© 2015 Navid H. Jafari

ELEVATED TEMPERATURES IN WASTE CONTAINMENT FACILITIES

BY

NAVID H. JAFARI

DISSERTATION

Submitted in partial fulfillment of the requirements
for the degree of Doctor of Philosophy in Civil Engineering
in the Graduate College of the
University of Illinois at Urbana-Champaign, 2015

Urbana, Illinois

Doctoral Committee:

Professor Timothy D. Stark, Chair
Professor Gholamreza Mesri
Professor Emeritus James H. Long
Professor Mark J. Rood
Professor R. Kerry Rowe

ABSTRACT

Municipal solid waste (MSW), construction demolition debris (CDD), industrial byproducts, and many other wastes are landfilled in waste containment facilities. A number of factors can lead to elevated temperatures and thus present a hazard to the public health and safety. For instance, MSW landfills can produce obnoxious odors, toxic gases, and aggressive leachates. In addition, they can damage gas extraction, leachate collection, interim cover, and composite liner systems. These events can result in expensive remediation and warrant the permanent closure of the facility.

The main objectives of this research are to: (1) identify causes and frequency of elevated temperatures; (2) develop a reactivity test for hazardous classification of aluminum production waste (APW); (3) develop an experiment to characterize gas generation and composition of APW; (4) identify progression of indicators for elevated temperatures in MSW landfills; (5) propose a classification system for landfill operators to assess the location and movement of elevated temperatures; and (6) evaluate the impact of elevated temperatures to high density polyethylene (HDPE) geomembrane service life.

MSW landfills with a gas collection and control system used to comply with federal regulations (40 CFR, Part 60, Subpart WWW) operate each gas extraction well with a landfill gas temperature less than 55°C (131°F) because methane production from mesophilic bacteria starts to significantly decrease if the temperature of the waste mass exceeds 55°C (Kasali and Senior 1989; Hartz et al. 1982). At temperatures beyond 64°C, Ahring et al. (1995) report that thermophilic methanogens are inhibited and methane production slows or ceases. Therefore, in this thesis waste temperatures above 65°C is considered to be elevated because anaerobic decomposition has been curtailed. Several factors can lead to elevated landfill temperatures, including aerobic decomposition, self-heating, partially extinguished surface fires, exothermic chemical reactions, and spontaneous combustion. Although the leading mechanism of elevated temperatures is air ingress, landfills are also experiencing elevated temperatures due to exothermic reactions from APW. Because aluminum production waste does not meet hazardous waste classification criteria, they are commonly disposed in MSW landfills. As a result, a novel bench-scale calorimeter is developed and calibrated to measure potential temperature escalation. The calorimeter experiments at varying sodium hydroxide (NaOH) strengths show temperatures can

rise to 100°C. For a landfill operator, the optimal concentration of NaOH was determined to be 1 M to 2 M NaOH because it provides sufficient alkalinity to react the metallic aluminum and fulfill the objectives of a rapid procedure to evaluate the reactivity criterion for hazardous waste classification. A gas generation test is developed and calibrated to evaluate hydrogen production and ammonia emissions from this waste stream. In addition, guidelines are provided for the disposal of APW in waste containment facilities.

Whether aluminum wastes, air ingress, or other mechanisms lead to elevated temperatures, these events start in a localized area and over time can expand and consume entire landfill facilities. A case study is used to consolidate changes in landfill behavior into an ordered sequence (referred herein as progression of indicators) to permit landfill operators and first responders to detect and identify the location of elevated temperatures. Expanding on the progression of indicators, two case histories are used to develop methods to illustrate spatial and temporal changes in landfill behavior. In particular, the first case study illustrates spatial movements with gas wellhead temperature, ratio of methane to carbon dioxide, and settlement, while the second case study demonstrates subsurface temperature migration. These two case studies along with the progression of indicators are used to classify MSW landfills into five zones: anaerobic biodegradation, gas front, heating front, smoldering front, and combustion/pyrolysis zone.

In addition, elevated temperatures can negatively impact engineered components in composite bottom liners, cover systems, leachate collection, and gas extraction and recovery systems. A case study is used to investigate the effect of elevated temperatures on HDPE geomembrane service life. When peak temperatures reach 60°C to 80°C, the geomembrane service life can be reduced to decades for the conditions examined and thus raises concerns regarding the integrity of the geomembrane at high temperatures.

To my parents, who raised me with a freedom to decide my career and supported me in all my pursuits

ACKNOWLEDGEMENTS

It is a great pleasure to thank the people who made this thesis possible. It is difficult to overstate my gratitude to my advisor, Professor Timothy D. Stark. It has been an honor to be his Ph.D. student. Throughout my research and thesis-writing, he provided encouragement, sound advice, and good teaching, company, and ideas. The joy and enthusiasm he has for his research was contagious and motivation for me, even during tough times of my Ph.D. pursuit. I am also thankful for the excellent example he has provided me as a successful geotechnical professional and professor.

I would also like to thank Professors Gholamreza Mesri, James H. Long, Mark J. Rood, and R. Kerry Rowe, for agreeing to serve as members of my committee. My special thanks to Professor R. Kerry Rowe of Queen's University, who in addition to participating in my committee, provided me with the geomembrane data and service life spreadsheet. In my later work of laboratory gas testing, I am indebted to Professor Mark Rood. He permitted access to his laboratory and aided in my understanding of air pollution control.

My time at University of Illinois at Urbana-Champaign was made enjoyable in large part due to the many friends and groups that became part of my life. I am grateful for this time spent with friends and their families. I am indebted to my many student colleagues for providing a stimulating and fun environment to learn and grow, especially my first officemates Randa Asmar and Seung Jae Lee. I am especially grateful to my friends Mohamad Jammoul, Ahmad Fawaz, Adolfo Caicedo, Luis Pazmino, Andrew Tangsombotvisit, Pouyan Assem, Steve Wilk, Cassie Dumoulin, Ziyue Yang, Ryan Wong, Ahmed Baghdady, Hamid Emamipour, John Atkinson, Andony Landivar, Mario Hernandez, and many others.

I would like to thank my family for all their love and constant encouragement during my studies: my brother, Kamron Jafari, and my sister Nauzanene Jafari. Most of all my supportive, encouraging, and patient mother, Faranak, and father, Mohammad, whose support during this Ph.D. is so appreciated.

Lastly, I offer my regards and blessings to all of those who supported me in any aspect of my courses and research.

TABLE OF CONTENTS

CHAPTER 1 INTRODUCTION 1

1.1 Statement of Problem 1
1.2 Research Objectives 2
1.3 Scope and Outline of this Study 3

CHAPTER 2 CAUSES AND FREQUENCY OF ELEVATED TEMPERATURES 5

2.1 Introduction 5
2.2 Occurrence of Elevated Temperatures 5
2.3 Causes of Elevated Temperatures in Waste Containment Facilities 7
2.4 Summary and Conclusions 15
2.5 Tables and Figures 16

CHAPTER 3 APW CLASSIFICATION AND REACTIVITY 27

3.1 Introduction 27
3.2 Review of APW Heat Generation 28
3.3 Waste Classification 29
3.4 Reactivity Test Criterion 32
3.5 Constant Pressure Calorimeter 33
3.6 Results 38
3.7 Discussion 40
3.8 Summary and Conclusions 43
3.9 Tables and Figures 44

CHAPTER 4 APW GAS PRODUCTION AND COMPOSITION 57

4.1 Introduction 57
4.2 Gas Production Background 57
4.3 Material and Test Methods 59
4.4 Results and Discussion 62
4.5 Summary of Gas Production Test Results 66
4.6 Recommendations for APW Disposal 66
4.7 Tables and Figures 69

CHAPTER 5 PROGRESSION OF ELEVATED TEMPERATURES IN MSW LANDFILLS . 89

5.1 Introduction 89
5.2 Overview of Case Study 90
5.3 Progression of Elevated Temperature Indicators 100
5.4 Field Manifestations and Landfill Operations 102
5.5 Elevated Landfill Temperature Processes 103
5.6 Summary and Conclusions 106
5.7 Tables and Figures 108

CHAPTER 6 CLASSIFICATION OF ELEVATED TEMPERATURES IN MSW LANDFILLS 121

6.1 Introduction 121

6.2 Case Study 1: Spatial Migration 122
6.3 Case Study 2: Subsurface Temperature Movement 127
6.4 Classification of Landfill Zones 131
6.5 Summary and Conclusions 136
6.6 Tables and Figures 138

CHAPTER 7 SERVICE LIFE OF HDPE GEOMEMBRANES SUBJECTED TO ELEVATED TEMPERATURES 151

7.1 Introduction 151
7.2 Effect of Temperature on HDPE Geomembranes 152
7.3 Elevated Temperature Case History 153
7.4 Evaluation of HDPE Geomembrane Service Life 161
7.5 Possible Remedial Measures 164
7.6 Summary and Conclusions 165
7.7 Tables and Figures 168

CHAPTER 8 SUMMARY AND CONCLUSIONS 177

8.1 Summary 177
8.2 Conclusions 178
8.3 Recommendations for Future Research 181

REFERENCES 183

CHAPTER 1

INTRODUCTION

1.1 Statement of Problem

Municipal solid waste (MSW), construction demolition and debris (CDD), compost, wood waste and saw dust stockpiles, shredded tires, wastewater sludge, industrial byproducts, and many other wastes are landfilled in waste containment facilities. These facilities are designed, constructed, and operated under federal and/or state regulations to reduce the risk of air pollution and groundwater contamination. A number of factors, e.g., air intrusion and reactive wastes, are causing elevated temperatures and thus presenting a hazard to the public health and safety. During elevated temperatures, the containment facilities can produce obnoxious odors, toxic gases, and aggressive leachates, as well as damage gas extraction, leachate collection, interim cover, and composite liner systems (Jafari et al. 2014a; Lewicki 1999; Øygard et al. 2005). The resulting odors and gases include carbon monoxide, benzene, volatile organic compounds (VOCs), dioxins and furans, reduced sulfur compounds, and particulate matter (Bates 2004; Nammari et al. 2004; Szczygielski 2008). Degradation of engineered barriers and maintenance of gas and leachate infrastructure can be accelerated by elevated temperatures (Jafari et al. 2014a; Stark et al. 2012; Martin et al. 2013) and result in expensive remediation.

MSW landfills with a gas collection and control system used to comply with federal regulations (40 Code of Federal Regulations (CFR), Part 60, Subpart WWW) operate each gas extraction well with a landfill gas temperature less than 55°C (131°F) because methane production from mesophilic bacteria starts to significantly decrease if the temperature of the waste mass exceeds 55°C (Kasali and Senior 1989; Hartz et al. 1982). At temperatures beyond 64°C, Ahring et al. (1995) report that thermophilic methanogens are inhibited and methane production slows or ceases. Therefore, in this thesis waste temperatures above 65°C is considered to be elevated because anaerobic decomposition has been curtailed.

Elevated temperatures are generally defined by the depth at which they occur: shallow (depths < 5 m) or deep-seated (depths > 10 m). Surface events involve recently buried or uncompacted waste, situated on or close to the landfill surface in the aerobic decomposition layer, i.e., generally 1 to 3 m in depth. They generally are characterized by the emission of dense white

smoke and the products of incomplete combustion. The smoke can include irritating agents, such as organic acids. Subsurface events occur at depths > 10 m, so the physical effects can range from distressed soil cover system, leachate outbreaks, excessive and rapid settlement, and possible slope instability. Although surface events occur more frequently (Martin et al. 2013), this research is focused on deep-seated cases because they are difficult to identify and delineate; are difficult to extinguish; can damage engineered components; and can warrant permanent closure of the facility.

1.2 Research Objectives

The main research objectives are to: The main objectives of this research are to: (1) identify causes and frequency of elevated temperatures; (2) develop a reactivity test for hazardous classification of aluminum production waste (APW); (3) develop an experiment to characterize gas generation and composition of APW; (4) identify progression of indicators for elevated temperatures in MSW landfills; (5) propose a classification system for landfill operators to assess the location and movement of elevated temperatures; and (6) evaluate the impact of elevated temperatures to HDPE geomembrane service life.

To accomplish these objectives, the study involved the following major tasks:

1. Identify factors leading to elevated temperature events.
2. Develop a bench-scale calorimeter to evaluate APW reactivity and heat generation potential.
3. Develop a procedure to quantify APW gas production and measure ammonia and hydrogen concentrations.
4. Measure heat generation and gas production using constant pressure calorimeter.
5. Analyze field case histories of elevated temperature events at MSW landfills.
6. Develop a progression of indicators for elevated landfill temperatures.
7. Develop a methodology to track spatial and temporal variations in elevated temperatures.
8. Evaluate the service life of high density polyethylene (HDPE) geomembrane.
9. Propose geomembrane service life criteria and possible remedial measures.

1.3 Scope and Outline of this Study

This thesis is divided into eight chapters. Chapter 1 is the introduction, and Chapter 2 presents a review of factors that cause elevated temperatures in waste containment facilities. In many cases, more than one factor can lead to development of elevated temperatures.

Chapter 3 discusses hazardous waste classification and lack of reactivity criterion for industrial wastes, particularly secondary aluminum production industry. A test procedure to measure reactivity, or heat generation potential, under simulated landfill conditions is presented. APW is used as an example of an industrial waste to show the efficacy of the reactivity test to evaluate heat generation potential. The work presented in Chapter 3 is published under the title "Classification and Reactivity of Secondary Aluminum Production." in 2014 in the ASCE Journal of Hazardous, Radioactive, and Toxic Waste, Volume 14, Number 4, p. 1-11.

Chapter 4 reviews gas related reactions from APW and describes an experimental setup to quantify gas production and measure hydrogen and ammonia concentrations. Measurements of several types of APW samples are presented and corroborated with x-ray diffraction results.

Chapter 5 uses a case study to develop a progression of landfill indicators to show elevated temperature events follow a systematic sequence. The progression of indicators allows landfill operators and first responders to detect and identify the location of elevated temperatures.

Chapter 6 uses two landfills to investigate the spatial and temporal changes in landfill indicators. In particular, the first case study (reported in Chapter 5) illustrates spatial movements with gas extraction wells and settlement points, while the second case study demonstrates subsurface temperature migration. These two case studies along with the progression of indicators in Chapter 5 are used to classify MSW landfills into five zones.

Chapter 7 presents the effect of elevated temperatures on HDPE geomembrane service life and proposes geomembrane service life criteria and possible remedial measures. The work presented in Chapter 7 is published in 2014 in the ASCE Journal of Hazardous, Radioactive, and Toxic Waste, Volume 14, Number 1, p. 1-11, and is titled "Service Life of HDPE Geomembranes subjected to Elevated Temperatures."

Finally, Chapter 8 presents the summary and conclusions of the research.

In summary, the contributions of this thesis include: (1) developing a criterion and test to assess the reactivity characteristics of industrial wastes; (2) evaluating the gas generation potential and composition of APW; (3) identifying a progression of landfill indicators that defines the

timeline of elevated temperatures; (4) developing a methodology to classify an elevated temperature landfill into anaerobic biodegradation, gas front, heating front, smoldering front, and combustion/pyrolysis zone; and (5) developing a time-temperature history plot at elevated temperatures to asses HDPE geomembrane service life.

CHAPTER 2

CAUSES AND FREQUENCY OF ELEVATED TEMPERATURES

2.1 Introduction

The waste industry, environmental regulators, fire scientists, first responders, and landfill engineers have labeled elevated temperature events as fires, smoldering combustion, glowing combustion, pyrolysis, subsurface oxidation, spontaneous oxidation, hot spots, and metallic reactions. The diverse terminology stems from different causes of elevated temperatures, regional and local precedence, and environmental regulations and policies. For the purposes of this thesis, elevated temperature landfills encompass all of these types of events. This chapter is focused on reviewing case histories and reports to understand the occurrence and causes of elevated temperatures. In Section 2.1, the author's terminology is used to maintain consistent definitions when presenting statistics of elevated temperature events.

2.2 Occurrence of Elevated Temperatures

2.2.1 United States

FEMA (2002) estimates that ~8,400 landfill fires occur every year in the U.S.A. The majority of landfill fires that occur are relatively small, easily contained surface events at the working face that are suppressed by the landfill operator. Surface fires generally do not result in operational problems or regulatory violations, are not typically reported to the regulatory community, and do not pose a serious threat to the public, environmental control systems, or site personnel. Although the majority of fires are surface events and small in nature, large-scale subsurface events (< 1% of landfill fires) do occur in the United States.

Large-scale events within the past decade were collected from press releases, literature, and personal communication with state regulators. The sites in which the author visited or obtained data are shown in Figure 2.1. In particular, DeHavilland (personal communication, 2014) reports that 15 Ohio landfills are experiencing elevated temperatures, with 8 sites having landfilled APW and recirculated leachate and another 3 facilities having only recirculated leachate. The two elevated temperature sites in Tennessee are attributed to aluminum waste reactions. Miller (2007)

describes a case study in Georgia detailing changes in gas well field temperature and gas composition due to air ingress. The Waimanalo Gulch sanitary landfill in Oahu, Hawaii has experienced elevated temperatures of about 85°C (Geosyntec 2008).

2.2.2 International

Ettala et al. (1996) states that ~60% of operational landfills in Finland reported fires annually, and more than one fire occurred at 20% of these sites. Moreover, approximately 95 sites (15% of total) in Finland reported deep-seated (depths > 2 m) events. In Sweden, 200 to 250 fires were reported in 400 MSW landfills (Ruokojarvi 1995; Naturvardverket 1994; Ettala et al. 1996). In most cases, the fires are shallow (depths < 8 m) and continued for 1 day to 1 week. In the United Kingdom, 57 incidents were reported to the environmental agency over a 10 month period in 2002 (Environmental Agency 2007). In another study, records from the Fire Service and Environment Agency show 26 fires occurring on landfill sites within Northamptonshire, United Kingdom between 1998 and 2003 (Bates 2004). A study in Ontario, Canada showed that out of 43 sites 10% reported daily fires, 20% weekly, 20% monthly (Chiblow 2004). In 1994, a survey carried out in Germany found that over four years and 63 landfills, there had been 13 fires which required assistance of the fire authority (Bothman 1994).

Parker et al. (2001) describe a landfill fire in Australia that was first reported in 1980. Remedial actions by the local fire authority attempted to smother the fire, but outbreaks of fire continued on site over the next two years. In particular, smoke was reported to be emanating from the landfill sporadically, but only investigative works and construction of passive venting in boreholes were undertaken to combat the fire. A national review of all landfills in New Zealand was undertaken in 1995 by the Ministry for the Environment (MOE). They reveal that more than half of the landfill operators who responded had experienced fires in the previous year (Parker et al. 2001). They indicate that the majority of fires were accidental, but almost a third of these fires were intentional. Burning occurred more commonly at small landfills, although a significant proportion of large landfills also experienced fires. As a result of concern about landfill fires, the New Zealand MOE released guidelines on the hazards of burning waste at landfills, which explicitly banned deliberate burning (NZ MOE 2001). An approximate 50% reduction in the occurrence of landfill fires was reported, but the New Zealand Fire Service for 2000-2001 shows that there were still around 130 fires at public and private landfills (NZ MOE 2001).

Poorly managed MSW landfills and dumps are also prone to fires. A possible methane explosion and fire may have contributed to the slope failure at Payatas landfill near Quezon City, Manila, Philippines (see Figure 2.2(a)) that killed at least 330 people (Jafari et al. 2013; Merry et al. 2005). Figure 2.2(b) shows smoke and/or steam emanating from a smaller landfill directly south of Payatas, which provides evidence that a possible deep-seated event at the Payatas landfill was occurring at the time of failure. Koelsch et al. (2005) report that a smoldering fire at the Leuwigajah dumpsite near Bandung, Indonesia destroyed the reinforcement nature of MSW, i.e., eliminated interlocking between MSW particles, and was a mechanism that triggered the slope failure and death of 141 people.

Table 2.1 presents a list of case histories reported in the literature. In particular, a summary of pertinent data and trends, mechanisms causing fires, and environmental impacts are provided. The leading mechanism of landfill fires is air ingress and subsequent combustion. Six case histories reported subsurface temperatures, including 800°C at a hazardous landfill, 690°C at a MSW landfill, and 240°C at an industrial waste fuel storage pile. Two case histories found that non-invasive geophysical techniques proved capable of delineating fire areas. For example, electromagnetic resistivity measurements indicate that fire areas (hot and/or dry material) are characterized by high resistivity. In regards to air pollution, two cases report elevated carbon monoxide concentrations (> 1,000 ppmv) and particulate matter ($PM_{2.5}$). Alberta Environment (2012) found that $PM_{2.5}$ concentrations ranged from 560 to 1,250 $\mu g/m^3$, which exceeded local ambient air quality guidelines. In addition, Oygard et al. (2005) monitored leachate before and after a fire. The leachate color changed from a pale brown to black color with high particulates and strong foul odor. They measured an increase in the chemical oxygen demand (COD) and heavy metals (lead, cadmium, and chromium), with the COD up to 15 times higher and the heavy metals 10–50 times higher than normal leachate.

2.3 Causes of Elevated Temperatures in Waste Containment Facilities

MSW landfills with a gas collection and control system used to comply with federal regulations (40 CFR, Part 60, Subpart WWW) operate each gas extraction well with a landfill gas temperature less than 55°C (131°F) because methane production from mesophilic bacteria starts to significantly decrease if the temperature of the waste mass exceeds 55°C (Kasali and Senior 1989; Hartz et al. 1982). At temperatures beyond 64°C, Ahring et al. (1995) report that thermophilic methanogens

are inhibited and methane production slows or ceases. Therefore, in this thesis waste temperatures above 65°C is considered to be elevated because anaerobic decomposition has been curtailed. Several factors can lead to landfill temperatures above 65°C, including aerobic decomposition, self-heating, partially extinguished surface fires, exothermic chemical reactions, spontaneous combustion, and smoldering combustion.

2.3.1 Aerobic Decomposition

The most common mechanism of elevated temperatures is introducing ambient air into landfills during gas collection and control operations (see Table 2.1). The typical vacuum for a gas extraction well is about 125 to 250 mm (5 to 10 inches) of water column (USACE 2008). Because landfill operators can overdraw the gas collection system, i.e., apply excessive vacuum, to capture methane for energy production, oxygen can enter the landfill through damaged gas wellhead seals and cracks. Aerobic decomposition can start from other actions that allow oxygen to enter the waste, such as fissures in the soil cover or rapid settlement, an abandoned gravel access road, poorly compacted or inadequate interim covers, uncapped borings, leachate sumps, drainage systems, and passive venting systems. Changes in atmospheric pressure can move landfill gas out or move air into the landfill body (Young 1992; Nastev et al. 2001; Ishigaki et al. 2005). In addition, the chimney effect draws humid and warm air into the landfill as higher temperature gas moves and expands upward. This convection process causes air to flow into the landfill body, delivering oxygen to the heat generating processes.

MSW landfills undergo aerobic decomposition to produce carbon dioxide, water, and heat (Meraz and Dominguez 1998). As available oxygen is consumed, biological decomposition changes to anaerobic with resultant production of methane, carbon dioxide, and heat. Aerobic transformation of glucose as representative of the organic matter in the waste can be expressed by Reaction 2.1 (Meraz and Dominguez 1998):

$$C_6H_{12}O_6\,(s) + 6\,O_2\,(g) \rightarrow 6\,CO_2\,(g) + 6\,H_2O\,(l) \quad \Delta H = -2{,}815\ \mathrm{kJ/mol} \tag{2.1}$$

Transformation of glucose under anaerobic condition can be expressed by Reaction 2.2 (Meraz and Dominguez 1998):

$$C_6H_{12}O_6\,(s) \rightarrow 3\,CO_2\,(g) + 3\,CH_4\,(g) \quad \Delta H = -145\ kJ/mol \tag{2.2}$$

Comparing the enthalpies of both reactions, heat generated in anaerobic decomposition is about 5% of the heat produced from the aerobic reaction (Meraz and Dominguez 1998; El-Fadel 1999). Waste temperatures in aerobic conditions are in the range of 60 to 80°C (Haug 1997; Lefebvre et al. 2000; Merz 1969; Hudgins and Harper 1999) whereas anaerobic landfills typically range from around 25°C to 45°C (Yesiller et al. 2005; Hartz et al. 1982; Mata-Alvarez and Martinez-Viturtia 1986; Pfeffer 1974). For example, Figure 2.3 presents changes in gas wellhead temperature and composition due to air intrusion at a MSW landfill in Illinois. Prior to October 2006, gas wellhead temperatures are below the New Source Performance Standards (NSPS) limit of 55°C and the gas composition consists of 50% v/v methane and carbon dioxide. Oxygen levels initially remain below 1% v/v until September 2006, and then increase to 6% v/v. Air ingress into the well caused the surge in oxygen because methane levels and gas temperature decreased concomitantly. After four months, methane levels and temperature rebounded to anaerobic conditions. However, another air ingress event in February 2007 introduced oxygen (~8% v/v) into the waste mass. Methane concentrations and temperature decreased again but in this case methane (see February 2007) continued to drop and by June 2007 had reached < 10% v/v. As methane levels decreased, temperatures fueled by aerobic decomposition and possible smoldering combustion increased to 75°C in October 2007. Wellhead temperatures gradually increased to 80-85°C and CO_2 concentrations replaced CH_4 in the following two years.

2.3.2 Self-Heating

A common strategy to reduce long-term environmental risks and to enhance methane recovery is to stimulate microbial activity by adding moisture to the waste via leachate recirculation and addition of supplemental liquids (Benson et al. 2007; Barlaz et al. 2008). The process accelerates decomposition and heat generation, resulting in waste temperatures of 50-60°C (Kumar 2007; Yazdani et al. 2006). Researchers have also investigated injecting air and moisture in landfills because of the ability of aerobic landfills to degrade the solid waste at higher rates than conventional anaerobic landfills (Stessel and Murphy 1992; Read et al. 2001a,b; Reinhart et al. 2002). With accelerated

biodegradation, the insulating properties of MSW minimize heat flux from the landfill to the surroundings, so MSW self-heating can ultimately continue to raise temperatures (Rees 1980; El-Fadel 1999). During MSW self-heating, organic matter undergoes chemical oxidation and temperatures rise to initiate possible pyrolysis and/or smoldering combustion. Although chemical oxidation is similar to aerobic biodegradation in terms of the final products and total released heat, rates of heat generation and oxygen consumption are higher during chemical oxidation. For example, Springer et al. (1971) studied spontaneous heating in piled wood chips. In this study, they measured the oxygen consumption and calculated the released heat for aspen and Douglas-fir wood during biological degradation and chemical oxidation. They found that oxygen consumption during aerobic biodegradation was about 39% and 50% of the oxygen consumption during chemical oxidation for aspen and Douglas-fir wood, respectively. Research shows moisture is an accelerator for the chemical oxidation of different organic materials, including coal, yard waste, and wood chips (Brownring and Crone 1950; Shea and Hsu 1972; Kubler 1987; Buggeln and Rynk 2002; Kucuk et al. 2003; Kadioglu and Varamaz 2003).

2.3.3 Surface Fires

Temperatures also can increase and remain elevated because of partially extinguished, buried surface fires (depths of 1 m to 5 m). Surface fires are common at landfills and can be attributed to the burial of hot loads, spontaneous combustion, sparks from construction vehicles, incompatible chemicals, reactive metals, and ignition of methane and air. Wastes affected by surface fires are excavated, but if the fire is not completely extinguished, the smoldering waste can continue as a hot spot for a long period of time.

2.3.4 Reactive Industrial Wastes

Landfills are experiencing elevated temperatures due to exothermic chemical reactions of industrial wastes (Stark et al. 2012; Jafari et al. 2014b; OEPA 2011; Klein et al. 2003). For example, several facilities in Figure 2.1 observed increased wellhead temperatures when MSW landfill operators began to recirculate leachate to accelerate biodegradation. However, the consequence of additional moisture was that an APW reaction was instigated (Calder and Stark 2010; Jafari et al. 2014b). Other landfill chemical reactions with industrial wastes include MSW

incinerator ash and bottom ash (Klein et al. 2001; Klein et al. 2003), tires (Wappett and Zornberg 2006), iron waste, steel mill slag, petroleum coke, flue gas desulfurization gypsum, fluidized bed combustion residues (Anthony et al. 1999), lime kiln dust, and dried wastewater sludge (Zerlottin et al. 2013). Table 2.2 summarizes several possible exothermic reactions in landfills. They primarily involve oxidation of alkali metals and iron (Fe), corrosion of metallic aluminum (Al), and hydrolysis of calcium oxide (CaO). Exothermic chemical reactions can become the primary source of heat for pyrolysis and/or combustion.

2.3.4.1 APW

Aluminum production waste is recognized as a toxic and hazardous waste per the European Union, Australia, Brazil, and others (Amer 2002; Bruckard and Woodcock 2007; Lucheva et al. 2005; Miškufová et al. 2006; Shinzato and Hypolito 2005). In the USA, treatment processes developed for recycling APW into saleable salt fluxes, metal, and value-added non-metallic derivatives are adversely influenced by the current low cost alternative of landfill disposal, which has resulted in APW reactions in MSW landfills (Stark et al. 2012; Martin et al. 2013). For example, the U.S. DOE (1999) estimates that at least 1 million metric tons of APW are placed annually in Resource Conservation and Recovery Act (RCRA) Subtitle D landfills. Subtitle D landfills address non-hazardous solid wastes, including certain hazardous wastes which are exempted from the Subtitle C regulations.

Aluminum waste is commonly referred to as “skimmings”, “white dross”, “black dross”, and “salt cake.” These terms refer to the amount of aluminum present and the morphology of the wastes raked from the surface of molten aluminum during primary and secondary processing and purification (Manfredi et al. 1997). The generation of white dross occurs at primary aluminum smelters, extruding plants, sheet mills, foundries, and dies casters (Kulik and Daley 1990). Because these facilities operate without fluxing, white dross skimmed from the furnaces have a grey or metallic white color (Figure 2.4(a)) and consist of 15-70% metallic Al content (Kulik and Daley 1990). Black dross is created during melting of scrap and recycled aluminum with a salt flux (Figure 2.4(b)). When melting aluminum scrap in open charging well furnaces, a salt flux is often used on the open surface of the bath to eliminate the formation of oxides and to cause the agglomeration of small beads of aluminum, thus improving metal recovery. A common flux contains about 47.5% NaCl, 47.5% KCl, and 5% fluoride salt (Sreenivasarao et al. 1997). At high

molten temperature, the added salt flux becomes dark colored and thus is referred to as "black dross." Black dross is usually granular with a relatively high metal content in the coarse fraction and chiefly oxides and salt in the fine. The content of the black dross varies depending on the scrap type being charged and the processing conditions, but usually varies from 12 to 18% metallic Al, 40-55% salt flux mixtures, and 20-50% Al_2O_3 (Kulik and Daley 1990). To capture metallic Al in white and black dross, they can be melted in a rotary furnace with additional salt flux. The discharge from this process is salt cake. The composition of salt cake depends on the black dross, but it often contains 3–5% metallic Al, 15–30% Al_2O_3, 30–55% NaCl, and 15–30% KCl, and depending on the scrap type may contain carbides, nitrides, sulfides, and phosphides (Peterson and Newton 2002). Almost 726,000 metric tons of salt cake is annually landfilled in the U.S. (Sreenivasarao et al. 1997) and is usually disposed in landfills in solid blocks (Figure 2.4(c)). Baghouse dusts consist of particulate matter produced during salt cake hammering and crushing and furnace off-gas. These wastes may contain cadmium (Cd) and lead (Pb) above the limits of the EPA Toxicity Characteristics Leaching Procedure (TCLP) test (Hwang et al. 2006; Stanforth 1991) and are frequently disposed in landfills (Figure 2.4(d)). Because lime is injected into the foundry ductwork to protect against sparks and improve dust collection, baghouse dusts are a source of alkalinity and fine aluminum dust particles in landfills. This makes baghouse dust highly reactive when disposed with other forms of APW.

The disposal of APW in landfills or other venues can cause environmental pollution through its high reactivity with leachate, infiltrating rain, or even humidity in air, leading to the heat generation and formation of toxic, explosive, and odorous gases. As early as 1955, the aluminum industry acknowledged the generation of excessively elevated temperatures and hydrogen gas as a result of aluminum wastes contacting water (Chen 1955). The most likely heat-generating reaction of APWs in a Subtitle D landfill or non-hazardous industrial landfill involves the amphoteric reaction of aluminum metal with water (Calder and Stark 2010):

$$2\mathrm{Al(s)} + 6\mathrm{H_2O(l)} \rightarrow 2\mathrm{Al(OH)_3} + 3\mathrm{H_2(g)} \quad \Delta H = -415\ \mathrm{kJ/mol} \tag{2.3}$$

These reactions can release large amounts of heat and possibly flammable hydrogen gas. Internal temperatures of waste masses undergoing this reaction have been observed between 88°C (170°F) and 110°C (230°F), at which desirable microbial activity is terminated and corresponding

methane production is severely curtailed. Figure 2.5 shows an example of two gas wells in an APW monofill in Ohio where downhole temperatures were measured at 3 and 7.6 m below the ground surface. At a depth of 7.6 m, the maximum temperature increased to 112°C within the first 50 days after disposal and gradually decreased thereafter. The maximum temperatures measured at a depth of 3 m is 108°C, but the average trend line from both gas wells indicate that the maximum temperature produced is more likely between 80 and 90°C. Lower temperatures are observed in Figure 2.5(a) due to heat loss to the surface. In areas where APW was co-disposed with MSW and leachate was recirculated, temperatures rose to 95°C (205°F) and remained steady or slightly decreased to 85°C (185°F) after five years. Temperatures remained constant because the reaction occurred in the middle of the waste height (~31 m thick), hence heat loss is limited. In contrast, waste temperatures in APW only cells show similar behavior to Figure 2.5. That is, the APW reacts with liquid (most likely rain) and temperatures reach a peak value before decreasing because of heat loss to the atmosphere. These cells are under construction so the effect of thermal insulation is not known.

The exothermic aluminum reaction and associated changes in gas composition and increased gas pressure also usually cause intense nuisance odors (e.g., ammonia) and possible combustion of surrounding MSW. The temperature in APW landfills depends on both the availability of liquids and free metallic aluminum. Whereas the maximum temperature in MSW landfills is located within the middle third of the depth of the waste, the maximum temperature in APW landfills depends on the location of APW and amount of metallic aluminum in Reaction (2.3).

2.3.5 Spontaneous Ignition

Sustained heat generated by aerobic biodegradation and/or exothermic waste reactions may not be easily dissipated because of the insulating properties of MSW. Because heat is retained in the waste, internal chemical oxidation reactions are accelerated and further contribute to elevated temperatures. This self-heating is a pathway to spontaneous ignition, which induces even higher temperatures and accelerates thermal breakdown of MSW (Lönnermark et al. 2008). Hogland and Marques (2003) monitored the initiation of spontaneous ignition in an open-stored MSW fill. They measured waste temperatures as high as 240°C, which corresponds to MSW ignition temperatures of 180 to 300°C reported in Moqbel et al. (2010).

2.3.6 Smoldering Combustion and Pyrolysis

After MSW is exposed to elevated temperatures for a sustained period of time, pyrolysis and/or smoldering combustion can occur. The process of pyrolysis degrades MSW to lower weight molecules in the absence of oxygen (Babrauskas 2003). Pyrolysis is an endothermic process, i.e., not self-sustaining, that precedes the exothermic processes of flaming or smoldering combustion (Pitts 2007). Sørum et al. (2001) show that the major weight loses of the cellulosic matter in MSW occurred between 250–400°C. In addition, the charred waste products of pyrolysis also have a lower ignition temperature than the original material, which ultimately can lead to spontaneous combustion.

Fires are a self-sustained, exothermic reaction between a fuel and oxidizer (Kuo 1986; Griffiths and Barnard 1995; Warnatz et al. 1996; Drysdale 1999). Two types of fires can develop in MSW landfills: (1) surface fires (flammable combustion) by burning of volatilized compounds and (2) subsurface fires (smoldering combustion) (Kuo 1986). Subsurface fires typically propagate in landfills through smoldering combustion, which occurs directly on the surface of a solid fuel (Shafizadeh 1982). Reaction 2.4 indicates that the incomplete smoldering combustion of cellulose yields carbon dioxide, carbon monoxide, water vapor, and heat (Huggett 1980). The rate of combustion is generally limited by the amount of oxygen available, but it can still propagate at low oxygen levels of <3% v/v (DeHann 2007; Pitts 2007). Smoldering combustion has been documented to persist within a solid waste landfill between 100°C and 120°C (Ettala et al. 1996). Once initiated, smoldering combustion temperatures observed in MSW landfills have ranged from 200 to 300°C and as high as 700°C (Ettala et al. 1996; Lönnermark et al. 2008; Ruokojarvi et al. 1995). In addition, temperatures of 80 – 230°C were also measured for a deep fire and 309 – 406°C for a surface fire (Bergstrom and Bjorner 1992).

$$C_6H_{10}O_5 + 5.7\,O_2 \rightarrow 5.4\,CO_2 + 0.6\,CO + 5\,H_2O \qquad \Delta H = -2,440\,\text{kJ/mol} \tag{2.4}$$

Figure 2.6 relates a timeline of MSW landfill operations with development of smoldering combustion and pyrolysis. Figure 2.6(a) shows that aerobic biodegradation begins soon after the waste is placed in a landfill and continues until all of entrained oxygen is depleted from the voids in the waste. During Stage I, aerobic biodegradation may continue from 6 to as long as 18 months and raise waste temperatures to 80°C (EMCON 1981). As the oxygen is consumed, acid forming

bacteria begin to hydrolyze and ferment the complex organic compounds in the waste. Biodegradation then enters an anaerobic phase (Stage II) and waste temperatures are typically 38 to 54°C. Stage II will continue until all of the carbonaceous (organic) material is depleted. In Figure 2.6(a), anaerobic biodegradation continues for 9.5 years until an incident of oxygen ingress reverts the landfill to aerobic conditions, thereby increasing waste temperatures to 80°C. The presence of oxygen and heat source (aerobic biodegradation) provide the necessary conditions for smoldering combustion to occur. As a result, smoldering combustion causes temperatures to increase to possibly 400°C or higher. As temperatures increase above 250°C, the cellulosic fraction and plastic components of MSW begin to thermally degrade via pyrolysis. The pathway to elevated temperatures in Figure 2.6(b) is similar to Figure 2.6(a) except that after Stage II the reaction of APW and leachate generates sufficient heat to spontaneously ignite MSW. In addition, the APW reaction provides self-sustaining chain reaction if limited oxygen is available to fuel smoldering combustion, which leads again to pyrolysis.

2.4 Summary and Conclusions

This chapter reviewed the frequency and mechanisms causing landfill elevated temperatures. In particular, a review of case studies shows that MSW, construction debris, industrial landfills are prone to fire hazards. Fires occur in modern engineered containment facilities and sanitary dumps and can continue for several months to years. The leading mechanism in both cases is oxygen ingress and subsequent aerobic reactions. Industrial landfills are experiencing elevated temperatures due to chemical reactions. In addition, there are short and long-term consequences of landfill fires. Two case studies in Southeast Asia indicate that smoldering combustion can be a triggering mechanism to waste slides. Another case study found temperatures increased solubility of heavy metals into the landfill leachate, which can lead to groundwater pollution. Studies have documented air emissions due to MSW combustion, but the long-term risks to the public and environment remain unknown.

2.5 Tables and Figures

Table 2.1 Summary of case histories documented in literature

Description and Notes	Event Duration	Location/Reference
A fire was discovered in an active hazardous waste landfill containing industrial waste sludge and other chemical manufacturing by-products. Thermocouple measurements in the vicinity of the fire measured temperatures of ~800°C.	11 months	U.S.A. Adams et al. (1997)
An experimental MSW landfill was constructed to investigate optimum extinguishment practices during smoldering combustion. The test site was 7 m deep, 3 m wide, and 6 m long and was instrumented with 66 type K thermocouples, and CO, CO_2, and O_2 gases were measured. They observed temperatures of 350 and 690°C at two thermocouples. The study also found that MSW above and below these two hot spots were not affected, thus proving the heterogeneity and insulating properties of MSW. CO concentrations reached 1,600 ppmv and limited oxygen supply slowed the smoldering combustion process	Not Reported	Finland Ettala et al. (1996)
Four fire-prone landfills were investigated with integrated electrical resistivity tests, temperature, and gas composition measurements. The waste type at four landfill fires consists of construction waste only, mixed MSW and construction (2 sites), and mixed industrial and MSW. Two facilities are located in old quarries. One is located on a valley slope and another is a man-made embankment. Maximum subsurface temperatures measured at ~0.6 m depth in the smoldering area were about 113°C and 162°C.	Not Reported	Israel Frid et al. (2010)

Table 2.1 (cont.)

Description and Notes	Event Duration	Location/Reference
Two landfill fires were investigated using infrared and geophysical instruments. Maximum temperatures measured by the infrared camera were ~300°C. Electromagnetic resistivity measurements characterized fire areas as high resistivity (hot and/or dry material) while low resistivity zones indicated higher moisture waste.	Not Reported	France Riquier et al. (2003)
A fire started because of air ingress from an abandoned storm water drain below the landfill. Temperature probes measured waste temperatures of ~100°C. The operators tried liquefied CO_2 injection to mitigate elevated temperatures. Temperatures subsided only after the storm drain was abandoned.	7 months	California Gale et al. (2007)
The paper describes spontaneous combustion events for industrial waste fuel and refuse derived fuel (RDF) compacted storage piles. Spontaneous combustion in the industrial waste resulted in temperatures of 240°C. For the RDF pile, the study found elevated levels of cadmium, lead, and chromium in the leachate.	5 days	Sweden Hogland and Marques (2003)
A construction, demolition, and debris landfill was initiated by spontaneous combustion. CO concentrations above 1,000 ppmv were measured in the fire area. Limited CO (< 100 ppmv) was found in non-impacted areas. The author suggests temperatures above 75°C as a strong indication of fire.	2 – 3 months	North Delta, near Vancouver, Canada Henderson and Sperling (2001) Sperling (2001)

Table 2.1 (cont.)

Description and Notes	Event Duration	Location/Reference
The landfill was established in 1993 and stopped receiving waste in 2002. In March 2003, a subsurface fire was first noticed when smoke escaped out of the landfill. Prior to the fire, the leachate was a pale brown color, but it changed to black color with high particulates and a strong foul odor. Immediately after the fire started, there was a large increase in the chemical oxygen demand (COD) and heavy metals (lead, cadmium, and chromium), with the COD up to 15 times higher than normal and the heavy metals 10–50 times higher than normal.	10 days	Western Norway Øygard et al. (2005)
In July 2000, a slope at the Payatas Landfill failed, killing at least 300 people. One possible factor in the slope failure was a subsurface fire. Evidence of a fire in a smaller landfill immediately southeast of the waste failure showed a combination of steam/smoke emanating from the surface. In addition, the slide mass caught fire after the failure because of downed electrical lines, fired stoves in buried huts, or from spontaneous combustion.	Not Reported	Quezon City, Manila, Philippines Jafari et al. (2013); Merry et al. (2005)
In February 2005, the Bandung dump slope failed, which unfortunately led to 141 deaths. Forensic investigations found that the failure was most likely triggered by pore-water pressure from significant rainfall and damage to the reinforcement nature of MSW caused by the smoldering fire. The operators of the dump confirmed that the landfill regularly burned. A photo captured in 1992 showed smoke emanating from the landfill.	Several months to years	Bandung, West Java, Indonesia Koelsch et al. (2005)

Table 2.1 (cont.)

Description and Notes	Event Duration	Location/Reference
The fire occurred in construction and demolition materials. Alberta Environment and Sustainable Resource Development conducted ambient air quality monitoring to assess potential impact on local air quality. They found exceedances of 1-hr Alberta Ambient Air Quality Guidelines for PM2.5. Concentrations ranged from 560 to 1,246 µg/m^3.	3 days	Southwest boundary of Calgary, Canada Alberta Environment (2012)
Dump sites are common in Nigeria. The author cataloged air pollution from five municipal solid waste dump sites that frequently burn. They found particulate matter and CO emissions at concentrations of 773 to 801 µg/m^3 and 134 to 142 ppmv, respectively.	Not Reported	Niger Delta, Nigeria Rim-Rukeh (2014)
There are a number of uncontrolled dumps in Greece and fires are common, especially during the summer. The Tagarades landfill consists mainly of domestic trash as well as hospital and commercial wastes and wastewater treatment sludge. Landfill gas is not collected so the fire is hypothesized to have started because of spontaneous ignition of methane.	10 days	Near Thessaloniki, Greece Chrysikou et al. (2008)
The subsurface fire stated in the summer of 2006. The authors examined pollutant emissions to the atmosphere, but no measurements were provided.	Several weeks to months	Thessaloniki, Greece Nikolaou (2008)

Table 2.1 (cont.)

Description and Notes	Event Duration	Location/Reference
Old MSW landfill used for more than 35 years (until mid-1970s) as open combustion. Although the site was covered with soil, the burning process is still ongoing because combustion was not complete.	Partially extinguished fire mid-1970s to 1990s	Marka, Jordan Alawi et al. (1996)
The Solous landfill is a non-engineered facility that has experienced several landfill fires since 2008. The authors describe two incidents in 2009 and 2011 that caused dark smoke to emanate from the landfill. No measurements were provided.	Several days to weeks	Lagos, Nigeria Aderemi and Otitoloju (2012)

Table 2.2 Exothermic reactions in MSW landfills

Reaction	Enthalpy of reactions, ΔH (kJ/mol)
$CaO + H_2O \rightarrow Ca(OH)_2$	-65.3
$4Fe + 3O_2 + 6H_2O \rightarrow 4Fe(OH)_3 + H_2 \uparrow$	-340.7
$2Al + 6H_2O \rightarrow 2Al(OH)_3 + H_2 \uparrow$	-422
$FeS + (9/4)O_2 + (5/2)H_2O \rightarrow Fe(OH)_3 + H_2SO_4$	-921



Figure 2.1 Locations of elevated temperature events in the U.S.A. the author obtained data (map with permission from Wikipedia)



(a)



(b)

Figure 2.2 Aerial view of Payatas Landfill: (a) Slope failure and homes visible in foreground and (b) Stable landfill south of slide showing smoke/steam plumes (photos by S.M. Merry)

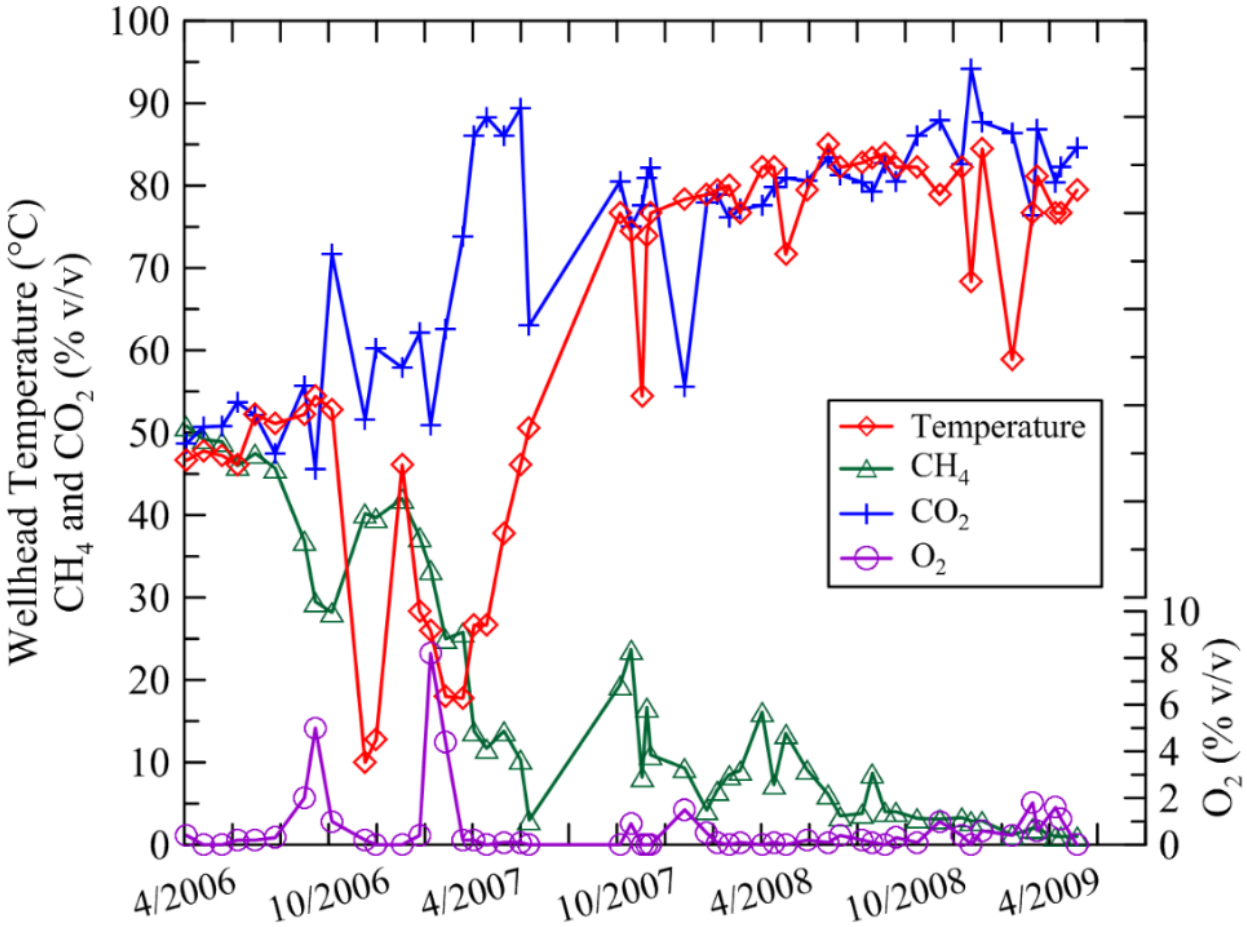

Figure 2.3 Elevated temperatures caused by air ingress and aerobic decomposition



(a) white dross



(b) black dross



(c) salt cake



(d) baghouse dust

Figure 2.4 Types of aluminum production waste: (a) white dross, (b) black dross, (c) salt cake, (d) and baghouse dust

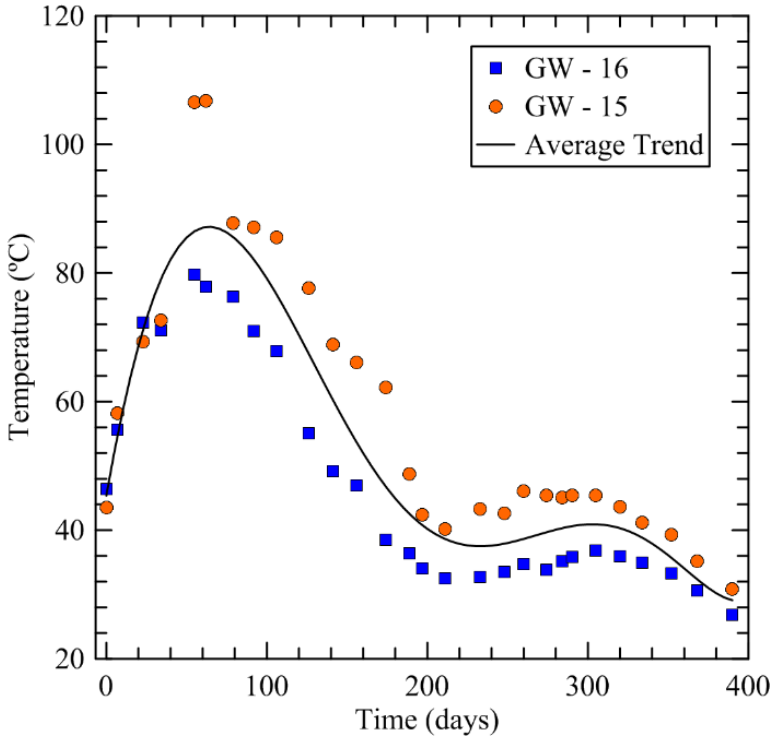

(a) Depth 3 m

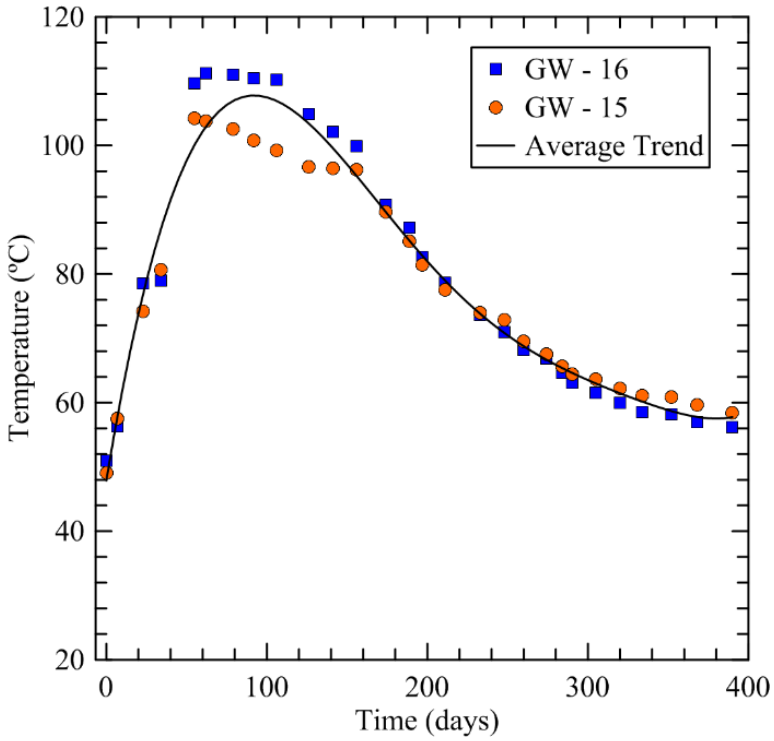

(b) Depth 7.6 m

Figure 2.5 Maximum temperatures Gas Well (GW) 15 and 16 at an APW monofill in Ohio: (a) Depth 3 m; and (b) Depth 7.6 m (from Jafari et al. 2014)

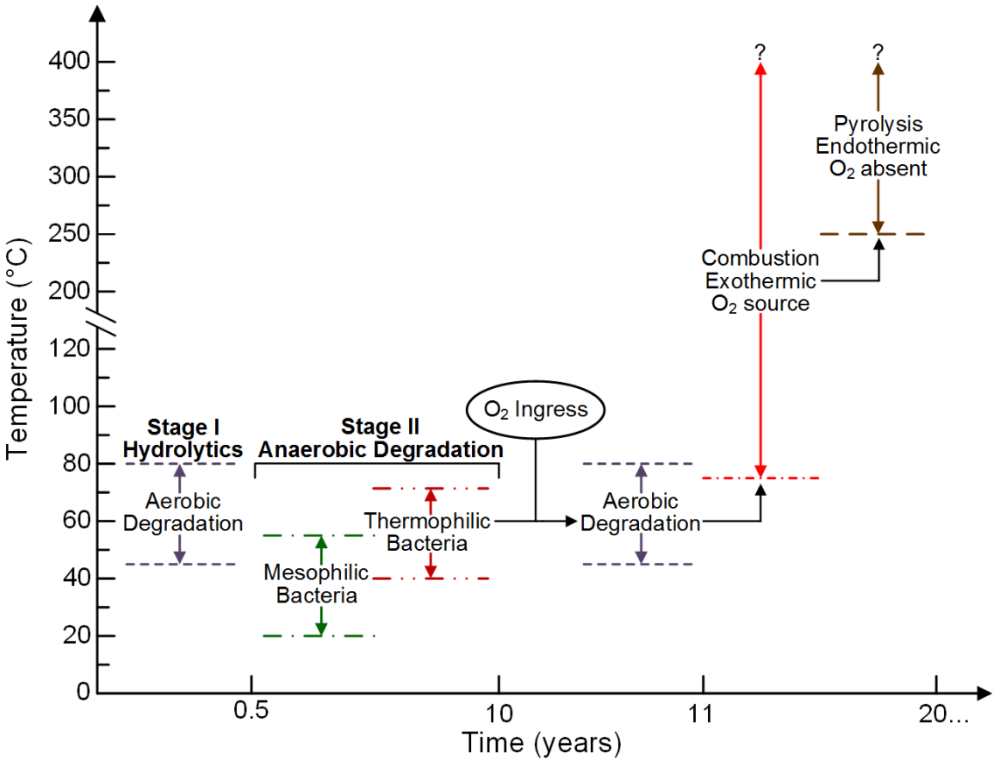

(a) Aerobic biodegradation

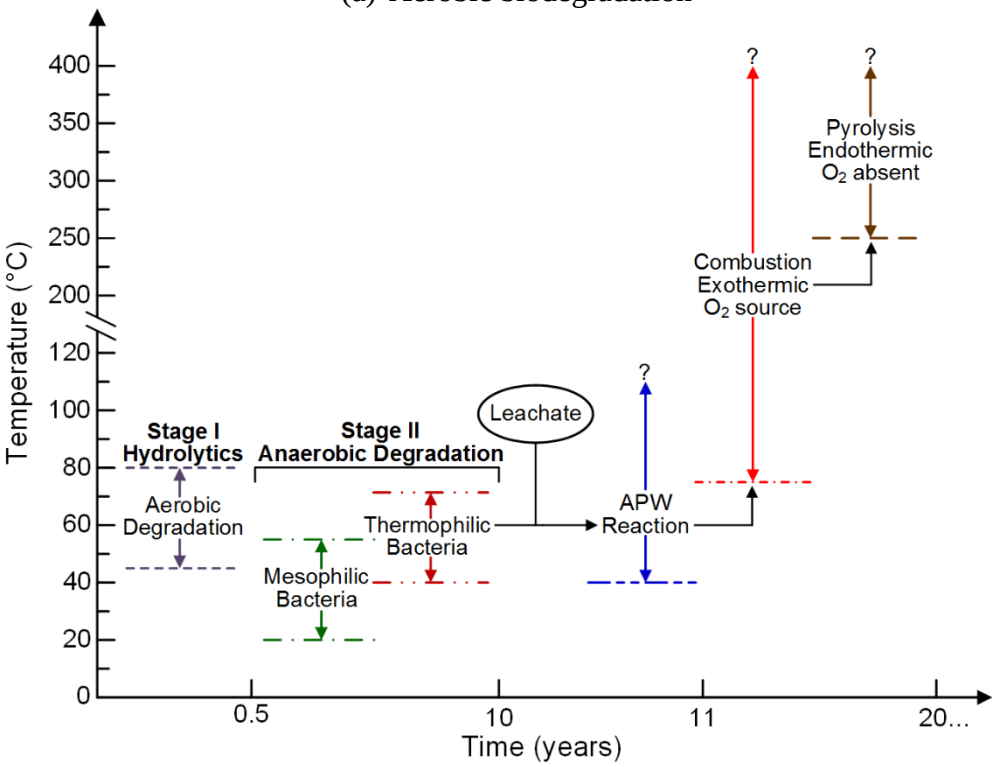

(b) APW reactions

Figure 2.6 Development of elevated temperatures by two pathways: (a) Aerobic biodegradation and (b) APW reactions

CHAPTER 3

APW CLASSIFICATION AND REACTIVITY

3.1 Introduction

Residential, institutional, and commercial refuse from a municipality or region comprise the bulk of the waste streams disposed in a Subtitle D (MSW) landfill. Subtitle D landfills also can accept industrial wastes which are generally referred to as "special wastes". For example, APW is generally classified as a special waste in Tennessee and Ohio landfills. The primary purpose of referring to a waste streams as "special waste" is to provide the operator of Subtitle D landfills with a mechanism to ensure that prohibited wastes, especially RCRA Subtitle C hazardous and TSCA (Toxic Substances Control Act) wastes, are not placed in a Subtitle D landfill. A secondary purpose of classifying certain types of waste as "special waste" is to ensure that receipt of such wastes will not adversely affect the near-term or long-term operation of the facility.

A solid waste is deemed hazardous in two ways, either of which would make it ineligible for disposal in a Subtitle D facility. First, 40 CFR Sec. 261, Subpart D explicitly lists the materials that are defined as hazardous and these materials cannot be placed in a Subtitle D regulated landfill. APW, including dross, salt cake, and baghouse dust, are not explicitly listed in 40 CFR Sec. 261. Second, if a waste exhibits any one of the four characteristics of a hazardous waste, i.e., ignitability, corrosivity, reactivity, or toxicity, the waste is classified as a hazardous waste under 40 CFR Sec. 261, Subpart C and cannot be placed in a Subtitle D facility. Because of APW related reactions observed in Subtitle D landfills in the past (e.g., Brantley, Huelger Kronquist, Countywide, Middle Point, and Arkansas Red River), toxicity, reactivity, and corrosivity under 40 CFR Sec. 261, Subpart C are potentially relevant to APW. For example, corrosivity and toxicity can be an issue because APW leachate consists of high concentration of salts and may include of heavy metals (arsenic, cadmium, lead, mercury) (Xiao et al. 2005; Swackhamer 2006). Reactivity is the most applicable to APW because of liquid induced aluminum reactions. As defined by CFR Sec. 261.23, reactive wastes can cause explosions, toxic fumes, gases, or vapors when mixed with water. Test methods to evaluate reactivity are not currently available. As a result, this chapter provides a brief review of APW heat generation and summarizes two case histories in which APW was evaluated under hazardous waste regulations. In addition, a bench-scale test using a constant pressure

calorimeter is presented to help APW generators and Subtitle D landfill operators decide whether a certain shipment of APW will cause an adverse reaction and thus result in excessive increase in landfill temperature.

3.2 Review of APW Heat Generation

3.2.1 Huang et al. (2014)

Huang et al. (2014) collected 36 salt cake samples from 9 landfill sites to characterize chemical composition, physical characteristics, and waste reactivity. In particular, they measured moisture content, water holding capacity, pH, and specific conductance, and chemical properties, such as total element analysis, leachate element analysis, and X-ray Diffraction (XRD). Huang et al. (2014) assessed reactivity by measuring heat generation potential, i.e., temperature increase from an initial control temperature (ΔT), for the salt cakes samples in acidic and basic solutions, two control temperatures, three particle sizes, and various solid to liquid ratios.

Heat generation potential of salt cake samples was conducted in a temperature controlled container by reacting 10 g of salt cake with 10 mL water in a 60 mL vial. The salt cake samples were sieved so that test samples were < 2 mm in particle size. Figure 3.1(a) and 3.1(b) show histograms of temperature increase (ΔT) from initial control temperatures of 37°C and 50°C, respectively. The control temperatures were selected because they represent typical waste temperatures found in MSW landfills (Yesiller et al. 2005). In Figure 3.1(a), ΔT is < 20°C for 25 of 36 samples, yet one sample yielded a maximum ΔT of 64°C. Raising the control temperature to 50°C (Figure 3.1(b)) caused the mean temperature to increase from 22.0 to 28.6°C, thus indicating reactivity increases with increasing control temperatures. Figure 3.2 shows a plot of 37°C data on the abscissa and 50°C results as the dependent variable. When samples tested at 37°C generated ΔT > 30°C, raising the control temperature to 50°C did not significantly affect ΔT. This is illustrated by the data plotting on the 1:1 trend line in Figure 3.2. For temperatures below 30°C, Figure 3.2 indicates that the maximum temperature observed increases by an average factor of 1.5 and maximum factor of 2. The data in Figure 3.2 suggest that initially less reactive salt cake samples ($\Delta T \leq 30$°C) can yield significantly higher temperatures with increasing control temperatures. It is suggested that the metallic aluminum reaction is the governing reaction for ΔT

> 35°C. Photos and visual descriptions of the materials were not provided. These salt cake samples may contain large metallic aluminum pieces that are easy to react and less dependent on the initial control temperature to facilitate the reaction. In addition to increasing reactivity, the time to reach maximum temperatures (t_{max}) is reduced. Figure 3.3 compares t_{max} values for 37 and 50°C control experiments. Increasing control temperature to 50°C causes t_{max} values to decrease by an average factor of two compared to the 37°C control experiment.

Figure 3.4 shows maximum temperature response for salt cake particle sizes of < 0.25 mm, < 2 mm, and < 9 mm from three samples (Samples A through C). The experiments were conducted at a control of 37°C. All three samples show that the maximum temperature increases with decreasing particle size. For example, Sample B yielded temperatures of 41.1°C, 46.2°C, and 133.2°C for decreasing particle sizes. Because small particle diameters increases surface area, reactivity also increases. This is important because the amount of finely graded fraction of APW increases with grinding/milling processes. In addition, an APW sample must be collected from the shipping container, and obtaining a finer fraction should result in higher reactivity.

Huang et al. (2014) also conducted heat generation tests with salt cake samples in 0.1 M NaOH (pH~13), deionized water (pH~6.8), and MSW leachate (pH not reported). Table 3.1 summarizes reactivity for three samples at an initial control temperature of 37°C. For all three samples, reactivity was higher for deionized water and 0.1 M NaOH than MSW leachate. As an example, sample 1 produced ΔT of 55.9 and 49.8°C for 0.1 M NaOH and deionized water, respectively, while MSW leachate generated a ΔT of 12.4°C. The MSW pH and chemistry was not provided by Huang et al. (2014) to explain the lower reactivity attributed to MSW leachate.

3.3 Waste Classification

3.3.1 Ohio Landfill

From 1995 through 2008, a MSW landfill located in Ohio (referred herein to Site 1 in Chapter 3 and Chapter 4) received approximately 661,000 metric tons (651,000 tons) of APW. Annually, APW comprises 30-50% of the total site tonnage (176,000 metric tons). Because another Ohio landfill experienced APW reactions (Stark et al. 2012; Martin et al. 2013), the county health district issued special terms and conditions to prevent a similar situation. The terms and conditions

included monitoring leachate characteristics, gas production and composition, and temperatures within the waste mass. The special terms and conditions requested the facility to characterize the reactivity, ignitability, chemical composition, and leaching characteristics of APW from each generator. Table 3.2 presents total elemental composition (EPA 3051 Method) for three types of APW. The APW elemental content varies significantly and hence are difficult to interpret, but presumably result from different feed-stocks and differences in operating practices. For example, magnesium, iron, manganese, and silicon in APW are linked to alloys used to enhance aluminum properties during production. Chloride, potassium, and sodium with trace amounts of calcium and fluoride in Table 3.2 are ingredients comprising the salt flux.

Starting in 2007, Ignitability and Department of Transportation (DOT) Dangerous When Wet Tests (CFR Part 173.124) were performed monthly for each APW in Table 3.2. The ignitibility test evaluates whether the waste is spontaneously combustible, e.g., waste oils and used solvents. The ignitability tests proved negative. The DOT test is described in Title 49 Transportation (CFR Part 173.124) – Shippers - General Requirements for Shipments and Packing and involves the reaction of a material with distilled water at 20°C and atmospheric pressure. A “dangerous when wet” material is defined as a material in contact with water that becomes spontaneously flammable or gives off flammable or toxic gas at a rate greater than 1 L/kg-hr. The Dangerous When Wet Test were generally below the maximum gas evolution rate of 1 L/kg-hr. However, several baghouse dust samples yielded maximum gas evolution rates above 1 L/kg-hr, e.g., 3.0, 6.6, and 10.1 L-kg-hr. Based on the characterization testing, the APW was not deemed hazardous and continued to be disposed at the facility. Although extensive APW characterization and testing was performed, waste temperatures over 100°C measured in landfill gas, ammonia emissions, and hydrogen gas production suggest current test procedures to do not capture APW reactivity.

3.3.2 Indiana Landfill

An Indiana secondary aluminum facility generated 3,600 metric tons per month of APW from its aluminum dross reclamation process and disposed these wastes at an onsite monofill. From July 2006 to January 2007, three “thermite fires” (oxidation of metallic aluminum at high temperatures) occurred in the landfill (RMT, Inc. 2007). Subsequently the Indiana Department of Environmental Management (IDEM) requested assessment of the APW as a hazardous waste according to 40 CFR

Sec. 261, Subpart C. The fires ceased after modifications to the mechanical post-process reduced the metallic aluminum content of the APW being disposed. Specifically, the top screen mesh size was increased from 25.4 mm to 50.8 mm before mechanical grinding. The bottom screen sieve was decreased from No. 16 (1.19 mm) mesh to No. 25 (0.707 mm). The screen size modifications allowed larger APW granules to pass (thereby increasing the post-processed volume of dross to capture more metallic aluminum before disposal). By retaining more of the crushed metallic aluminum particles on the final mesh, mainly salts and non-metal oxides passed the final sieve and were identified for landfill disposal.

The generator concluded that APW was not a reactive or ignitable hazardous waste under 40 CFR Secs. 261.2 and 261.4(a) because the reaction between APW and water occurred over several hours. The reaction did not exhibit violent reaction, i.e., characterized by a rapid evolution of energy. Laboratory testing showed that upon contact with water, gas release was slow, at less than 1 liter/kg-hour in six out of seven hourly increments as measured in the (DOT Dangerous When Wet Test (CFR Part 173.124).

To measure heat generation, this Indiana facility decided to immerse the APW in tap water in an insulated chamber. The testing procedure consisted of thoroughly mixing 1 kg of APW and 150 mL of tap water in a plastic beaker. After quickly filling a quart size container with moist APW and placing a thermometer inside the waste, the container was sealed and placed inside an insulated chamber. Figure 3.5 summarizes the results that include maximum temperatures of 130°C (266°F). The data show that about one-third of the samples tested exceed temperatures of 65°C, which is an upper bound temperature measured in MSW landfills (Hanson et al. 2010). Although the metallic aluminum content was not evaluated, the amount of oxidized metallic aluminum necessary to reproduce temperatures in Figure 3.5 was about 1%. This indicates that only a small amount of oxidized metallic aluminum is required to elevate the temperature to 130°C. Complete metallic aluminum reaction in the described experiments was unlikely and under more favorable conditions, e.g., finer particle size and a basic solution, higher temperatures should be anticipated.

The reaction between APW and water (under controlled conditions) did not generate toxic gases, e.g., ammonia, acetylene, methane, or sulfur compounds, in a quantity sufficient to present a danger to human health in an outdoor environment (see Table 3.3). Ammonia concentrations were measured using Dräger tubes positioned less than 150 mm above the processed materials.

Ammonia concentrations ranged from 2 to 23 ppmv which is below the OSHA Personal Exposure Limit (PEL) of 50 ppmv. The gas composition in Table 3.3 confirms that hydrogen is the dominant gas generated from APW, and the metallic aluminum reaction is the source of temperature rise. Based on the data in Table 3.3, IDEM concluded that APW did not meet reactivity characteristics as described by 40 CFR Part 261.23 and allowed disposal to continue in the site's Subtitle D facility.

3.3.3 Summary of APW Classification

The Indiana and Ohio cases corroborate that APW is reactive but not necessarily hazardous under 40 CFR Sec. 261, Subpart C. Other landfill facilities and researchers (IMP 2002; David and Kopac 2012; Fukumoto et al. 2001; Huang et al. 2014) suggest the reaction is slow and depends on leachate chemistry. If sufficient time is allowed and an alkaline environment persists, the APW can react and increase temperatures, and thus should not be disposed in MSW landfills. The slow activating reaction is also a drawback of the Dangerous-When-Wet test method (40 CFR Sec. 170, Appendix E) because the reacting solution is distilled water. This liquid does not represent actual landfill leachate, which ha percolated through APW. In fact, Huang et al. (2014) found that APW reaction with water requires over an hour before maximum temperatures are observed. Given the field observations of reactivity (US EPA 1994; Swackhamer 2006; RMT, Inc. 2007; Calder and Stark 2010; Stark et al. 2012) and variability of reactivity test methods, a new test and criterion is proposed here to determine whether an APW displays a characteristic of reactivity under 40 CFR Sec. 261, Subpart C and thus whether a specific APW should be considered suitable for disposal in Subtitle D landfills.

3.4 Reactivity Test Criterion

One of the most important parameters used to assess whether or not a Subtitle D Landfill is operating normally is temperature (Hanson et. al. 2010; Crutcher et al. 1982). For an active gas collection system that meets New Source Performance Standards (NSPS; 40 CFR 60.753) requirements, landfill gas temperature within each extraction wellhead must be monitored monthly (US EPA 1999). Monitored routinely, temperature provides a reliable parameter to evaluate APW reactivity and landfill behavior.

Anaerobic decomposition proceeds within three temperature ranges: the psychophilic range with temperatures less than 20°C; the mesophilic range with temperatures between 20° and 45°C; and the thermophilic range with temperatures greater than 45°C (Kotze et al. 1969). Yesiller et al. (2005) report that most Subtitle D landfills operate in the mesophilic range, although optimal landfill gas production can be achieved in the thermophilic range. The anaerobic processes that regulate methane generation occur best within a temperature range of 40° to 42°C for mesophilic bacteria (Hartz et al. 1982; Mata-Alvarez and Martinez-Viturtia 1986; Pfeffer 1974). Characterizing optimal temperatures in the thermophilic range are less certain. For example, methane production starts to significantly decrease if the temperature of the waste exceeds 55°C (Kasali and Senior 1989; Hartz et al. 1982). Zinder et al. (1984) suggest that the optimal temperature range for thermophilic methanogenesis is between 55°C and 60°C. At temperatures beyond 64°C, Ahring et al. (1995) report that acetotrophic methanogens are inhibited and methane production slows or ceases.

Under normal conditions, the temperature of solid waste and landfill gas generated by an MSW landfill ranges between 25° and 45°C (77° to 113° F) (ASTDR 2001), and the maximum allowable gas wellhead temperature is 55°C (131°F) (40 CFR 60.756). In particular, NSPS (40 CFR 60.753) require that a facility demonstrate that combustion is not occurring within the waste mass if a wellhead temperature exceeds 55°C. Based on NSPS requirements and anaerobic landfill environment, it is desirable to maintain landfill temperatures below 65°C (150°F) for healthy anaerobic decomposition, optimal methane gas production, and safe landfill operations. Therefore, the reactivity test should yield a temperature less than 65°C (149° F) to ensure NSPS compliance and prevent adverse consequences to landfill engineered components.

3.5 Constant Pressure Calorimeter

Aluminum production waste composition and physical properties, e.g., pH, particle size, and metallic aluminum content, can vary significantly due to plant operation, smelting furnace, scrap and recycled materials used, and salts introduced. The most likely exothermic reaction of APW in a Subtitle D landfill or non-hazardous industrial landfill involve the amphoteric reaction of metallic aluminum with water.

$$2Al(s) + 6H_2O(l) \rightarrow 2Al(OH)_3 + 3H_2(g) \qquad \Delta H = -415\ kJ/mol \tag{3.1}$$

As an amphoteric metal, trivalent aluminum (Al^{3+}) dissolves in strong acids as well as strong basic solutions (see Figure 3.6). In addition, Figure 3.6 shows that an oxide layer passivates metallic aluminum between pH of 4 to 9, giving corrosion resistance in the atmosphere and almost neutral pH solutions. However, the oxide layer cannot exert its protective effect in strong acidic or alkaline solutions, which can be problematic in Subtitle D landfills because of significant alkalinity in the wastes and accompanying liquids. In particular, Table 3.1 shows that deionized water with a pH ~6.8 can release signficantly more heat than MSW leachate (pH not reported but typical leachate pH are about 7).

The pH value is not the sole parameter influencing the reaction of metallic aluminum. The lower corrosion rate in ammonium hydroxide demonstrates that the individual ions in the solution are more important than the degree of acidity or alkalinity. For example, the corrosion rate of metallic aluminum in a solution of NaOH at 0.1 g/L is 25 times greater than in an ammonia solution at 500 g/L, although both solutions have similar pH values of 12.7 and 12.2, respectively (Vargel 2004). The strong bases and acids in Figure 3.6 cause the reaction rate to increase with concentration. In addition to alkalinity, increasing temperature leads to an increase in rate of chemical reactions. This applies to inorganic acids (HCl) and bases (NaOH), especially when the temperature approaches their boiling point (Vargel 2004). Chatterjee and Thomas (1976) report that aluminum corrosion rates in 200 g/L NaOH solution increase by twenty times for temperatures of 30°C to 80°C, respectively. Therefore, depending on the specific chemical ions, concentration of hydroxide ions, and temperature, the metallic aluminum reaction in APW can range from superficial etching to rapid corrosion.

In Reaction 3.2, metallic aluminum and NaOH solution combine to yield sodium aluminate [$NaAl(OH)_4$], hydrogen, and heat. This reaction is the basis of the caustic etching reaction used as the initial operation in aluminum anodizing, i.e., electrolytic passivation process, that increases the thickness of the natural oxide layer.

$$2Al(s) + 2NaOH(aq) + 6H_2O \rightarrow 2NaAl(OH)_4(s) + 3H_2(g) \tag{3.2}$$

This important reaction is completed within a few a minutes and oxidizes the metallic aluminum. As a result, the bench-scale experiment developed herein uses Reaction 3.2 to identify whether the reactivity of the APW is sufficient to elevate temperatures in the landfill and classify it as a hazardous waste.

3.5.1 Calorimeter Theory

Calorimetry is the quantitative measurement of heat required or evolved during a chemical process (Chang 2005). The proposed constant pressure calorimeter is shown in Figure 3.7 and is an instrument for measuring the heat of reaction during a defined process. In a constant pressure calorimeter, the reaction between a liquid and APW generates heat. Because calorimeter acts as an insulator, minimal heat loss occurs between the calorimeter and the surrounding air, thus creating an isolated system. The heat of reaction (q_{rxn}) is a thermodynamic unit of measurement for calculating the amount of energy (kilojoules; kJ) released in a reaction.

$$q_{rxn} = m_{residue}\, c_{p,residue}\, \Delta T \tag{3.3}$$

where the change from final and initial temperature is ΔT (°C), $m_{residue}$ is mass of alkaline solution and APW (g), and $c_{p,residue}$ is the specific heat (J/g °C). The resulting value of q_{rxn} is the maximum amount of heat that could be generated in a Subtitle D landfill by a given amount of APW reacting with solution. The $c_{p,residue}$ is a weighted average between the specific heats of solution and solid APW. Using the arithmetic mean of the main constituents (metallic Al, Al_2O_3, NaCl, and KCl), the APW specific heat is about 0.837 J/g °C (0.2 cal/g·°C). Assuming 50 g of APW is reacted in 20 g of water (4.186 J/g·°C or 1 cal/g·°C), the $c_{p,residue}$ is about 1.79 J/g·°C (0.43 cal/g·°C). The example assumes the density of water is constant, but the solution density changes with varying concentrations of alkaline reagents.

3.5.2 Calorimeter Equipment and Procedure

The test equipment comprises an insulated calorimeter, NaOH solution, thermometer, and release valve. Typical insulated calorimeters use glass thermal insulation layers and are tightly sealed

using a rubber stopper. A variety of NaOH molarity (M) concentrations, e.g., 1 M, 5 M, and 10 M, can be prepared from NaOH pellets purchased at a chemical supply company. Although landfill leachate is usually represented by a pH of about 7 (Barlaz et al. 2010; Kjeldsen et al. 2002; Ehrig 1983), a basic solution is recommended in the test to ensure the metallic aluminum reacts. This will minimize the reaction time and maximize the temperature rise, i.e., representative APW reactivity assessment. A release valve serves to dissipate gas pressure generated by the APW reaction. As a result, it is anticipated that this test can be performed quickly at a secondary processor or a landfill weigh station.

The general test procedure consists of weighing a representative specimen of APW and placing it inside the insulated constant pressure calorimeter (Figure 3.7). The volume of NaOH should saturate the APW. This procedure is recommended instead of a solid to liquid ratio because some APW, e.g., baghouse dust, are extremely fine and require additional liquid to saturate and coat all dust particles. The predetermined NaOH solution is then added to the APW and quickly mixed by stirring or swirling. The calorimeter is quickly sealed tightly by placing the rubber stopper in the top of the container to prevent heat loss. The change in temperature inside the calorimeter is monitored by inserting a thermometer through the rubber stopper into the moist APW. In addition, a release valve is connected to the rubber stopper, which prevents pressure build-up from gas production. The temperature is monitored and recorded at regular intervals, e.g., every 20 seconds, until the maximum temperature is recorded. Because the heat lost from the insulated container is small, the constant pressure calorimeter provides a representative landfill temperature and heat of reaction. The constant pressure calorimeter is calibrated by evaluating the insulation efficiency of the container.

3.5.3 Calibration

Calibration of the constant pressure calorimeter is recommended before classifying APW as hazardous or non-hazardous. The calorimeter calibration test involves the dissolution of NaOH in water. Reaction 3.4 is exothermic and generates 44.5 kJ of energy. By measuring ΔT, q_{rxn} (kJ) is computed using Equation 3.3. To compare theoretical and experimental results in similar units, the computed q_{rxn} is divided by the moles of NaOH to obtain ΔH (kJ/mol).

$$NaOH(s) + H_2O \rightarrow Na^+(aq) + OH^-(aq) \qquad \Delta H = -44.5\ kJ/mol \tag{3.4}$$

Table 3.4 presents the results for the calorimeter calibration. In Test 1, 7.65 g NaOH (0.191 mole NaOH) is dissolved in 150.19 g H_2O. The measured ΔT was 12.6°C, resulting in q_{rxn}= 8.32 kJ and ΔH= 43.51 kJ/mol. For Test 1, the error is 2.1%, and the error for all tests is 5.1%. A likely source of error is the measurement of ΔT because the thermometer scale is in increments of 1°C. For example, Test 1 error would have increased from 2.1% to 6% if ΔT was increased by only 0.55°C (1°F).

3.5.4 APW Physical and Chemical Properties

Aluminum production waste was sampled from two Subtitle D facilities: Site 1 (Ohio landfill in waste classification section) and Site 2 (facility in Tennessee). Figure 3.8 presents samples of Sites 1 and 2 APW used in reactivity testing. The APW samples in Figure 3.8(a) through Figure 3.8(d) are milled black dross (MBD), baghouse dust (BHD), black dross (BD), and milled salt cake (MSC), respectively. Figure 3.9 shows the particle size gradation for both sites. The MBD in Figure 3.9(a) represents the remaining APW after black dross was mechanically milled and screened for metallic aluminum, resulting in gap-graded MBD. The BD in Figure 3.9(b) is representative of a well-graded fine sand. The MSC originates from mechanical grinding and crushing of salt cake blocks and sieving to recover metallic aluminum captured within the salt flux. The sieve processing results in a coarser gradation than black dross in Figure 3.9(b). BHD is not shown in Figure 3.9(a) because the dust particles are finer than No. 200 (0.074 mm). The pH of each sample was evaluated using ASTM 4972 (ASTM 2007). The pH ranged from 8 to 9 for all APW except baghouse dust, which indicated a pH of ~10.4.

The mineral phase of each APW was characterized using XRD by Heritage Environmental Services. The XRD patterns were collected on a Rigaku MiniFlex II Diffractometer from 5 to 110 degrees 2θ using Cu Kα radiation and scintillation counter with in-line monochromator. The phase identification of samples was carried out using Materials Data, Incorporated (MDI) software suite Jade 9 and the International Center for Diffraction Data PDF4+ database for reference patterns. After identification, semi-quantitative analysis was conducted on each sample using Jade 9 whole pattern fitting methods. The dominant minerals in the salt cake samples are summarized in Table

3.5 and comprise metallic aluminum, corundum (Al_2O_3), sylvite (KCl), halite (NaCl), and spinel ($MgAl_2O_4$). Some of the samples also contained quartz (SiO_2) and periclase (MgO). The average metallic aluminum content is about 2% for both sites, which is lower than average values reported in the literature. XRD results summarized in Table 3.5 also identified aluminum oxycarbide (Al_2CO), which is more commonly found in APW as Al_4C_3. Alumina and carbon react in the furnace to form Al_2CO. Then, additional carbon and Al_2CO combine to yield Al_4C_3. The XRD results also did not identify AlN even though an ammonia odor was noted from the APW during the calorimeter experiments. This observation suggests that certain minerals phases are present in APW but may not be identified and so XRD results should provide only a general overview of APW composition.

3.6 Results

3.6.1 Effect of NaOH Concentration

Experiments were performed on APW to investigate the role of metallic aluminum reaction on temperatures in a landfill. The test procedure consists of dosing 50 g of APW in 25 mL of NaOH solution and measuring the temperature increase. Figure 3.10 shows the effect of NaOH molarity (mole NaOH/L solution) on the APW from Sites 1 and 2. As the concentration of NaOH increases from 1 M to 15 M, the maximum temperature and reaction rate increase significantly. For example, Figure 3.10(a) shows the MBD in 15 M NaOH solution reaches a maximum temperature of about 130°C in 2 minutes. This reaction is violent and characterized by forceful gas release. Temperatures in the range of 100°C to 110°C are consistently observed in 4 M, 5 M, and 10 M NaOH for all APW samples. Experiments generally peaked at a temperature of 100°C because additional heat produced by the aluminum reaction vaporized moisture into steam. The 4 M and 5 M NaOH solutions yield similar temperatures of 100°C, but the reaction rate of 4 M is slightly slower, as illustrated in Figure 3.10(a) and 3.10(d). A larger decrease in maximum temperature and reaction rate is observed for 3 M NaOH solutions. This indicates that sufficient hydroxide ions are not present in 3 M NaOH to react the metallic aluminum and increase temperatures to 100°C. In Figure 3.10(b), the baghouse dust in 3 M NaOH reacts quicker due to the finer particles, i.e., increased surface area, and additional basicity from lime present in baghouse dusts. Higher

maximum temperatures (85°C) and reaction rates were also observed for baghouse dust in 1 M and 2 M NaOH. Figure 3.10(a) and 3.10(d) illustrate that APW in 10 M NaOH generates substantially greater temperatures (above 110°C) than 5 M NaOH. Both APW samples in Figure 3.10(a) and 3.10(d) are milled before landfill disposal, which may explain the slower reaction rates at lower NaOH concentrations.

In Figure 3.10(c) and 3.10(d), the black dross is more reactive than the milled salt cake. Using 4 M NaOH solution as an example, the milled salt cake requires about 9 minutes to reach 100°C, but the black dross increases to 105°C in about 3 minutes. Figure 3.10 demonstrates that in a strong basic environment, APW reacts to produce elevated temperatures and flammable, malodorous gasses. However, APW reactivity in water is slower and results in 5°C to 17°C temperature increase. In comparison, Huang et al. (2014) measured temperature increases of 3.4°C to 64.1°C with an average of 22°C for thirty-nine APW samples tested in distilled water and two initial temperatures (37°C and 50°C). Huang et al. (2014) report pH and XRD patterns but not APW particle gradation. Trends relating pH or metallic aluminum content to temperature increase were not directly correlated by Huang et al. (2014). More likely, APW reactivity in neutral solutions is governed by the fines content and lack of hydroxide ions to facilitate the reaction.

The 4 M NaOH experiments generate temperatures of 100°C because the strong alkaline solution drives the metallic aluminum reaction. However, the hydroxide ions in 3M NaOH concentration are consumed prior to 100°C, so temperatures increase to 80°C. Decreasing reactivity is also observed for 1 M and 2 M (see Figure 3.10(a) and 3.10(d)). APW samples tested in Figure 3.10 contain low metallic aluminum content, i.e., XRD results indicate an average of 2% wt. These samples likely represent the lower reactivity spectrum, thus the recommended concentration to evaluate APW reactivity is 1 M NaOH with a maximum concentration of 2M NaOH.

In summary, the temperatures in Figure 3.10 rapidly increase from 23°C to about 105°C in less than 10 minutes. Slower reaction rates in milled APW corroborates that milling and recovering metallic aluminum in APW also reduces reactivity. The XRD analyses verify that low concentrations of metallic aluminum in APW can generate high temperatures under strong alkaline conditions. The rapid reaction rate observed in Figure 3.10(b) is attributed to additional alkalinity in the form of lime in the baghouse dust. The reactivity of milled black dross in water, shown in Figure 3.10(a), may be attributed to the fine particle size. The results in Figure 3.10 and Figure

3.11 indicate that a strong basic solution (1 M NaOH) is required to initiate a reaction for the APW samples shown in Figure 3.8.

Because XRD results only provide semi-quantitative results, the metallic aluminum content in Table 3.5 may be higher than actually identified. A reliable method of evaluating metallic aluminum content is to directly measure the volume of hydrogen gas produced. For example, Chapter 4 presents a method to measure gas production and composition from APW.

3.6.2 Effect of Milling APW

After skimming salt residue from the smelting furnace, metallic aluminum entrapped in APW is recovered by impact milling. This process deforms or grinds the malleable metallic aluminum and reduces the size of brittle oxide and salt phases. Because aluminum will not break in the milling process, it will be screened out in the coarser fractions. The coarser fractions represent as low as 15% of the total weight of the milled APW but can contain as much as 80% metallic aluminum (Karvelas et al. 1991). After screening ball-milled black dross, Fair et al. (1987) found that 5.2% of the mass passing the No. 100 mesh (0.15 mm) can be metallic aluminum.

Impact milling recovers aluminum from APW before final disposal but also generates finer APW particles, which may liberate entrapped aluminum and increase APW reactivity. Fair et al. (1987) report that after impact milling 26.3% of APW was finer than No. 100 (0.15 mm) mesh. In comparison, laboratory ball-milling grinds particles to finer than the No. 200 sieve (0.074 mm), so use of ball-milled material will represent a conservative estimate on APW reactivity. Figure 3.11 compares Site 2 black dross for original particle gradation and ball-milled samples (< 0.074 mm). Using a 4 M NaOH solution, the effect of ball-milling slightly increases reactivity. More importantly, ball-milling increased temperatures from 25°C to 60°C in water. Although ball-milling conservatively reduces particle gradation to below 0.074 mm, the milling processes can exacerbate APW reactivity in neutral pH solutions.

3.7 Discussion

The constant pressure calorimeter experiments with NaOH demonstrate that APW is highly reactive yet APW can remain dormant for years in MSW landfills and monofills until some event inadvertently causes the waste to come into contact with an acidic or basic leachate. For example,

APW reactions occurred after facilities in Ohio (Stark et al. 2012; Martin et al. 2013) and Tennessee began recirculating leachate. MSW landfill leachates consist of dissolved organic matter, inorganic components, heavy metals, and organic compounds (Christensen et al. 1994). The pH levels are initially acidic (5-6) during the transition period from aerobic decomposition to stable methane production. After methanogenic decomposition is established, pH levels increase to average values of 7 to 8 (Ehrig 1983; Kjeldsen et al. 2002). The role of leachate chemical characteristics on initiating the metallic aluminum reaction is currently unknown. More likely, the leachate serves to saturate the dry APW, where the dissolution and reaction of other APW constituents activate that the metallic aluminum reaction. Huang et al. (2014) report that the pH of APW is about 10.5. Possible APW constituents responsible for increasing pH are MgO, CaO, AlN, and others. The reactivity increases for APWs comprised of alkaline pH and a large percentage of fines, e.g., baghouse dusts. Baghouse dusts are, in some instances, even more basic with pH values of 13 because of the addition of alkalinity (lime) to control sparks in ductwork and prevent leaching of heavy metals. As a result, moisture introduced into the landfill reacts with carbides, nitrides, and metal oxides and hence increases waste pH. The basic conditions begin to react with metallic aluminum to elevate temperatures and produce hydrogen gas.

Because a high pH (> 3 M NaOH) solution induces a vigorous APW reaction, the optimal concentration of NaOH was determined to be 1 M to 2 M NaOH. This concentration provides sufficient alkalinity to react the metallic aluminum and fulfill the objectives of a rapid procedure to evaluate APW reactivity in an alkaline environment. For example, Figure 3.12 presents the temperature increase with time for Site 1 APW samples for 1 M and 2 M NaOH. The reactivity tests performed at 1M are generally completed in 25 minutes while the 2M experiments are completed in a slightly lower time period (~15 minutes). Compared to 1 M NaOH, the 2M NaOH caused temperatures to increase by ~8°C for the milled black dross MBD and ~14°C for the salt cake. The baghouse dust did not show a visible increase in temperature from 1 M to 2 M NaOH. Never the less, Figure 3.12 shows that the lower NaOH concentrations can delineate more reactive (salt cake and baghouse dust) wastes than the milled black dross, thus providing the landfill operator a quantitative criterion to decide if a waste stream should be disposed within the landfill.

In situ landfill temperatures have been measured above 100°C in APW disposed facilities. For example, Site 1 (Ohio Landfill) is measuring downhole temperatures in gas wells. In May 2008, temperatures measured at 8 m (26 ft) and 20 m (65.5 ft) below the ground surface (bgs) were

about 96°C (205°F). Over two years later (September 2011) the temperatures decreased to ~70°C (158°F) at 8 m bgs but remained nearly constant at 93°C at 20 m bgs. The temperature decrease at 8 m bgs indicates that the metallic aluminum rapidly oxidizes after disposal, i.e., when soil cover is minimal and precipitation can infiltrate into the waste. As the waste height increases, moisture infiltration into the lower waste layers decreases. Because the reaction requires liquid to be sustained, heat loss is greater than heat generation and temperatures begin to decrease. The temperatures at 20 m bgs illustrate that minimal heat loss occurs in the middle third of the landfill. In the reactivity test, the insulated constant pressure calorimeter serves to simulate the center of the landfill where heat loss is minimal. The 4 M or 5 M NaOH solutions react the APW in a short time period to yield temperatures similar to the field. The field reaction most likely involves a less basic solution but more aluminum to react. Whereas the alkaline solution serves to accelerate the metallic aluminum reaction so the test completes in several minutes, the field reaction required several months. This suggests that the reaction is slower and that heat loss is an important influence.

The bench-scale reactivity test involves performing a temperature test at the generator or landfill weigh station to estimate the temperature rise that could occur in the landfill. The optimal test conditions should balance the strength of NaOH, solid to liquid ratio, APW sample size, and testing temperature. Because APW is generally transported from generator to the landfill facility by a transfer dump truck, a representative sample size of APW is necessary for the reactivity test. As indicated in Figure 3.9, APW particle gradation can vary based on the type of waste. APW fines are more reactive than the coarse fraction, so the landfill operator should pass the APW through a No. 40 mesh (0.425 mm) to obtain a representative sample. This sample, consisting of APW fines, is then used to measure 50 g for the reactivity test. If the APW consists primarily of lumps and granules, the sieve size may be increased to No. 10 (2.00 mm) and the sample mass increased to a reasonable value.

In addition, APW can be exposed to cold climates during transport as well as warmer temperatures during the summer months. Because metallic aluminum corrosion is influenced by temperature, a standard temperature is required. For instance, Huang et al. (2014) performed APW reactivity tests in distilled water and temperatures of 37°C and 50°C to simulate temperatures in landfills. They report that at 50°C maximum temperatures increased by an average of 7°C compared to 37°C. The proposed calorimeter test, however, is recommended to be performed at a

standard temperature of 20°C (68°F), similar to the Dangerous When Wet test. The standard temperature permits a baseline temperature for landfill operators to compare APW reactivity and ensures testing conditions are consistent between landfills, secondary aluminum generators, and other facilities.

3.8 Summary and Conclusions

Although recycling aluminum is beneficial and sustainable, the disposal of the resulting solid waste is a concern because of potential APW exothermic reactions. A review of two active sites indicate that APW is reactive but not necessarily classified as hazardous under 40 CFR Sec. 261, Subpart C. Potential problems can be avoided by the proposed calorimeter test that assesses reactivity of specific APW loads or sources prior to Subtitle D disposal. The reactivity is assessed via the maximum temperature generated by an APW reaction. The maximum recommended temperature for Subtitle D landfills is 65°C (~150°F) to permit waste decomposition and prevent elevated temperatures from impacting engineered components (composite liner system, gas vents, and leachate collection system).

Calorimeter experiments at varying NaOH strengths show temperatures rise to 100°C. The optimal concentration of NaOH was determined to be 1 M to 2 M NaOH, which provides sufficient alkalinity to react the metallic aluminum and fulfill the objectives of a rapid procedure to evaluate APW reactivity in an alkaline environment. It is possible that this higher NaOH strength compared to water and APW monofill leachates is because the tested APW samples consisted of low metallic aluminum content. XRD analyses or hydrogen gas production can complement the reactivity tests by corroborating the amount of Al present and similar temperature increase and reaction rates.

The progression of APW reactions in landfills is dependent on the presence of moisture via leachate recirculation, precipitation, groundwater, waste processing, and other sources. The alkaline APW, especially baghouse dusts, and moisture react with the nitrides, carbides, and salts to further increase the pH. After temperatures and pH begin to increase above background levels, the protective oxide layer is corroded and metallic aluminum reacts to produce heat and hydrogen gas. In the reactivity test, the insulated constant pressure calorimeter serves to simulate the center of the landfill where heat loss is minimal. The bench-scale test using a constant pressure calorimeter is presented to help APW generators and Subtitle D landfill operators decide whether

a certain shipment of APW will cause an adverse reaction and temperatures in the landfill and whether the APW should be classified as hazardous using the reactivity criterion.

3.9 Tables and Figures

Table 3.1 Effect of liquid on reactivity of salt cake samples (data from Huang et al. 2014)

	Temperature Increase, ΔT (°C) from Initial Control Temperature of 37°C		
	sample 1	sample 2	sample 3
0.1 M NaOH (pH~13)	55.9	20.1	53.8
De-ionized Water (pH~6.8)	49.8	19.1	43.0
MSW leachate (pH not reported)	12.4	9.2	12.6

Table 3.2 Site 1 Ohio APW total element content

Parameter	Milled Black Dross (mg/kg)	Salt Cake (mg/kg)	Baghouse Dust (mg/kg)
Aluminum	114,000	142,000	35,300
Magnesium	57,800	26,700	10,600
Iron	2,030	1,710	1,970
Manganese	533	186	199
Chloride	230,000	140,000	250,000
Potassium	122,000	70,900	71,300
Sodium	97,400	86,700	66,000
Calcium	7,980	7,820	206,000
Fluoride	950	640	150

Table 3.3 Composition of gas generated from Indiana landfill in laboratory tests using U.S. DOT Dangerous When Wet Test (data from RMT, Inc. 2007)

Gas	Composition (% v/v)
Hydrogen	95+
Methane	1 to 5
Hydrogen Sulfide	<0.2
Acetylene	<0.2
Phospine	<0.2
Arsine	<0.2%
Methane Thiol	<0.2%
Allene	Below detection limit*
Ammonia	Below detection limit*

*detection limit not specified in report

Table 3.4 Calibration results for constant pressure calorimeter

Test	NaOH (mole)	H_2O (mL)	ΔT (°C)	q_{rxn} (kJ)	$-\Delta H$ (kJ/mole)	Error (%)
1	0.191	150.19	12.6	8.32	43.51	2.1
2	0.379	150.32	22.8	15.79	41.65	6.3
3	0.376	150.31	22.4	15.50	41.19	7.3
4	0.209	150.08	13.2	8.75	41.96	5.6
5	0.207	151.27	13.6	9.08	43.86	1.3
6	0.308	187.45	15.6	13.04	42.40	4.6
7	0.217	149.24	13.4	8.85	40.80	8.2

Table 3.5 Summary of APW mineral phases

Mineral Phase (% wt)	Site 1		Site 2	
	Milled Black Dross	Baghouse Dust	Black Dross	Milled Salt Cake
Al	3.8	1.1	3.1	0.5
Al_2O_3	4.8	8.5	8.3	8.6
KCl	9.3	23.1	18.2	14.3
NaCl	38.2	32.4	42.3	33.8
$MgAl_2O_4$	6.7	30.9	16.1	34.4
Al_2CO	3.5	3.7	6	5
C	4.3	0.3	----	----
$KMgCl_3(H_2O)_6$	29.4	----	----	----
MgO	----	----	5.3	1.2
SiO_2	----	----	0.7	0.2
Pb	----	----	----	2
Total	100	100	100	100

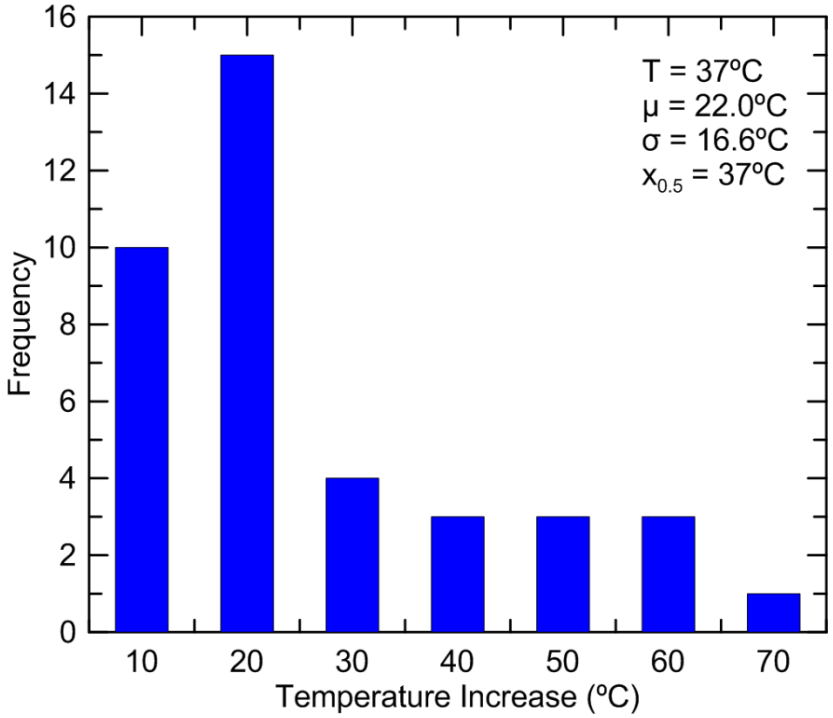

(a) T_c = 37°C

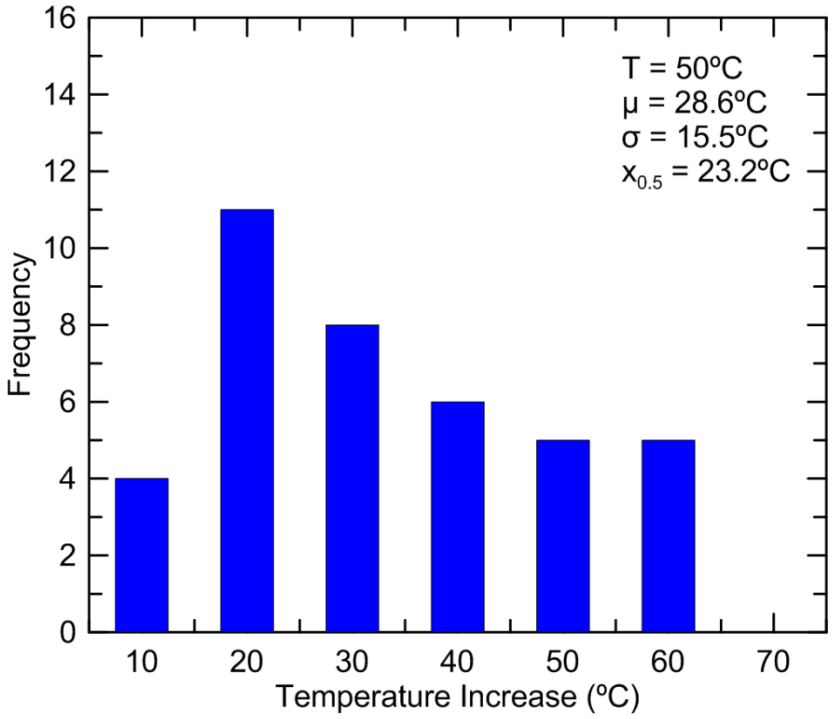

(b) T_c = 50°C

Figure 3.1 Heat generation potential and statistical parameters (μ = mean, σ = standard deviation, $x_{0.5}$ = median) for salt cake samples at two control temperatures: (a) 37°C and (b) 50°C

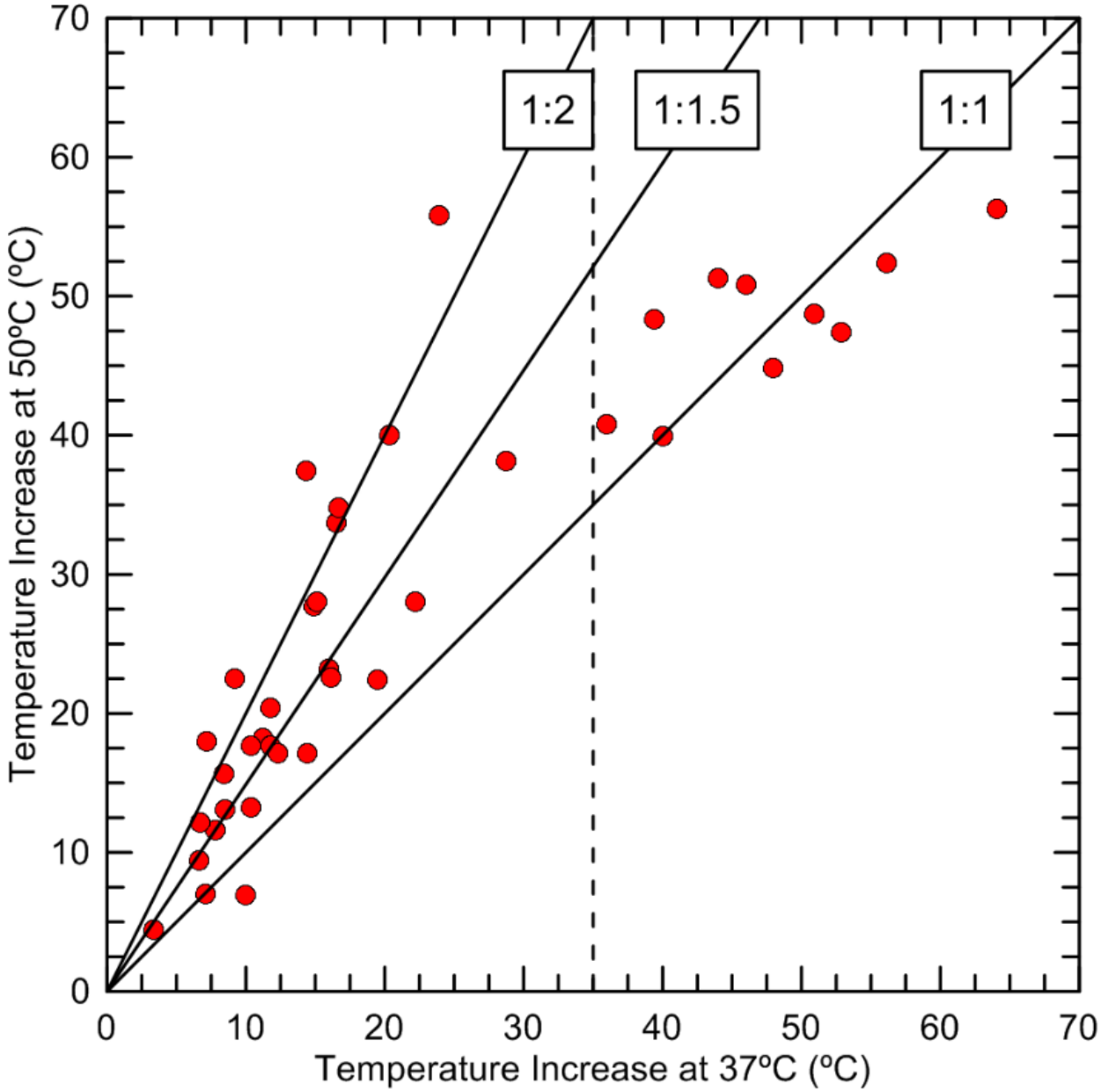

Figure 3.2 Comparison of temperature increase (ΔT) for control temperatures of 37°C and 50°C with trend lines of 1:1, 1:1.5, and 1:2 (1:1; ΔT at 37°C = ΔT at 50°C)

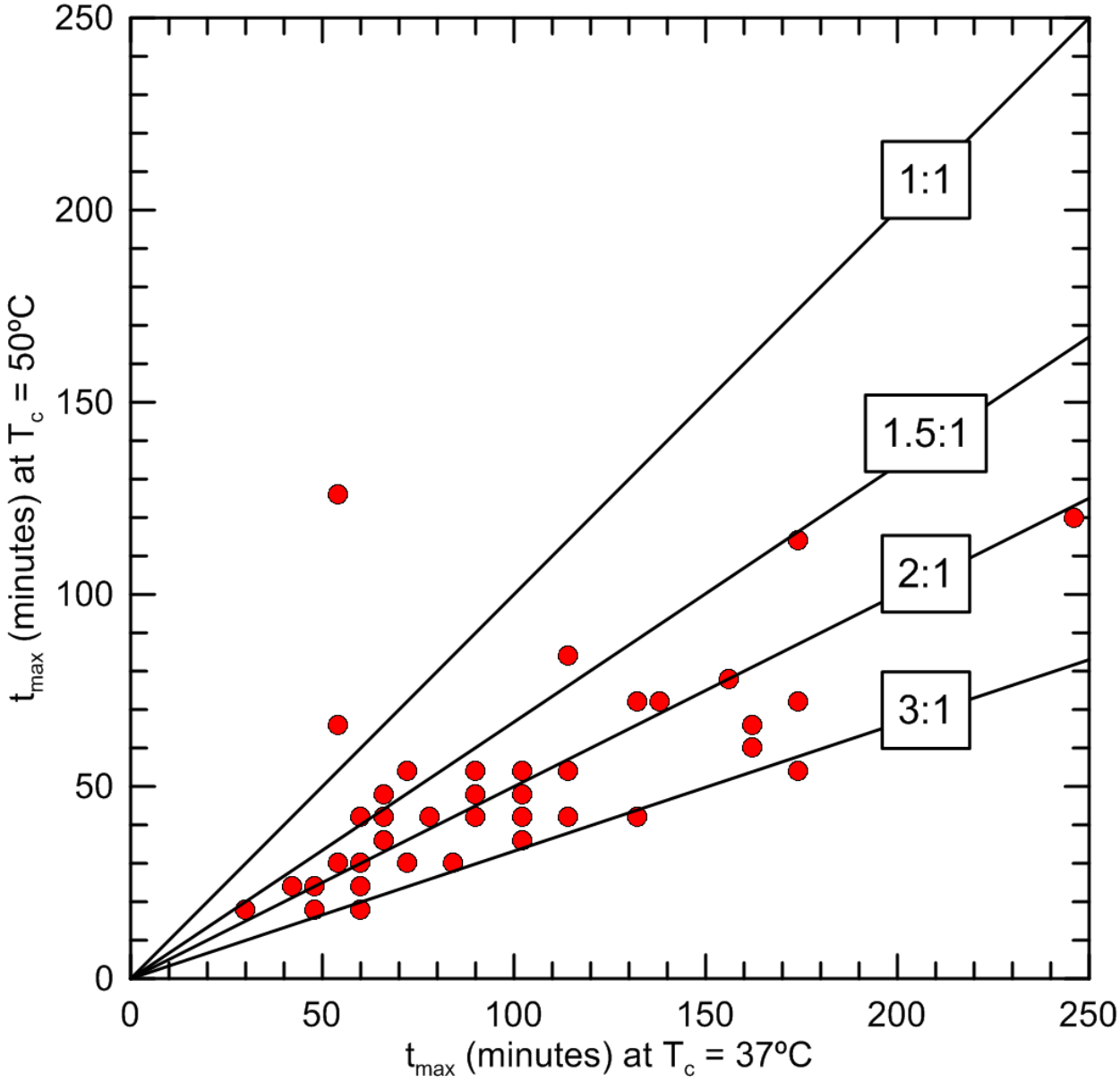

Figure 3.3 Comparison of time to maximum temperature (t_{max}) for control temperatures of 37°C and 50°C with trend lines of 1:1, 1.5:1, 2:1, and 3:1 (1:1; t_{max} at 37°C = t_{max} at 50°C)

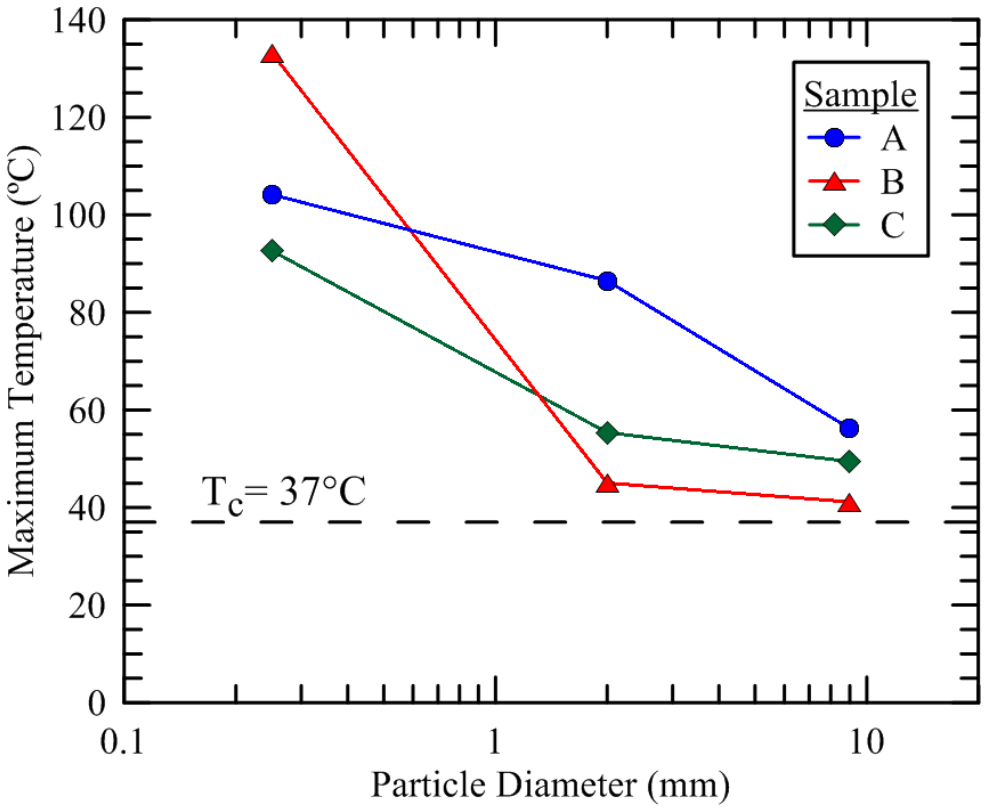

Figure 3.4 Decreasing particle size increases maximum temperatures observed

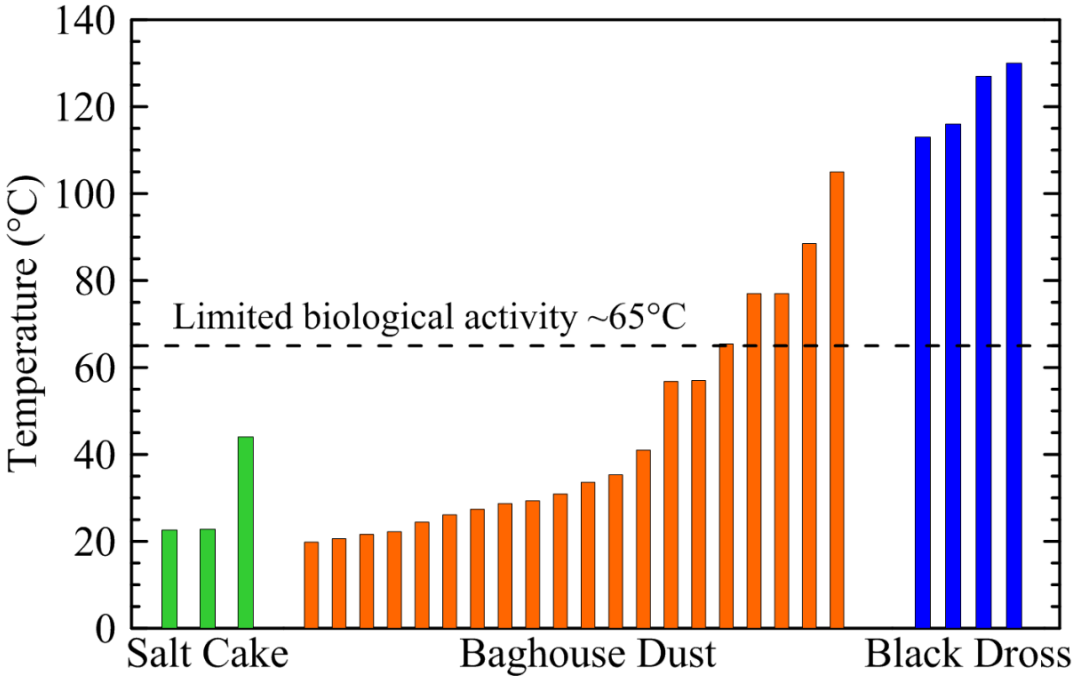

Figure 3.5 Temperature results from Indiana Landfill APW (data from RMT, Inc. 2007)

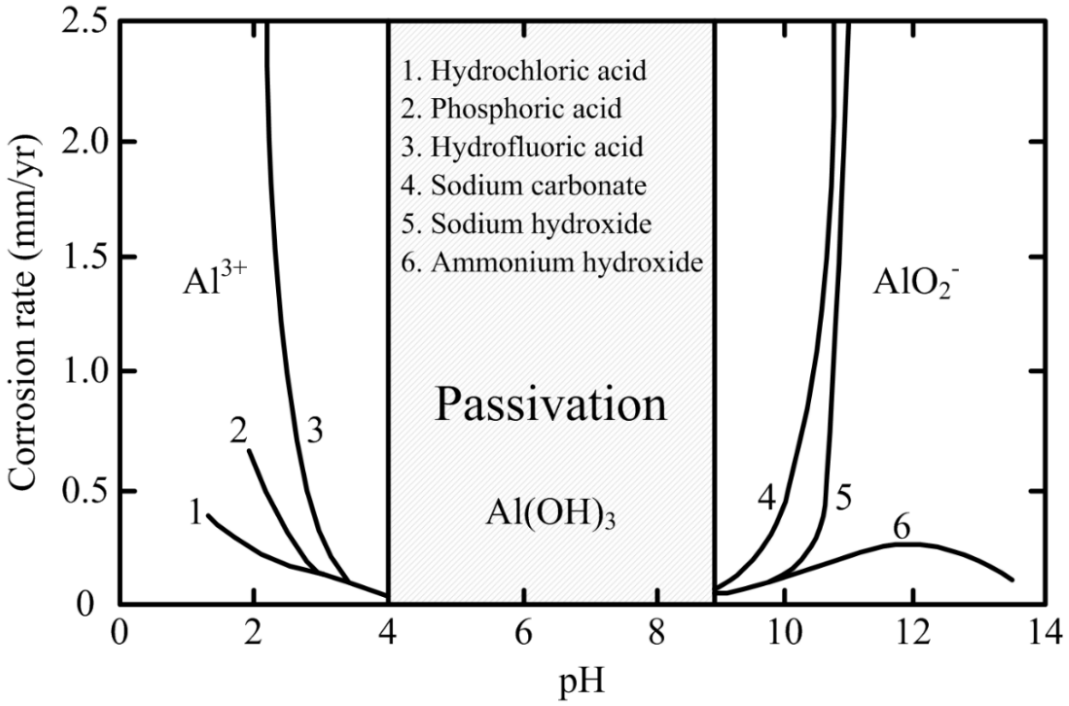

Figure 3.6 Effect of pH on corrosion of aluminum alloy 1100-H14 by various chemical solutions (data from Hollingworth and Hunsicker 1990)

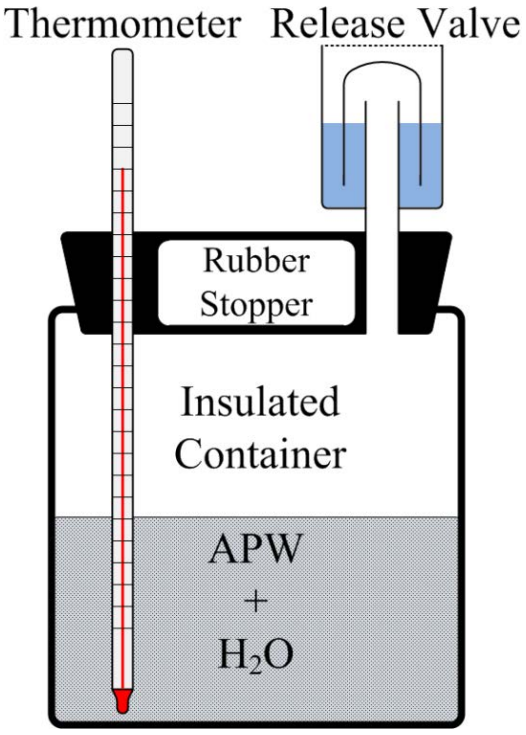

Figure 3.7 Schematic of constant pressure calorimeter for APW classification



(a) Site 1 MBD



(b) Site 1 BHD



(c) Site BD



(d) Site MSC

Figure 3.8 Samples of APW tested (a) Site 1 Milled Black Dross, (b) Site 1 Baghouse Dust, (c) Site 2 Black Dross, and (d) Site 2 Milled Salt Cake

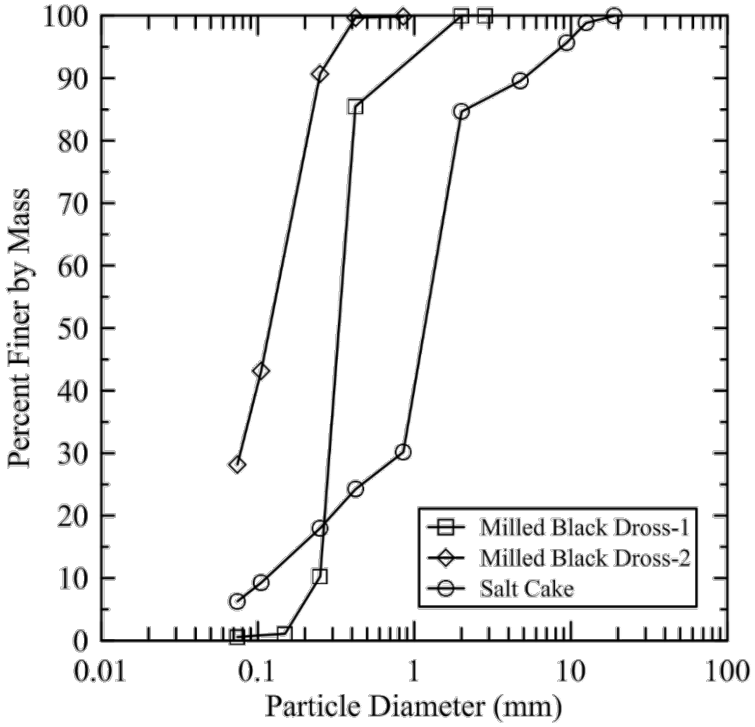

(a) Site 1

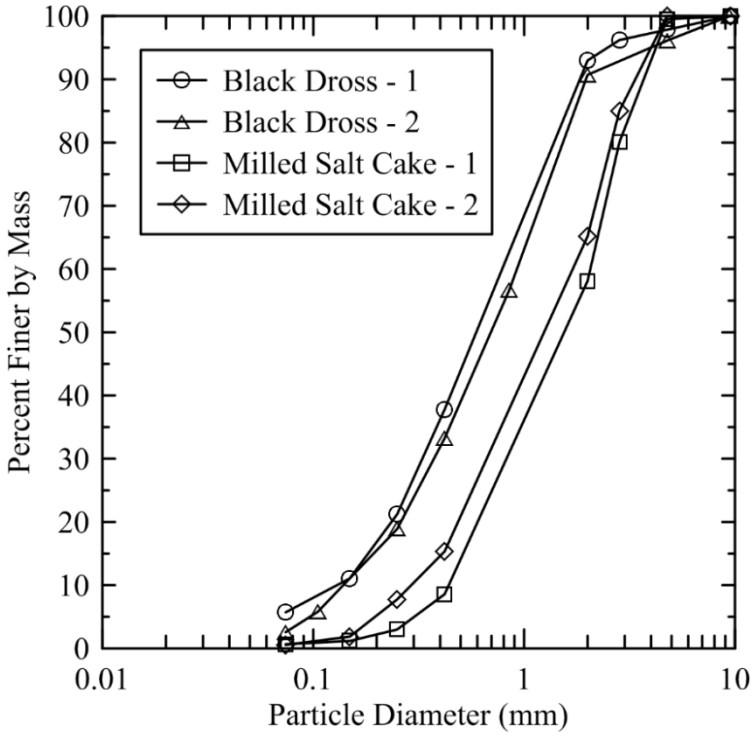

(b) Site 2

Figure 3.9 Particle size gradation: (a) Site 1 and (b) Site 2

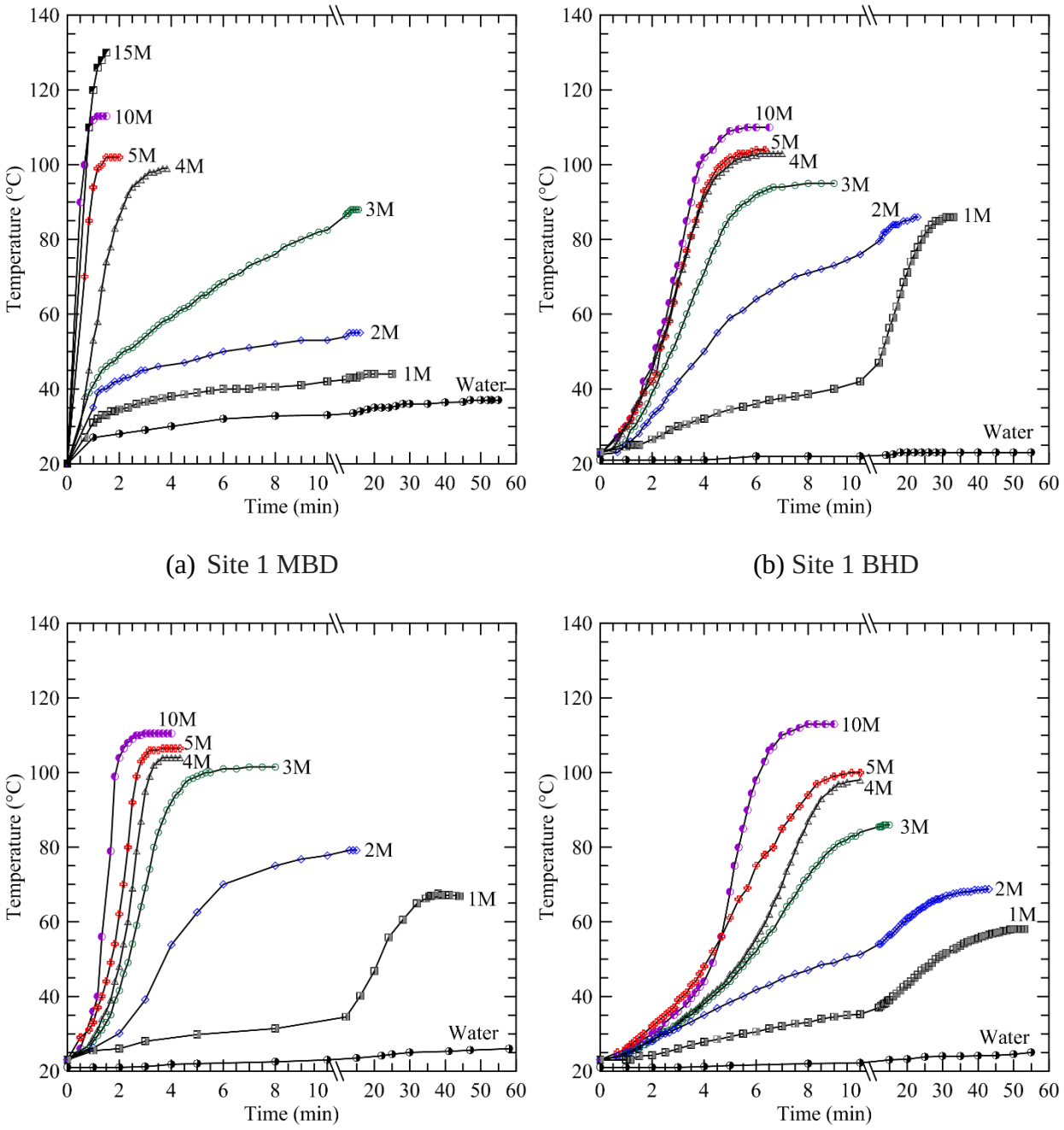

Figure 3.10 Effect of NaOH strength on temperature response for (a) Site 1 Milled Black Dross-1, (b) Site 1 Baghouse Dust, (c) Site 2 Black Dross, and (d) Site 2 Milled Salt Cake

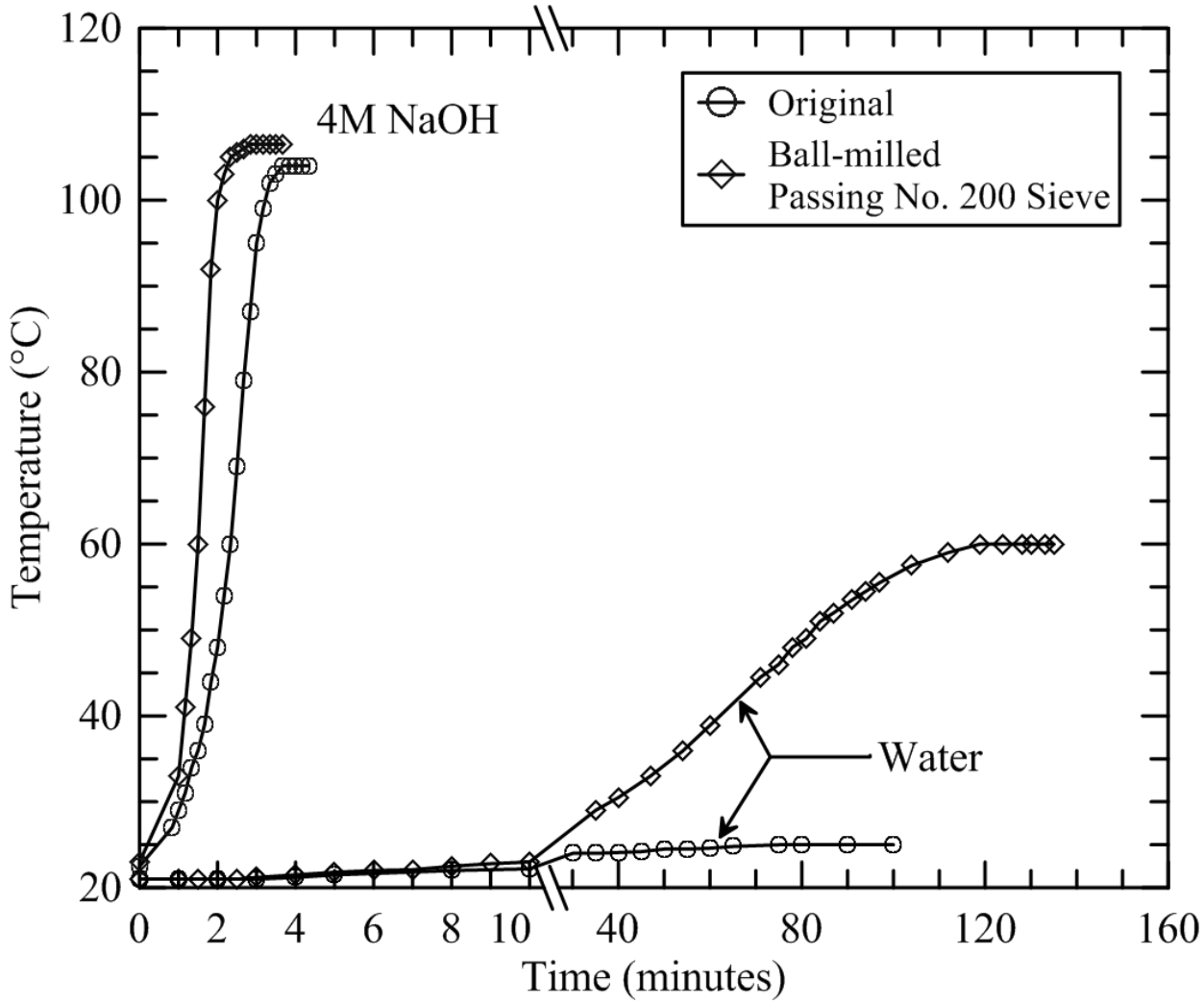

Figure 3.11 Effect of ball-milling on Site 2 Black Dross reacted with 4 M NaOH and water (milled particle diameter < 0.074 mm)

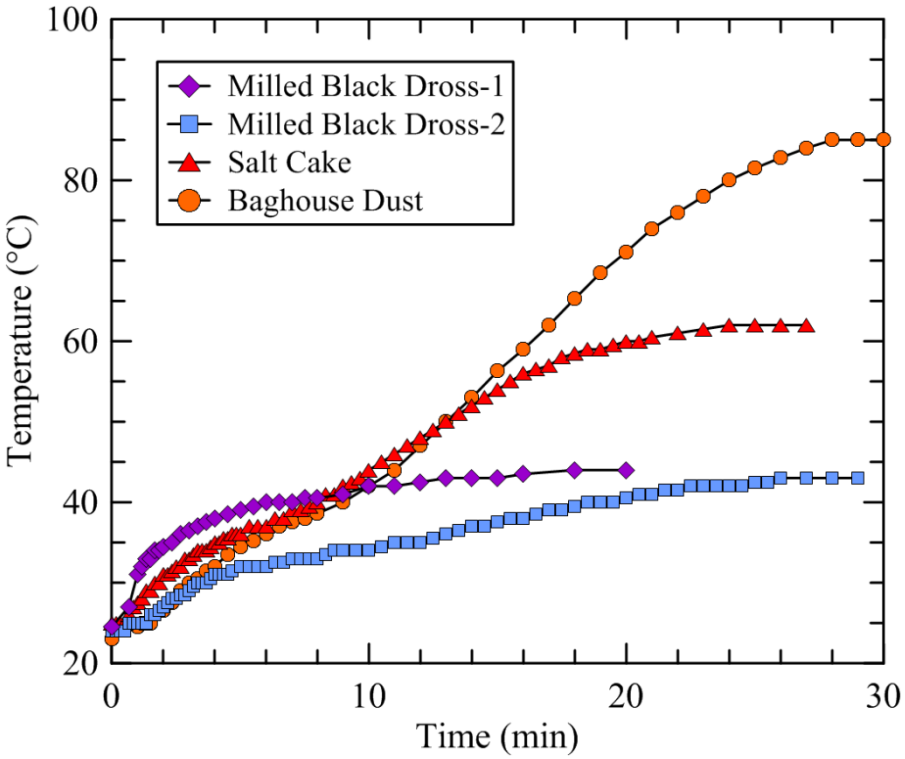

(a) 1 M NaOH

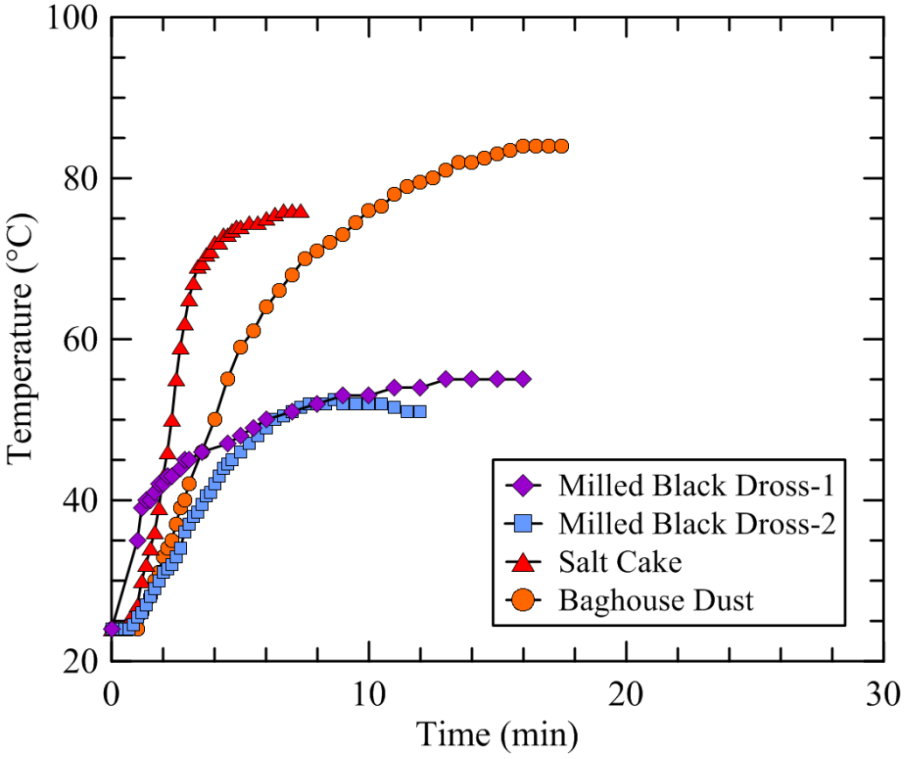

(b) 2 M NaOH

Figure 3.12 Site 1 APW calorimeter experiments: (a) 1M NaOH and (b) 2M NaOH

CHAPTER 4

APW GAS PRODUCTION AND COMPOSITION

4.1 Introduction

Characterizing gas production and composition from aluminum production waste (APW) is important to evaluate waste reactivity, evaluate pretreatment processes prior to disposal, and estimate landfill gas emissions. For example, the volume of gas generated from APW provides an indication of metallic aluminum content and possible recovery potential or use as renewable energy by capturing the hydrogen gas. In addition, ammonia odors emanating from a monofill in Tennessee is creating a public nuisance by impacting landfill personnel, the environment, and public health. The purpose of this chapter is to characterize gas production and composition from APW with emphasis on ammonia and hydrogen gases. To accomplish this objective, a laboratory bench-scale experiment was devised to assess gas generation rates and concentrations in terms of APW composition and reacting solution.

4.2 Gas Production Background

APW contains variable amounts of metallic aluminum (Al), salt flux, and non-metallic oxides. The important aluminum and non-metallic compounds that produce gases include metallic aluminum, aluminum nitride (AlN), aluminum carbide (Al_4C_3), aluminum phosphide (AlP), and aluminum sulfide (Al_2S_3). Aluminum nitride and carbide are formed from the rapid chemical reaction of nitrogen and carbon dioxide gases, respectively, after the dross is skimmed but before the molten aluminum cools (Peterson 2011). Aluminum carbides also can be produced from oils and organic contaminants of aluminum scraps during the melting process (Shinzato 1999). Doutre (2010) reports the reaction of metallic aluminum and magnesium with bone ash [$Ca_3(PO_4)_2$, which is widely used within casthouses to seal gaps and fill holes in metal transfer launders] produces AlP, calcium, and spinel ($MgAl_2O_4$). The presence of sulfur in the furnace atmosphere is a consequence of the combustion of impurities in the scrap leads to the formation of Al_2S_3.

Upon contact with water, APW is hydrolyzed to produce heat and malodorous and flammable gas (Narayanan and Sahai 1997; Totten and MacKenzie 2003). Metallic Al in basic or

acidic solutions can oxidize rapidly to produce heat and hydrogen gas (Reaction 4.1). A basic solution can be present near APW due to the reaction of AlN with water to produce ammonia (Reaction 4.2). The ammonia released from the reaction can dissolve in water to form basic ammonium hydroxide (NH_4OH). Another form of alkalinity is the hydrolysis of calcium oxide (CaO) in the baghouse dust. This can raise the pH of APW and lead to dissolution of the protective aluminum oxide layer. As indicated by Reaction (4.3), Al_4C_3 reacts with water to liberate methane (CH_4). AlP reacts with moisture in Reaction (4.4) to produce phosphine, which has a distinct garlic-like odor. Phosphine is also a pyrophoric substance and has been observed to ignite spontaneously upon contact with air and cause landfill fires (Doutre 2010). The reaction of Al_2S_3 in Reaction (4.5) leads to the formation of hydrogen sulfide (H_2S). In addition, the reported free energy of formation (ΔG) suggests that these reactions are spontaneous at standard temperature and pressure.

$$2\,Al + 6\,H_2O \rightarrow 2\,Al(OH)_3 + 3\,H_2\,(g) \quad \Delta H = -415\,kJ/mol,\ \Delta G = -426\,kJ/mol \tag{4.1}$$

$$AlN + 3\,H_2O \rightarrow Al(OH)_3 + NH_3\,(g) \quad \Delta H = -147\,kJ/mol,\ \Delta G = -206\,kJ/mol \tag{4.2}$$

$$Al_4C_3 + 12\,H_2O \rightarrow 4\,Al(OH)_3 + 3\,CH_4\,(g) \quad \Delta H = -1,695\,kJ/mol,\ \Delta G = -1,665\,kJ/mol \tag{4.3}$$

$$AlP + 3\,H_2O \rightarrow Al(OH)_3 + PH_3\,(g) \quad \Delta H = -248\,kJ/mol,\ \Delta G = -265\,kJ/mol \tag{4.4}$$

$$Al_2S_3 + 6\,H_2O \rightarrow 2\,Al(OH)_3 + 3\,H_2S\,(g) \quad \Delta H = -177\,kJ/mol,\ \Delta G = -255\,kJ/mol \tag{4.5}$$

Laboratory studies of APW gas production have been used to characterize composition and reactivity (Huang et al. 2014; Graczyk et al. 1997; Manfredi et al. 1997), measure the efficacy of treatment and/or recycling processes (Liu and Chou 2013; Huang et al. 2014; Schaefer et al. 2008; David and Kopac 2012), develop a landfill gas control system (RSGA 2011), and evaluate health and safety conditions (Hwang et al. 2006; Lorber and Antrekowitsch 2009). The gas evolution values reported in Table 4.1 indicate that APW is capable of producing 0.25 to 568.5 mL of gas/g APW. The variability in gas volume is attributed to properties of the APW and testing conditions reported in Table 4.1. For example, the maximum gas production reported in David and Kopac (2012) represents aluminum dross ball-milled into fine particles, which acts to disrupt the protective oxide layer and thus permits aluminum hydrolysis in water. In another case, Graczyk et al. (1997) used a strong acidic solution to ensure complete reaction of metallic aluminum for

various salt cake samples. Considering the results of Graczyk et al. (1997) and David and Kopac (2012) as upper bound estimates (e.g., up to 248.3 mL/g APW), the range of gas production from APW and water reaction (see Table 4.1) is 0.15 to 3.4 mL/g APW. Analyses based on theoretical material balance (Narayanan and Sahai 1997; Beckmann 1991; Unger and Beckmann 1992) imply that maximum gas production is 10 to 12 mL/g APW. Xiao et al. (2005) estimates that 9.5-10.5 mL CH_4/g APW, 1.5-13.5 mL NH_3/g APW, and 0.1 mL PH_3/g APW can be produced. In summary, relevant literature shows that complete APW reaction does not occur, but it is still reactive and generate significant amounts of toxic and flammable gases.

Hydrogen was reported as the dominant gas by Hwang et al. (2006), Graczyk et al. (1997), and David and Kopac (2012). Liu and Chou (2013) measured methane and ammonia production of 0.20 mL/g APW and 1.08 mL/g APW, respectively, while the formation of hydrogen and phosphine was not detected. Graczyk et al. (1997) also reported methane production of 2.5 mL/g APW. Depending on APW composition and experimental conditions, Table 4.1 shows that hydrogen, methane, and ammonia are the predominant gases that can be generated from APW. As a result, the laboratory experiments designed and conducted herein are focused on characterizing the concentrations of hydrogen, methane, and ammonia.

4.3 Material and Test Methods

4.3.1 APW Physical and Chemical Properties

The APW samples originate from the two Subtitle D facilities (referred herein as Site 1 and Site 2) described in Chapter 3. The APW samples from Site 1 (Figure 4.1) include two milled black dross collected in 2011 and 2013 (MBD-1 and MBD-2), baghouse dust (BHD), and salt cake (SC). The samples from Site 2 (Figure 4.2) are black dross (BD) and milled salt cake (MSC). MBD is the residue after black dross is mechanically milled and screened for metallic aluminum, resulting in a predominant particle size of < 0.5 mm. BD is skimmed from rotary furnaces and is similar to a well-graded fine sand (D_{50} = 0.3 mm). The MSC originates from mechanical grinding and crushing of salt cake blocks and sieving to recover metallic aluminum captured within the salt flux. The SC sample consists of pieces greater than 10 cm and a finer fraction of < 0.5 mm. The pH of

each sample was evaluated using ASTM 4972 (ASTM 2007). The baghouse dust pH is about 10.4 while the other dross and salt cake pH ranges from 8 to 9.

The mineral phase of each APW was characterized using XRD by Heritage Environmental Services. The XRD patterns are collected on a Rigaku MiniFlex II Diffractometer from 5 to 110 degrees 2θ using Cu Kα radiation and scintillation counter with in-line monochromator. The phase identification of samples was performed using Materials Data, Incorporated (MDI) software suite Jade 9 and the International Center for Diffraction Data PDF4+ database for reference patterns. After identification, semi-quantitative analysis is conducted on each sample using Jade 9 whole pattern fitting methods. The dominant minerals in the APW samples are summarized in Table 4.2 and comprise metallic Al, corundum (Al_2O_3), sylvite (KCl), halite (NaCl), and spinel ($MgAl_2O_4$). Some of the samples also contained quartz (SiO_2) and periclase (MgO). XRD analyses summarized in Table 4.2 also identified aluminum oxycarbide (Al_2CO), which is produced from of alumina and carbon. The XRD analyses also did not detect AlN and Al_4C_3 even though ammonia and methane were observed in the laboratory tests. As a result, the Table 4.2 provides only a general overview of APW composition.

4.3.2 Experimental Design

Figure 4.3 shows a schematic of the gas experiment equipment, which consists of: filter flask reactor, gas collection tank, mass balance, and gas sampling port. A 5 g sample of APW is placed inside the 200 mL filter flask reactor in Figure 4.3. The reaction is initiated by introducing 25 mL of NaOH (NaOH >99.5% purity, supplied by Aldrich). After introducing the basic solution, the flask is swirled and immediately corked with a rubber stopper. The gas volume is measured by the water displacement method and corrected to a gas volume at standard temperature and pressure (STP) of 20°C and 1 atm. The total gas generated is reported in units of standard mL per gram of APW (mL/g APW). The Nalgene™ 180 polyvinyl chloride tubing (Thermo Scientific™) is connected to the reactor directs the gas into the collection tank. Because ammonia is soluble in water, the liquid inside the collection tank is 1 M NaOH. A correction factor is included to account for the density of 1 M NaOH (~1.04 g/mL) solution in the collection tank. The gas displaces 1 M NaOH solution inside the collection tank into a holding container (also 1 M NaOH) that rests on a mass balance. The changing liquid mass in the holding tank is measured as a function of time. The

mass change with time provides an indication of the rate of gas generation from the reaction, and the difference between the initial and final mass balance readings determine the total gas yield. After the reaction proceeds to completion, the gases are allowed to equilibrate to STP. Figure 4.4 shows the cumulative gas generation for Site 1 MBD-2 and Site 2 BD reacted with 5 M NaOH. Both APW samples are homogenous, and they show the same cumulative gas volume with time trends in Figure 4.4. As a result, they indicate that the laboratory procedure is reproducible.

After pressure and temperature in the reactor flask comes to equilibrium, a portable low flow pump (SKC 222 Series) is used to extract gas from the collection tank into a 1 L multi-layer gas sampling bag (manufactured by Restek). The hydrogen and methane concentrations were evaluated per ASTM D1946 (2011) using a Hewlett Packard 5890 Series II GC-TCD (gas chromatograph – thermal conductivity detector), equipped with a Carboxen® 1010 capillary porous layer open tubular column (length 30 m, i.d. 0.32 mm) and molecular sieve. This column is ideal for separation of all major components in permanent gas (helium, hydrogen, oxygen, nitrogen, carbon monoxide, methane, and carbon dioxide). To measure hydrogen gas, samples (50 µL) were injected directly into the column, where ultra-high purity hydrogen (supplied by S.J. Smith) with a 5 point calibration from 10% v/v to 50% v/v was used as the standard. The temperatures of the injector, TCD, and oven were 200, 200, and 35°C, respectively. The TCD and oven carrier gas was nitrogen. For methane concentrations, samples (100 µL) were injected directly onto the column and the calibration standard used ultra-high purity methane (supplied by Matheson) with a 4 point calibration from 1% v/v to 10% v/v. The temperatures of the injector and TCD were both 200°C. The oven temperature was held at 35°C for 7 minutes before increasing to 150°C (24°C/min), where it remained for two additional minutes. The TCD and oven carrier gas was helium. The hydrogen and methane concentrations are reported within ±0.3% and ±0.08% v/v, respectively.

After a sample was obtained in the multi-layer gas sampling bag, a hand-held Dräger accuro pump and Dräger tube were inserted into the reactor filter flask to measure ammonia concentrations. When ammonia permeates the Dräger tube after one stroke, a pH indicator causes the tube color to change from yellow to violet. The length of discoloration is correlated to an ammonia concentration. The Dräger tube measuring range was 0.5 to 10% v/v NH_3, with a standard deviation of ±10 to 15%. The measuring range can be reduced by an order of magnitude (0.05 to 1% v/v) by squeezing 10 strokes of the accuro pump and diving the reading by 10.

The multi-layer gas sampling bag contains a mixture of air and APW gases (hydrogen, methane, and ammonia). Thus, the hydrogen and methane concentrations are reported based on the entire sample bag composition, e.g., 45% v/v H_2 ad 1.4% v/v CH_4, where the remaining mixture is assumed oxygen and nitrogen. To calibrate the test procedure, 25 mL of 5 M NaOH was reacted with aluminum foil (>97.9% purity, Reynolds Wrap). The volume of gas was compared to the theoretical yield from the aluminum content in the aluminum foil. Table 4.3 presents six calibration tests with various aluminum foil masses. For example, 0.09 g aluminum foil in Test 1 yielded 120.3 mL. Correcting for the temperature and metallic aluminum content in the foil, the experimental and theoretical yields were compared, resulting in a percent error of 1.6%. The average error for the six calibration tests is 3.1%. Uncertainty in the testing procedure may be attributed to measurement of aluminum foil mass to two significant digits and spatial variability of aluminum foil properties between sheets. Based on Figure 4.4 and Table 4.3, the experimental method is reproducible and produces stoichiometric quantities of hydrogen gas. Table 4.4 lists the 29 experiments performed to investigate the total gas generation, gas composition, and effect of NaOH concentration and are discussed herein.

4.4 Results and Discussion

4.4.1 APW Gas Composition

Table 4.5 summarizes the gas composition for the APW from Sites 1 and 2. The experiments were performed at 5 M NaOH except for Site 1 MBD-1, which used 2 M NaOH. Table 4.5 indicates that Site 1 MBD-1 and SC-1 produced the most gas (>190 mL/g APW). In general, the ammonia concentrations for both sites range from 2,600 to 6,200 ppmv. For both sites, the highest concentrations were observed in salt cake samples (SC-1 and MSC-1), while lower concentrations were found in the milled black dross (MBD-1 and MBD-2). These ammonia concentrations are conservative estimates because a strong alkaline solution drives the AlN reaction to completion and a small headspace limits dilution. Regardless, these APW emissions can pose a health hazard in a confined space. For example, AIHA (1971) reports that 5,000 to 10,000 ppm are reported to be fatal (Mulder and Van der Zahm 1967) and exposure for 30 minutes to 2,500 to 6,000 ppmv is considered dangerous to life (Smyth 1956). The hydrogen and methane concentrations provided

in Table 4.5 represent the concentration within the multi-layer sampling bag, which consists of air and APW gases. The methane levels range from 1 to 2% v/v, which suggests that a limited amount of Al_4C_3 or another carbon mineral is reacting to form methane. In addition, the methane levels are near the lower bound of the calibration standard, indicating a lower calibration concentration may be more appropriate. The hydrogen concentrations were found to correlate with the total gas generated. In particular, Figure 4.5 shows that a linear trend exists, i.e., increasing gas generation results in higher hydrogen levels. This trend corroborates that hydrogen is the dominant gas generated from APW with reaction with NaOH. In addition, the strong correlation in Figure 4.5 (R^2= 0.975) is comprised of several types of APW that originate from different secondary aluminum plants. As a result, it may serve as an empirical formula to determine the hydrogen content under similar laboratory conditions, which is beneficial for estimating possible landfill emissions and possible energy recovery.

4.4.2 Effect of NaOH Concentration

Figure 4.6 shows the total gas generated from each APW sample as a function of NaOH strength. In general, the total gas generation increases with increasing NaOH strength. For example, Figure 4.6(a) shows that SC-1 and MBD-1 increase from ~145 mL/g APW to maximum volumes >200 mL/g APW for 5 M and 10 M NaOH solutions. MBD-2 shows the same response with increasing NaOH molarity, but the maximum gas evolved is ~85 mL/g APW. Site 1 BHD-1 produced the least volume of gas because it consists of fine dust particles from the grinding and milling of salt cake and other secondary aluminum production processes. For Site 2 samples, Figure 4.6(b) shows that BD generates about ~85 mL/g APW while the MSC yields a lower value of ~45 mL/g APW. In comparison to Table 4.1, the total gas production summarized in Table 4.4 agrees with the conservative values reported in Graczyk et al. (1997) and David and Kopac (2012).

Duplicate measurements on several APW samples showed minor variability, e.g., Site 1 MBD-2 at 1 M and 5 M NaOH as well as Site 2 BD at 5 M NaOH (see error bars in Figure 4.6). In these instances, the variability was less than 6% of the measured value. However, Site 1 SC-1 and Site 2 MSC show greater variability, up to about 20% of the measured value. This variability could be attributed to non-uniformity in the metallic aluminum content between the test samples and broad APW particle size gradation. Visual observation of Site 1 SC-1 (Figure 4.1(d)) and Site

2 MSC (Figure 4.2(b)) indicates a higher percentage of coarser particles, including grain sizes as large as medium sand. Because a small sample mass (5 g) is necessary to accommodate the capacity of the gas collection tank in Figure 4.3, the APW samples with homogenous particles size shows less variability than the coarser Site 1 SC-1 and MSC samples.

Based on the XRD results in Table 4.2, it is evident that APW samples with higher metallic aluminum mineral phase produce higher gas yields. For example, the Site 1 MBD-1 and SC-1 contain higher concentrations of metallic Al compared to MBD-2 and BHD. The same trend follows for Site 2. Figure 4.7 shows the linear relationship (R^2=0.44) between XRD metallic aluminum and total gas generation. Five gas generation tests are shown for the Site 1 C sample in Figure 4.7. They are all plotted on one metallic Al content because only one XRD analysis was performed for each APW sample. This behavior is also depicted in Site 1 MBD-1 and Site 2 MSC, where gas generation variability is more pronounced.

Although the trend is not strong, XRD results provide a qualitative estimate of potential of gas generation between APW samples from the same site. By conservatively assuming the total gas generated is hydrogen and stoichiometric conditions are present, the aluminum content (% wt) was estimated using Equation (4.6):

$$\mathrm{Al}(\%) = \mathrm{H_2}\,(\mathrm{L}) \times \frac{\mathrm{P_{atm}}}{\mathrm{R}\cdot\mathrm{T}} \times \frac{2\,\mathrm{mol\,Al}}{3\,\mathrm{mol\,H_2}} \times \frac{\mathrm{MM_{Al}}}{\mathrm{mol}} \times \frac{1}{\mathrm{M_{initial}}\,(\mathrm{g})} \tag{4.6}$$

where R is the ideal gas constant 0.082057 (L·atm/K·mol), P_{atm} is atmospheric pressure (atm), T is 293°K or 20°C (68°F), *2 mol Al/ 3 mol* H_2 is the molar ratio of Al and H_2 reaction coefficients shown in Reaction (4.1), MM_{Al} is the molar mass of aluminum (27 g/mol), and $M_{initial}$ is initial mass of APW sample (5 g). Figure 4.8 shows the comparison of metallic aluminum determined by the laboratory gas experiments (abscissa) and XRD metallic aluminum (ordinate). Similar to Figure 4.7, the measured aluminum contents are based on multiple gas generation tests that are reported for a single XRD value. Although the laboratory measured aluminum contents are lower than the XRD predictions for all samples except Site 1 SC-1, they are within 20% of the XRD estimates. The exceptions (Site 1 SC-1 and Site 2 BD) to the solid trend line (Measured aluminum = XRD) in Figure 4.8 are likely caused by sample preparation issues in XRD analyses or variation in the APW. XRD requires the sample

to be ball-milled so samples such as Site 2 BD, which contain larger particles (see grain sizes in Figure 4.2(a)), may liberate entrapped metallic aluminum in conglomerated salt granules (Jafari et al. 2014) and yield a higher aluminum content. As a result, XRD results indicate that Site 2 BD contains a relatively high metallic aluminum content but conglomerated salt and aluminum particles reduce the ability for gas production in the laboratory gas experiments.

4.4.3 Gas Generation Rates

Figure 4.9 through Figure 4.14 show the cumulative total gas volume and generation rate for the APW samples from Sites 1 and 2. As the NaOH molarity increases, the reaction rates increase and the time to reach the maximum evolved gas decreases. In all experiments, the reaction started in a few seconds and typically continued until the cumulative volume approached a horizontal asymptote. Limited temperature increase was observed in the gas generation tests because only 5 g of APW was reacted with 25 mL of 1 to 10 M NaOH solution.

Chapter 3 calorimeter experiments provide insight into the comparison of temperature response and gas generation. For NaOH concentrations greater than 3 M, calorimeter temperatures increased rapidly and reached a maximum value within 10 to 20 minutes. In comparison, the gas generation tests require significantly longer period to reach equilibrium, e.g., over 1,000 minutes. However, the highest gas evolution rates occur before an elapsed time of 30 minutes, and they precipitously decline to rates < 0.5 mL/g APW/min by an elapsed time of 60 minutes. The gas rate trends indicate the majority of gas production occurs during this period. As a result, there is a temporal connection between the calorimeter and gas generation experiments. One possible reason for the discrepancy in reaction time is that 50 g APW was reacted with 25 mL NaOH solution for the calorimeter tests while the gas generation tests use only 5 g APW in 25 mL NaOH solution. In essence, more APW is available to react with the NaOH solution so the reaction rate occurs at a faster rate.

In general, cumulative gas volume approaches a horizontal asymptote, i.e., constant volume, after 100 minutes and continues to gradually increase until about 1,000 minutes. However, Site 1 MBD-2 in Figure 4.10 exhibits a two stage increase in gas volume. The gas volume appears to level off at an elapsed time of 60 minutes. Then, it begins to increase at a time of 200 minutes before reaching the maximum gas volume at ~750 minutes. The first stage generates about ~ 30

mL/g APW while the second stage yields an additional 45 mL/g APW. This behavior was observed for all NaOH concentrations except for 1 M NaOH, which suggests the second stage is influenced by pH, i.e., the amount of hydroxide ions available.

Figure 4.15 provides a gas generation with time comparison for all APW samples with a 5 M NaOH solution. Figure 4.15(a) shows that Site 1 MBD-1 is significantly more reactive than MBD-2 and BHD-1. Site 1 SC shows similar reactivity to MBD-1, but the two different SC samples (SC-1 and SC-2) suggest the sample selected affects the gas generation potential. In Figure 4.15(b), Site 2 BD reacts faster than both of the MSC samples. However, Site 2 samples are less reactive compared to Site 1 SC and MBD-1.

4.5 Summary of Gas Production Test Results

This chapter describes laboratory equipment and experiments used to characterize APW gas production and composition. Laboratory results show cumulative gas volumes increase with increasing NaOH strength and 5 M NaOH was determined to provide sufficient alkalinity to maximize gas production for the APW samples tested. Total gas generation from all APW samples range from about 20 to 220 mL/g APW, with Site 1 SC and MBD-1 generating over 210 mL/g APW. Variability in gas production was found to depend on waste type and particle gradation, e.g., salt cake consists of a larger percentage of coarse fraction than baghouse dust. A qualitative correlation was found between total gas generated and metallic aluminum content evaluated from XRD analyses. Hydrogen is the dominant gas generated from the APW reaction because of the strong correlation to total gas generated. In addition, ammonia concentrations range from 2,600 to 6,200 ppmv and methane concentrations were < 2% v/v.

4.6 Recommendations for APW Disposal

The potential environmental hazards of APW disposal along with high disposal costs have caused secondary aluminum producers in Europe, Japan, and Australia to consider recycling technologies to reduce the volume of waste. The conventional recycling treatment consists of grinding and sieving the APW to recover the metal value, followed by water leaching at ambient or at higher temperature and pressure to dissolve and separate the salt in water from residue oxide. The salt is recovered back by filtering and evaporation techniques from the water. The residue, which

contains primarily alumina and other alloying elements, can be used after washing (or calcination) in various industries, such as, cement, ceramic, and building industries (Bodnar et al. 1997; Skoch and Collins 1995; Dash et al. 2008; Bahr and Kues 1978).

Gil (2005) reports that the total recycling process of APW is not economically viable. As a result, the best solution is to maximize the recovery of aluminum and dispose of the residue in controlled landfills. These controlled landfills are referred to as monofills, which are constructed to Subtitle D regulations in the U.S.A. and accept only this waste stream. The advantages of APW monofills are:

- There is no risk of starting combustion of MSW because MSW is not present unless the monofill is inside an MSW disposal facility
- Depending on economic viability, the monofill may be mined in the future to further capture aluminum and/or react the aluminum to generate heat and hydrogen gas as an energy resource.

Given these positive advantages, exothermic reactions still do occur in monofills. For example, Site 1 is measuring elevated waste temperatures of over 100°C (see Figure 2.5) while Site 2 is experiencing localized elevated temperatures and emanating ammonia odors that are causing a nuisance to nearby commercial businesses and residential communities. As a result, Figure 4.16 illustrates a flow chart for disposal of APW in monofills.

The recommended procedure for APW disposal involves first using the calorimeter device described in Chapter 3 to evaluate APW reactivity. The temperature of 65°C is the criterion used to define reactive wastes. The gas generation test works in parallel with the calorimeter and can be conducted to evaluate the hydrogen production and estimate aluminum content. The secondary aluminum producer and/or landfill owner then can decide if further recycling or energy recovery, e.g., mechanical treatment via grinding/crushing and harnessing hydrogen gas for energy, is economically viable given the estimated aluminum content and APW physical characterization, i.e., particle size gradation. Four conditions are shown in Figure 4.16 based on a yes/no answer for the reactivity and gas generation tests. If a “no” is answered for both tests, it can be landfilled but immediately covered with 0.3 m of fine-grained soil to limit moisture contact. If a “yes” is observed for the reactivity test but a “no” is selected for aluminum recycling, the reactive APW

should be mixed with fine-grained soil in equivalent mass ratios, e.g., one metric ton of APW and fine-grained soil. This mixing will reduce the concentration of available aluminum to react in the APW and will require more energy to increase the temperatures of soil and APW. The final two scenarios are: (1) reactivity test is “no” but recycling is “yes”; and (2) both requirements are “yes”. The recommended procedure for both scenarios is aluminum recovery via mechanical grinding/crushing and/or hydrogen capture from a large-scale reactor. For the latter scenario (two “yeses”), the APW exhibits temperature and gas reactivity so preemptive action should be taken to reduce the possibility of an exothermic reaction after disposal. If the reactivity test indicates temperatures are below 65°C, harnessing energy may still be viable because the APW could produce plentiful amounts of gas, e.g., see Site 1 MBD-1. Given the four conditions, all wastes should be disposed in a monofill facility per federal and state regulations. Prior to disposal in the monofill, it is recommended to isolate the baghouse dust waste from other APW in the monofill. This is beneficial because baghouse is usually a source of lime and alkalinity, which can initiate and/or exacerbate the reaction of other APW. The facility operator can evaluate the efficacy of the calorimeter and gas generation test for reducing adverse aluminum reactions by: (1) installing temperature arrays in the waste to monitor heat generation; (2) constructing a gas collection system to evaluate hydrogen production and ammonia emissions; and (3) measuring leachate volume and characterizing leachate chemistry to evaluate the amount of liquid infiltration and the constituents leaching from the APW that are contributing to the reaction.

4.7 Tables and Figures

Table 4.1 Review of APW gas evolution and composition in literature

APW Type and Properties	Experimental Conditions*	Gas Evolution (mL/g APW)†	Reference
Salt cake Particles < 149 μm pH ~ 10-11	Deionized water, 22°C, N/A	H_2 = 1.93	Hwang et al. (2006)
Salt cake	6 N HCl, 20°C, 1:300 to 1:6	H_2 = 27.8-248.3	Graczyk et al. (1997)
Granular dross D_{50} = 10 mm pH ~ 9.5-10.1	Distilled water, 20°C, 1:10	Total = 0.25-1.7	Manfredi et al. (1997)
Dross D_{50} = 200 μm	Water, 25°C, 1:0.3	Total = 2.4	Liu and Chou (2013)
Ball-milled dross Particles ~ 45μm	Water, 21°C, 1:26	H_2 = 568.5	David and Kopac (2012)
Dross/salt cake	Water, 20°C, 1:0.53	Total = 3.4	RSGA (2011)
Dross excavated from landfill experiencing APW reaction	Leachate, 77°C, 1:1.4	Total = 2.6	Schaefer et al. (2008)
Dross excavated from landfill after 20 yrs	Water, 24°C, N/A	Total = 0.15	Lorber and Antrekowitsch (2009)

Note: *Reported in the reference: reacting solution, ambient temperature, and solid to liquid ratio (g APW: ml solution)
†Gas evolution is reported in actual testing conditions.

Table 4.2 Chemical properties of Site 1 and Site 2 APW samples

Site 1					Site 2		
Mineral	MBD-1 (% wt)	MBD-2 (% wt)	BHD (% wt)	SC (% wt)	Mineral	MSC (% wt)	BD (% wt)
Al	3.8	1.5	1.1	2.4	Al	0.9	3.2
Al_2O_3	4.8	20.8	8.5	14.4	Al_2O_3	7.7	7.5
Al_2CO	3.5	2.3	3.7	7.6	Al_2CO	4.5	3.7
NaCl	38.2	42	32.4	33.4	NaCl	34	41.8
KCl	9.3	15.5	23.1	16.8	KCl	15.2	18.7
$MgAl_2O_4$	6.7	12	30.9	22.8	$MgAl_2O_4$	34.7	17.1
Graphite	4.3	---	0.3	0.9	MgO	1.6	6.4
SiO_2	---	2.4	---	---	SiO_2	0.5	0.7
$MgAl_4O_7$	---	---	---	1.8	Pb	0.8	0.9
$KMgCl_3(H_2O)_6$	29.4	---	---	---			
$CaMg(CO_3)_2$	---	3.4	---	---			

Table 4.3 Calibration of gas yield using aluminum foil and 5M NaOH

Test	Al (g)	Experimental H_2 yield (mL)	Theoretical H_2 yield (mL)	Reactor Temperature (°C)	Percent Error (%)
1	0.09	120.3	122.3	25	1.6
2	0.13	176.0	186.1	41	5.4
3	0.19	263.4	269.4	38	2.2
4	0.21	299.8	300.6	41	0.3
5	0.23	314.4	329.2	41	4.5
6	0.14	181.1	190.2	25	4.8

Table 4.4 Testing regime for APW gas generation experiments

Site	Waste Type	NaOH (M)	Total Gas Volume (mL/g APW)
1	MBD-1	1	134.4
1	MBD-1	2	193.3
1	MBD-1	5	233.2
1	MBD-1	10	213.3
1	MBD-2	1	20.5
1	MBD-2	1	24.7
1	MBD-2	3	74.5
1	MBD-2	5	81.5
1	MBD-2	5	82.2
1	MBD-2	10	86
1	BHD	5	38.9
1	BHD	10	34.9
1	SC	1	153.1
1	SC	3	196.5
1	SC	5	169.3
1	SC	5	260.2
1	SC	10	168.1
1	SC	10	193.2
2	BD	1	75.5
2	BD	3	82.6
2	BD	5	81.3
2	BD	5	81.6
2	BD	10	84.1
2	MSC	1	33.7
2	MSC	5	40.8
2	MSC	5	47.5
2	MSC	10	31.9
2	MSC	10	37.1
2	MSC	10	50.6

Table 4.5 Preliminary Site 1 and Site 2 gas composition results

Site	APW	Mass (g)	NaOH (M)	Total Gas (mL/g APW)	NH_3 (ppmv)	H_2 (% v/v)	CH_4 (% v/v)
1	MBD-1	6	2	193.6	3,100	40.3	1.3
1	MBD-2	5	5	83.8	2,600	17.2	1.1
1	BHD-1	5	5	41.9	3,800	13.5	1.2
1	SC-1	5	5	260.2	6,200	47.4	1.5
2	BD-2	5	5	81.6	4,500	21.6	1.9
2	MSC-1	5	5	46.8	5,500	10.5	<1.0

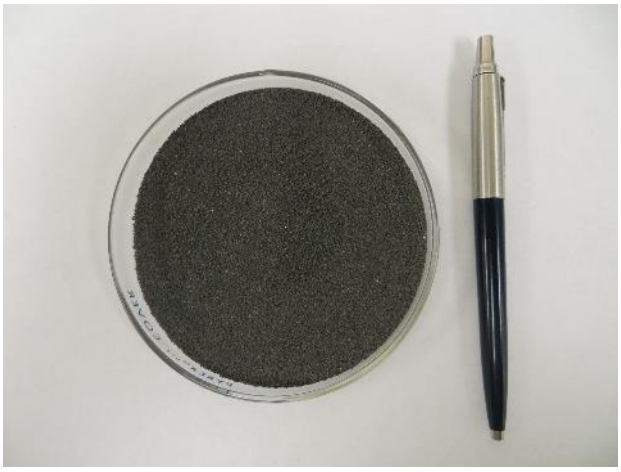

(a) Milled Black Dross-1



(b) Milled Black Dross-2



(c) Baghouse Dust-1

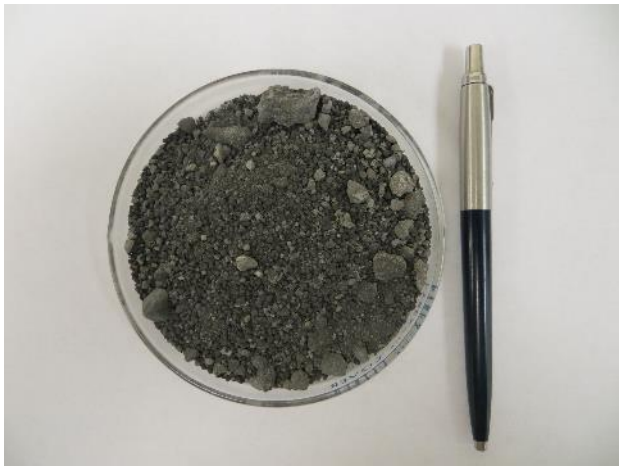

(d) Salt Cake-1

Figure 4.1 Photos of Site 1 APW samples: (a) MBD-1, (b) MBD-2, (c) BHD-1, and (d) SC-1



(a) Black Dross-1 (b) Milled Salt Cake-1

Figure 4.2 Photos of Site 2 APW samples: (a) BD-1 and (b) MSC-1

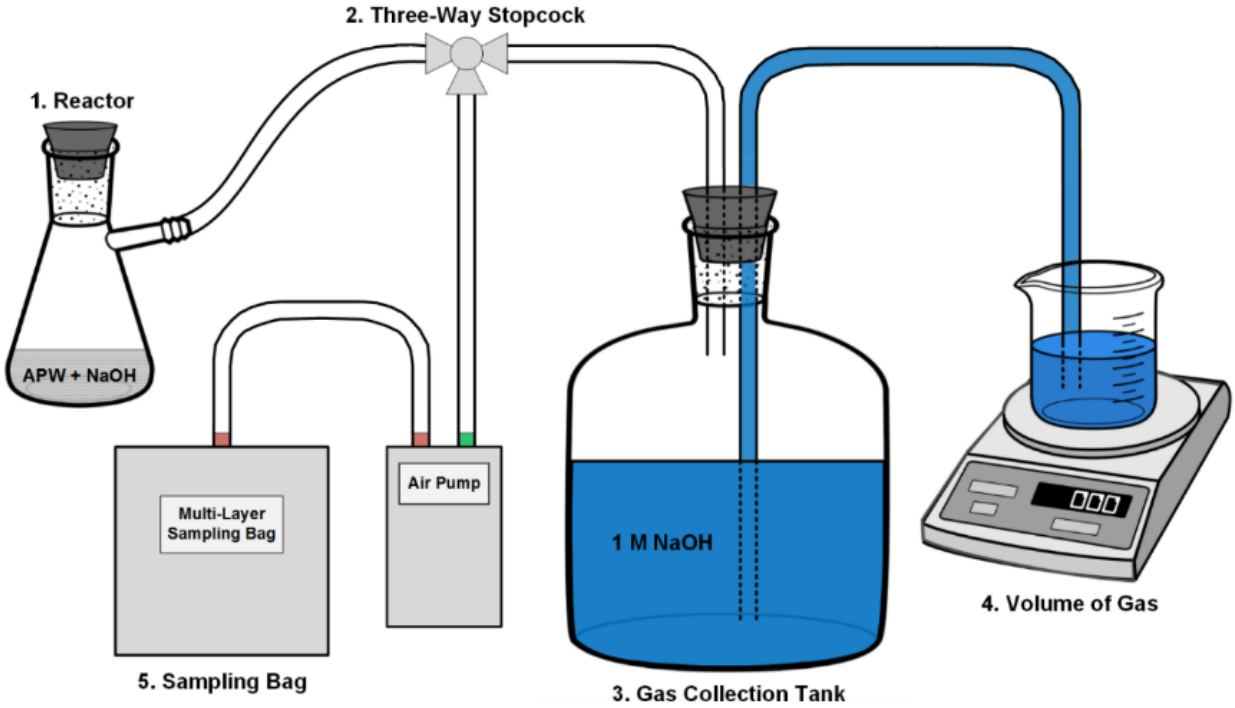

Figure 4.3 Schematic of APW gas generation experiment

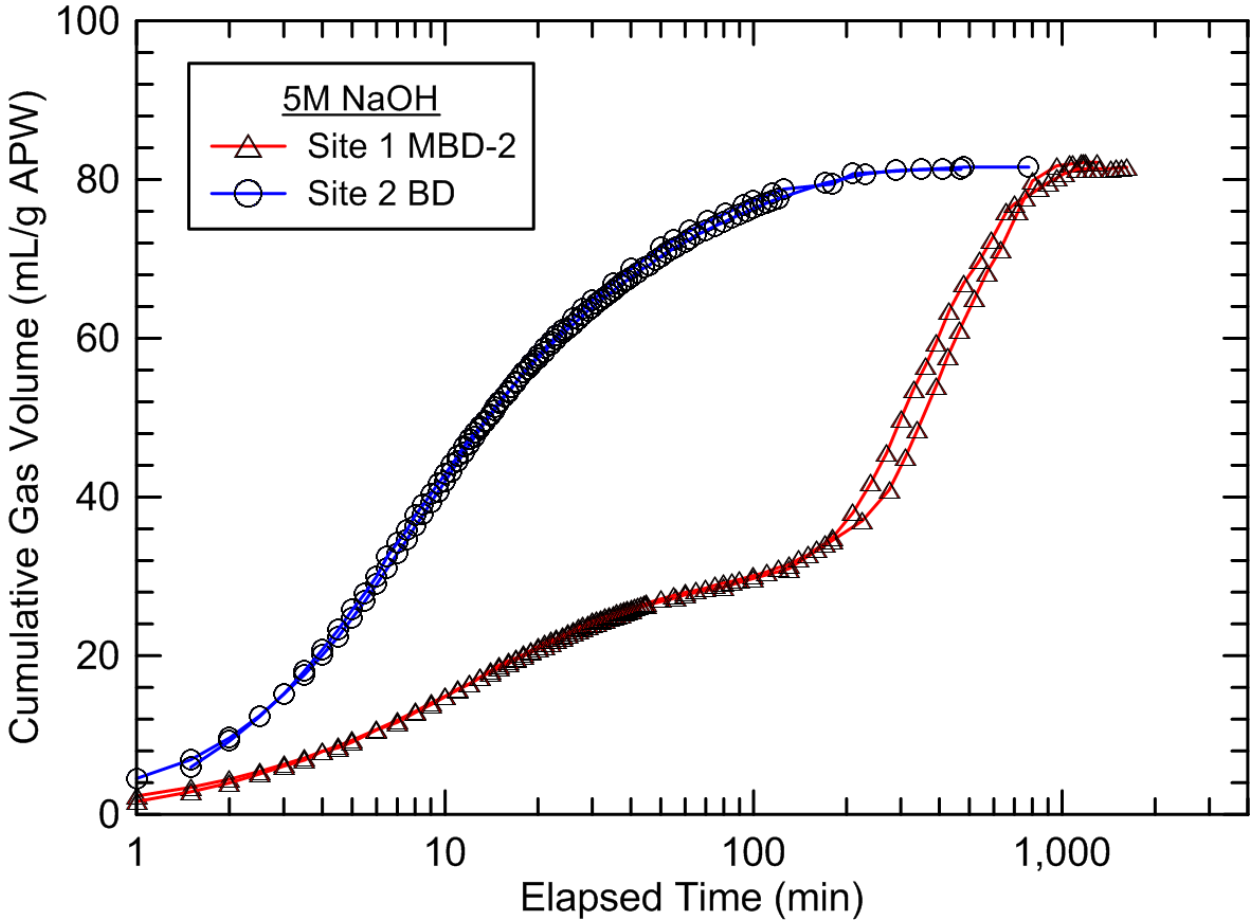

Figure 4.4 Reproducibility of total gas generation at 5M NaOH

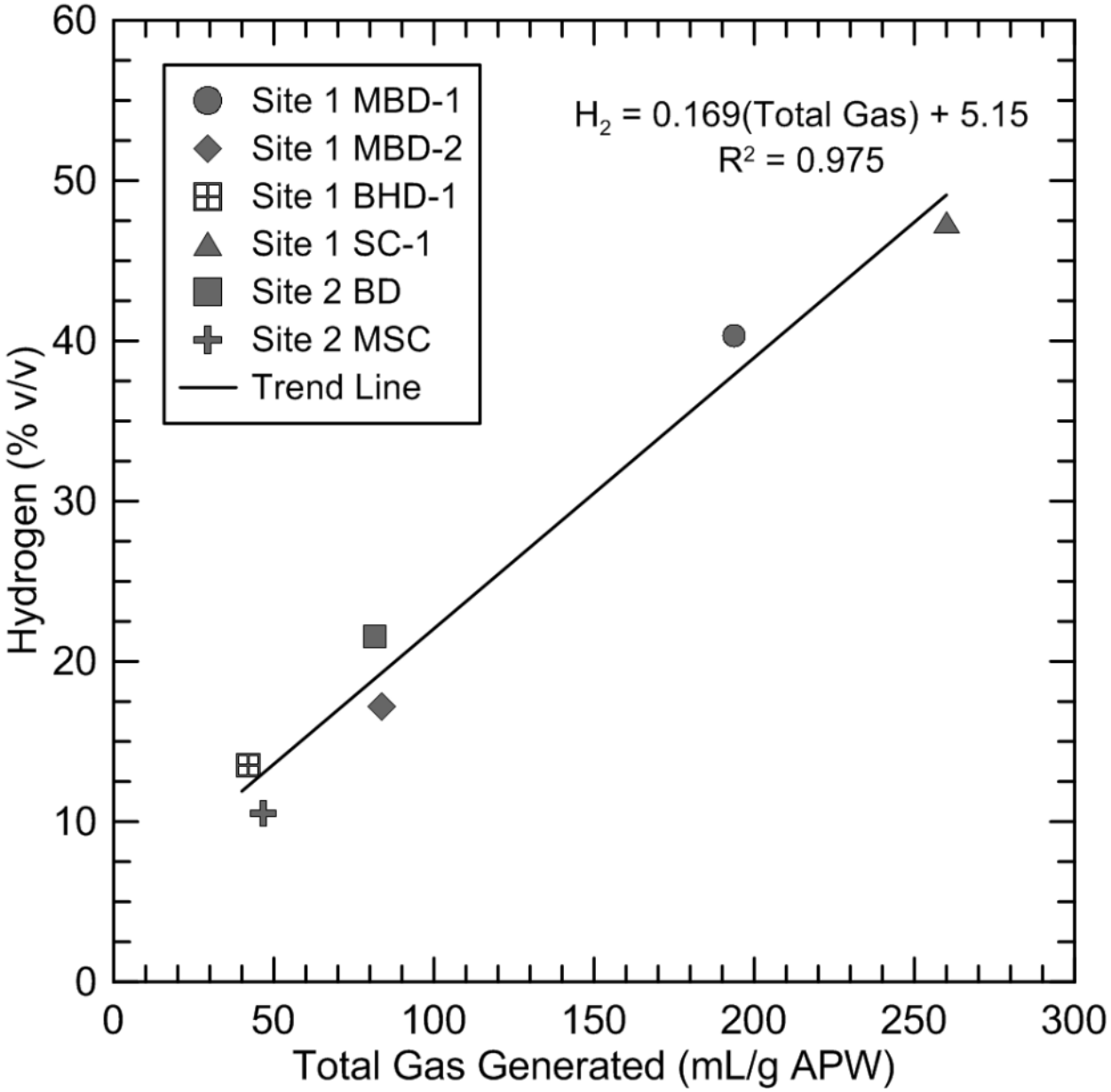

Figure 4.5 Trend of total gas generated and hydrogen concentrations for Sites 1 and 2

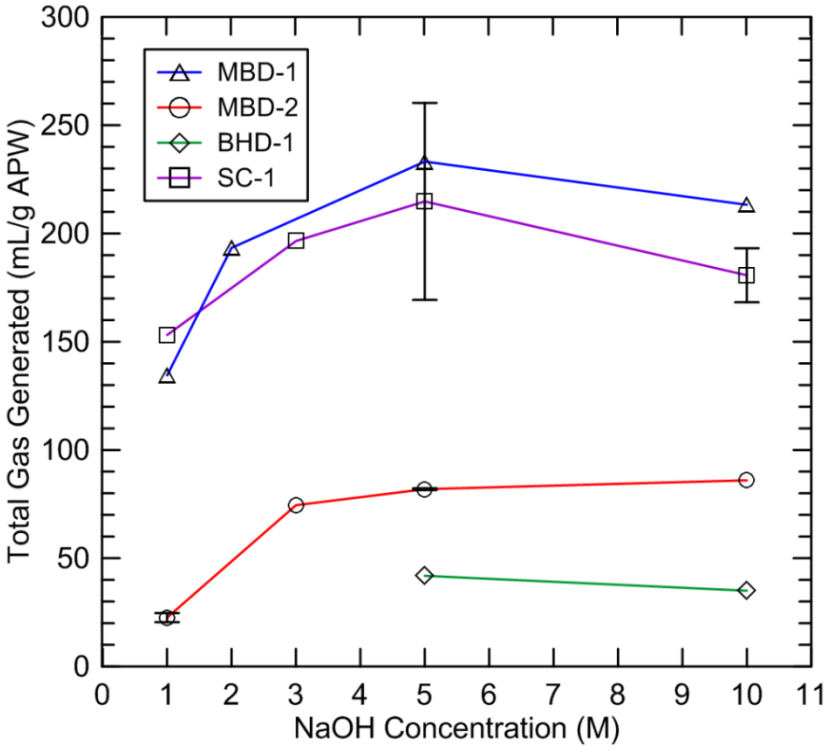

(a) Site 1

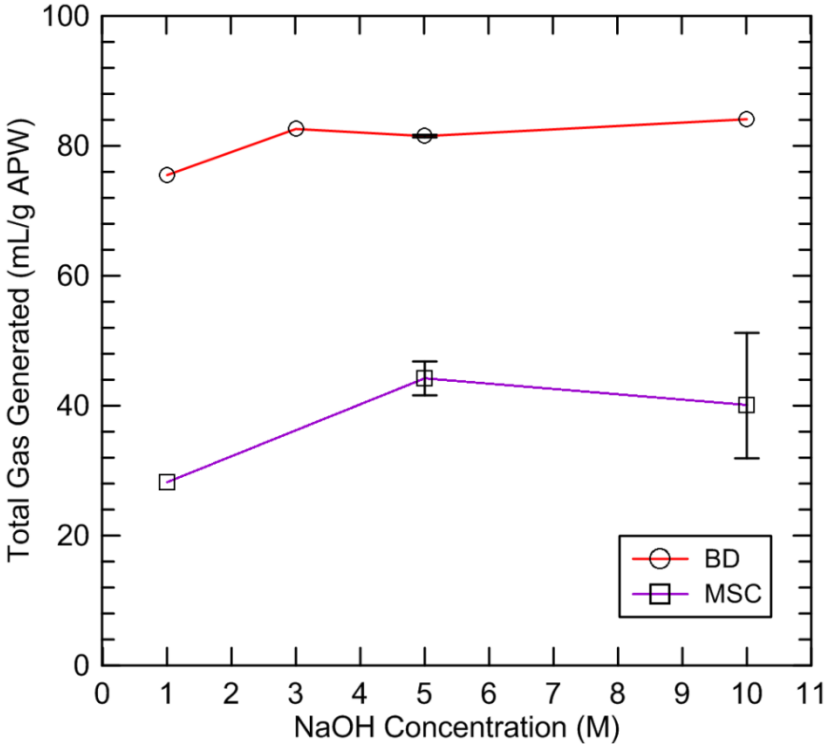

(b) Site 2

Figure 4.6 Effect of NaOH concentration on total gas generated for (a) Site 1 and (b) Site 2

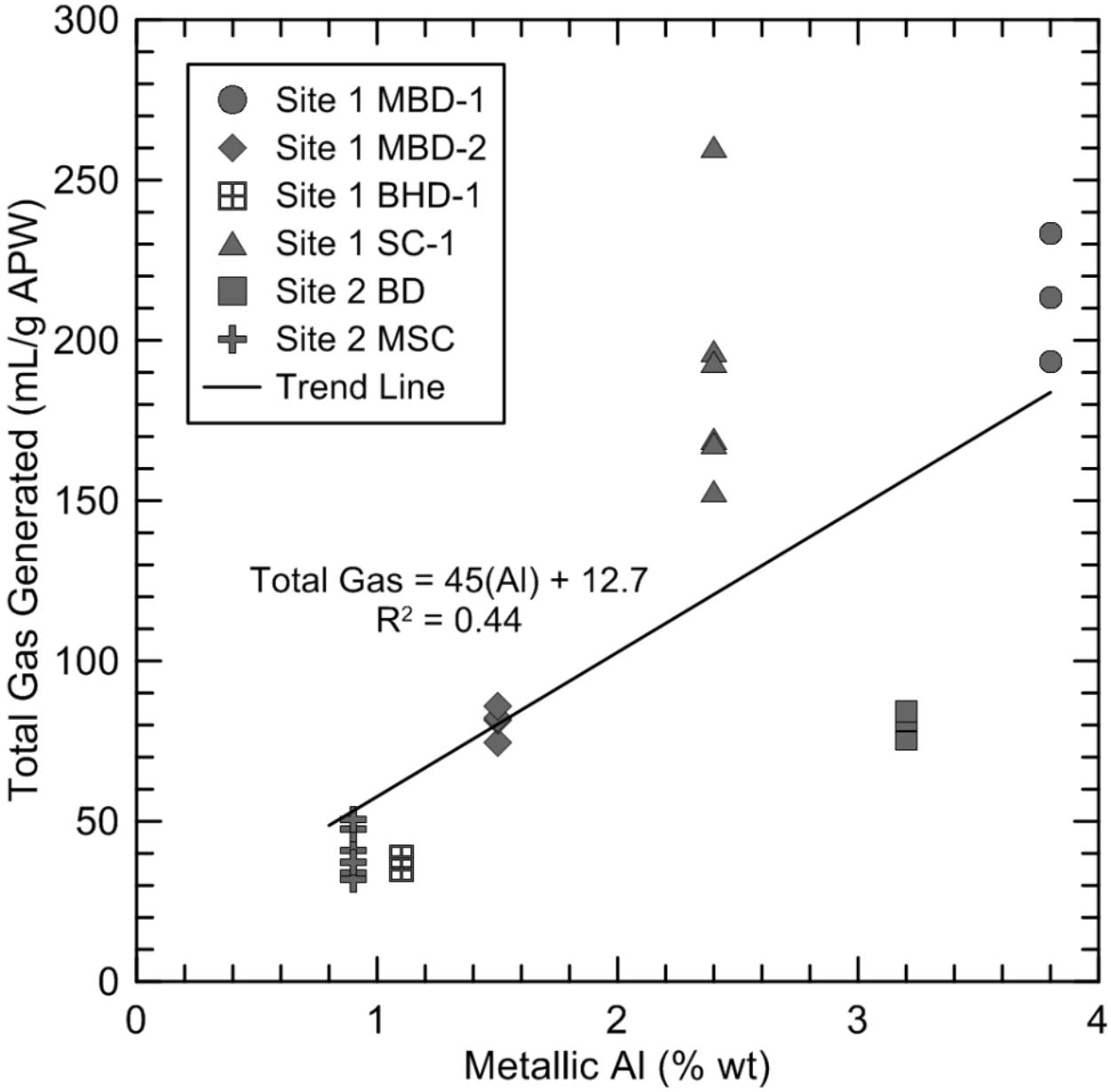

Figure 4.7 Trend of XRD metallic Al and total gas generated for Sites 1 and 2

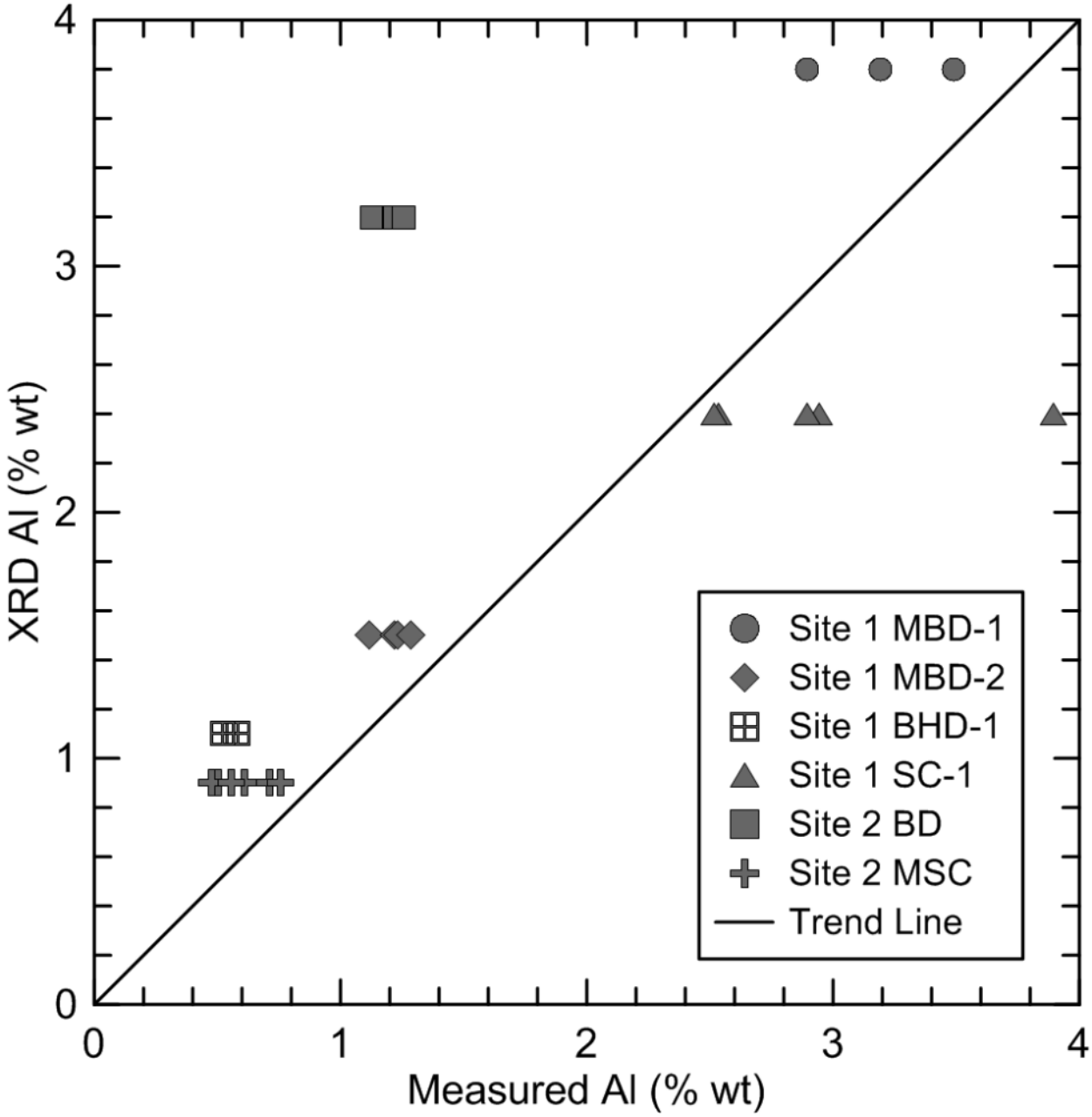

Figure 4.8 Comparison of XRD Al and measured Al for Sites 1 and 2

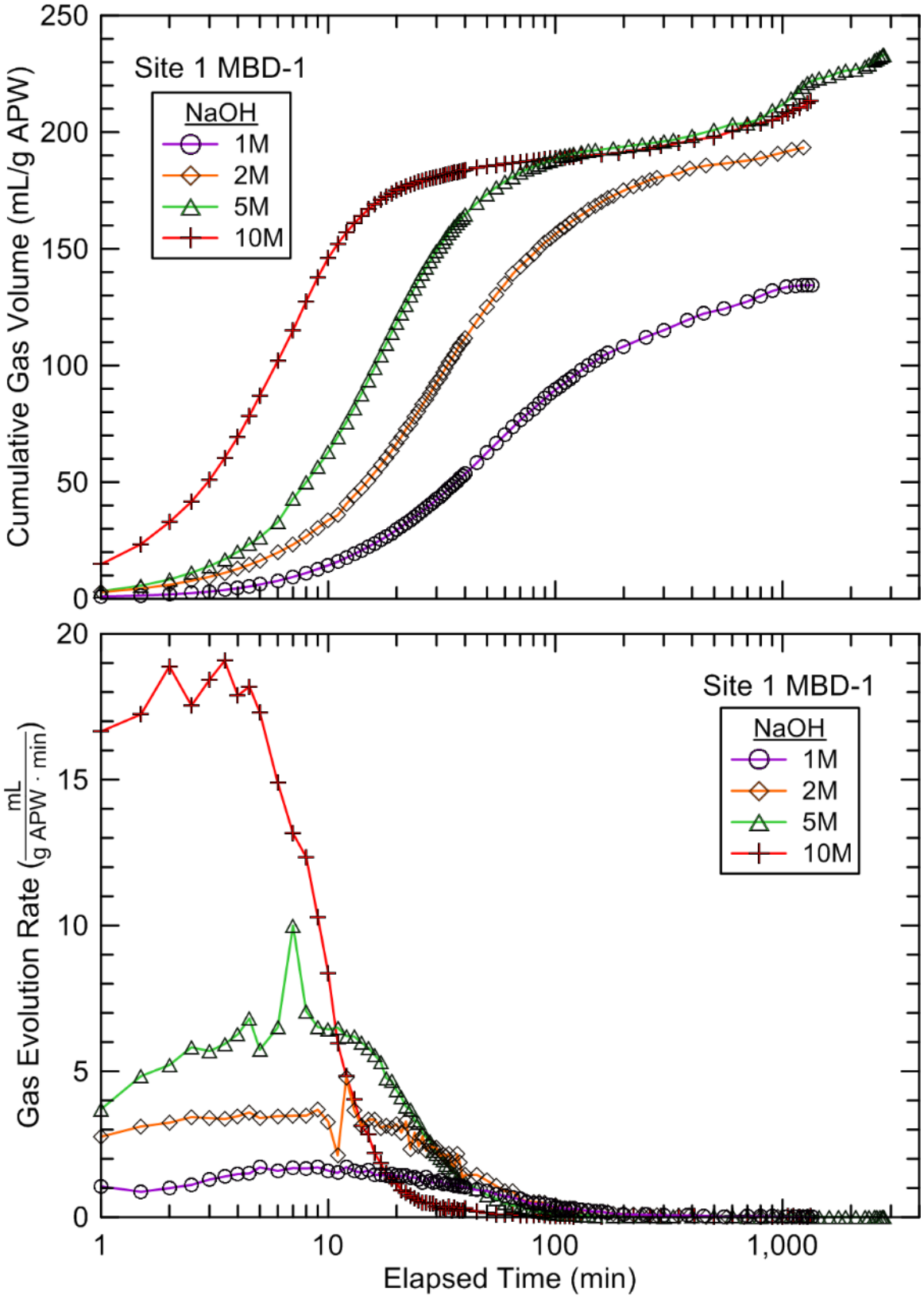

Figure 4.9 Site 1 MBD-1 total volume of gas and production rate

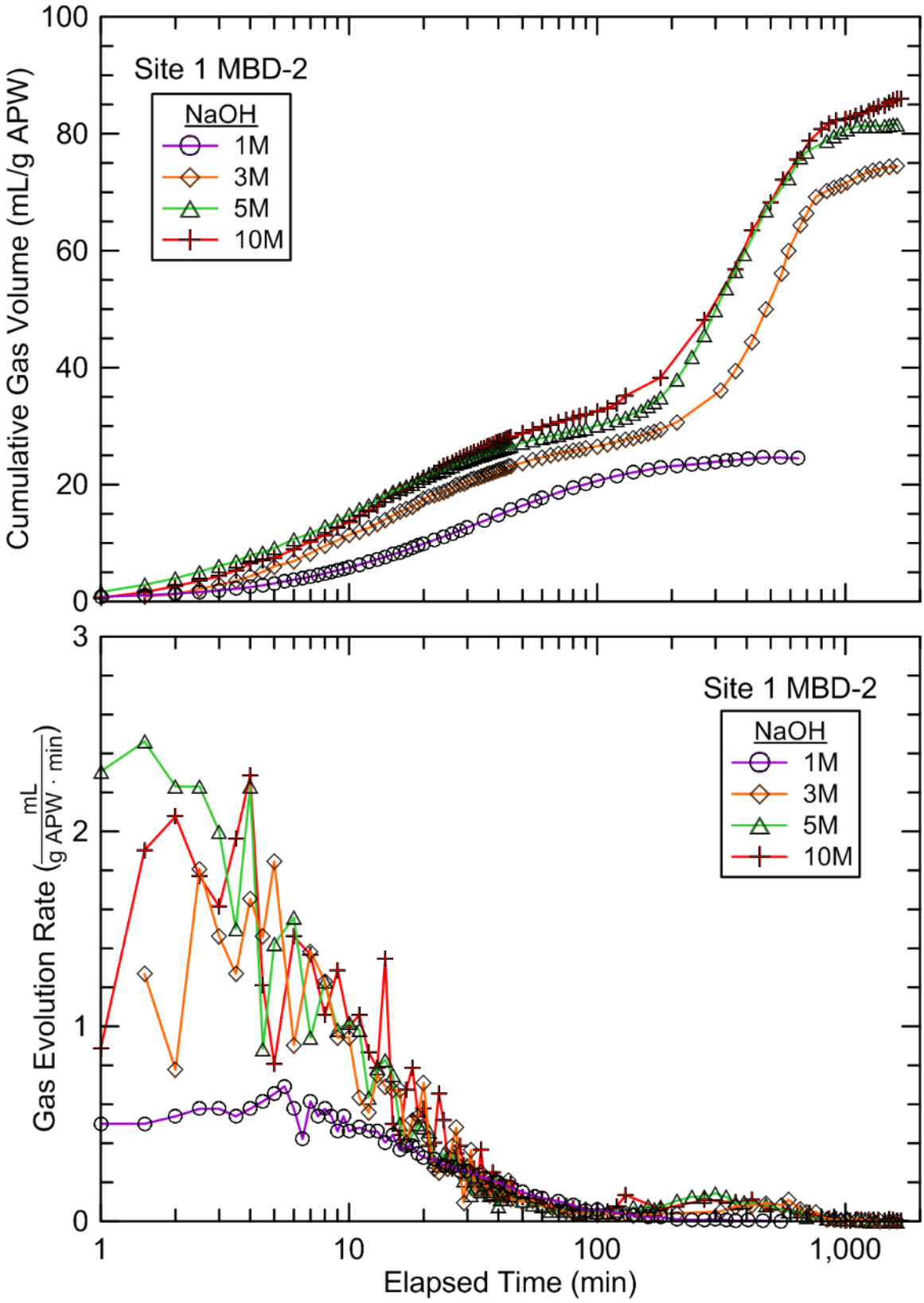

Figure 4.10 Site 1 MBD-2 total volume of gas and production rate

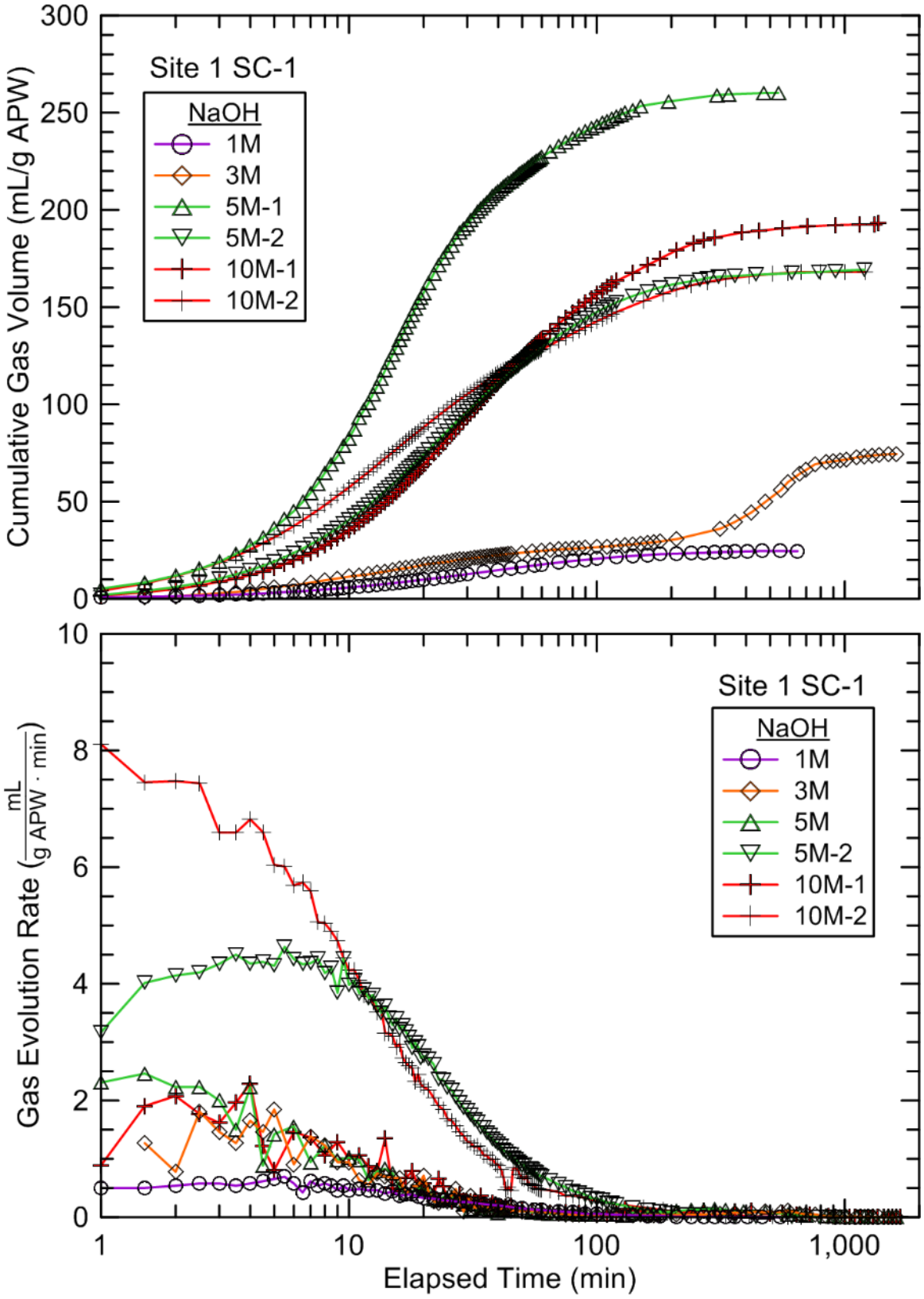

Figure 4.11 Site 1 SC-1 total volume of gas and production rate

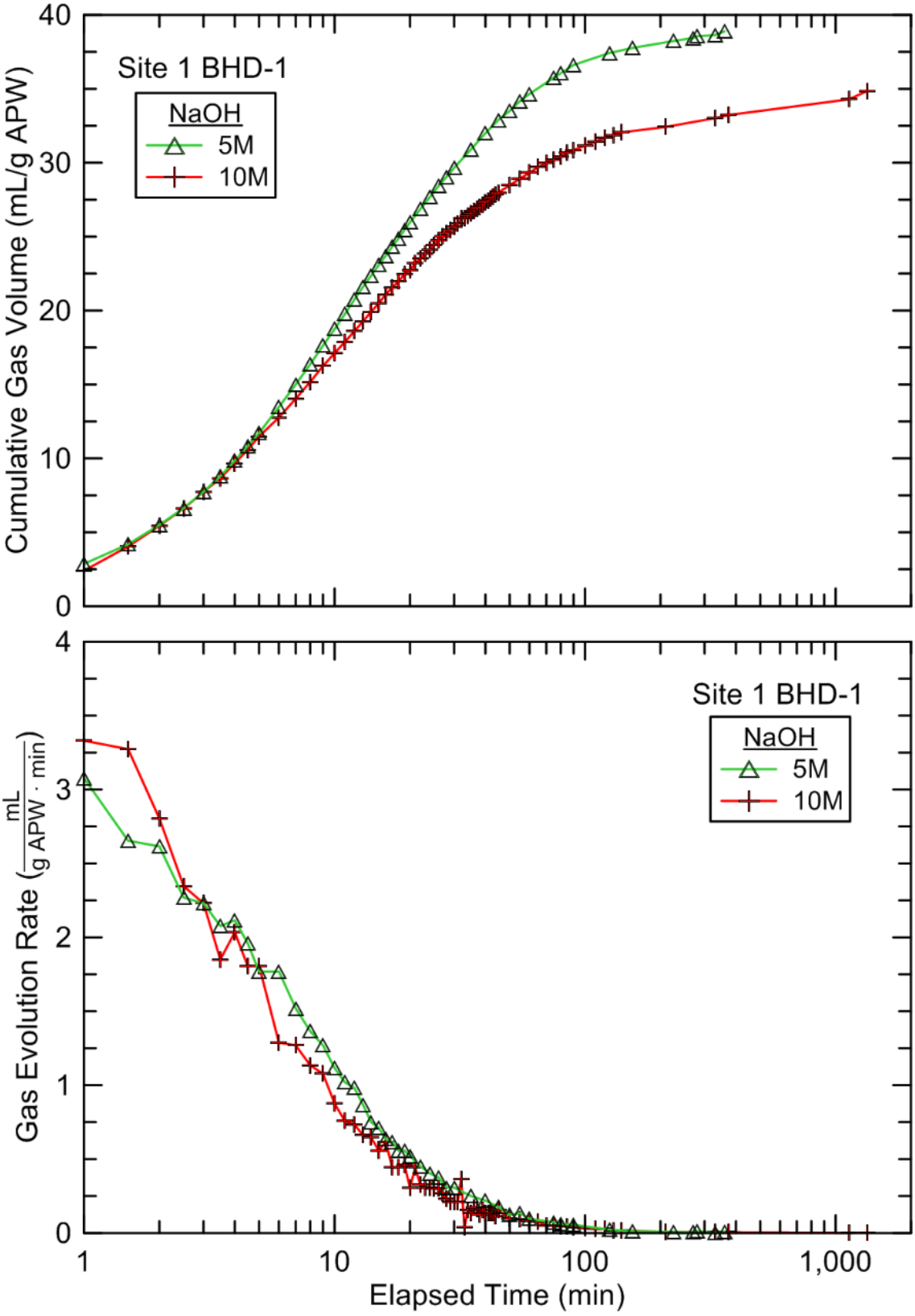

Figure 4.12 Site 1 BHD-1 total volume of gas and production rate

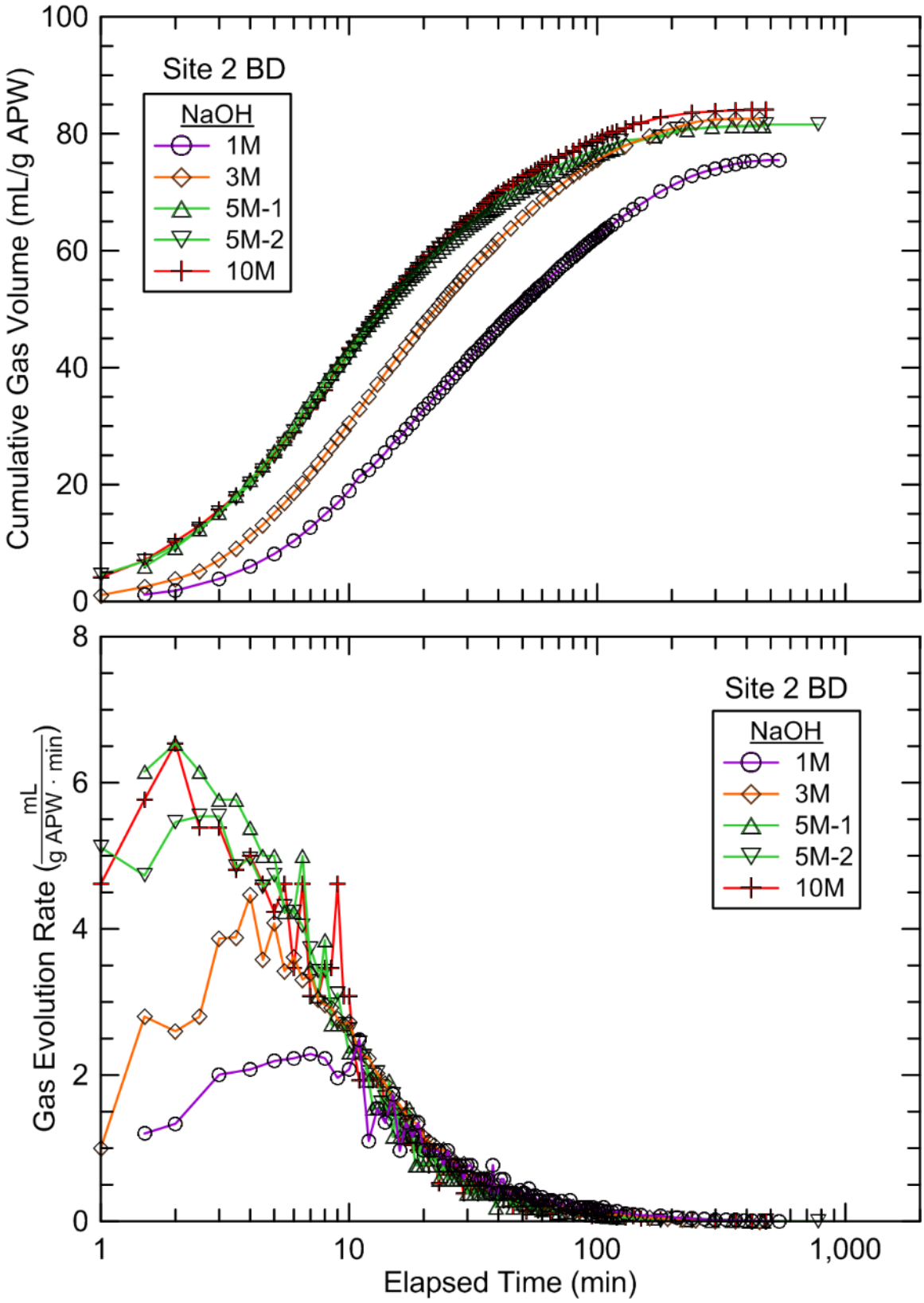

Figure 4.13 Site 2 BD total volume of gas and production rate

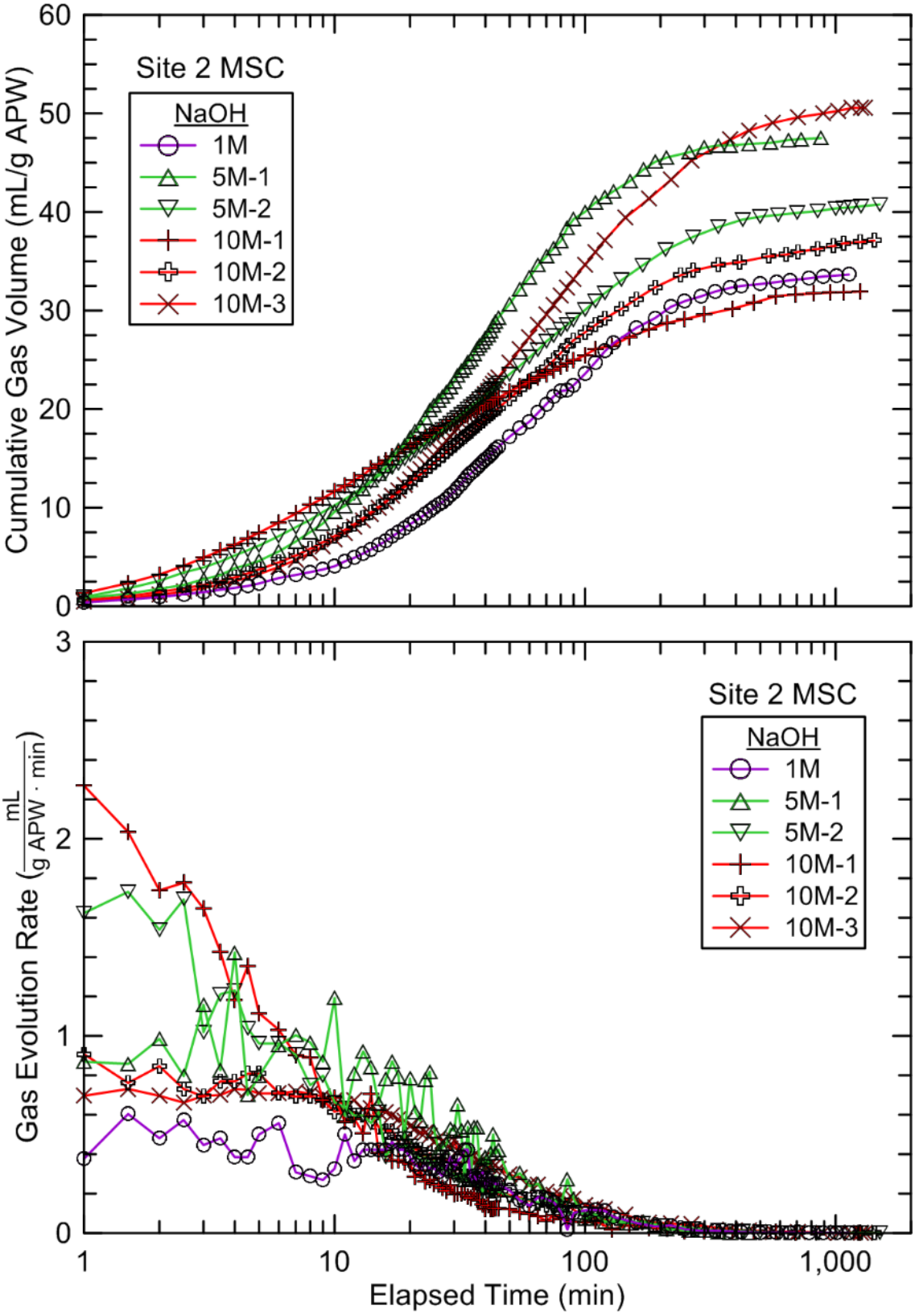

Figure 4.14 Site 2 MSC total volume of gas and production rate

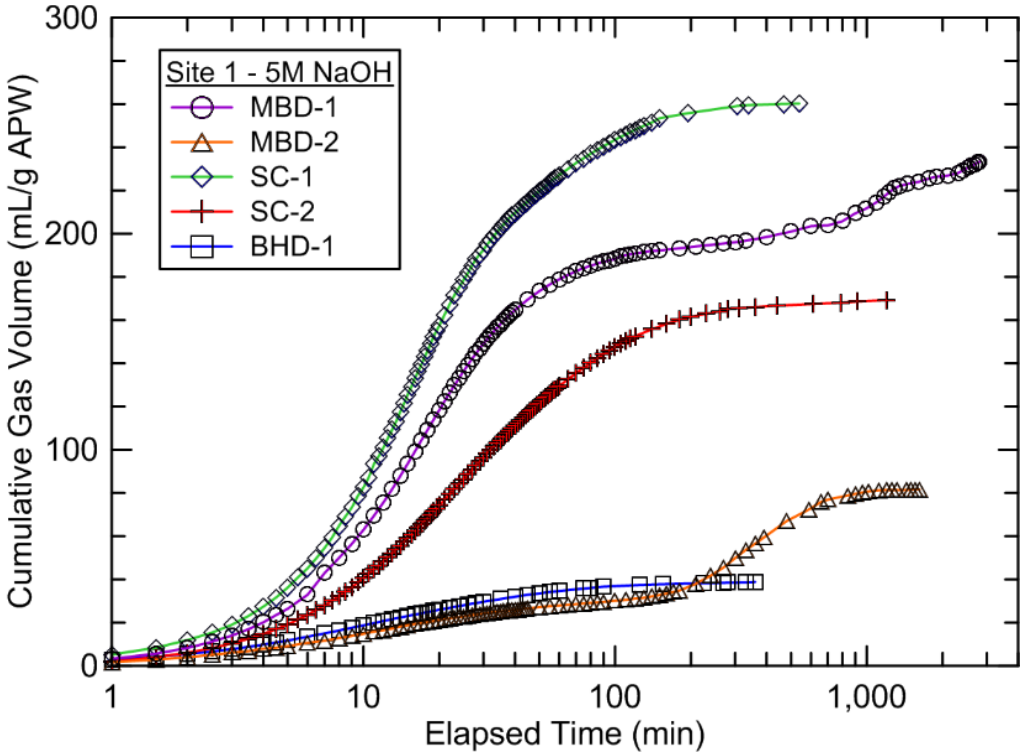

(a) Site 1

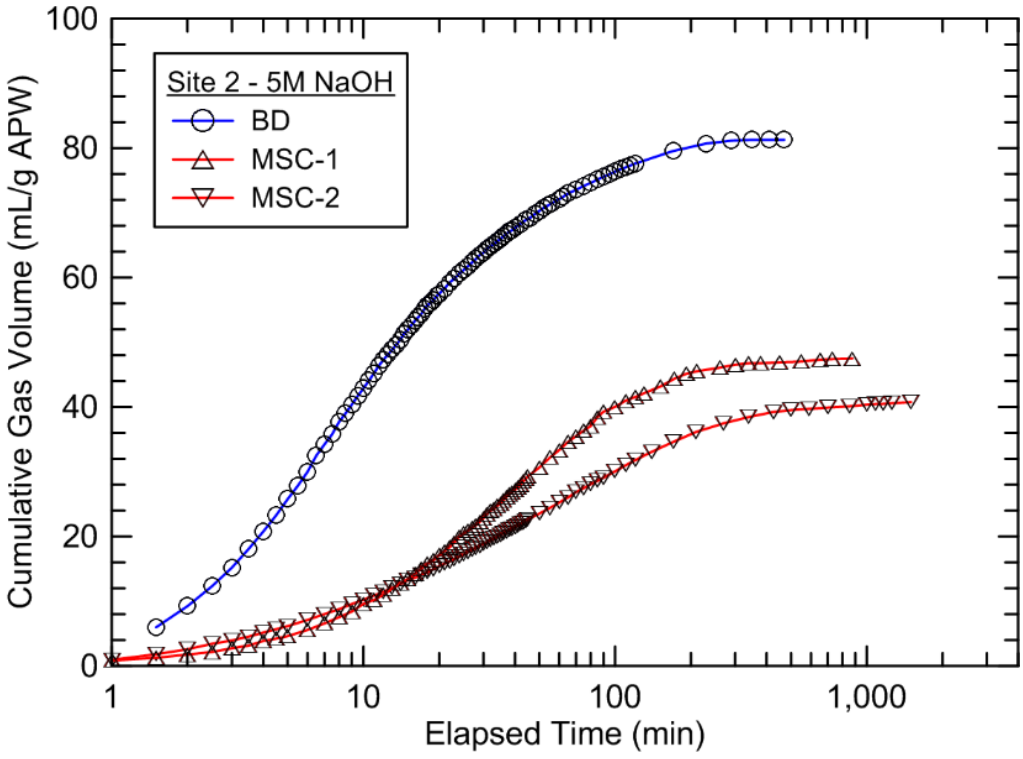

(b) Site 2

Figure 4.15 Total gas production at 5 M NaOH: (a) Site 1 and (b) Site 2

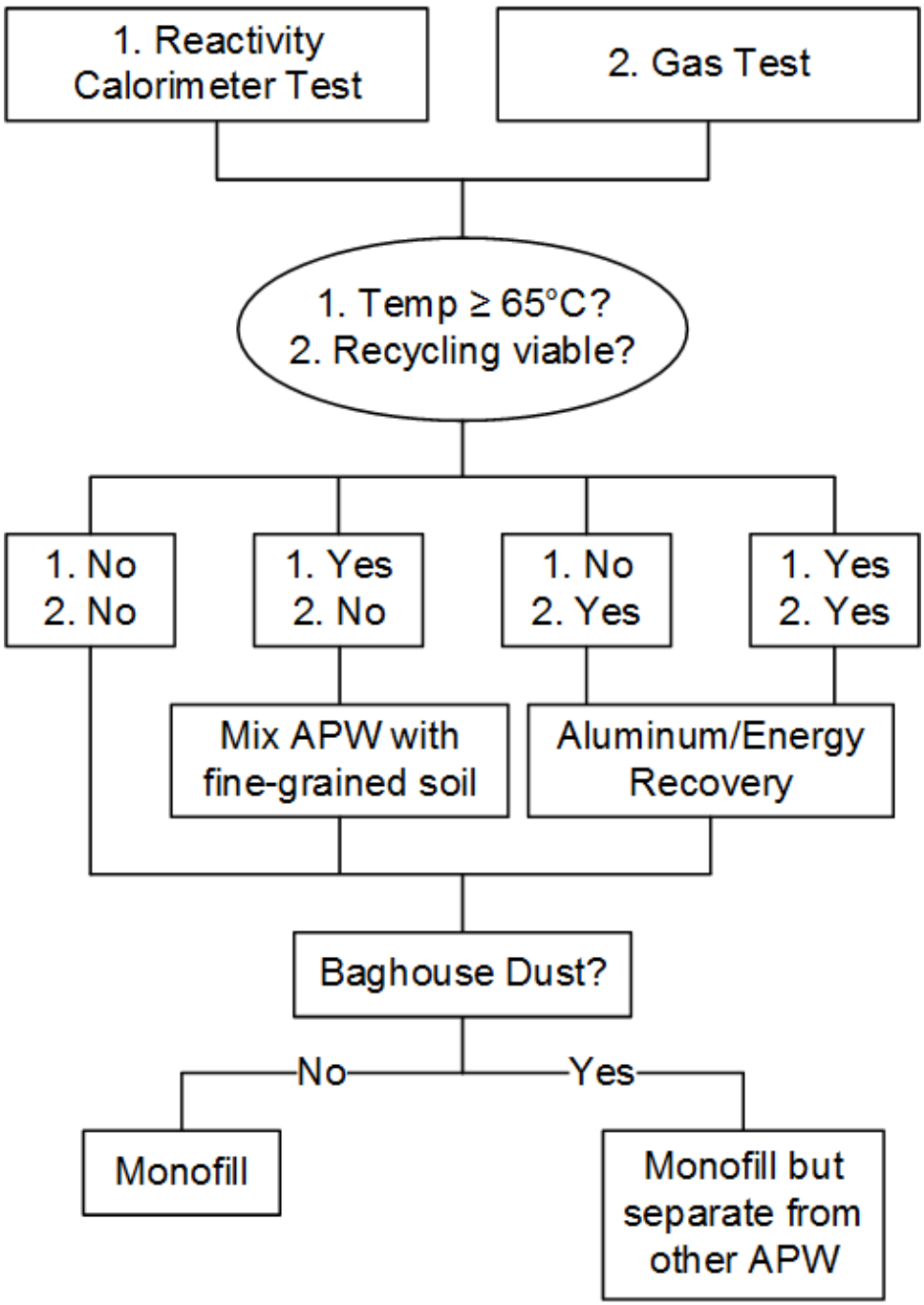

Figure 4.16 Flow diagram for evaluating APW reactivity and recommending disposal options of aluminum/energy recovery and mixing APW with fine-grained soil

CHAPTER 5

PROGRESSION OF ELEVATED TEMPERATURES IN MSW LANDFILLS

5.1 Introduction

Elevated temperatures have been documented in MSW landfills, CDD landfills, industrial waste monofills, and sanitary dumps (Martin et al. 2013; Sperling and Henderson 2001; Hogland and Marques 2003; Ettala et al. 1996; Riquier et al., 2003; Øygard et al. 2005; El-Fadel et al. 1977; Nikolaou 2008; Merry et al. 2005; Koelsch et al. 2005; Frid et al. 2009). The presence of elevated temperatures, particularly in MSW landfills, can impact the integrity of the cover and liner systems, leachate quality, gas composition, slope stability, differential settlement, odor generation and migration, and leachate outbreaks (Lewicki 1999; Øygard et al. 2005; Jafari et al. 2014a; Stark et al. 2012; Øygard et al. 2005). In addition, they present a significant threat to the environment by emitting to the atmosphere incomplete combustion by-products, e.g., carbon monoxide (CO), reduced sulfur compounds, and particulate matter (Nammari et al. 2004; Ruokojarvi et al. 1995a,b; Lönnermark et al. 2008; Chrysikou et al. 2008).

To rapidly detect elevated temperatures, landfill operators, consultants, and regulatory agencies have used infrared imagery, geophysical (electric and electromagnetic) methods, visual observations (surface settlement, smoke, and steam), and monitoring of waste temperatures, gas composition and temperature, and leachate quality (Stearns and Petoyan 1984; Lewicki 1999; Riquier et al. 2003; Sperling and Henderson 2001; Riviere et al. 2003; Ohio EPA 2011; Hall 2007). For instance, Stark et al. (2012) use a case study to illustrate gas and leachate indicators for APW reactions in MSW landfills. Building on the work of Stark et al. (2012), Martin et al. (2013) provide operational criteria and landfill trends to rapidly detect if an APW reaction is occurring within an MSW facility and how to distinguish between APW reactions and subsurface smoldering or combustion.

Detection criteria and methods are readily available (Stark et al. 2012; Martin et al. 2013; Stearns and Petoyan 1984), but a comprehensive understanding of the spatial and temporal variation of landfill gas, temperature, leachate migration, and settlement of elevated temperature events and the underlying mechanisms are lacking. As a result, this chapter presents data from an MSW facility that is experiencing elevated temperatures to relate elevated gas and waste

temperatures, changes in gas composition and production, leachate migration, slope movement, and settlement and uses it to develop a progression of indicators for the presence and migration of elevated temperatures in MSW landfills.

5.2 Overview of Case Study

The case study is an MSW landfill regulated under Subtitle D regulations. The site is permitted for waste disposal in 178 ha and receives up to 9,000 metric tons of MSW per day. Figure 5.1 shows the site layout and location of impacted area in Cells 4-7 (see red dashed box). The cells encompass 26.2 ha and were constructed in phases, with Cell 4 completed in late 1997, Cell 5 in early 1999, Cell 6 in late 1999, and Cell 7 in early 2001. After reaching the permitted elevations in 2005, Cells 4 through 7 were capped with a layer of 0.6 m thick fine-grained soil and a gas control and collection system was installed through the soil cover.

In August 2009, five gas wellheads in Cell 5 experienced temperatures above 68°C and as high as 95°C. Associated laboratory gas sampling from the wellheads reported carbon monoxide concentrations greater than 1,000 ppmv, with a maximum of 10,200 ppmv (Ohio EPA 2010). In response to the elevated temperatures, the facility reduced vacuums to all landfill gas wells in the impacted area, i.e., they were tuned to allow passive flow into the gas collection system. The facility suspended dewatering pumps inside the wellhead pipes, which were operated to increase the capture of methane gas for energy recovery. An additional 0.3 m clay soil cover was placed over a 4.8 ha area in Cell 5 to control increasing and stronger odors. In October 2009, the facility observed cracks at the crest of the Cell 5 slope and a month later toe bulging was observed at the same slope. As a result, the facility constructed stability berms at the toe of the Cell 5 and Cell 7 slopes. In mid-October, the facility began surveying the landfill and measured settlements in the affected area exceeded 4 m within five month, i.e., by March 2010. Odor complaints by residents and commercial businesses increased from 121 in 2009 to 437 in 2010 and 566 in 2011 (Hamilton County Public Health 2014). To reduce the odor nuisance, the facility installed an exposed ethylene vinyl alcohol (EVOH) geomembrane over Cells 5, 6, and 7, increased flare capacity, immediately transported odorous leachate from the site, and operated odor neutralizing systems.

Based on the Findings and Orders issued by the Ohio EPA (Ohio EPA 2010), the facility initiated an expanded monitoring program to monitor and delineate the area of elevated temperatures and their migration. The program includes:

- Weekly measurement of gas wellhead temperature, flow rate, and pressure.
- Weekly measurement of methane, nitrogen, oxygen, hydrogen, carbon dioxide, and carbon monoxide with a portable field gas chromatograph.
- Monthly topographic surveys.
- Monthly measurement of stability pins to monitor slope movement and elevation in Cells 4 through 7.
- Weekly downhole temperature measurements in Cell 4.

Gas temperature, flow rate, and vacuum pressure were sampled at the gas port located on the wellhead (located above the surface) and recorded using the GEM™ 2000 meter (LandTec 2010). Fixed gases (CO_2, CH_4, N_2, O_2, H_2, and CO) were measured by a portable field gas chromatograph. Stability pins were installed through the exposed EVOH geomembrane over Cells 5, 6, and 7 and anchored in the underlying cover soil to monitor changes in northing, easting, and elevation. Downhole temperatures were obtained from Type T thermocouples installed in sand backfilled boreholes in the MSW. Leachate was collected and removed at sumps located in each cell (Figure 5.2(b)). The facility reports the number of hours each sump was operated but not the volume of leachate removed. Although the volume of leachate is unknown, a comparison between sump operations before and after elevated temperatures can be used to infer the migration of leachate into each cell.

Elevated temperatures were first observed in Cell 5 in late 2009 and they migrated to Cells 6 and 7 over the next four years. During the monitoring period, Cell 4 remained unaffected by elevated temperatures. Data collected from the monitoring program is discussed herein to show the correlations and the progression of temperature increase to changes in gas composition and pressure, leachate quantity and composition, slope movement, and surface settlement. Figure 5.2(a) shows the location of gas extraction wells and stability pins used to correlate the landfill trends. Figure 5.2(b) shows the bottom liner system contour elevations, which are used to estimate the waste thicknesses in Figure 5.2(c).

5.2.1 Elevated Waste and Gas Temperatures

One of the most important parameters used to assess whether or not a MSW landfill is operating normally is temperature (Hanson et al. 2010; Crutcher et al. 1982; Pfeffer 1974; Hartz et al. 1982). Landfill temperatures can be measured: (1) at the gas wellhead with a gas analyzer, e.g., GEM™ 2000 gas meter, (2) from MSW samples recovered during drilling, and (3) with thermocouple arrays installed at various depths in gas extraction well pipes, in boreholes, and in leachate collection pipes. Gas extraction wells collect gas from a slotted pipe, so the measured wellhead temperatures represent an average temperature over the length of the slotted well pipe and radius of influence of the gas extraction well. Temperatures of waste cuttings generated during drilling operations can be immediately measured by a thermal infrared camera or thermometer. Downhole thermocouple arrays are extremely useful because they provide a time history of temperatures with depth.

An example of temperatures from each of these methods is presented in Figure 5.3. The gas extraction well utilized was installed in 2005 to a depth of 33.2 m, with the final 24.4 m consisting of slotted pipe, i.e., starting at a depth of 8.8 m. In October 2010, the landfill installed downhole thermocouple arrays to monitor waste temperatures in Cell 4. The borehole was advanced using a 152.4 mm (6 in) casing and drilled with a 101.6 mm (4 in) core barrel using the rotosonic drilling method. Seven Type T thermocouple sensors spaced 6.1 m with depth were attached to a chlorinated polyvinyl chloride (CPVC) pipe and then lowered into the borehole. As the casing was removed, the borehole was backfilled with sand. The final 2.1 m to the ground surface was backfilled with a 1.5 m bentonite plug and 0.6 m of cover soil. The waste samples recovered during drilling were immediately scanned with a thermal infrared camera. The gas wellhead, thermal infrared, and thermocouple measurements used in Figure 5.3 were collected at the same time (mid-October 2010) and after the thermocouples had reached equilibrium with the surrounding waste. The gas wellhead temperature of 46°C represents an average value over the 24.4 m length of slotted pipe. The thermocouple arrays measured a waste temperature of 42°C near the ground surface and a maximum temperature of 65°C within the middle one-third (depths 15 m to 35 m). Downhole temperatures decreased slightly to 55°C near the landfill bottom (waste thickness is ~58 m). The thermal infrared temperatures show a similar trend with depth compared to the thermocouples, but the values vary significantly because of heat loss during sample recovery.

Figure 5.3 shows the thermal infrared camera can provide an approximate profile of waste temperature because of agreement with the thermocouple readings and thus can be used to verify the initial thermocouple readings. For one-time sampling events, such as the thermal infrared camera, temperatures are less accurate because heat gain or loss may occur during drilling operations or during removal of samples from the landfill. Gas wellhead temperatures in Figure 5.3 are about 20°C lower than downhole temperatures because wellhead temperatures are influenced by mixing with surrounding gases in the wellhead, convective heat loss from waste to the ground surface, and a lower ambient temperature. In addition, a gas wellhead represents a composite temperature over finite waste thickness. For example, the slotted pipe extends to about 55% of the waste thickness, so the gas extraction well may not show evidence of elevated temperatures in the bottom 45% of waste thickness because of the shallow pipe depth.

The downhole temperature array in Figure 5.3 is located in Cell 4 and is part of a system of sentinel wells that monitor the movement of elevated temperatures towards Cell 4. These sentinel wells act as an early warning system for the landfill operators to install an isolation break that would separate Cell 4 from the rest of the landfill, thereby reducing the chance of the elevated temperatures consuming the entire facility. The maximum waste temperatures in Cell 4 have remained in the range of 65 to 70°C since monitoring began in October 2010. The landfill operators attempted to install downhole temperature arrays in Cell 5, but significant gas pressure prevented completion of the drilling activities. Gas wellhead temperatures in Cell 5 reached over 90°C. Because thermocouple arrays are not available in Cell 5, the data in Figure 5.3 suggests that the subsurface temperatures exceed 100°C in Cell 5 because maximum wellhead temperatures are reported above 90°C.

5.2.2 Changes in Landfill Gas Composition

Relevant publications show that typical temperatures in normally operating MSW landfills are within the mesophilic range of 38 – 54°C (EMCON 1981; Yesiller et al. 2005; Houi et al. 1997). The anaerobic processes that regulate methane generation occur best within a temperature range of 40 to 42°C for mesophilic bacteria (Hartz et al. 1982; Cecchi et al. 1993; Mata-Alvarez and Martinez-Viturtia 1986; Pfeffer 1974). Thermophilic methanogens have a temperature optimum of about 65°C with 70°C as an approximate upper limit for acetate conversion to methane (Zinder

1993). Thermophilic bacteria can yield higher gas generation rates but the production is significantly influenced by the initial population of thermophilic methanogens in the waste (Buivid et al. 1981).

Although there is not a simple upper temperature limit for methanogens, laboratory reactors simulating anaerobic decomposition of MSW indicate the methane production starts to significantly decrease if waste temperature exceeds 55°C (Kasali and Senior 1989; Hartz et al. 1982). This decrease is attributed to mesophilic bacteria population being significantly curtailed (Farquhar and Rovers 1973; McBean et al. 1995). Therefore, it is important to understand the relationship between gas composition and gas wellhead temperature above the mesophilic range for extraction wells because of MSW heterogeneity, variable gas collection operations, and internal landfill processes.

Normal landfill gas is composed mostly of methane (45–60% v/v) and carbon dioxide (40–60% v/v), and a ratio of CH_4 and CO_2 close to unity provides a useful measure of degree of anaerobic decomposition (Barlaz et al. 2010; Powell et al. 2006). The advantage of using CH_4 and CO_2 flow rates rather than concentrations is that flow rate is a measure of the actual gas production from the waste mass, whereas concentration is simply a measure of the percentage of gas. The flow rates of CH_4 and CO_2 were calculated by multiplying the average percentage of CH_4 and CO_2 gas by the adjusted flow rate at the wellhead. Wellhead temperatures were used to standardize the flow rates to standard pressure and temperature of 20°C and 101 kPa. Temperature and flow rate were measured at the gas wellhead using the gas analyzer GEM™ 2000, while the gases were measured by a portable field gas chromatograph.

Figure 5.4 presents the relationship between wellhead temperature, the ratio of CH_4 to CO_2 flow rate, hydrogen, and carbon monoxide for a single gas extraction well in this MSW facility. In Figure 5.4(a), the gas extraction well is operating under normal conditions because wellhead temperatures are below the New Source Performance Standard (NSPS) limit of 55°C and a ratio of CH_4 to CO_2 greater than unity (see Figure 5.4(b)). The gas and temperature conditions remain steady until an elapsed time of 550 days when the ratio of CH_4 to CO_2 precipitously decreases from 1.2 to 0.3 in only 50 days (elapsed time = 600 days). Wellhead temperatures exceeded the NSPS threshold of 55°C at an elapsed time (t) of 580 days, i.e., about a month after methane levels began decreasing, and gradually increased to 75°C at t of 800 days. A decreasing ratio of CH_4 to CO_2 before wellhead temperatures increase is a trend among several gas extraction wells at this

facility. The delay between wellhead temperature increase and CH_4/CO_2 decrease may be attributed to the difference in gas flow and heat conduction through the landfill. For example, heat conduction is a slower process than gas flow to an extraction well because of the void space available in MSW, so elevated temperatures may arrive after gas decrease have been detected. This observation suggests that changes in gas composition can precede the arrival of elevated gas wellhead temperatures. Therefore, increasing wellhead temperature can be a conservative indication of the presence of an elevated temperature event because changes in the gas composition may have already occurred.

Hydrogen levels were less than 2% v/v and carbon monoxide (CO) was not measured when the ratios of CH_4 to CO_2 remained above unity. Figure 5.4(c) shows that hydrogen increased at t= 550 days to a maximum concentration of 20% v/v. Similar to hydrogen, CO increased to ~1,800 ppmv at an elapsed time of t= 550 days, and remained in the range of 2,000 to 2,500 ppmv for the duration of the monitoring period. Combining the timeline in Figure 5.4(b) to 5.4(d), it is evident that changes in CH_4/CO_2, hydrogen, and CO occur at the same time. Moreover, the ratio of CH_4 to CO_2 and CO are characterized by steep slopes, i.e., changes occur within a short time frame, while hydrogen increase occurs at a slower pace, similar to the wellhead temperature trend.

5.2.3 Leachate and Moisture Migration

The convection of moisture rich gas from dehydration of MSW due to elevated temperatures can facilitate/force redistribution of leachate within the waste mass. When water vapor condenses, it can gravitate to the leachate collection system and contribute to increased leachate volume. For example, Stark et al. (2012) report a 35.7 ha facility generated between $3.8x10^6$ L and $23x10^6$ L of leachate prior to an elevated temperature event. After the elevated temperature event began and expanded, leachate increased from $11.8x10^6$ L in 2004 to $45.7x10^6$ L in 2005. Leachate volumes continued to increase to $127.1x10^6$ L in 2008, thus representing a seven fold increase from after the detection of elevated temperatures.

Figure 5.5 shows the cumulative number of operated hours for each sump in Cells 4 through 7 of the subject MSW facility. The sump locations are shown in Figure 5.2(b). The data was collected bi-monthly and represents the number of hours the pump was operated. Figure 5.5 does not quantify if leachate volume increased but it allows a comparison of sump productivity as the

elevated temperature area expanded. Based on Figure 5.5, sump pump operation in Cells 5 and 7 increased significantly during the monitoring period. For example, Cell 5 sump pump operated for ~7,000 cumulative hours while Cell 7 sump pump reached almost 16,000 hours of operation by November 2013. In contrast, Cells 4 and 6 sumps were operated for only ~2,000 hours after 1,500 days. Elevated temperatures were first observed in Cell 5 in 2009 with gas wellheads reported temperatures of 95°C being measured. Because subsurface temperatures are higher (20-30°C based on Figure 5.3 than wellhead temperatures, sufficient heat is present to drive moisture from the MSW in Cell 5 to other cells, where it condenses in gas extraction pipes and/or gravitates to one of the sumps. For example, as temperatures advanced into Cell 7 (Figure 5.5), water vapor and leachate moisture are gravitating to the Cell 5 and Cell 7 sumps. Although Cell 6 is affected by the elevated temperatures, Figure 5.5 shows that leachate collection is lower than in Cells 5 and 7. A possible reason for this difference is the zone of elevated temperatures is migrating from Cell 5 to Cell 7 so moisture is being projected towards Cell 7 instead of Cell 6. In addition, leachate is not increasing in Cell 4 because the leachate sump in Cell 4 is located 20 m above the Cell 5 and Cell 7 sumps so leachate drainage and pump operation hours are significantly lower in Cell 4.

5.2.4 Elevated Gas and Leachate Pressures

Table 5.1 shows that MSW landfills under anaerobic biodegradation typically exhibit pressures up to 3 kPa. Stark et al. (2012) found that gas pressures increased to 45 kPa in a facility experiencing APW reactions and smoldering combustion. Subsurface combustion has been found to display significant gas pressures, in some cases as high as 75 kPa (Illinois EPA 2006). Several mechanisms can contribute to increased gas pressures, which are discussed below. Following the ideal gas law and assuming a landfill is a constant volume boundary, gas temperature and pressure are directly proportional and thus increase simultaneously as shown below:

$$PV = nRT \tag{5.1}$$

where P is pressure (kPa), V is volume (L), n is moles of gas, T is temperature (Kelvin), and R is the ideal gas constant (8.314462 L kPa K^{-1} mol^{-1}). For example, landfill gas is approximately atmospheric pressure (101.3 kPa) at a temperature of 40°C (Young 1992; Bogner et al. 1988). If

subsurface temperature increases to 100°C, internal gas pressures should increase by 19.5 kPa. Convection can also drive hotter gases to the surface where they can accumulate under a soil or geomembrane cover and result in odors. Furthermore, warmer gases carry a higher percentage of water vapor that will condense and reduce the efficiency of the gas collection system wells and lateral header pipes. The clogged or "watered-in" wells can reduce gas extraction capability thus permitting subsurface pressures to build-up. Similar to the APW reaction reported in Stark et al. (2012), elevated temperatures can initiate gas generating processes, such as combustion and pyrolysis. For temperatures of 300 to 700°C, pyrolysis yields about 30 to 50% by weight (wt) of char, 30 to 50% wt liquid, and 20 to 40% wt of gas (Buah et al. 2007; Rampling and Hickey 1988; Williams and Besler 1993; Lin et al. 1999). In addition, Baggio et al. (2008) report that pyrolysis at 500°C of 1 kg of MSW generates around 300 g of gas. As a result, elevated gas pressures could be explained by the increased gas production caused by combustion and pyrolysis. In conjunction with additional gas production, temperatures can damage and/or compromise gas extraction wells and lateral headers by melting. Eventually, the gas collection system can become overwhelmed and lead to elevated gas pressures.

When gas and leachate migrate to landfill side slopes and are impeded by the cover system (soil or flexible geomembrane), gas pressures and leachate can accumulate and cause gas and leachate outbreaks. The elevated leachate and gas pressures occasionally manifest themselves as a "leachate geyser" (Figure 5.6) and can eject 9 to 11 m into the air (Stark et al. 2012). These leachate geysers also can be encountered when borings are drilled in the waste to install gas wells or for exploratory purposes. In some instances, the soil cover system is replaced with an exposed flexible geomembrane to control odors. Although the geomembrane encapsulates the surface, outbreaks can still occur at seams, geomembrane defects, and gas wellhead connections.

5.2.5 Slope Movement and Settlement

Slope instability and movement have occurred at landfills with elevated temperature, leachate, and/or gas pressures (Stark et al. 2012; Stark et al. 2010; Koelsch et al. 2005; Jafari et al. 2013; Hendron et al. 1999; Blight 2008). The slope failure described by Stark et al. (2012) resulted in over 6 m of displacement and waste being located outside of the permitted landfill boundary. In general, slope movement is preceded and accompanied by forceful gas and leachate outbreaks in

elevated temperature situations. Mechanisms for slope instability include elevated gas pressures, perched leachate surfaces, and/or reduced MSW shear strength (Stark et al. 2010). For example, the interconnecting plastics and other reinforcing materials that contribute to the high shear strength of normal MSW are consumed, degraded, burnt, and/or decomposed at elevated temperatures (see Figure 5.7 showing charred waste). The shearing or tilting of vertical gas wellheads, tension cracks at the slope crest or at some point along the slope, and bulging of the slope toe or some point along the slope are indications of slope movement.

Figure 5.8 shows the cumulative slope movement and settlement obtained from stability pins installed throughout Cells 4 through 7 at the subject landfill (locations shown in Figures 5.2(a) and 5.2(c)). The northing, easting, and elevation of the stability pins were measured monthly to evaluate time-lapse slope movement and settlement. The change in elevation is compounded each month to determine the cumulative settlement. Surface movement is represented by vectors that show the direction and magnitude of slope movement. The vector angle is computed each month from the delta northing and easting values and the vector length is defined by the total distance travelled since the start of stability pin monitoring (September 2009). As an example, a stability pin was originally located at a northing and easting of 400 m and 500 m, respectively. After two years, the pin moved a total of 3 m and 4 m in the positive northing and easting directions, respectively. The cumulative distance is 5 m and the angle of movement is ~325° (reference: 0° points in the easting direction; angle increases counterclockwise).

In September 2010, i.e., one year after the detection of elevated temperatures, (see Figure 5.8(a)), a cumulative settlement of ~4 m had occurred and formed a bowl-like shape in the surface of Cell 5. Two years after the onset of elevated temperatures, i.e., September, 2011, (see Figure 5.8(b)), the settlement bowl depth increased to 6 m and the bowl expanded radially into Cell 6. From September 2011 to February 2012, settlement significantly increased to 14 m and the settlement bowl extended into Cell 7 for the first time and approached the boundary of Cells 4 and 5. Cumulative settlement in the elevated temperature epicenter continued to rapidly increase through September 2012 and 2013. Figure 5.8(e) shows that about 20 m of settlement has occurred in Cell 5 by 2013. In this four year period, i.e., September 2009 to 2013, the average settlement rate in the “bowl” is 5 m/yr. The initial waste height in Cell 5 is 85 m and the corresponding strain is ~24% by 2013. During the four years of monitoring, the settlement bowl migrated into Cell 6 before advancing to Cell 7. More importantly, Figure 5.8 shows the settlement associated with

elevated temperatures did not impact Cell 4. The settlement within Cell 4 ranges between 0 and 2 m, which corresponds to a much lower average settlement rate of 0.5 m/yr.

In September 2010 (Figure 5.8(a)), the slope movement vectors in Cells 4, 6, and 7 are barely visible, i.e., slope movements are less than 0.15 m. However, slope movement vectors in Cell 5 (along cross-section A-A') indicate that ~2 m of slope movement had occurred by September 2010. In Cells 6 and 7 in Figure 5.8(b), the movement vectors are still small, e.g., cumulative movements are less than 0.5 m, but it is evident they are pointing out towards the landfill perimeter. The vector arrows in Cell 5 have increased to ~4 m and they project in the direction of the Cell 5 slope because of the outward migration of the settlement bowl. After significant deepening of the settlement bowl by February 2012, slope movement can be directly linked to the movement of the settlement bowl (Figure 5.8(c)). For example, the movement vectors projecting outward of Cell 5 are smaller in Figure 5.8(c) because the epicenter of the settlement bowl has settled sufficiently and it is dragging the slope crest into the settlement "crater" or bowl. The migration of the settlement bowl into Cell 7 shows vector arrows projecting towards the exterior slope of Cell 7, with slope movements of ~2 m outward. This trend continues through September 2012 and 2013. In Figures 5.8(d) and 5.8(e), the movement vectors indicate the Cell 7 slope has moved about 15 m. Thus, Figure 5.8 illustrates the dual nature or time dependence of the slope movement due to migration of the elevated temperatures. First, as the settlement bowl expands, gas and leachate pressures exert a force that thrusts the adjacent exterior slope outward. Second, if the settlement bowl continues to deepen, the slope movement can reverse directions and drift backwards into the center of the elevated temperature zone or settlement bowl. This explains why the vector arrows can increase and decrease in size with time and vector angles can reverse direction. The comparison of slope movement and settlement in Figure 5.8 shows the subject elevated temperature event started in Cell 5 and expanded into Cells 6 and 7. The settlement bowl advanced into Cell 6 first and the movement vectors indicate cumulative slope movements of ~4 m, but Figure 5.8 shows the major thrust from the elevated temperatures is primarily towards Cell 7.

5.3 Progression of Elevated Temperature Indicators

The case study described in Section 5.2 identified the following progression indicators after the onset of elevated temperatures: (1) changes in landfill gas composition, (2) elevated gas and waste temperatures, (3) increased leachate migration and volume, (4) elevated gas and leachate pressures, (5) slope movement, and (6) settlement. This section arranges these indicators into a chronological sequence to facilitate understanding of the location and movement of the elevated temperatures. In particular, a two-dimensional (2-D) cross-section through the subject landfill is used to illustrate gas composition changes along a line of gas wells with time. In particular, cross-section A-A' in Figure 5.2(a) traverses from Cell 5 to Cell 7 and bisects the elevated temperature region that started in Cell 5 in 2009. The profile of cross-section A-A' and location of gas extraction wells B-1 to B-6 are shown in Figure 5.9. Furthermore, a stability pin and gas extraction well in Cell 5 provides a means to relate changes in gas composition with MSW settlement with time.

Figure 5.10 shows the trends in the CH_4/CO_2 ratio for gas extraction wells B-1 through B-6 in cross-section A-A'. Gas wells B-1 and B-2 are located in Cell 5 and the initial elevated temperature zone, so the CH_4/CO_2 ratio is about 0.1 in September 2009 and remains below 0.2 throughout the monitoring period. However, gas wells B-3 through B-6 are located outside of the immediate elevated temperature zone and they show CH_4/CO_2 ratios near unity from September 2009 to December 2010. In February 2011, the CH_4/CO_2 ratios decrease rapidly in these wells to values below 0.3. This decline in each well suggests that internal landfill processes changed simultaneously even though the distance from B-3 to B-6 is only about 250 m.

Similar to the gas extraction well in Figure 5.4, Figure 5.11 shows that the decline in CH_4/CO_2 ratio is accompanied by increased CO and hydrogen levels. For example, Figure 5.11(a) shows that CO concentrations begin to increase at CH_4/CO_2 ratios of 0.8. Carbon monoxide levels continue to increase from 500 to 8,000 ppmv for CH_4/CO_2 ratios below 0.3. Figure 5.11(b) shows that hydrogen levels are generally less than 8% v/v when the CH_4/CO_2 ratio is above unity. As the gas ratio decreases to 0.4, hydrogen levels continue to increase to ~36% v/v. Figure 5.11(b) indicates that hydrogen is present at CH_4/CO_2 ratios above unity. However, the gas wellheads in Cell 4, which were not impacted by elevated temperatures, show no evidence of hydrogen gas. This indicates the presence of hydrogen (< 5% v/v) when the CH_4/CO_2 ratio is above unity and is a result of internal landfill gases mixing from elevated temperature and biodegradation areas. Therefore, hydrogen concentrations of about 35% v/v at low CH_4/CO_2 ratios in gas extraction

wells B-3 to B-6 are a consequence of the elevated temperatures. Based on Figure 5.10 and Figure 5.11, landfill methane and carbon dioxide change across the landfill to primarily carbon dioxide, carbon monoxide, and hydrogen during the movement/expansion of the elevated temperatures.

Figure 5.12 shows the cumulative settlement of two stability pins. One pin is located in Cell 5 and subjected to elevated temperatures while the other pin is in Cell 4, where normal anaerobic biodegradation still prevails. The Cell 4 or biodegradation pin shows that settlement for a 60 m waste height is about 1.3 m in ~1,300 days, which corresponds to a settlement rate ~0.5 m/yr. The Cell 5 or elevated temperature pin initially settles at the same rate as the biodegradation pin or about 0.5 m/yr. However, settlement begins to accelerate as the influence of elevated temperatures expands towards the stability pin. For example, vertical settlement is 0.5 m after an elapsed time of 800 days. By the end of the monitoring period, settlement is over 10 m (elapsed time of 1,600 days). The corresponding settlement rate of 4.6 m/yr is about a magnitude greater (factor of ~9) than the biodegradation rate of ~0.5 m/yr. Figure 5.12 also compares settlement with the CH_4/CO_2 ratio obtained from a gas extraction well located in the immediate vicinity of the Cell 5 pin. The CH_4/CO_2 ratio is above unity until an elapsed time of 600 days by which it declines to a ratio of ~0.35 in 50 days. The CH_4/CO_2 ratio gradually decreases to ~0.1 after t= 1,150 days. Before settlement transitions from normal biodegradation to an accelerated rate, the CH_4/CO_2 ratio decreased to values that indicate anaerobic processes are inhibited. Thus, Figure 5.12 shows that rapid settlement occurs after methane composition decreases and is a delayed indicator of elevated landfill temperatures and cannot be used to estimate the current location of the smoldering combustion. In this landfill case, a time gap of ~200 days occurs during which landfill gas is quickly changing composition, gas/leachate pressures and volume are increasing significantly and contributing to slope movement before the onset of excessive settlement. As a result, the case study discussed herein shows that the initiation and expansion of elevated temperatures results in a sequence of indicators that delineates the location, boundary, and movement of the zone of elevated temperatures. These indicators follow this systematic progression:

(1) Decreased ratio of CH_4 to CO_2 flow rate ratios;
(2) Elevated waste and gas temperatures;
(3) Elevated carbon monoxide and hydrogen levels;
(4) Increased leachate volume and migration;

(5) Elevated gas and leachate pressures;

(6) Slope movement; and

(7) Excessive settlement.

5.4 Field Manifestations and Landfill Operations

The flow chart in Figure 5.13 couples the progression of landfill indicators with field observations and landfill operations. For example, odors can emanate from the cracked soil cover as the landfill gas composition changes. In addition, combustion residue in gas well pipes may accumulate. Hydrogen gas can reduce flare combustion efficiency corrode integral parts of the flare system. The landfill operator is tasked to ensure soil cover integrity, expand the capabilities of the gas extraction and collection system, and install odor neutralizers to combat foul odors and possible air intrusion. Elevated gas and waste temperatures manifest when wellhead temperatures are > 55°C (131°F) and damage to the wellhead or cracked soil cover are observed. The landfill operator applies to the regulatory agency for Higher Operating Variances (HOVs) for each gas wellhead. HOVs allow the landfill operator to show that methane production is not inhibited at the elevated wellhead temperatures of 65°C (149°F). During the HOV, monitoring frequency of oxygen levels (< 5% v/v), wellhead vacuum (negative pressure), and gas temperature are increased. Leachate color typically changes from a pale brown to black color, contains high concentrations of particulates, and resembles an oil-like consistency. The facility operator is often required to construct a pre-treatment plant on-site to address the contaminants in the leachate before transporting it off-site. When elevated gas and leachate pressures cause outbreaks, the operator is recommended to install a temporary flexible membrane liner (FML). Indicators of slope instability include tension cracks in the soil cover, toe bulging, and possible titled or pinched gas wellheads. For affected slopes, a toe buttress is constructed to balance the driving forces, and a slope monitoring system is devised for slopes that may experience instability due to elevated temperatures. Rapid settlement can cause large drops in landfill height, which can tear and rip the FML cover system. It is imperative that the landfill operator monitor the integrity of the FML to prevent air intrusion. In practice, the landfill operator can use Figure 5.13 and the field manifestations to identify the current progression of elevated temperatures in the landfill and develop an operational response.

5.5 Elevated Landfill Temperature Processes

This section discusses biological and/or chemical processes that can elevate temperatures to generate carbon dioxide, hydrogen, and carbon monoxide gases, increase gas and leachate production and pressures, initiate slope movement, and cause excessive settlement.

5.5.1 Biological Processes

Acetogenesis is the biological process that bridges the acidogenesis and methanogenesis stages in anaerobic decomposition (Barlaz et al. 1989). Acetogenic microorganisms break down the end of acidogenesis into acetic acid, carbon dioxide, and hydrogen. Next, methanogenic microorganisms convert these products into methane and carbon dioxide. Methanogenic activities are reduced at temperatures above 55°C and generally inhibited at temperatures exceeding 65°C (Hartz et al. 1982; Cecchi et al. 1993; Mata-Alvarez and Martinez-Viturtia 1986; Pfeffer 1974). However, acetogens have a higher temperature tolerance than methanogens. For example, Lee et al. (2008) monitored the performance of anaerobic digesters fed with artificial kitchen waste and operated at thermophilic temperatures. Although methane conversion efficiencies were high at 55°C, they decreased with increasing temperature and methane was not produced over 73°C. The researchers characterized the microbial population and found that methanogens were dominant below 65°C and acetogens were dominant over 73°C. Similarly, Ueno et al. (2007) reports that fermentative hydrogen accumulation from pulverized garbage and shredded paper waste dominated over methane production in a digester seeded with thermophilic fermentative bacteria and operated at 60°C. Under an elevated temperature scenario, methanogenesis is reduced or inhibited while hydrogen, carbon dioxide, and acetic acid may build up as a result of ongoing acetogenesis processes. However, waste temperatures should be in the thermophilic region and less than 80°C because biological activity is inhibited when temperatures exceed 80°C (Hogland and Marques 2003).

Carbon monoxide is typically not detected or found at low concentrations, e.g., < 100 ppmv, in normal operating anaerobic and bioreactor landfills (FEMA 2002; Christensen et al. 1996; Rettenberger and Stegmann 1996; Christensen and Manfredi 2011). Powell et al. (2006) monitored an aerobic landfill and detected average CO levels of 245 ppmv with a maximum concentration of 1,200 ppmv. The study reports waste temperatures remained below 76°C, so

Powell et al. (2006) conclude the CO was not produced by combustion even though CO concentrations significantly increased in locations where the impact of air addition was more pronounced. However, Evidence of biological sources of CO is reported in relevant literature (Thauer 1998; Diekert et al. 1984; Bott and Thauer 1987). For example, methanogenic archaea can utilize CO as a nutrient to produce methane (Thauer 1998). Diekert et al. (1984) found that acetogenic bacteria can mediate the formation of CO from carbon dioxide. Bott and Thauer (1987) demonstrate that cell suspensions of methanogens incubated in serum bottles at 37°C and 65°C formed up to 15,000 ppmv (1.5% v/v) CO in presence of a mixture 80% v/v hydrogen and 20% v/v carbon dioxide. The laboratory experiments suggest that CO can be formed by biological processes but the experiments require mesophilic and/or thermophilic temperatures and precise gas concentrations, e.g., 80% v/v H_2 and 20% v/v CO_2. In contrast, MSW landfills are heterogeneous mixtures of waste, gas, and leachate and elevated wellhead temperatures are above 80°C.

5.5.2 Chemical Processes

The presence of CO in MSW landfills is associated with subsurface fires (Ettala et al. 1996; Frid et al. 2009; Bates 2004; Martin et al. 2013; Stearns and Petoyan 1984; Sperling and Henderson 2001). Carbon monoxide is generated during smoldering combustion when insufficient oxygen gas is present to allow complete combustion and generation of water vapor and carbon dioxide (Shafizadeh and Bradbury 1979; Quintiere et al. 1982; Pitts et al. 1994; Ohlemiller 1995). The stoichiometric CO concentration determined from Reaction 2.4 is about 54,500 ppmv, which represents an upper bound estimate. The average and maximum CO concentrations for the case study are 5,300 and 14,400 ppmv, respectively. In comparison, Quintiere et al. (1982) state that smoldering combustion results in CO of 100 to 10,000 ppmv. This suggests that increased CO concentrations are a manifestation of smoldering combustion.

Hydrogen can be generated from the hydrolysis and/or corrosion of aluminum (Reaction 2.3) and iron. The presence of aluminum dross and salt cake wastes in landfills has resulted in temperature increase and hydrogen generation (Jafari et al. 2014a). For example, Stark et al. (2012) found hydrogen levels increased to 40% v/v after an APW reaction was initiated. However, this reaction depends on certain wastes to be disposed at the site. For the case study described herein,

an exhaustive search through weight station receipts did not yield substantial evidence of aluminum/iron waste disposal and possible reaction.

Hall et al. (2007) report that landfill gas emitted hydrogen levels in excess of 20% v/v from regions where water was slowly introduced into an area with a suspected hot spot. The authors do not provide the mechanism for elevated hydrogen levels. One possible explanation is pyrolysis, i.e., the chemical breakdown of a substance to lower weight molecules in the presence of elevated temperatures and absence of oxygen (Fire 1996). Pyrolysis of cellulosic materials can cause the generation of carbon monoxide, carbon dioxide, and hydrogen gases, but typically not until temperatures are in the range of 250 to 500°C (Kubler 1982; Pitts et al. 1994; Shafizadeh and Bradbury 1979). In particular, Shafizadeh and Bradbury (1979) state that pyrolysis of cellulosic materials, such as wood, paper, and other fibrous products, at temperatures less than 300°C yields products of char and a gas mixture containing carbon monoxide and carbon dioxide. Typical carbon monoxide and carbon dioxide concentrations are 0.25 kg and 0.75 kg, respectively, for 1 kg of total gas produced (Neves et al. 2011). At temperatures above 300°C, the cellulose is decomposed by an alternative pathway, and the major evolved product is liquid, gases (carbon dioxide, carbon monoxide, hydrogen), and char (Antal et al. 1980). The evolution of hydrogen gas during pyrolysis first appears at low concentrations at 600°C, and generally reaches 20% v/v of gas composition by 700°C (Neves et al. 2011).

Alternatively, hydrogen gas can be generated at lower pyrolysis temperatures (200 to 250°C) by the water gas shift reaction. In this moderate exothermic reaction, carbon monoxide reacts with steam to form carbon dioxide and hydrogen gases (Demirel and Azcan 2012).

$$CO + H_2O \rightleftarrows CO_2 + H_2 \qquad \Delta H = -41.1\,kJ/mol \tag{5.1}$$

The conversion of carbon monoxide to hydrogen is thermodynamically favored at the low pyrolysis temperatures, but the reaction rate is kinetically favored at elevated temperatures (700°C). In other words, the process is temperature dependent, which means carbon monoxide is converted to hydrogen at 250°C but the conversion rate is slow.

5.5.3 Summary of Landfill Processes

Visual evidence of elevated temperatures is revealed through excessive MSW settlement. For rapid and excessive settlement to occur, combustion or another exothermic reaction is necessary to generate heat for the burning of MSW (see Figure 5.7). Thermogravimetric analyses provide a range of temperatures for MSW to thermally decompose. For example, Sørum et al. (2001) pyrolysed the cellulosic fraction and plastic components of MSW and showed that the major weight loses of the cellulosic matter occurred between 250–400°C. The thermal degradation of polystyrene, polypropylene, low-density polyethylene and high-density polyethylene occur between 350–500°C. Williams and Besler (1996) investigated the thermal decomposition of cellulose and hemicellulose and establish that thermal decomposition of hemicellulose begins at 250°C while cellulose decomposition occurs starts at 325°C. Therefore, temperatures in the settlement bowl should be 240 to 380°C to degrade the cellulosic fraction of MSW, while temperatures ranging from 410 and 500°C degrade the plastic components. Subsurface temperatures sufficient to initiate pyrolysis have been measured in MSW landfills. For example, smoldering combustion temperatures observed in MSW landfills have ranged from 200 to 300°C and as high as 700°C (Ettala et al. 1996; Lönnermark et al. 2008; Ruokojarvi et al. 1995). In addition, temperatures of 80 – 230°C were also measured for a deep fire and 309–406°C for a surface fire (Bergstrom and Bjorner 1992).

Because subsurface temperatures are not available in Cell 5 of this case study, evidence of CO within reported smoldering combustion concentrations suggests that incomplete combustion is occurring and generating heat for temperatures to be elevated for pyrolysis to occur. Because pyrolysis produces about 35% v/v CO (Neves et al. 2011) and MSW contains considerable moisture (30 to 40% wt) which is transformed into steam, the water-gas shift reaction seems a plausible explanation for appearance of hydrogen in gas extraction wells. Pyrolysis can also directly generate hydrogen gas, if the appropriate temperatures are present in the waste.

5.6 Summary and Conclusions

Elevated temperature events can significantly impact the behavior and operation of a MSW landfill. If not addressed in an expedient manner, elevated temperatures can result in damage to the landfill infrastructure (i.e., gas extraction, leachate collection, and liner system), slope

instability, and environmental conditions that adversely affect health and welfare of the local community. This chapter presented a case study to identify the indicators of elevated temperatures and arrange these parameters into a chronological sequence, as follows: (1) changes in landfill gas composition; (2) elevated waste and gas temperatures; (3) increased leachate volume and migration; (4) elevated gas and leachate pressures; (5) slope movement; and (6) excessive and rapid settlement. In addition, the case study provides the following conclusions:

- Gas wellhead temperatures should be correlated with downhole temperatures because they are more reliable, provide maximum temperatures, and show time-lapse changes. Wellhead temperatures typically under predict waste temperatures, e.g., by 20°C in the reported case, before the onset of elevated temperatures.
- During the expansion and/or migration of elevated temperatures, landfill gas changes from predominantly methane and carbon dioxide to carbon dioxide, hydrogen, and carbon monoxide in a short time period.
- The settlement rate estimated for anaerobic biodegradation is ~0.5 m/yr and ~4.6 m/yr for elevated temperatures (combustion and possible pyrolysis), which led to rapid and excessive settlement of 20 m in the center of the settlement bowl.
- A flow chart is provided to relate the progression of indicators to field observations and remedial measures taken by landfill operators. The field manifestations permit the landfill operators to understand the stage of the progression of indicators. Typical operation and maintenance recommendations are provided for the landfill operator to address elevated temperatures, odors, gas pressures, slope stability, and settlement.
- Biological and chemical processes were proposed to explain the changes in gas composition and settlement. Smoldering combustion and pyrolysis explain excessive settlement and generation of carbon monoxide. The water gas shift reaction and pyrolysis were proposed for hydrogen production. However, further research is necessary to determine the mechanism of hydrogen generation in MSW landfills when subjected to elevated temperatures.

5.7 Tables and Figures

Table 5.1 Summary of gas pressures for various landfill processes

Landfill Process	Gas pressure (kPa)
Biodegradation[a]	0.5 – 3
APW reaction[b]	0.5 – 45+
Subsurface combustion[c]	5 – 75+

[a]Bogner et al. 1988; Kerfoot 1993; Kjeldsen and Fischer 1995; Williams and Aitkenhead 1991; Wittman 1985; Nastev et al. 2001; Young 1992
[b]Stark et al. 2012; Martin et al. 2013
[c]Author's files

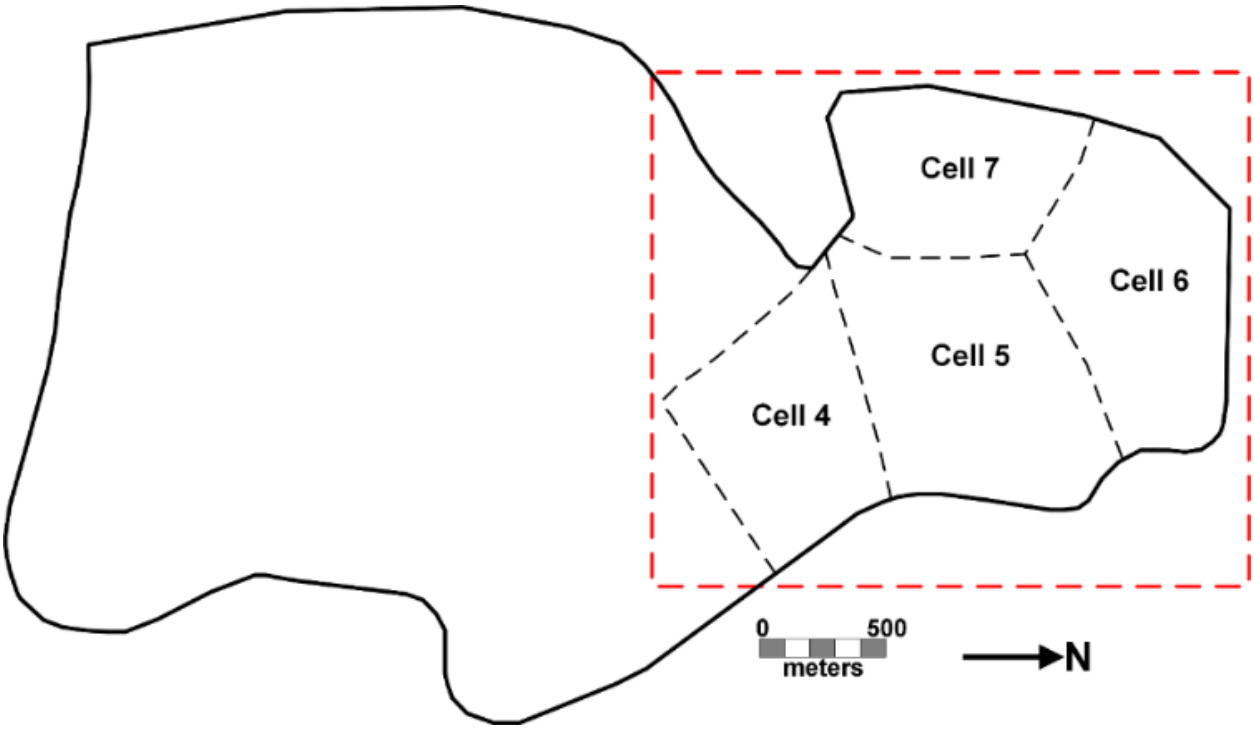

Figure 5.1 Site layout of case study (dashed box is impacted area)

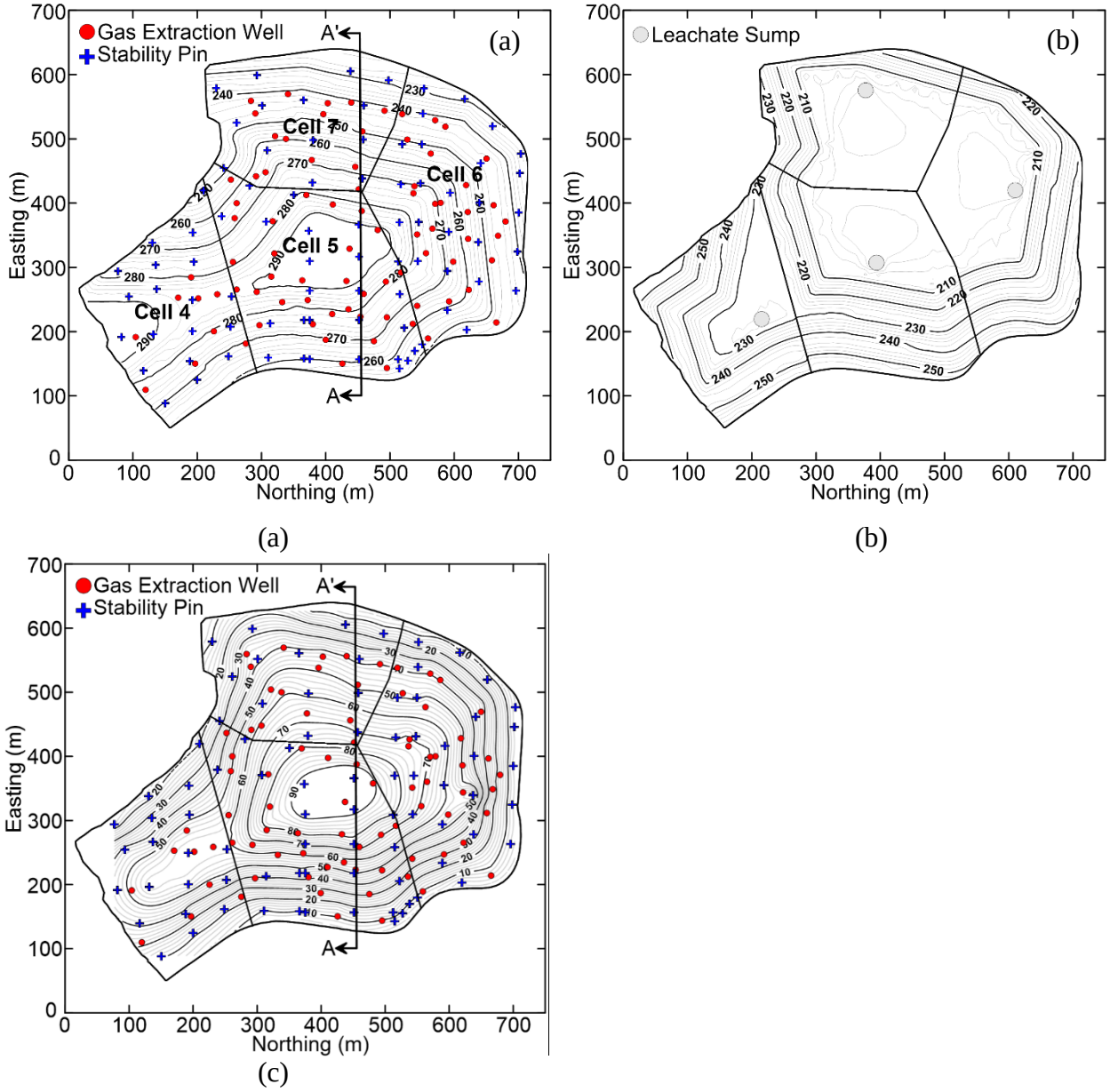

Figure 5.2 Plan view of Cells 4 through 7 showing: (a) location of gas extraction wells and stability pins, (b) leachate and composite liner system elevations, and (c) waste thickness contours

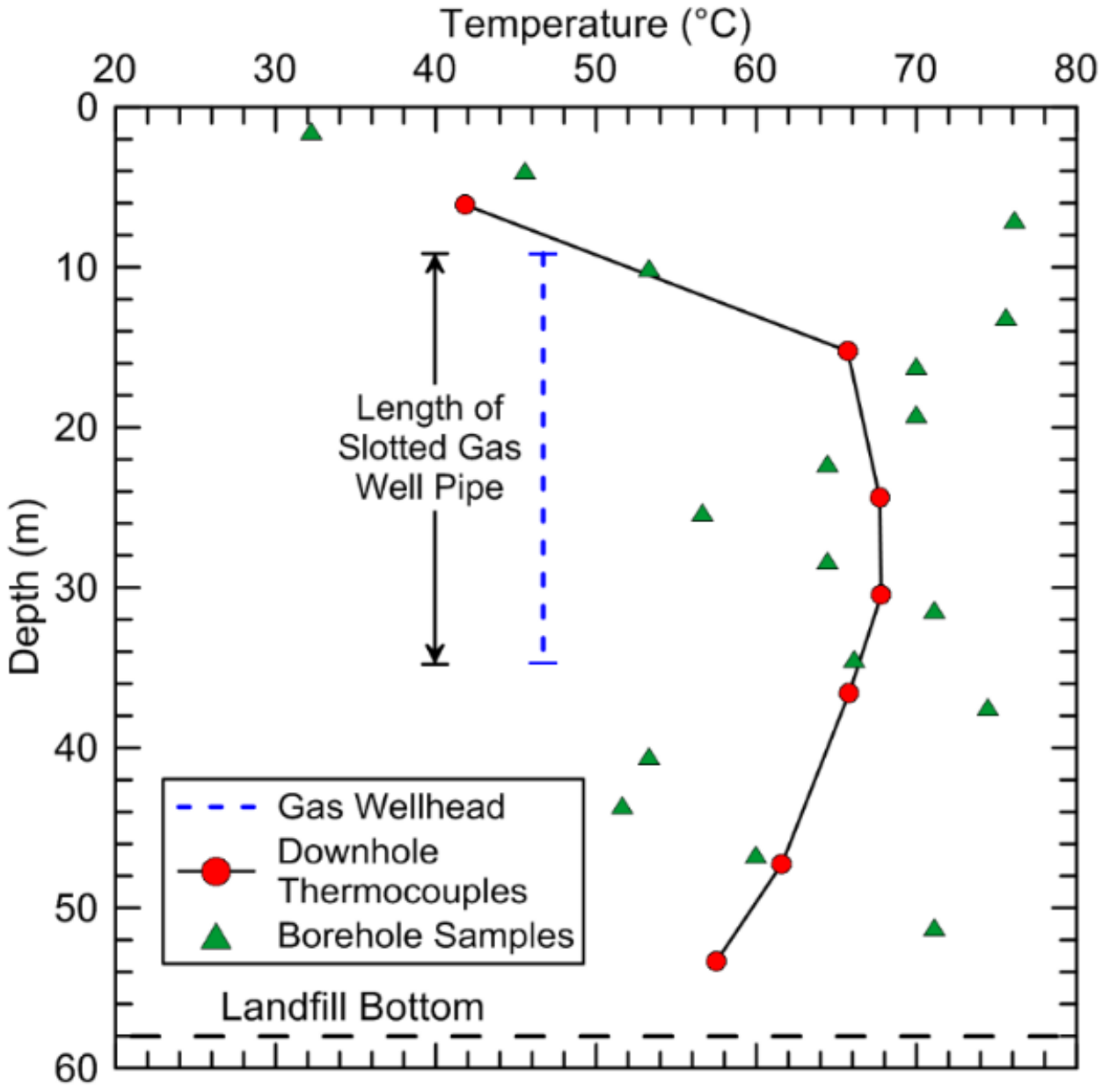

Figure 5.3 Comparison of subsurface temperatures in Cell 4 prior to elevated landfill temperatures

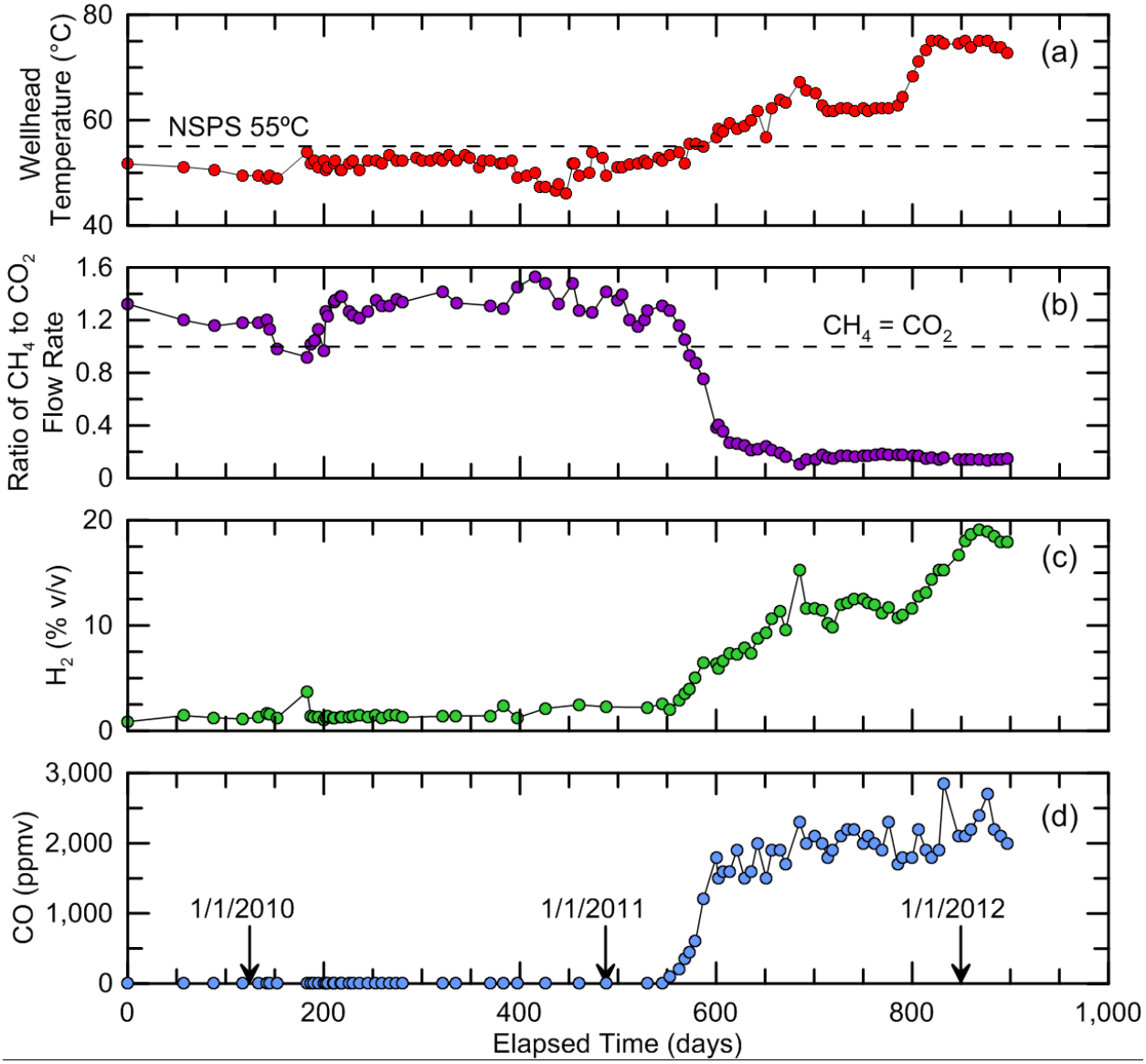

Figure 5.4 Gas extraction well trends in (a) temperature, (b) ratio of CH_4 to CO_2 flow rate, (c) hydrogen, and (d) carbon monoxide

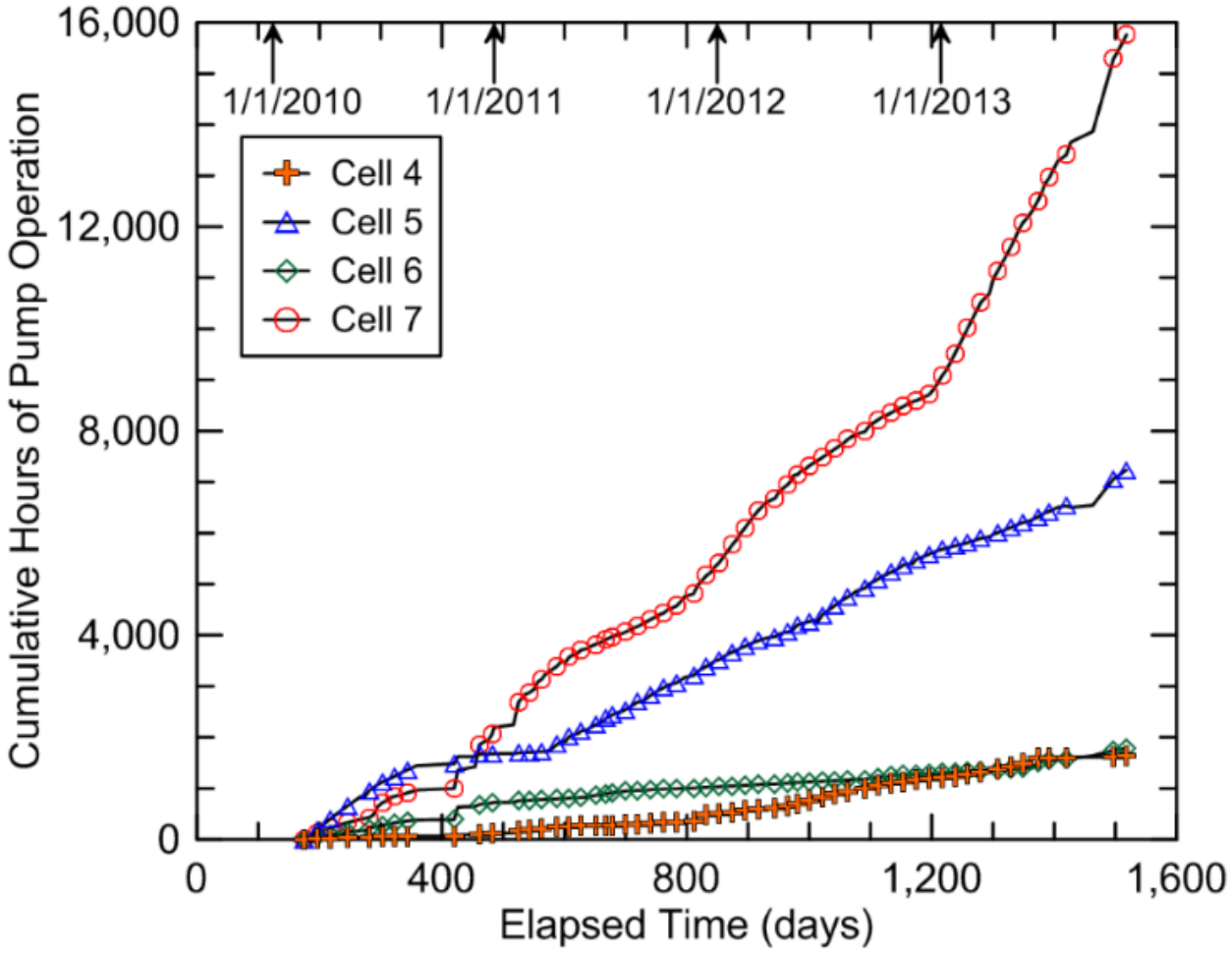

Figure 5.5 Leachate pumped from sumps located in Cells 4 through 7



Figure 5.6 Leachate outbreak of 2 to 4 m at MSW landfill side slope located in Northeast Ohio (photo courtesy of Ohio EPA)



Figure 5.7 Thermally degraded (combusted) waste from 100 mm diameter sample (MSW landfill located in Northeast Ohio)

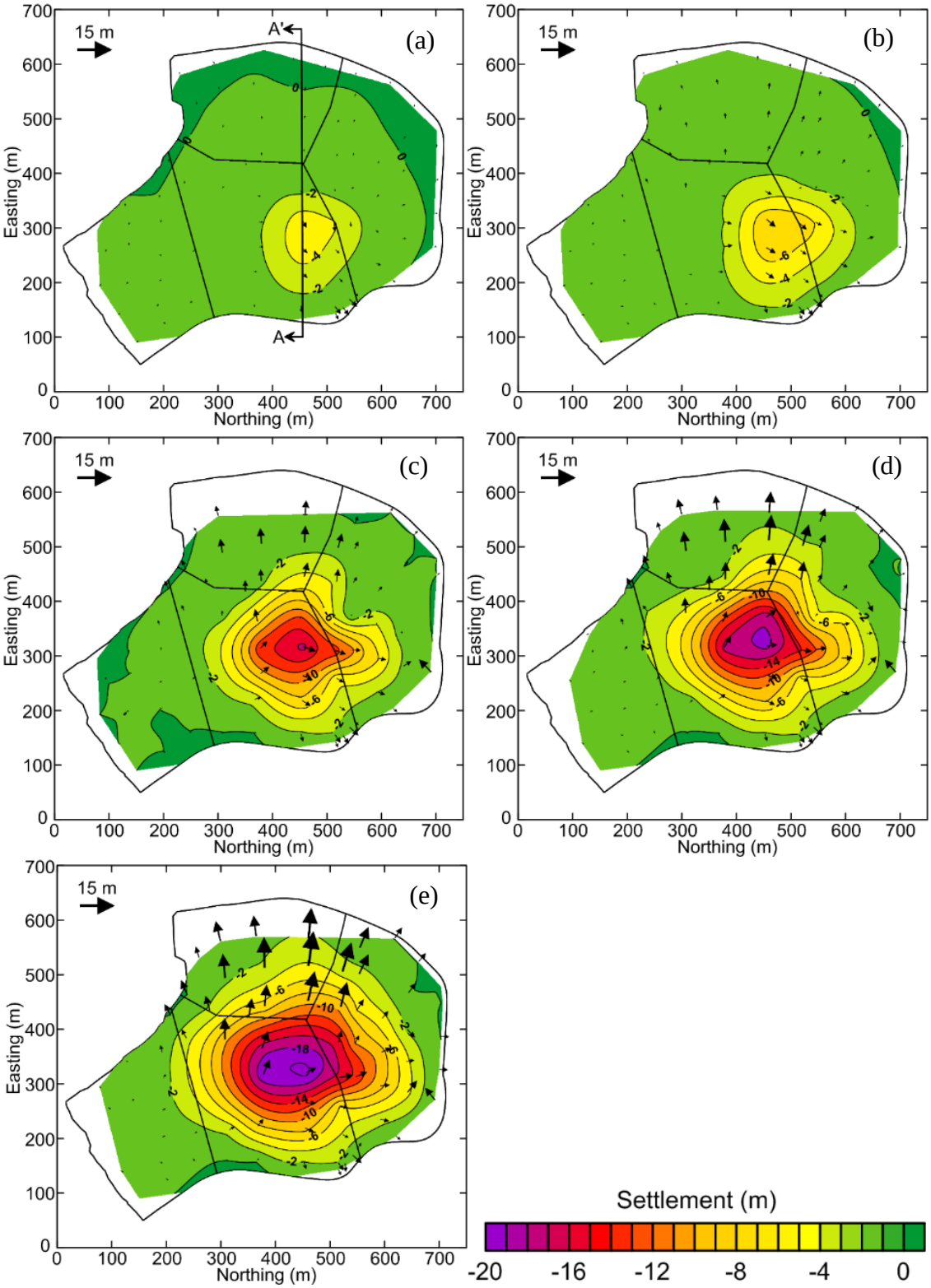

Figure 5.8 Spatial expansion of settlement and corresponding slope movement for: (a) September 2010, (b) September 2011, (c) February 2012, (d) September 2012, and (e) September 2013

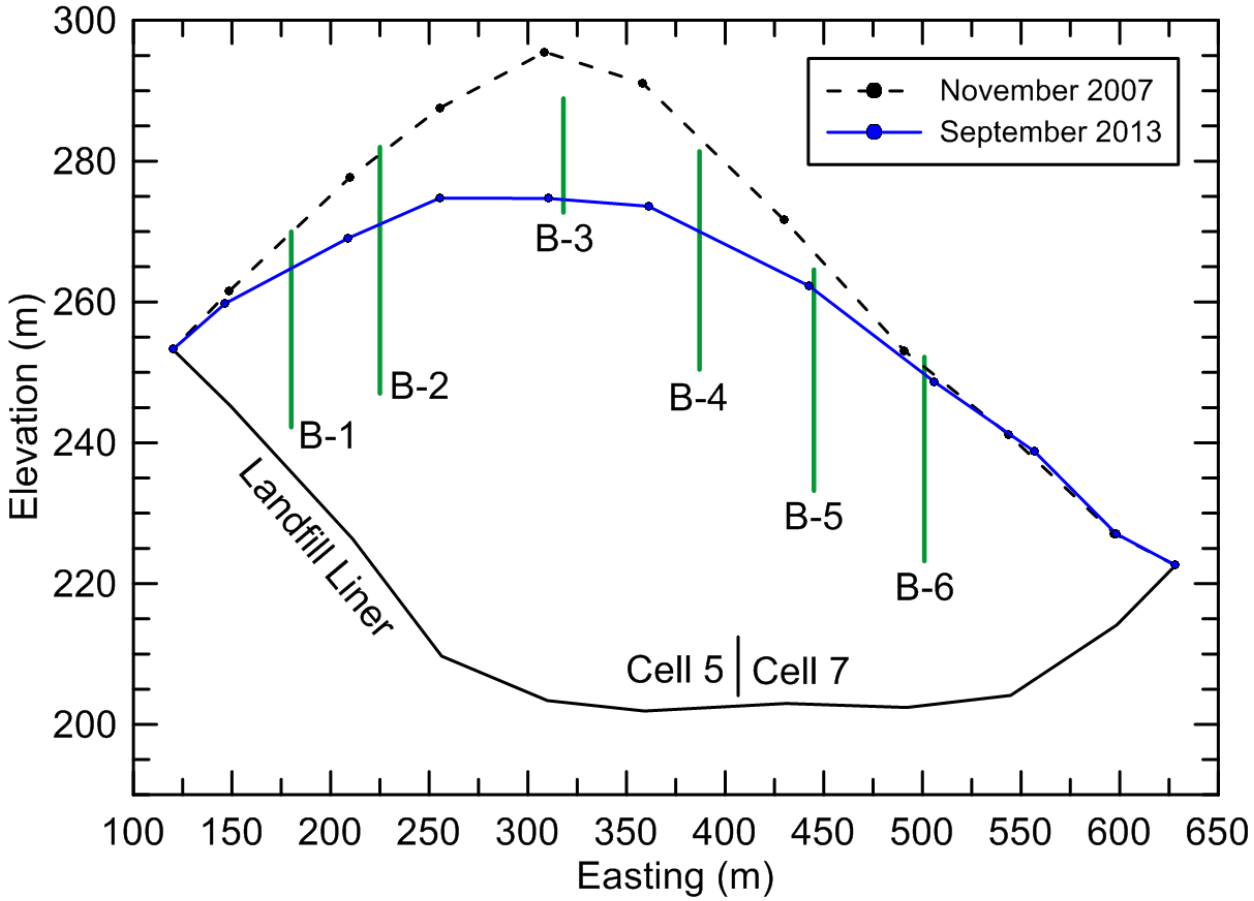

Figure 5.9 Profile of cross-section A-A' showing gas extraction wells B-1 to B-6 and landfill surface in November 2007 and September 2013

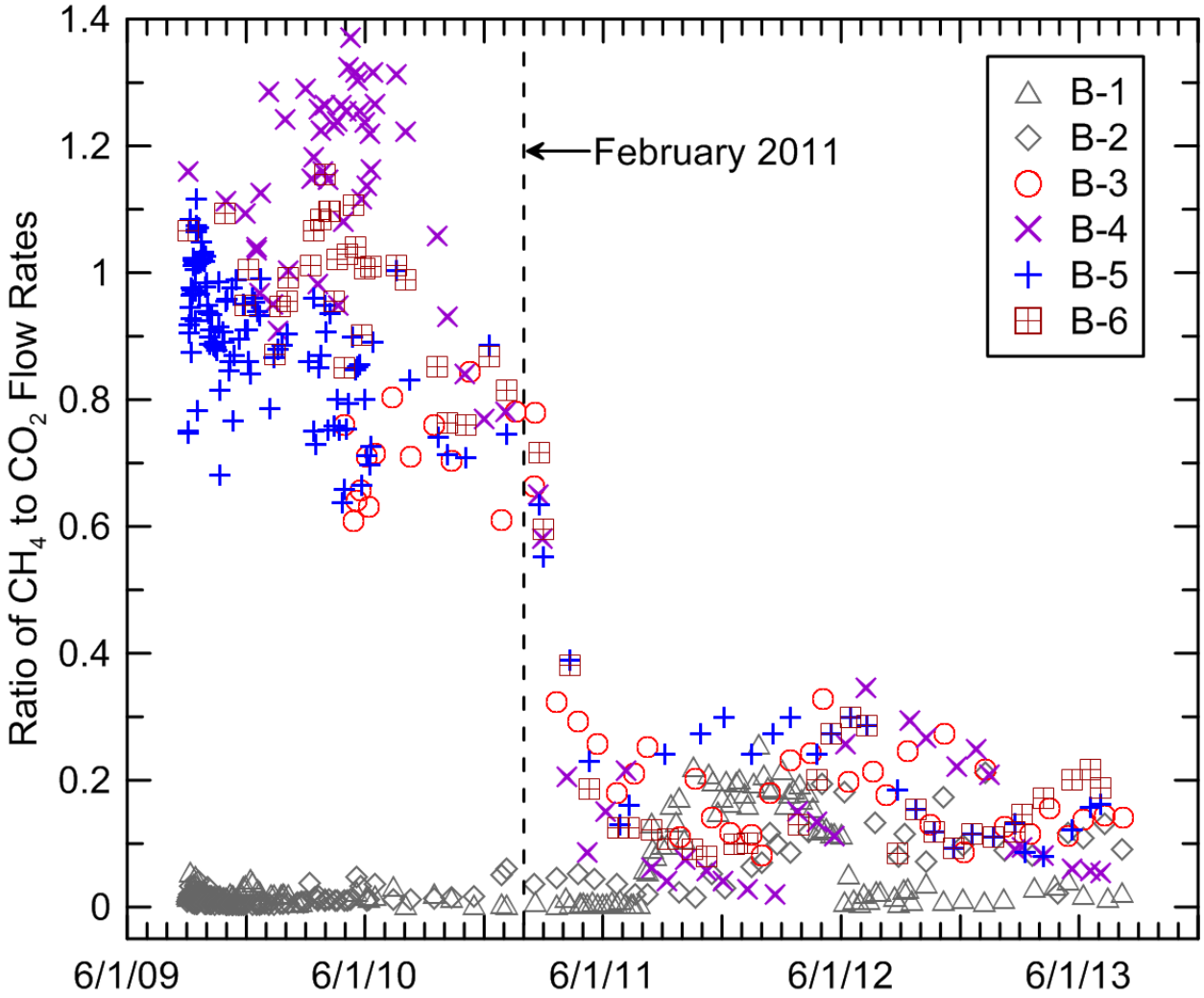

Figure 5.10 Trend of ratio of CH_4 to CO_2 flow rates along cross-section A-A' for gas extraction wells B-1 to B-6

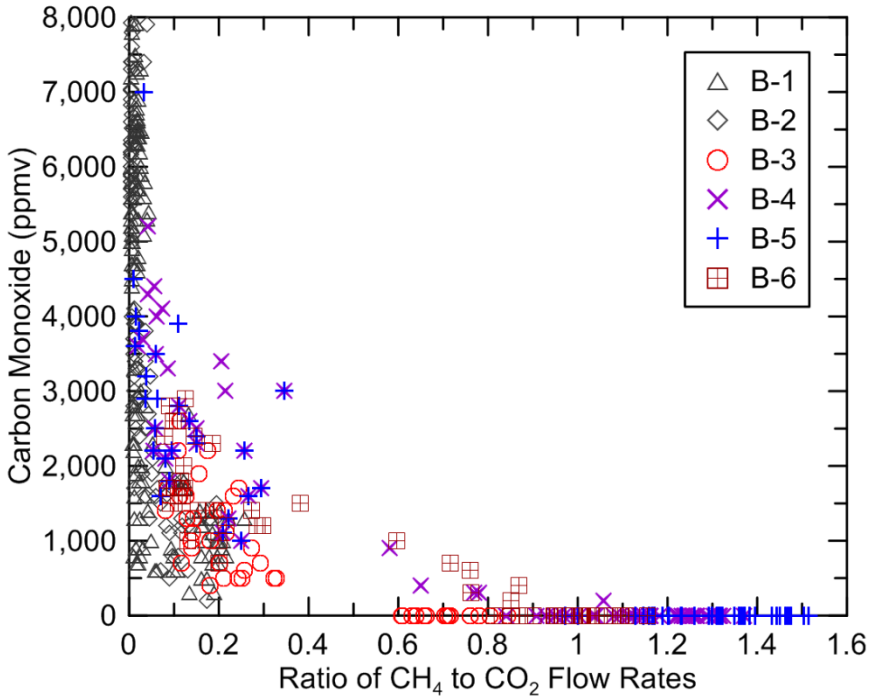

(a) Carbon monoxide

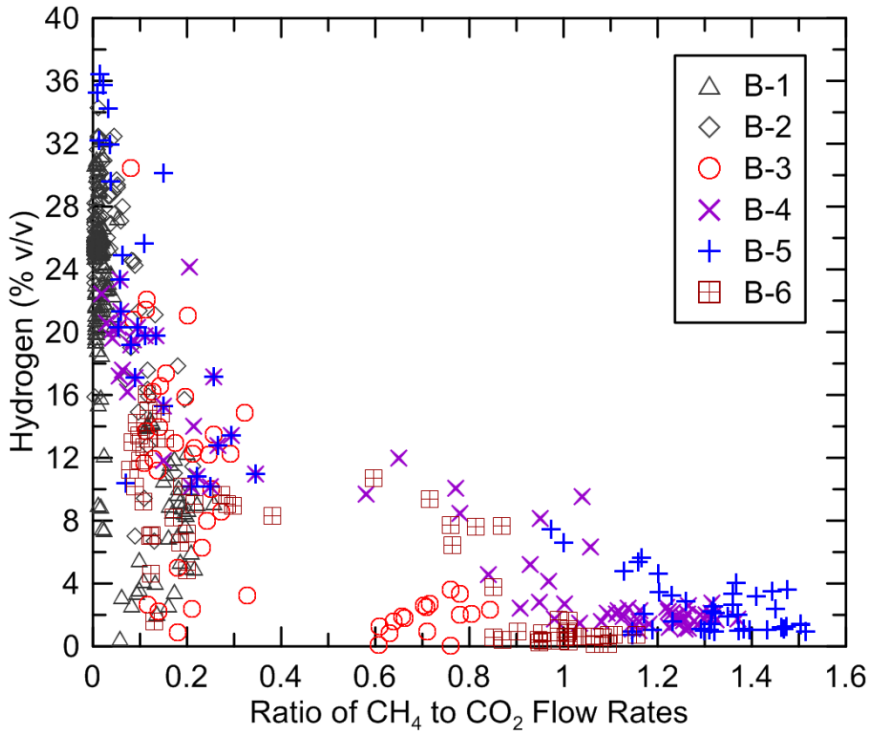

(b) Hydrogen

Figure 5.11 Gas extraction wells B-1 to B-6 trends for ratio of CH_4 to CO_2 flow rates with: (a) carbon monoxide and (b) hydrogen

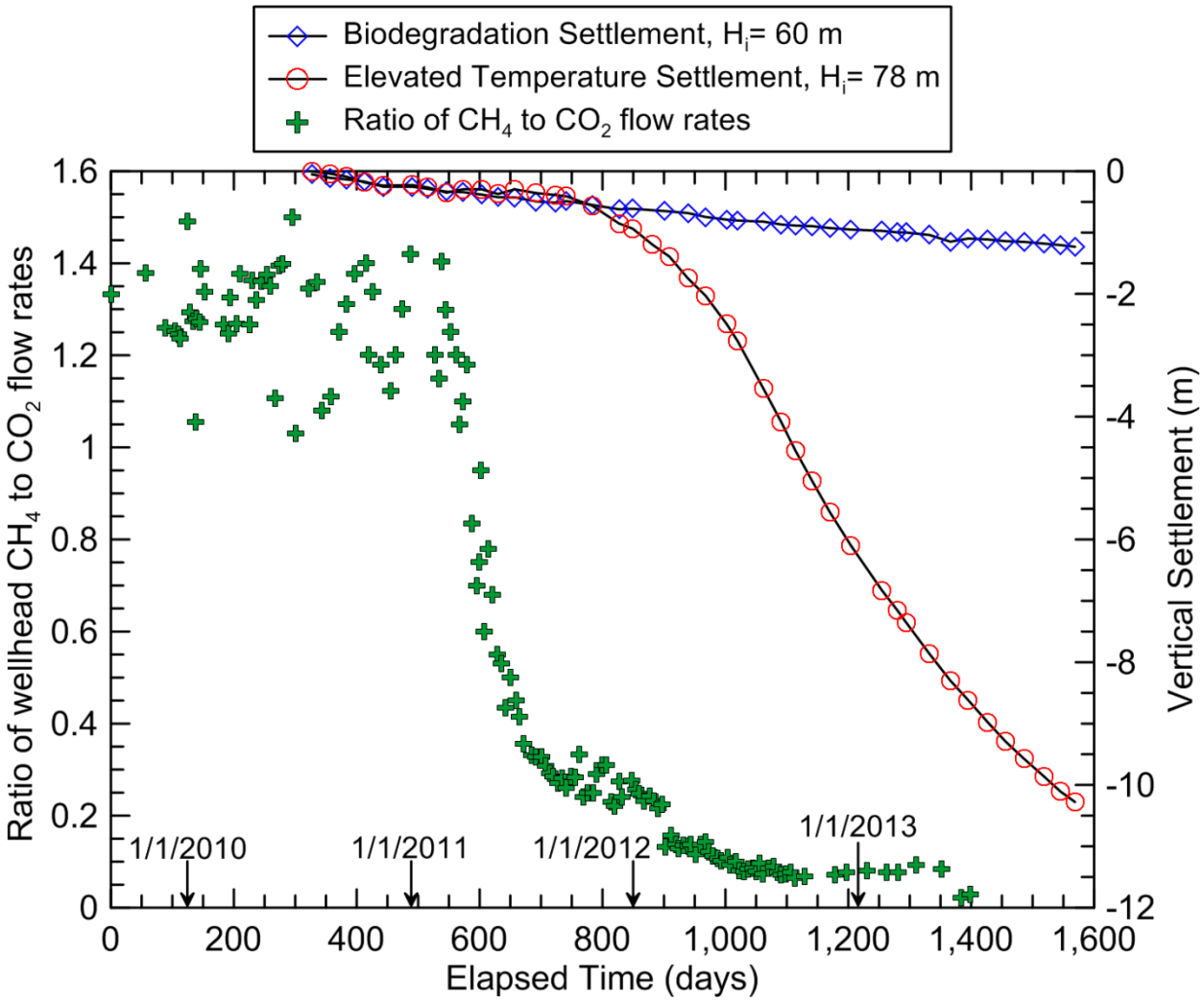

Figure 5.12 Comparison of elevated temperature and biodegradation settlement with timeline of decreasing ratio of CH_4 to CO_2 flow rates

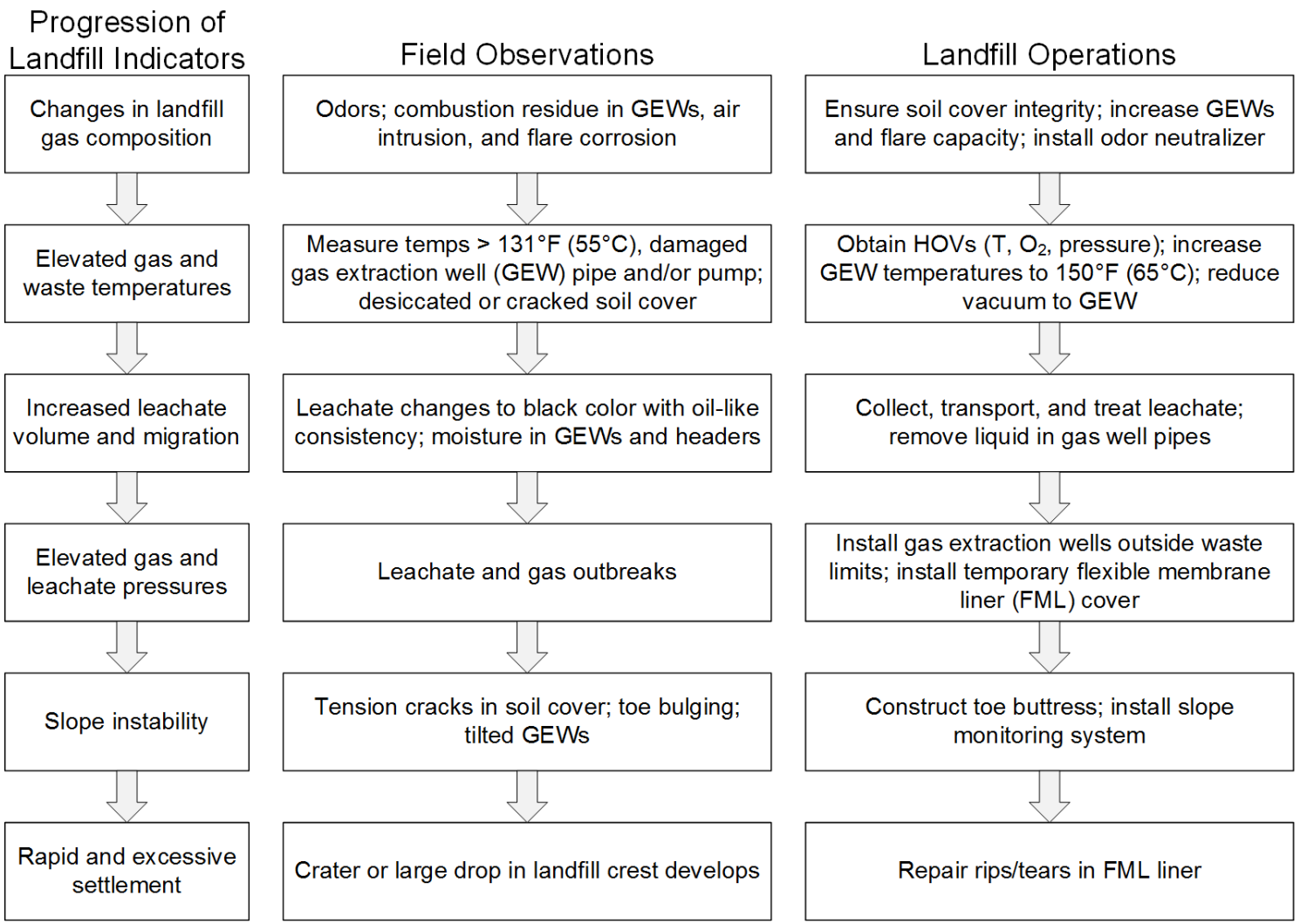

Figure 5.13 Flow chart showing progression of landfill indicators in conjunction with field manifestations of elevated temperatures and remedial measures acted by the landfill operators

CHAPTER 6

CLASSIFICATION OF ELEVATED TEMPERATURES IN MSW LANDFILLS

6.1 Introduction

A number of factors, such as aerobic decomposition, APW reactions, and smoldering combustion, can elevate temperatures in MSW landfills that subsequently impact operations, integrity of the cover and liner systems, degrade leachate quality and gas composition, decrease slope stability, and cause excessive settlement, odor migration, and leachate outbreaks operations (Lewicki, 1999; Jafari et al., 2014a; Stark et al., 2012; Øygard et al., 2005). In addition, elevated temperatures present a significant threat to the environment by emitting combustion byproducts and particulate matter to the atmosphere (Nammari et al. 2004; Ruokojarvi et al. 1995a,b; Lönnermark et al. 2008; Chrysikou et al. 2008).

After the onset of elevated temperatures, the impacted area can expand and advance to areas still undergoing anaerobic biodegradation. Chapter 5 presents a case study that shows the progression of indicators and describes the transition of landfill behavior with advancing elevated temperatures. These indicators include: (1) decreased ratio of CH_4 to CO_2 flow rates; (2) elevated waste and gas temperatures; (3) generation and accumulation of carbon monoxide and hydrogen gases; (4) increased leachate production and migration; (5) increased gas and leachate pressure; (6) slope movement; and (7) excessive waste settlement. Given this progression of landfill indicators, it is necessary to determine the appropriate indicators for characterizing the spatial and subsurface migration of elevated temperatures. This is important because landfill operators, consultants, and environmental agencies need a framework to demarcate the boundary of normal and elevated temperatures and movement rate and direction with time to evaluate contingency measures, such as installing an isolation break or containment barrier.

The objective of this chapter is to use the aforementioned indicators to delineate the three-dimensional (3D) boundary of elevated temperatures and monitor the growth and/or movement of the temperatures with time. To achieve these objectives, two case studies are presented to illustrate spatial migration and movement of subsurface elevated temperatures with time. The first case study involves the same facility described in Chapter 5 and shows trends in gas wellhead temperature, CH_4/CO_2 flow rates, and vertical strain rate. The second case study highlights the

application of downhole temperature arrays to monitor subsurface temperatures and then provides a comparison between gas wellhead and waste temperatures. Using this data, a conceptual model is proposed to classify an MSW landfill into five zones to determine the transition from normal operating areas to the elevated temperature region, which is important for public health, environmental safety, and appropriate response by landfill personnel, first responders, and regulatory agencies.

6.2 Case Study 1: Spatial Migration

Figure 6.1 shows an outline of the facility reported in Chapter 5, which is used herein to illustrate the spatial migration of elevated temperatures. Elevated temperatures were first noticed in Cell 5 in 2009 and during the course of four years, the impacted area expanded into Cells 6 and 7. In 2005 the site completed waste disposal, constructed an intermediate 0.6 m thick compacted soil cover, and installed a gas extraction and collection system to collect and combust methane gas as renewable energy. Prior to the elevated temperature event, the gas collection system for Cells 4 through 7 consisted of 82 gas extraction wells, lateral headers, and a flare station.

For an active gas collection system that meets NSPS requirements (40 CFR 60.753), landfill gas temperature, flow, pressure, and composition within each wellhead must be monitored monthly (US EPA 1999). As a result, the network of gas wellheads distributed across Cells 4 through 7 was used to generate contour plots of temperature and the ratio of CH_4 to CO_2 flow rates to define the onset of elevated temperatures and spatial expansion of the zone of elevated temperatures with time. In addition, the facility installed approximately 85 stability pins or surface survey monuments to monitor slope and soil cover movement with time. These pins or monuments were used to determine the vertical strain rate behavior for the site and develop contour plots showing locations of excessive settlement.

6.2.1 Gas Wellhead Temperatures

Although Chapter 5 indicates that gas wellhead temperatures may underestimate waste temperatures at depth, they provide an easy and routine procedure to evaluate changes in subsurface temperatures. Figure 6.2 shows temperature contours constructed using data from 82 gas extraction wells and the kriging interpolation function. In addition, gas wellhead oxygen levels

above the NSPS regulation of 5% v/v are shown in Figure 6.2. Elevated temperatures at this facility began in late 2009 in five (5) gas extraction wells in Cell 5 (Figure 6.2(a)) and by March 2010 (Figure 6.2(b)) the facility operators observed an expanded area of gas extraction wells experiencing temperatures above 65°C and as high as 90°C. At that time, temperatures remained between 30°C and 50°C in the unaffected cells. In September 2010, several gas wellhead temperatures in Cell 6 exhibited temperatures below 40°C. These isolated hot spots and cooler areas indicate that some gas wellheads are measuring elevated temperatures while the neighboring gas wellheads are reporting lower temperatures because of intrusion of cooler air that is cooling the waste and/or gas well pipe. For example, Figures 6.2(c) and 6.2(d) show high oxygen levels correspond to areas with cooler gas wellhead temperatures. Oxygen levels of 18 to 21% v/v typically indicate the extraction well pipes and/or wellhead connections may be compromised which is allowing air intrusion. As a result, the wellhead oxygen concentrations are similar to the ~21% v/v found in the atmosphere. However, there are areas where elevated oxygen concentrations were observed within the region of elevated temperatures (Figure 6.2(a)). These elevated oxygen levels could be stimulating smoldering combustion and/or aerobic biodegradation processes. As a result, wellhead temperatures should be compared with oxygen levels to understand if air intrusion is a factor.

Gas extraction wells usually only penetrate a portion of the waste height. For example, in Cells 4 to 7 gas extraction wells were installed to depths of 15 to 40 m, with an average of 24 m. The average waste thickness across Cells 4 to 7 is 50 m and about 80 m in the center of Cell 5. A comparison of waste thickness and gas well depth indicates that extraction wells extend only a third to half of the waste thickness at the site. Thus, wellhead temperatures and gas composition may not represent internal landfill processes along the entire waste column. Regardless, Figure 6.2 shows that wellhead temperatures above 65°C can be an early indicator of elevated waste temperatures. Temperature contour plots are advantageous to project the growing boundary, but they usually under predict elevated waste temperatures because they reflect ambient temperatures because of the shallow nature of the wellhead and possible air intrusion.

6.2.2 Ratio of CH_4 to CO_2 Flow Rates

Chapter 5 shows landfill gas is composed mostly of methane (45–60% v/v) and carbon dioxide (40–60% v/v), thus a ratio of CH_4 and CO_2 greater than unity provides a useful measure of degree of anaerobic decomposition (Barlaz et al. 2010; Powell et al. 2006). Figure 6.3 presents contours of the CH_4/CO_2 ratio developed using average monthly values of CH_4 and CO_2 from each gas wellhead. Temperature and flow rate were measured at the gas wellhead using a GEM™ 2000 gas analyzer while the gas concentrations were measured by a portable field gas chromatographer. The CH_4 and CO_2 flow rates were calculated by multiplying the average percentage of CH_4 and CO_2 gas by the adjusted flow rate at the wellhead. Wellhead temperatures were used to standardize the flow rates to standard pressure and temperature of 20°C and 101 kPa, respectively.

In January 2010, almost 1.5 years after the elevated temperatures were first observed, Figure 6.3(a) shows the CH_4/CO_2 flow rate ratio remains at or above unity in Cells 4 and 7. In the elevated temperature region (Cells 5 and 6), the CH_4/CO_2 ratio rapidly decreases to values below 0.6 (red zone), indicating methanogenesis is being curtailed. The area encompassing Cells 5 and 6 also corresponds to the shaded region in Figure 6.1(a), which demarcates the gas wellheads that showed CH_4/CO_2 ratios below 0.6 in late 2009. The red area denoting reduced methane production expanded further into Cell 6 (Figure 6.3(b)) and by April 2011 the reduced methane production (red area) engulfed Cells 5 and 6 (Figure 6.3(c)). The elevated temperatures are shown to advance into Cell 7 in Figure 6.3(c). The red zone did not change from Figure 6.3(c) to Figure 6.3(d), which suggests the event is remaining stationary. Through the CH_4/CO_2 ratio, Figure 6.3 shows that anaerobic biodegradation became inhibited in Cells 5 through 7 from September 2009 to April 2011, while Cell 4 remained normal with CH_4/CO_2 ratios above unity.

6.2.3 Vertical Strain Rate

Chapter 5 analyzed settlement at Site 1 and found the typical settlement rate for Cell 4, which is under anaerobic biodegradation, is ~0.5 m/yr while the settlement rate in Cell 5 experiencing elevated temperatures is about a magnitude higher (~9.2 m/yr). After determining the waste thickness below each stability pin prior to the start of elevated temperatures, the vertical strain rate (%/year) was calculated for each settlement data point. Settlement was measured monthly so each data point in Figure 6.4 represents the vertical strain rate per month. Figure 6.4 shows a typical

trend of vertical strain rate and elapsed time for two stability pins in Cell 4 and Cell 5 (see Figure 6.1(b)). The vertical strain rate for the stability pin in Cell 4 ranges from 0.2 to 1.5 %/yr, with an average of about 0.7 %/yr. For Cell 5, the initial strain rate is similar to Cell 4 because both are operating under anaerobic biodegradation. However, the rate increases from normal conditions at an elapsed time (t) of 750 days to about 4%/yr by t= 900 days and continues to a peak value of 9.5%/yr at t= 1,100 days. After increasing to a peak value of 9.5%/yr, Figure 6.4 shows the vertical strain rate gradually decreases f to ~3%/yr at t= 1,600 days. In total, the biodegradation pin settles only about 1.4 m during the entire monitoring period (~3.4 years) while the elevated temperature pin settles about 4.1 m in only 350 days, i.e., t= 750 to 1,100 days. The behavior in Cell 5 indicates the vertical strain rate follows anaerobic biodegradation until elevated temperatures cause thermal degradation of the waste, which finally appears as accelerated vertical strain rates. In addition, the decreasing vertical strain rate suggests the combustion and possibly pyrolysis processes are slowing down because the MSW has been consumed and/or subsurface temperatures are decreasing from limited smoldering combustion.

Based on the behavior in Figure 6.4, vertical strain rates below 2%/yr indicate normal biodegradation settlement while strain rates greater than 3%/yr indicate elevated temperatures and smoldering combustion. Figure 6.5 shows the development of vertical strain rate contours with time. The shaded region in Figure 6.1(b) denotes the location where excessive settlement was observed during the first months of elevated temperatures. Since 2009, Figure 6.5(a) shows that the center of the hot spot moved between Cells 5 and 6, and the maximum vertical strain rates within the settlement bowl are about 11%/yr. In October 2011 (Figure 6.5(b)), the accelerated strain rates form an arc that extends from Cell 5, boundary of Cell 7, and into Cell 6. This indicates the elevated temperature region is migrating towards Cell 7 and is consuming Cells 5 and 6. In addition, the vertical strain rates in Cell 5 (see northing and easting of 500 m and 200 m, respectively) are less than 3%/yr in Figure 6.5(b). These lower strain rates, also observed in Figure 6.4, still represent elevated temperatures even though the strain rates are equivalent to biodegradation. The strain rates in May 2012 (Figure 6.5(c)) are located in the center of Cells 5 and 6, where the waste thickness is about 80 to 90 m and maximum strain rates are above 10%/yr. From November 2012 to October 2013, it is evident that strain rates are decreasing in Cells 5 and 6. For example, accelerated strain rates are found only in localized areas in Cells 6 and 7 by

October 2013. In Figure 6.5(d), Cell 4 is not affected by elevated temperatures because the strain rates remain below 2%/yr.

6.2.4 Recommendation for Characterizing Spatial Movement

Case study 1 was used to illustrate spatial movement of elevated temperatures. By comparing the contour plots in Figure 6.2, Figure 6.3, and Figure 6.5, it is evident that gas wellhead temperatures provide an initial boundary of elevated temperatures, but they are prone to inconsistencies from possible air intrusion and ambient temperature fluctuations. In contrast, Figure 6.3 and Figure 6.5 show the CH_4/CO_2 ratio and vertical strain rate can capture the spatial migration of elevated temperature events. A visual comparison between similar reported months (e.g., September 2010) shows the region where the CH_4/CO_2 ratio is below 0.6 corresponds to areas of strain rates >3 %/yr. In fact, combining the CH_4/CO_2 ratio and vertical strain rate contour plots provides a temporal comparison of where anaerobic biodegradation is inhibited and thermal degradation is dominant.

The CH_4/CO_2 ratio of 1.0 to 0.6 was chosen to depict the transition from anaerobic biodegradation to elevated temperatures or the heating front. The upper limit of 1.0 characterizes healthy anaerobic decomposition while the contours from 1.0 to 0.6 are selected because they represent a declining CH_4/CO_2 ratio trend. The strain rates of -3 and -4 %/yr were selected based on Figure 6.4 and additional comparisons between Cell 4 strain rates and stability pins that exhibited biodegradation and excessive settlements. Figure 6.6(a) and 6.6(b) show CH_4/CO_2 ratio contours from September and October 2010, respectively. The trends in both figures indicate limited movement of the elevated temperatures occurred between the two months. When comparing to the initial impacted area in Figure 6.1(a), the CH_4/CO_2 ratio initially follows the perimeter of Cells 5 and 6. However, the CH_4/CO_2 ratio contours in Figure 6.6(a) progress into the center of the landfill. The same behavior is observed for the vertical strain rate contours. For example, Figure 6.1(b) shows the shaded area in which vertical strain rates are accelerated when settlement monitoring was initiated. In Figure 6.6(b), this boundary has advanced farther into the center of the landfill. The CH_4/CO_2 ratio and vertical strain rate contours expand at different rates in Figures 6.6(c) and 6.6(d). For example, the CH_4/CO_2 ratio contours have migrated into Cell 4 and through Cell 7. However, the progression of vertical strain rate contours cover Cell 5 and a

portion of Cell 6 in Figure 6.6(c). The strain rate contour first extends into Cell 7 in October 2011 (Figure 6.6(c)). As stated in Chapter 5, the vertical strain rates are delayed because heat is transferred by conduction and time is required to thermally degrade the waste. In summary, Figure 6.6 shows that decreasing CH_4/CO_2 ratios project in front of the accelerated vertical strain rates. In addition, Figure 6.6 provides a useful method to characterize where thermal degradation is the dominant process.

6.3 Case Study 2: Subsurface Temperature Movement

Gas composition and concentrations from gas extraction wells represent internal landfill processes around that well and gases transported from adjacent locations where other processes may be dominant. For example, methane levels in an elevated temperature zone should approach values below 5% v/v, but concentrations of 20% v/v are frequently reported. These higher values may represent a nearby area where methanogenesis is still the dominant process. Therefore, installation of downhole temperature arrays (DTAs) provides important information to:

1. Validate wellhead gas composition and determine if methanogenesis is the dominant landfill process.
2. Allow comparison between subsurface and gas wellhead temperatures.
3. Provide elevated temperature thickness and depth, which is important for determining whether or not waste excavation is a possible containment technique and the condition of the liner system components.
4. Understand progression of subsurface temperatures, which can be used to estimate rate and direction of subsurface movement.

6.3.1 Case Study 2: Site Overview and Layout

Case study 2 was operated as a limestone quarry from 1939 until 1988. In 1974, landfilling began in the north section of the quarry and continued until 1985 when the landfill underwent expansion to the southwestern areas (Figure 6.7). In August 2005, the facility stopped receiving waste and initiated closure and post-closure activities. The landfill covers an area of approximately 22.3 ha (52 acres), and extends a maximum of ~73 m below ground surface with a total waste thickness of ~98 m. The landfill accepted approximately 13 million m^3 of waste, including commercial,

industrial, and MSW, and was constructed without a bottom liner or side slope liners. The final cover/cap consists of 0.6 m of compacted clay and 0.3 m of soil for vegetation. Leachate is collected by pumping from six leachate collection risers constructed of stainless steel piping that reaches to the base of the quarry. The landfill gas collection and control system includes gas extraction wells, a system of header lines, and a blower flare station.

6.3.2 Subsurface Temperature Movement

From November to December 2010, landfill operators noticed that three landfill gas extraction wells in the southern quarry portion were experiencing increasing wellhead temperatures and changes in gas composition. By January 2011, the wellhead temperatures at two gas extraction wells exceeded ~90°C and methane levels dropped from ~50% v/v to ~1% v/v. To monitor the subsurface movement of elevated temperatures from the southern to northern landfill area, the facility operators installed nine DTAs in November 2012 and an additional five in March 2013 (see Figure 6.7). Figure 6.8 shows a typical schematic of the DTA, which consists of vertical borings drilled using rotary sonic or auger methods. Type T thermocouples were installed at 6.1 m spacing to the bottom of the borehole. The thermocouples were protected in a 50.8 mm chlorinated polyvinyl chloride (CPVC) pipe for the first 6 m, which was replaced with an abrasion protection sheath for the remaining borehole depth. A rebar was added to the CPVC pipe for structural rigidity. The well casing was backfilled with cement bentonite grout to ensure a consistent thermal conductivity along the well casing and prevent contact with leachate. The thermocouple were attached to the rebar and the associated wires were transferred to a junction box where the thermocouples are recorded on a weekly basis.

Figure 6.9 depicts waste temperatures versus elevation for the cross-section A-A' depicted in Figure 6.7. The cross-section utilizes four DTAs (referred to as DTA-1 through DTA-4) to evaluate subsurface temperatures and monitor rate of movement. The elevated temperatures are moving from DTA-1 towards DTA-4, i.e., DTA-1 is the closest to the elevated landfill temperatures. In addition, DTA-2, DTA-3, and DTA-4 are located 40 m, 55 m, and 80 m, respectively, from DTA-1. The kriging interpolation function was used to interpolate between the thermocouples, and thus develop the temperature contours in Figure 6.9.

After the DTAs were installed and began recording data in November 2012, the thermocouples in Figure 6.9(a) measured baseline temperatures of about 70°C in the center of the waste mass, with decreasing temperatures to the ground surface and final bottom depth. This shows at the time of DTA installation the typical temperature regime prior to the elevated temperatures. Assuming the upper boundary of biological activity is 80°C (Merz 1969; Hudgins and Harper 1999), the 80°C temperature contour can be used to delineate movement of the hot spot. The 80°C contour was first observed two months after installation (Figure 6.9(b)), and modest advancement was observed between months two and six (see Figure 6.9(c)). During month 7 (Figure 6.9(d)), the 80°C contour rapidly advanced towards DTA-2 and temperatures in the hot spot area increased to about 110°C. Over the next month (see Figure 6.9(e)), the smoldering area became more prominent and temperatures at the middle depth of the landfill increased to 130°C. These temperatures were maintained through month 15 (see Figure 6.9(f)). According to DTA-1, the maximum measured temperature in the hot spot area is 135°C.

The hot spot area in Figures 6.9(e) and 6.9(f) encompasses about 40% of the total waste depth, i.e., temperatures ≥ 80°C extend from 145 m to approximately 105 m. The 80°C contour projects towards the ground surface because of rising hot gases and elevated internal landfill pressures. In addition, the leachate level during the monitoring period was at elevation 95 m and hence may be preventing expansion of the hot spot to greater depths. Figure 6.9(f) also shows a developing isolated temperature event near the ground surface at or near DTA-3. This isolated area could daylight to the ground surface and produce flames and emit smoke into the atmosphere and connect to the main elevated temperature region near DTA-1.

Figure 6.10 shows temperature trends in gas wellheads GW-A and GW-B and DTA-2. GW-A and GW-B are located approximately 30 m and 45 m from DTA-1, respectively. The maximum waste temperatures in DTA-2 are used in Figure 6.10 to provide a comparison of wellhead temperatures as the 80°C contour approaches. These data illustrate the following two important characteristics of elevated temperatures in MSW landfills:

1. Comparison of gas wellhead and downhole temperatures with time indicate downhole temperatures exceed wellhead temperatures by about 15°C before the elevated temperatures develop, which is in agreement with observations by Martin et al. (2013) and in Chapter 5. For example during months 1 through 4, DTA-2 temperatures were 70°C while wellhead temperatures remained at 55°C.

2. As the 80°C contour approaches (after month 7) and eventually passes DTA-1, the gas wellhead temperatures increase to about the waste temperatures. This behavior indicates that convective heat transfer is raising the wellhead temperatures. Gas temperatures are higher in GW-A than GW-B, which may attributed to GW-A drawing gas from the hot spot. In addition, carbon monoxide concentrations (Figure 6.10(b)) are above 1,500 ppmv in GW-A throughout the monitoring period. The presence of carbon monoxide indicates smoldering combustion and confirms that gas composition changes before elevated temperatures have advanced to DTA-1. The significant drop in GW-B temperature at month 5 correlates to air intrusion because nitrogen levels in GW-B increased to ~30% v/v (see Figure 6.10(c)).

Downhole temperatures can also be used to estimate the rate of movement of the 80°C contour. Quantifying the rate of movement allows landfill operators and regulatory agencies to plan future instrumentation, a construction timeline for an isolation break or containment barrier, or a new operation plan. Because the temperature front is assumed at 80°C, the change in horizontal distance of the 80°C contour in each month represents the horizontal movement rate. For example, the 80°C contour is located 26.4 m from DTA-1 in month 7 (see Figure 6.9(d)) and 30.9 m in month 8 (see Figure 6.9(e)). Therefore, the temperature front advanced 5 m over 1 month period. Figure 6.10(d) shows the cumulative movement of the temperature front. From months 3 to 5 and again months 7 to 9, the positive rate of movement is 2.5 to 5 m/month. However, Figure 6.10(d) shows the cumulative movement decreased from month 5 to month 6, i.e., the 80°C contour moved backwards. This trend is attributed to air intrusion, i.e., high nitrogen levels in month 5 in GW-B (see Figure 6.10(c)), which led to cooler waste temperatures and an oxygen source. The significant progression after month six (6) indicates that oxygen possibly fueled combustion, which caused the temperature front to rapidly advance 15.9 m in one month. The constant cumulative movement of ~30 m from month 9 to month 15 indicates the elevated temperatures did not advance. In Figure 6.10(d), DTA-2 corroborates this observation because temperatures peaked at 80°C during months 5 and 6 but decreased to ~75°C in month 7 and remained constant for the remainder of the monitoring period. Possibilities for the impeded progress include lack of oxygen to propagate smoldering combustion, a layer of inert material, e.g., soil cover, acting as a thermal barrier, the

elevated temperatures migrating in an alternate direction than the line of DTAs, and/or changes in gas management operations.

6.3.3 Summary

The second case study shows the importance of monitoring subsurface waste temperatures. For example, the maximum recorded subsurface waste temperature was 135°C during the monitoring period. However, the thermocouples in DTA-1 failed before they could measure temperatures within the center the hot spot so the waste temperatures likely exceeded 135°C. A comparison of wellhead and waste temperatures confirms gas temperatures are initially at least 15°C lower than the maximum waste temperatures. As the 80°C contour approaches, gas wellhead temperatures fluctuate similar to the cumulative movement, i.e., changes in gas wellhead temperatures are linked with the approaching elevated temperatures. The gas composition in wells GW-A and GW-B shows evidence of carbon monoxide concentrations greater than 1,500 ppmv prior to elevated temperatures advancing to DTA-1. Smoldering combustion is the likely mechanism producing carbon monoxide, but temperatures at DTA-2 reach only ~80°C. This sequence of gas and temperature observations suggest that gas generated in close proximity to smoldering combustion can project in front of elevated temperatures, thus demonstrating the elevated temperature spatial boundary is greater than in reality.

6.4 Classification of Landfill Zones

Municipal solid waste normally degrades by biological and chemical processes. Biological processes, such as anaerobic biodegradation, are established by microorganisms using MSW as a carbon and energy source. Chemical processes are not governed by microorganisms and include dissolution, reduction/oxidation processes, and thermal degradation. The thermal degradation processes relevant in MSW landfills during elevated temperature events are smoldering combustion and possibly pyrolysis. Smoldering combustion is the slow, low temperature, flameless form of combustion that is sustained by the heat evolved when oxygen directly attacks the surface of MSW (Kuo 1986; Griffiths and Barnard 1995). When organic materials are subjected to sufficient heat flux from combustion or another exothermic reaction, they can degrade and gasify via pyrolysis if oxygen is not present (Ohlemiller 1985). When thermal degradation

becomes the dominant landfill process, smoldering combustion and pyrolysis can occur concurrently because the products of pyrolysis are oxidized in combustion. If smoldering combustion ceases because of limited oxygen supply, pyrolysis may continue for extended periods of time, depending on the temperature reached during combustion, the location and size of the landfill hot spot within the waste mass, and the duration of the combustion event. This is an important distinction because pyrolysis is an endothermic reaction in the presence of no oxygen.

Differentiating areas of anaerobic degradation and thermal degradation is important for emergency and environmental response and containment of these events. Therefore, a framework is proposed that includes a progression of indicators from anaerobic to thermal degradation and can be used to describe the spatial and subsurface movement with time. Figure 6.11 shows a schematic of elevated temperatures that is separated into five possible zones: (1) anaerobic biodegradation, (2) gas front, (3) heating front, (4) smoldering front, and (5) combustion/pyrolysis zone. Anaerobic biodegradation is represented by temperatures below 60°C and CH_4/CO_2 ratios greater than unity. The gas and heating fronts are located between anaerobic biodegradation and the smoldering front and are characterized by increasing waste and wellhead temperatures and changes in gas composition (decreasing methane concentration and CH_4/CO_2 ratios). The smoldering front follows the heating front and is the driving force of elevated temperatures. The heat generated from the smoldering front permits combustion/pyrolysis of MSW, which yields increased gas flow and water vapor (see blue arrows in Figure 6.11), toxic and odorous gases, and settlement.

Together, the gas, heating, and smoldering fronts are captured by the progression of indicators and can be used to delineate the location, boundary, and subsurface movement of the elevated temperatures. The parameters that can be used to assess the landfill zones include gas composition and temperature, subsurface temperature, and settlement. Subsurface temperatures are the most accurate because they illustrate the smoldering front geometry migration with time and can corroborate gas compositions. The pertinent gases for evaluation landfill zones are methane, carbon dioxide, and carbon monoxide. Settlement is usually monitored via topographic surveys. In this instance, exact settlement locations should be monitored continuously to determine the change in strain rates from biodegradation to thermal degradation.

6.4.1 Gas and Heating Front

The size and movement of the intermediate region (gas and heating fronts) depends on the heat transfer mechanisms from the smoldering front. Heat generated from smoldering combustion, or another exothermic reaction, can be transferred by conduction and convection. Conduction transmits heat by direct contact between MSW particles while convection transfers heat by movement of liquid and/or gas. In Figure 6.11, the smoldering front conducts heat to the landfill waste and projects gases in advance of the elevated temperatures. Convection forces the hot and saturated gas to rise, where it comes in contact with cooler waste material. The water vapor then condenses to leachate, which can accumulate in gas wellhead pipes, lateral headers, and develop a perched water level between the ground surface and smoldering front. The leachate from condensed water vapor and dehydrated MSW can also seep toward cooler waste in the center of the landfill or gravitate to the leachate collection system.

The gas and heating front location criteria proposed herein uses the CH_4/CO_2 flowrate ratio because it demonstrates sustainable anaerobic biodegradation when the ratio is greater than unity. In addition, temperature controls the quality (methane and carbon dioxide) and quantity of landfill gas generated within two temperature ranges: (1) the mesophilic range where temperatures are between 20 and 45°C; and (2) the thermophilic range with temperatures greater than 45 to 65°C (Meima et al. 2008; Mora-Naranjo et al. 2004; ATSDR 2001; Kotze et al. 1969). Therefore, the CH_4/CO_2 flow ratio and gas temperature are used in Figure 6.12 to characterize the gas and heating fronts.

Figure 6.12 provides a compilation of CH_4 to CO_2 ratio and wellhead temperature trends for 12 gas extraction wells at Case Study Site 1. The location of the gas extraction wells used in Figure 6.12 are displayed in Figure 6.1(a). The purple squares and green triangles represent gas wells in Figures 6.12(a) and 6.12(b), respectively. The wellheads started as normal operating wells before the smoldering front advanced towards these wells, resulting in decreasing CH_4/CO_2 ratios with increasing temperatures. Figure 6.12(a) shows a direct relationship between decreasing CH_4/CO_2 ratio and increasing wellhead temperature while Figure 6.12(b) shows the CH_4/CO_2 ratio decreases significantly before wellhead temperatures increase. For example, Figure 6.12(a) shows wellhead temperatures range from 40 to 55°C with CH_4/CO_2 ratios above 0.8. As the CH_4/CO_2 ratio decreases from 0.8 to 0.1 and methanogenesis has been inhibited (Kasali and Senior 1989; Hartz et al. 1982; Pfeffer 1974; Ahring et al. 1995), the average wellhead temperature

increases from 50 to 65°C. Wellhead temperatures continue to rise to 90°C for CH_4/CO_2 ratios less than 0.1. In contrast, Figure 6.12(b) shows the CH_4/CO_2 ratio decreases from values above unity to ~0.3 before an increase in wellhead temperature is observed. Both trends in Figure 6.12 indicate that the CH_4/CO_2 ratio is decreasing but the increase in wellhead temperature can be delayed. Based on the gas well locations, it is evident the purple squares are located next to the elevated temperature shaded region, which is characterized by the CH_4/CO_2 ratio being below 0.6. The close proximity of the gas wells experiencing elevated temperatures and low CH_4/CO_2 ratios, suggests that wellhead temperatures increase because heat is being conducted from the nearby smoldering front. In contrast, the green triangles are located farther away from the shaded region and gas composition changes before heat transfer via conduction has sufficient time to reach the gas extraction well. The appearance of carbon monoxide in advance of elevated temperatures at Case Study Site 2 also corroborates the concept of a gas front.

As a result, the gas and heating fronts are located between normal anaerobic decomposition and the smoldering front. The heating front is the zone adjacent to the heat source and is defined by increasing wellhead temperatures and decreasing CH_4/CO_2 ratios. The gas front projects outward to areas unaffected by the hot spot to a greater extent than the heating front. This region is characterized by decreasing CH_4/CO_2 ratios and mesophilic derived landfill temperatures.

6.4.2 Smoldering Combustion Front and Pyrolysis

The first indication of elevated temperatures is localized because the heat source is a discrete location or event, e.g., aluminum dross reaction in a specific cell or air introduced into the waste mass via cracked soil cover or leaking gas well. The expansion/movement of elevated temperatures from the original heat source signifies that smoldering combustion is present. The indicator synonymous with smoldering combustion in landfills is carbon monoxide (Ettala et al. 1996; Frid et al. 2009; Martin et al. 2013; Stearns and Petoyan 1984; Sperling and Henderson 2001). In particular, FEMA (2002) states that carbon monoxide concentrations exceeding 1,000 ppmv is indicative of a subsurface combustion. Although carbon monoxide is an established indicator, defining the boundary of the smoldering front is difficult because of internal mixing of landfill gases caused by MSW heterogeneity and operation of the gas extraction system. As a result, the

proposed framework defines the smoldering front using a combination of carbon monoxide concentrations, subsurface temperatures, and waste settlement.

Figure 6.13 shows the increasing trend of carbon monoxide with decreasing CH_4/CO_2 ratio for four gas extraction wells found in the gas and heating fronts. The trend line in Figure 6.13 shows an increase of carbon monoxide from 0 to ~800 ppmv when the CH_4/CO_2 ratio decreases from 1.0 to 0.6. This trend verifies that carbon monoxide is present in the gas and heating front, with maximum concentrations reaching ~1,200 ppmv. After the CH_4/CO_2 ratio declines to < 0.2, Figure 6.13 indicates that carbon monoxide concentrations increase significantly. Martin et al. (2013) recommend methane levels < 15% v/v and carbon monoxide concentrations > 1,500 ppmv be used to identify areas undergoing smoldering combustion. Based on Figure 6.13, the smoldering front may be defined by a CH_4/CO_2 ratio < 0.2 and carbon monoxide > 1,500 ppmv. Similar to Martin et al. (2013), a more conservative carbon monoxide value of 1,500 ppmv was recommend compared to FEMA's threshold of 1,000 ppmv to differentiate between carbon monoxide measured in the heating front and at the combustion front.

In addition to the carbon monoxide criteria, subsurface temperatures and settlement are important in defining the smoldering front. In particular, subsurface temperatures provide an indication of the combustion front boundary, e.g., see DTA-1 in Figure 6.9(e). Assuming a temperature contour to represent smoldering combustion, e.g., 80°C, a line of DTAs can be used to draw a cross-section and map the location of the smoldering front. Smoldering combustion temperatures observed in MSW landfills range from 200 to 300°C and as high as 700°C (Ettala et al. 1996; Lönnermark et al. 2008; Ruokojarvi et al. 1995). In addition, the maximum temperatures measured by DTA-1 at Case Study Site 2 is 135°C. Smoldering combustion may also develop at relatively low temperatures, and has been documented in a wood member exposed to heating at temperature as low as 77°C (170°F) for time periods ranging from several months to several years (Babrauskas 2003). Because the exact temperature where smoldering combustion is initiated in MSW is not known, a conservative temperature of 80 to 100°C may be appropriate.

A conservative estimate of the smoldering front can be made with vertical strain rate contour plots because of the delayed nature of the settlement. For example, Figure 6.6 shows the area within the 3 %/yr contour is undergoing combustion and possibly some pyrolysis. Therefore, this contour can act as a conservative boundary of the smoldering front because the waste has been combusted. Because pyrolysis is the mechanism leading to thermal breakdown of MSW without

oxygen, a contour plot of vertical strain rates can also delineate areas of thermal degradation. However, settlement is a delayed indicator of elevated temperatures so the vertical strain rates provide only the boundary where thermal degradation has been the dominant process. Subsurface temperature changes over time or space are also useful as part of an evaluation to differentiate between smoldering combustion and pyrolysis. Combustion is an exothermic and self-generating reaction with oxygen, so temperature increases over time and space are indicative of combustion. Conversely, pyrolysis is an endothermic and not self-generating reaction, i.e., temperatures should decrease over time and not spread significantly, without oxygen. Given the many sources of oxygen at shallow depths in a landfill, it is anticipated that pyrolysis can only occur a significant depth in a landfill where no oxygen is present. For example, the smoldering combustion front in Figure 6.9 is migrating towards DTA-4 until month 9. After this time, waste temperatures remain constant and pyrolysis may be the dominant process where oxygen is not present, i.e., significant waste depth.

6.5 Summary and Conclusions

The sources of heat generation that cause elevated temperatures include aerobic decomposition, self-heating via accelerated biodegradation, exothermic chemical reactions, and smoldering combustion. Although elevated temperatures are initially localized events, they can expand and advance to areas still undergoing anaerobic biodegradation and severely impact the operation and infrastructure of an MSW landfill. This chapter provides techniques to characterize the spatial and subsurface migration of elevated temperatures. These methods were combined into a framework that classifies a landfill into five zones, which can delineate the boundary and movement of elevated temperatures with time to evaluate contingency and containment measures. The following is a summary of trends and indicators for identifying the movement of elevated temperatures discussed herein:

1. Contour plots of the CH_4/CO_2 ratio provide a reasonable estimate of where internal landfill processes are transitioning from anaerobic biodegradation to thermal degradation. Vertical strain rate contours provide a useful method to characterize the location where thermal degradation is or has been the dominant process. Combining both contour plots allows a spatial and temporal comparison of internal landfill processes.

2. Gas wellheads temperatures should be correlated with downhole temperatures because they are more reliable and provide maximum temperatures in the smoldering front, heating front depth and thickness, and rate of subsurface movement. Wellhead temperatures typically under predict waste temperatures, e.g., by 15°C in the reported case, prior to smoldering front arrival. Comparison of gas composition and downhole temperatures indicate that gas from smoldering combustion projects ahead and results in accumulation of carbon monoxide in lower waste temperature areas so monitoring changes in the CH_4/CO_2 ratio is important.
3. Increased wellhead temperatures coupled with decreasing CH_4/CO_2 flow rate ratio can be used to delineate the gas and heating front from the normal MSW biodegradation area.
4. The smoldering front should be defined by carbon monoxide concentrations and subsurface temperatures. This study recommends a carbon monoxide concentration of 1,500 ppmv and subsurface temperatures ranging from 80 to 100°C. Because settlement can also be used to delineate areas where V vertical strain rate greater than 3 %/yr can be used.

6.6 Tables and Figures

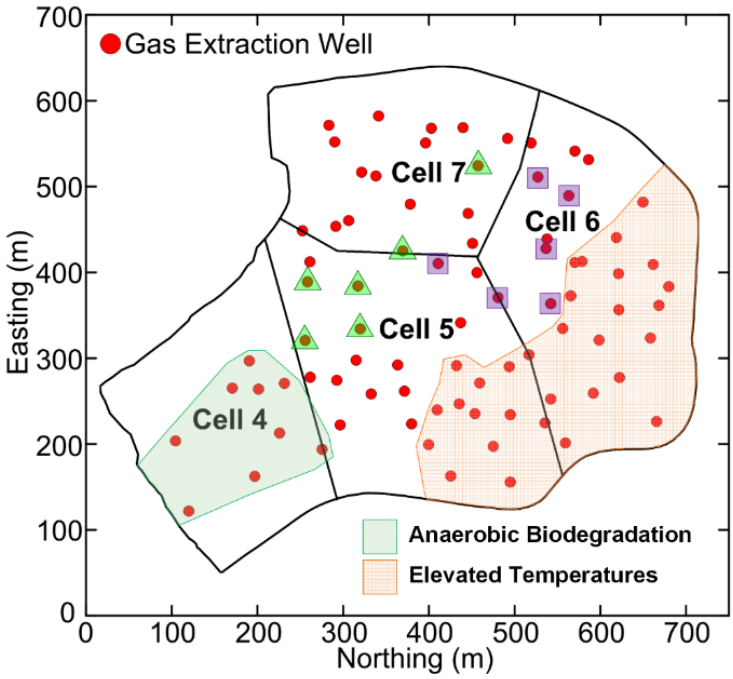

(a) Gas extraction wells

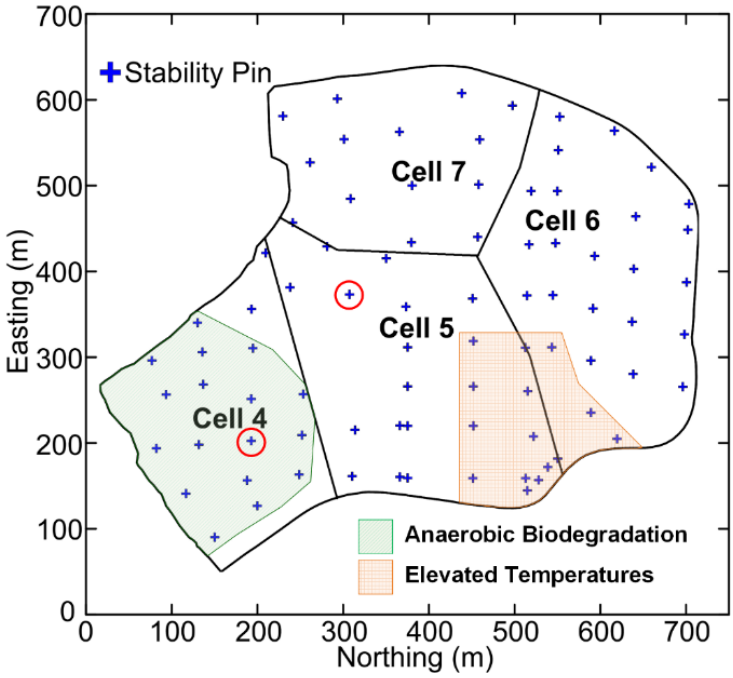

(b) Stability pins

Figure 6.1 Site 1 delineation of anaerobic degradation and elevated temperatures in late 2009: (a) Gas extraction wells and (b) Stability pins

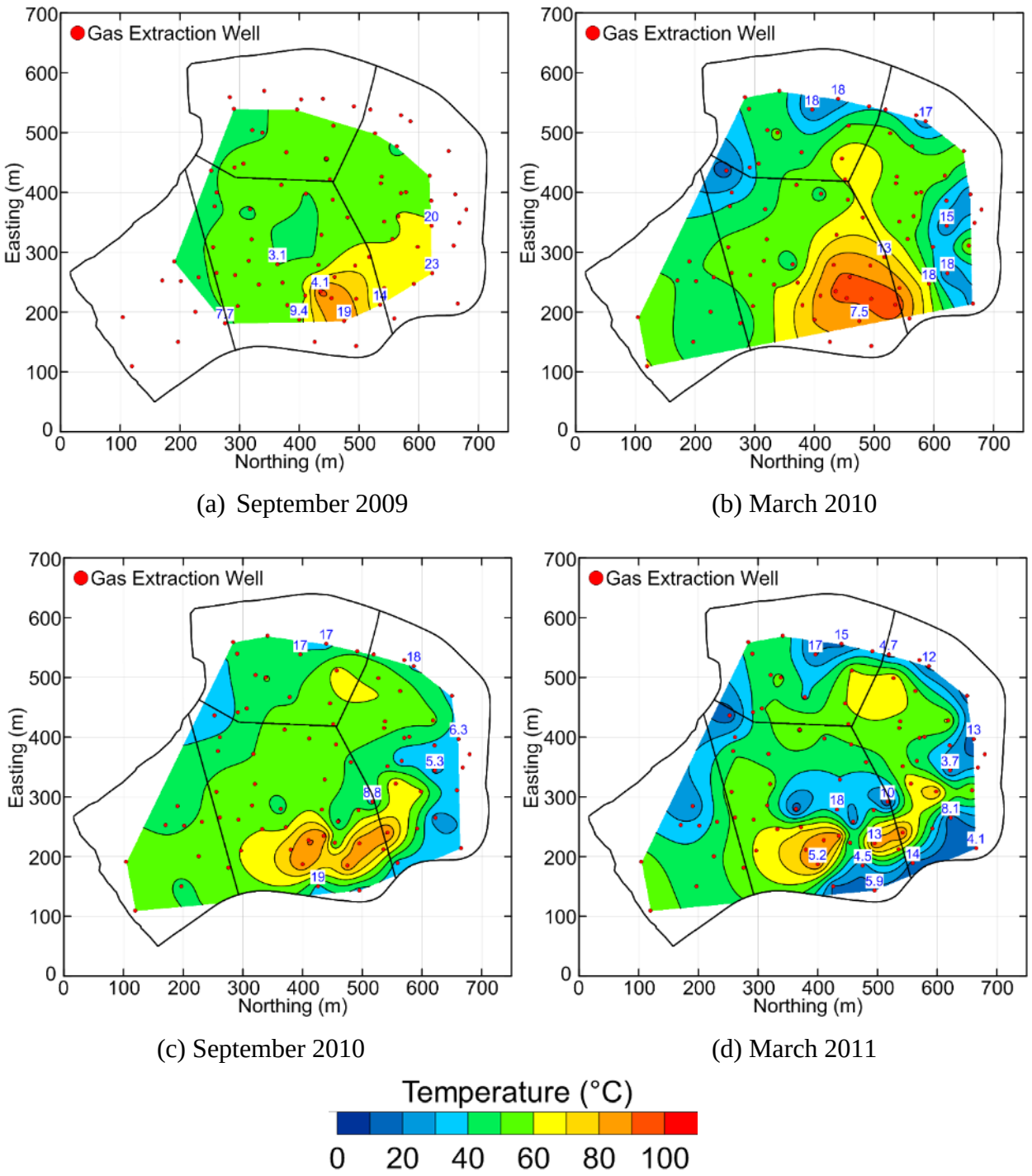

Figure 6.2 Gas wellhead temperatures (°C) and O_2 levels (% v/v) in (a) September 2009, (b) March 2010, (c) September 2010, and (d) March 2011

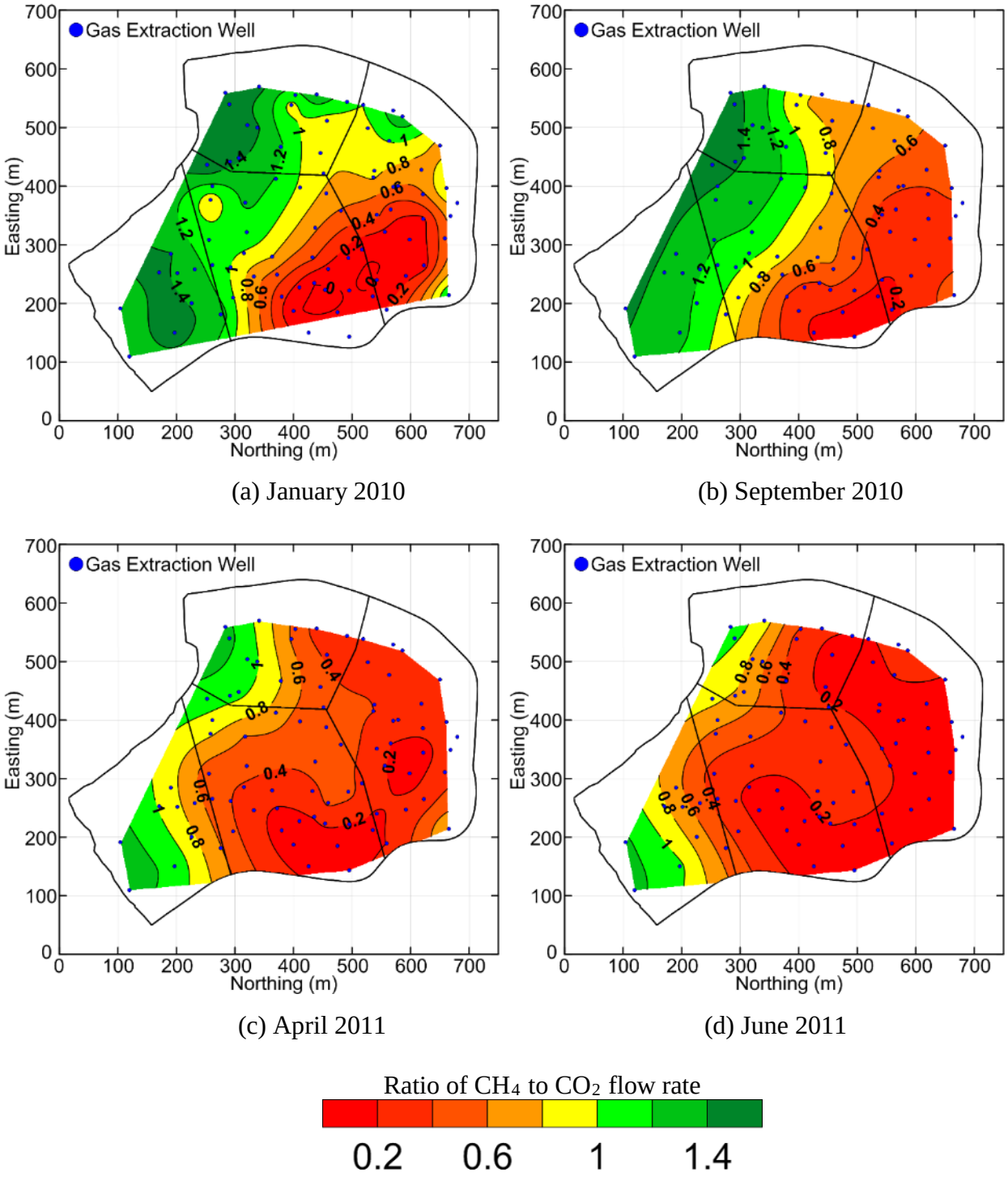

(a) January 2010

(b) September 2010

(c) April 2011

(d) June 2011

Figure 6.3 Gas wellhead ratio of CH_4 to CO_2 flow rates in (a) January 2010, (b) September 2010, (c) April 2011, and (d) June 2011

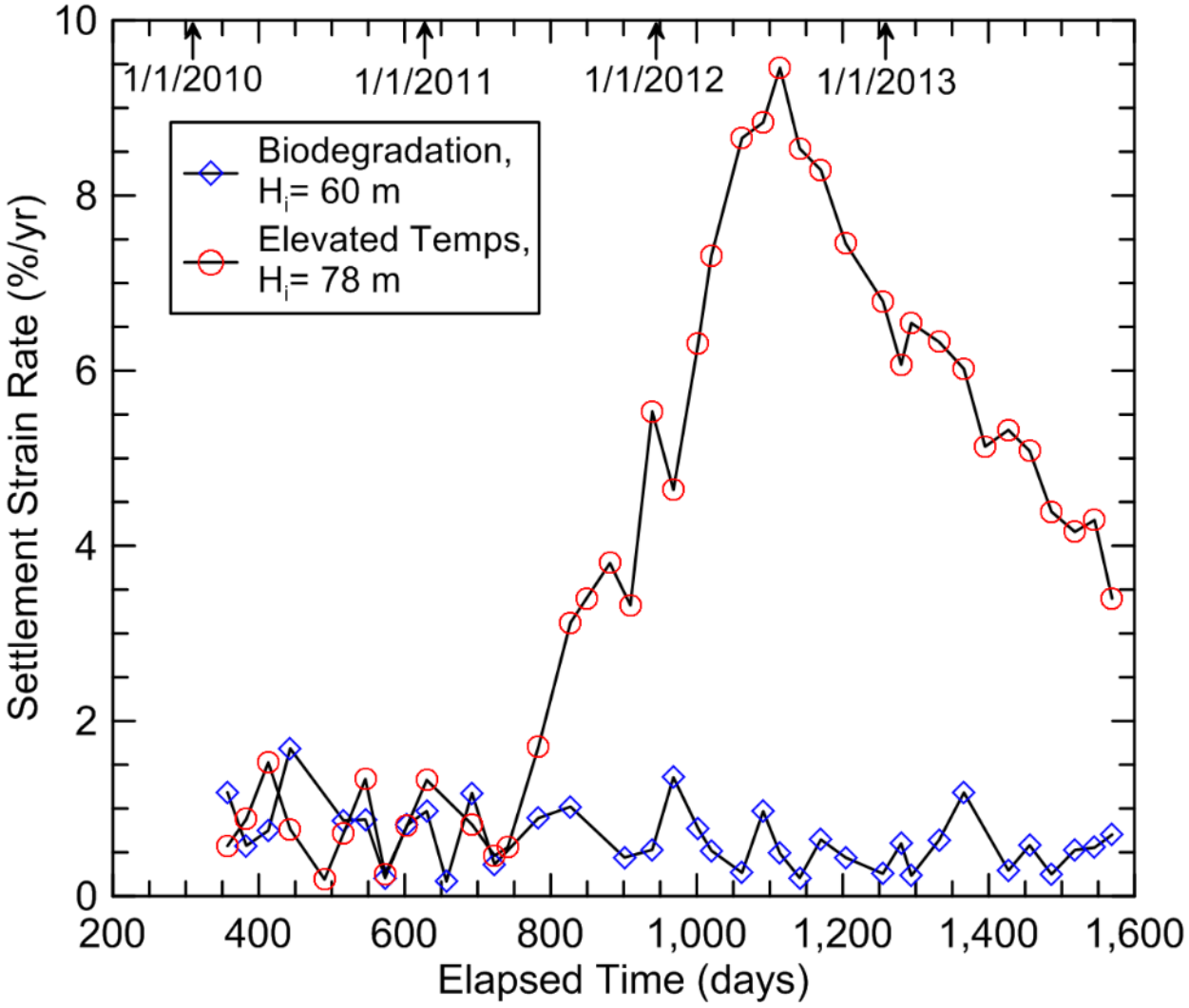

Figure 6.4 Typical strain rate of normal biodegradation and elevated tempeartures

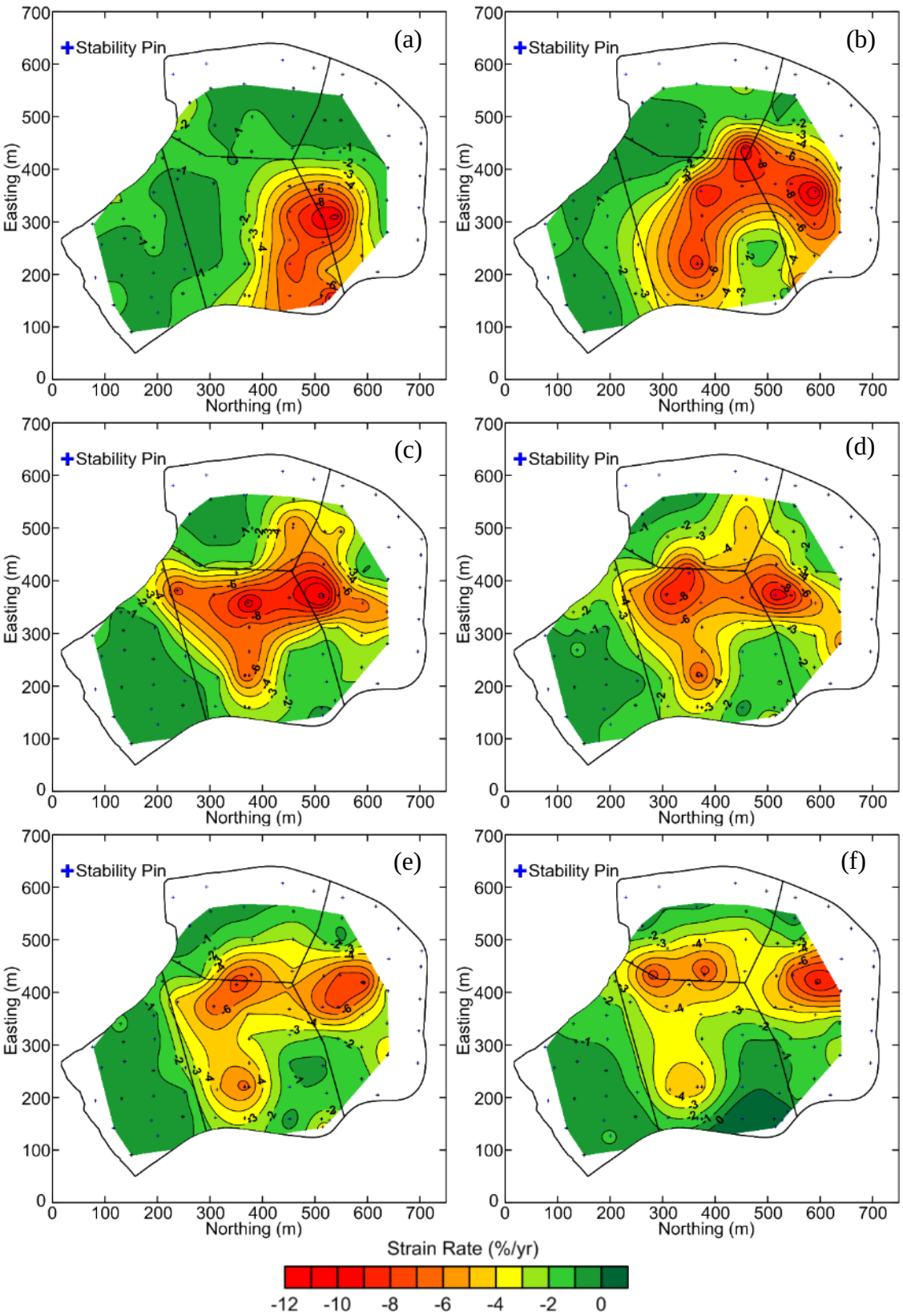

Figure 6.5 Spatial movement of strain rates: (a) September 2010, (b) October 2011, (c) May 2012, (d) November 2012, (e) May 2013, and (f) October 2013

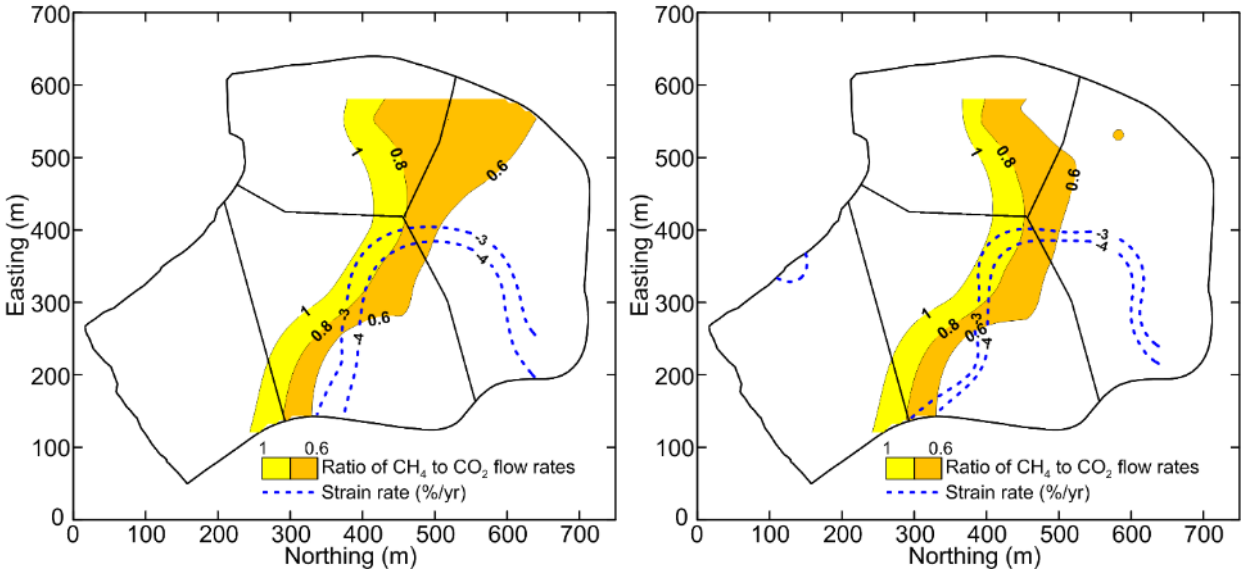

(a) September 2010 (b) October 2010

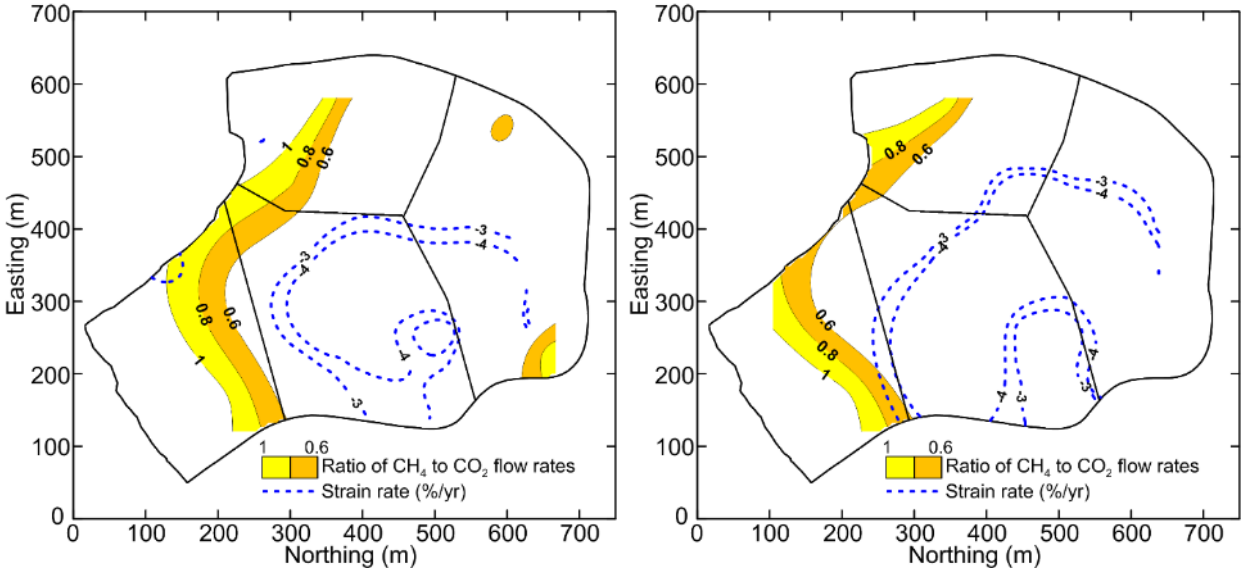

(c) May 2011 (d) October 2011

Figure 6.6 Combined movement of ratio of CH_4 to CO_2 flow rates and strain rate: (a) September 2010, (b) October 2010, (c) May 2011, and (d) October 2011

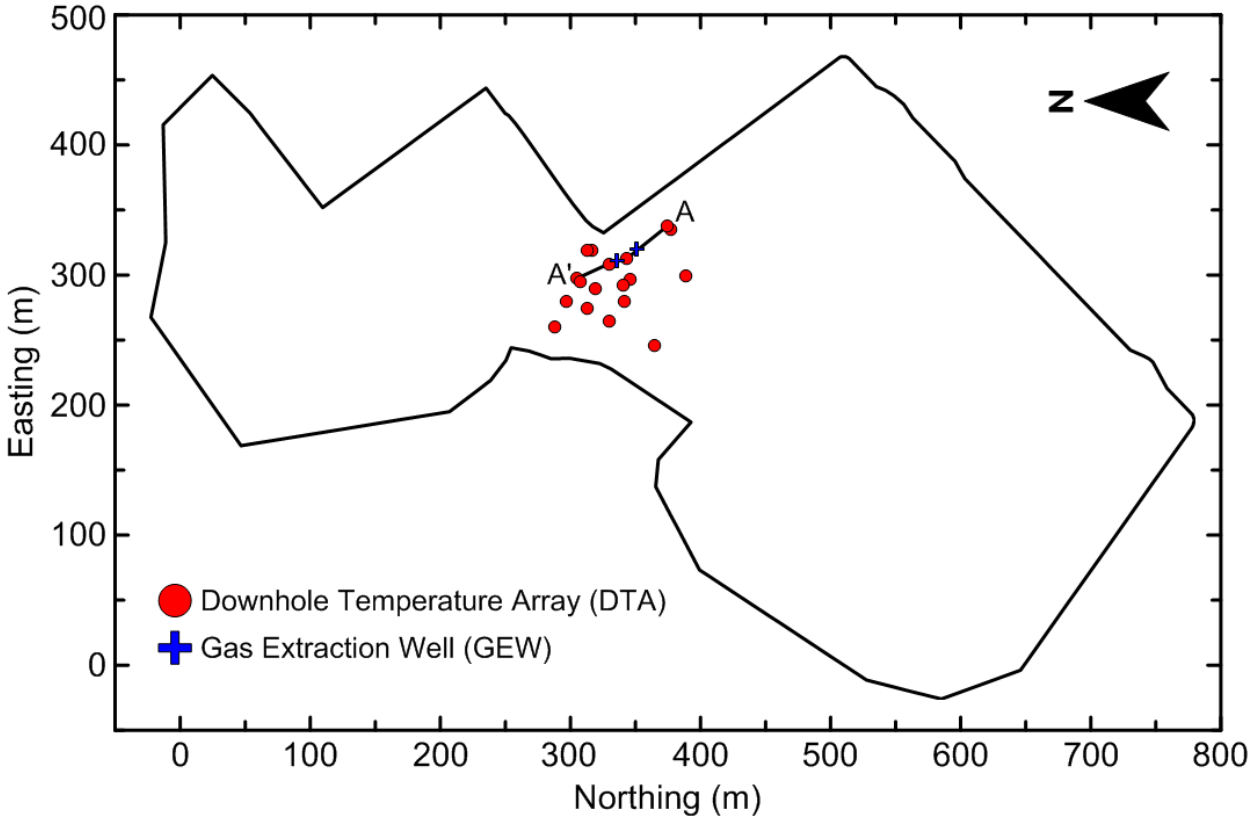

Figure 6.7 Site layout and locations of DTAs and cross-section A-A’

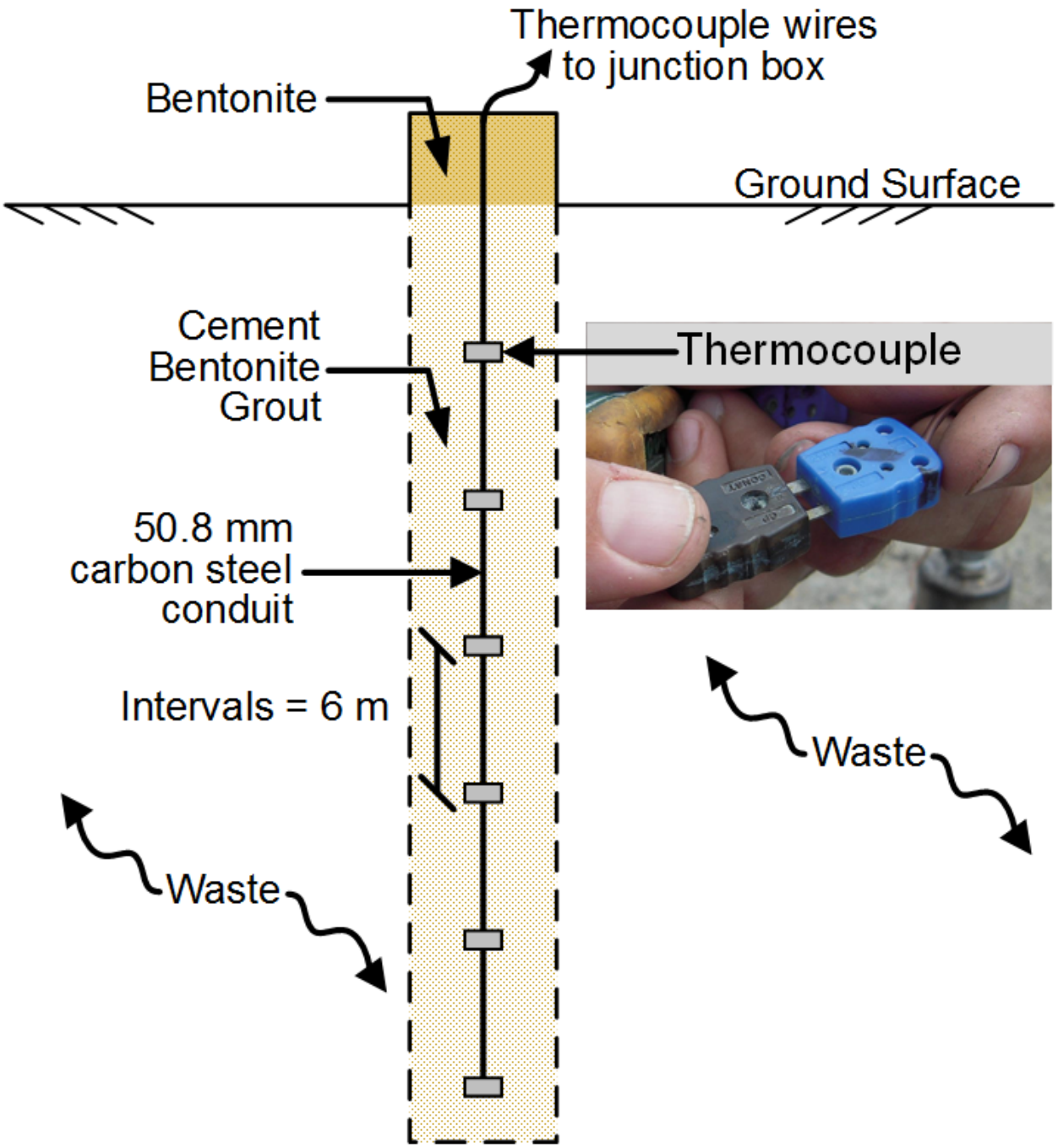

Figure 6.8 Schematic of temperature monitoring point with six thermocouples

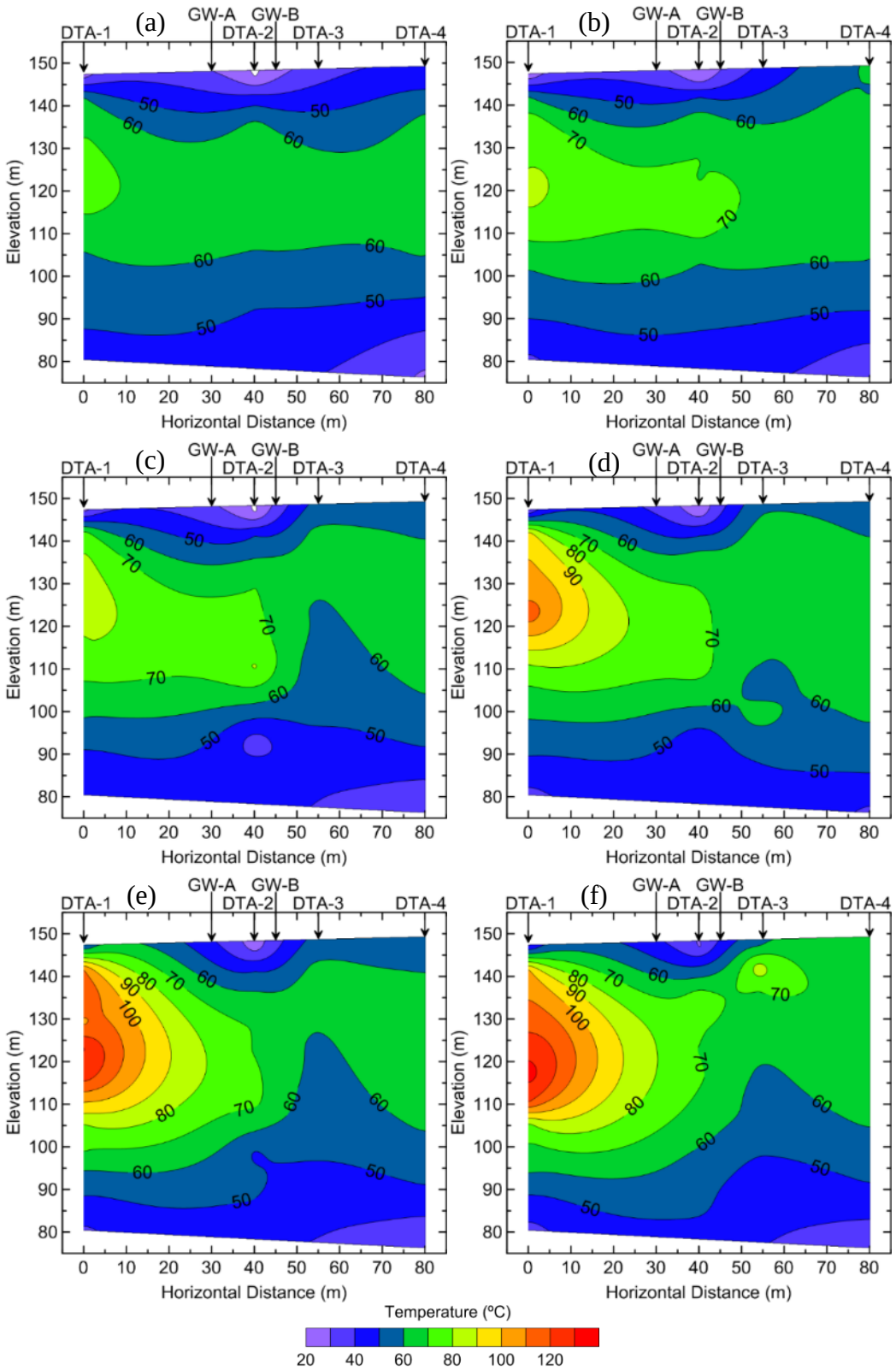

Figure 6.9 Cross-section A-A' showing subsurface temperatures at time of (a) installation [November 2012], (b) 2 months [January 2013], (c) 6 months [May 2013, (d) 7 months [June 2013], (e) 8 months [July 2013], and (f) 15 months [January 2014]

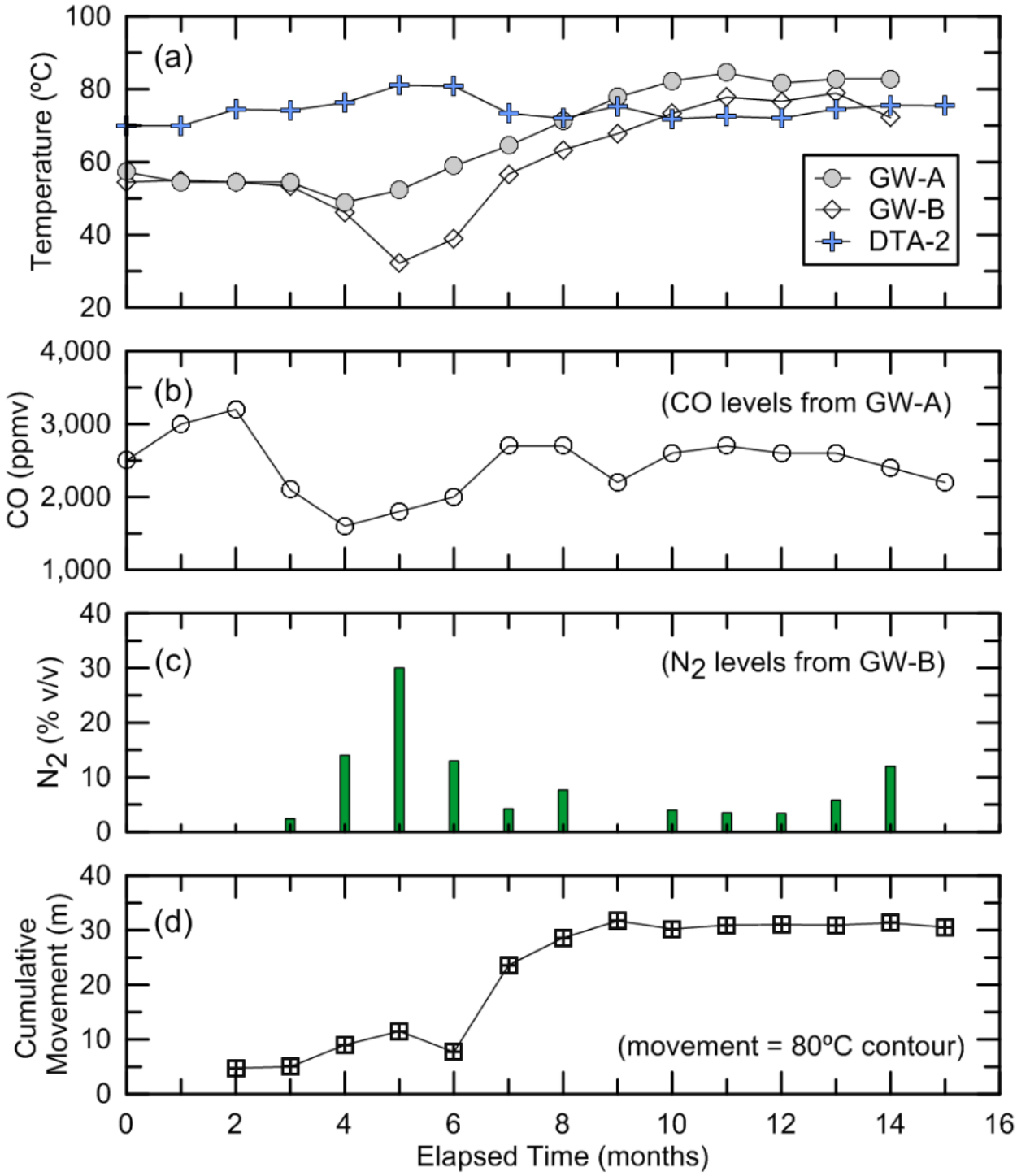

Figure 6.10 Trends in (a) landfill gas wellhead and waste temperatures, (b) CO concentrations in GEW-A, (c) N_2 levels in GEW-B, and (d) cumulative subsurface movement

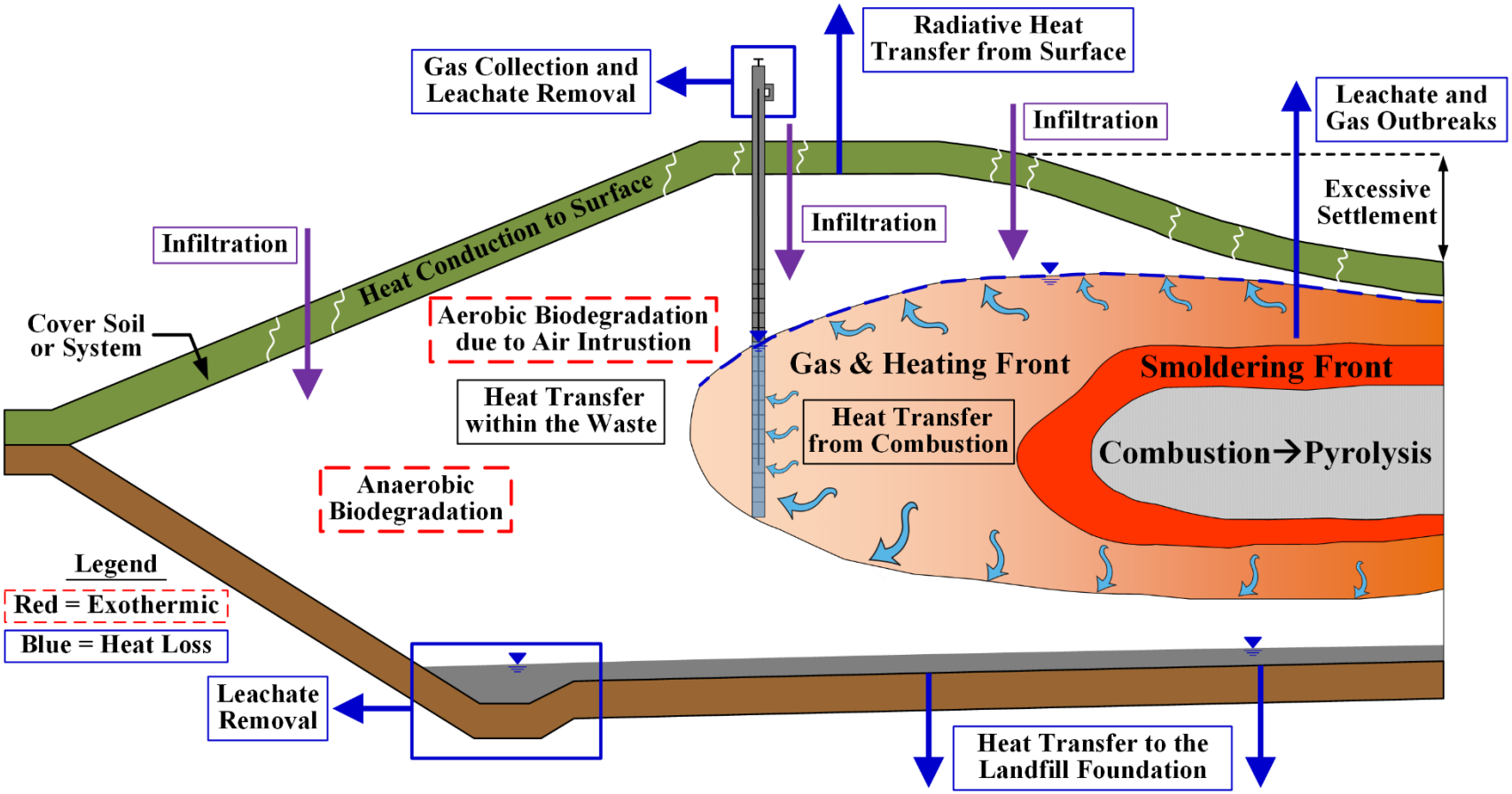

Figure 6.11 Schematic of landfill energy balance classification of landfill zones: anaerobic biodegradation, gas front, heating front, smoldering front, and combustion/pyrolysis

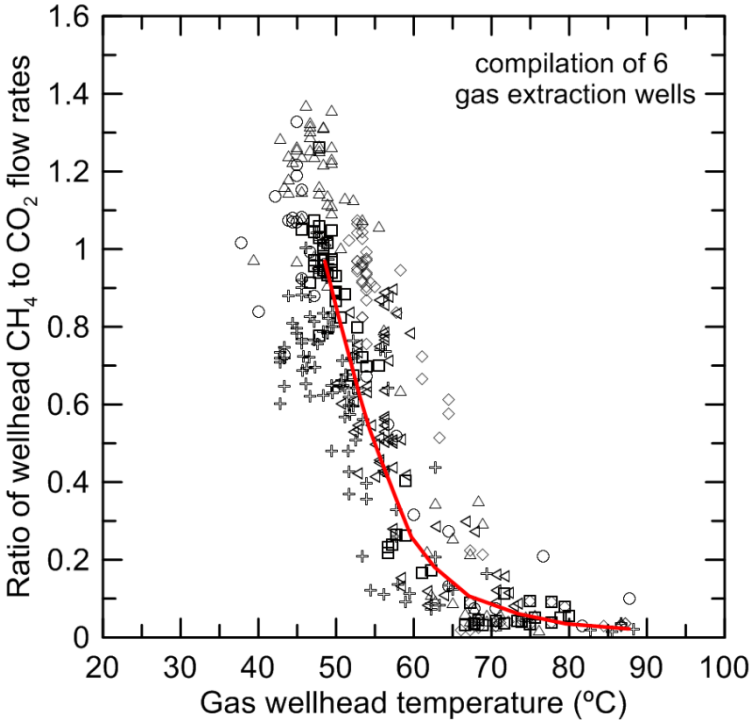

(a) Heating Front

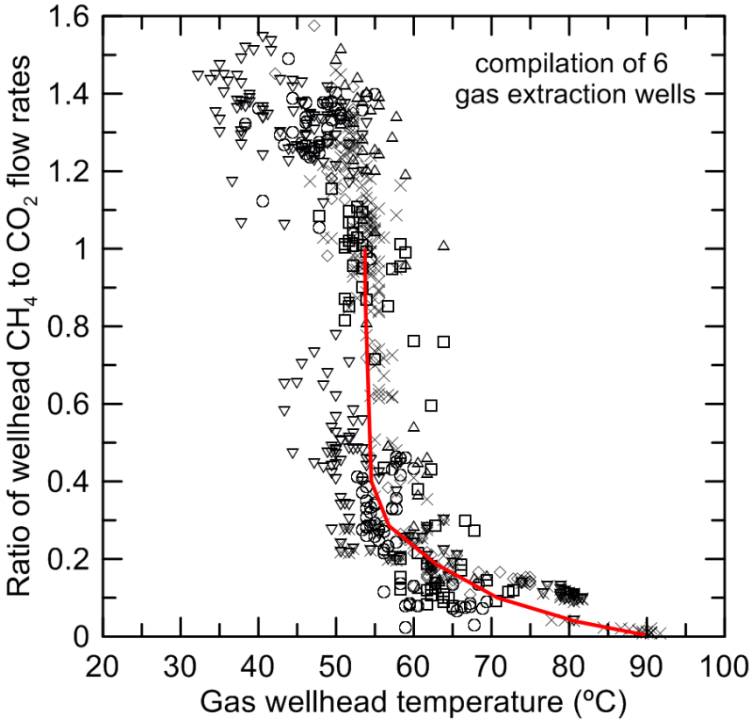

(b) Gas Front

Figure 6.12 Ratio of wellhead CH_4 to CO_2 flow rate as a function of wellhead temperature at Site 1: (a) Heating Front and (b) Gas Front

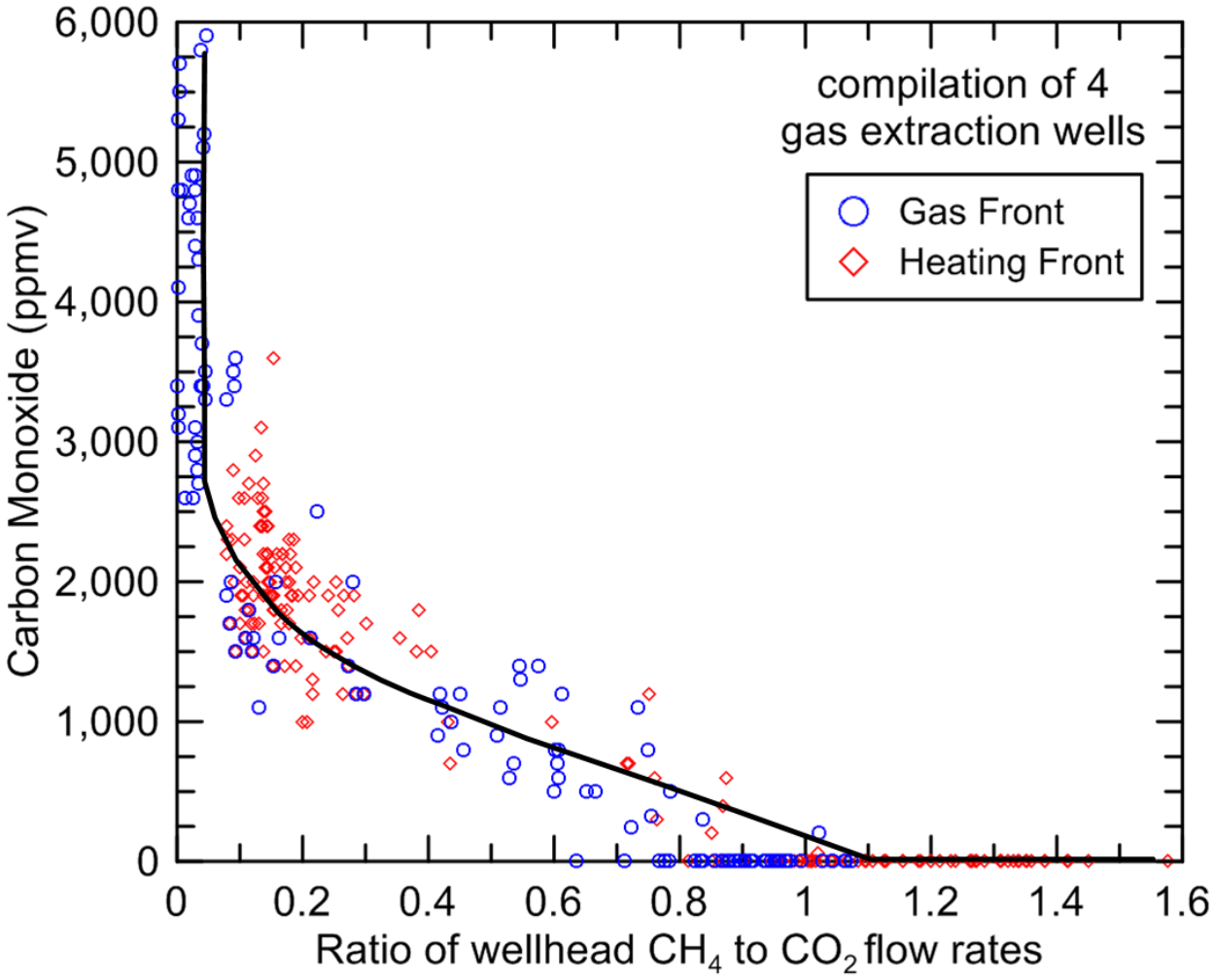

Figure 6.13 Trend of ratio of CH_4 to CO_2 and CO from gas extraction wells at Site 1

CHAPTER 7

SERVICE LIFE OF HDPE GEOMEMBRANES SUBJECTED TO ELEVATED TEMPERATURES

7.1 Introduction

Municipal solid waste facilities are required to construct a barrier system to control the escape of contaminants from the waste to groundwater or surface water bodies to negligible levels. Landfill temperature is important because it can impact performance of various barrier system components, such as the geomembrane (GMB), low hydraulic conductivity compacted soil liner (LHCSL), geotextiles (GTX), geonet drainage component (GDC), and geosynthetic clay liner (GCL). In particular, elevated temperatures can reduce the service life of HDPE geomembrane and induce possible desiccation of LHCSLs and GCLs in both single and double composite liner systems (Southen and Rowe 2004; Rowe 2005; Southen and Rowe 2005a,b; Rowe et al. 2008, 2009, 2010b; Rowe and Hoor 2009; Southen and Rowe 2011; Azad et al. 2011, 2012; Rowe 2012; Hoor and Rowe 2013).

The heat generated by anaerobic decomposition of MSW is a function of waste accepted management practice (e.g., leachate recirculation and gas system operation), and nature of the waste degradation process. For instance, Brune et al. (1991) report an increased rate of waste placement correlates with an increased rate of temperature increase. Available moisture can also accelerate the rate of temperature increase and temperature in the landfill by increasing the rate of waste degradation (Rowe 2005). As a result, liner system temperatures of 30–40°C are expected (Klein et al. 2001; Yoshida and Rowe 2003; Rowe et al. 2004; Rowe 2005; Koerner and Koerner 2006; Koerner et al. 2008; Yesiller et al. 2005; Hanson et al. 2005, 2008, 2010; Rowe and Islam 2009; Rowe 2012). However, landfill monitoring shows that heat generated by industrial waste, e.g., APW and combustion ash reactions, and smoldering combustion can significantly increase the temperature at the underlying liner system. For example, some cases temperatures up to 80°C have been measured (Calder and Stark 2010; Stark et al. 2011; Martin et al. 2012).

Rowe and Islam (2009) provide an assessment of liner temperature history for all three stages of service life based on published geomembrane ageing data. However, the liner temperature history proposed in Rowe and Islam (2009) is focused on landfills with normal MSW anaerobic

decomposition. HDPE geomembrane manufacturers do not recommend sustained temperatures greater than 57ºC (160ºF) for HDPE and 46ºC (140ºF) for linear low-density polyethylene (LLDPE) which are primarily used for final cover systems and not composite liner systems (personal communication, 2005). In particular, elevated temperatures can accelerate the depletion of antioxidants added during geomembrane manufacturing process and accelerate subsequent oxidation of the polymer leading to a loss in stress crack resistance and a decrease in geomembrane service life (Rowe et al. 2009, 2010b). Therefore, the objective of this chapter is to develop an idealized temperature history for elevated temperature events and to predict the service life of a primary HDPE geomembrane liner and hence provide insight regarding the long-term performance of engineered barrier systems.

7.2 Effect of Temperature on HDPE Geomembranes

HDPE geomembranes consist of, by weight percentage, 96 to 97% polyethylene resin, 2 to 3% carbon black, and approximately 0.5 to 1% antioxidants (Hsuan and Koerner 1998). Antioxidants are added to HDPE geomembrane formulations to reduce polymer degradation during processing and oxidation reactions during the initial stage of geomembrane service life (Hsuan and Koerner 1998). The degradation of HDPE geomembranes has been examined by a number of researchers (Hsuan and Koerner 1998; Sangam and Rowe 2002; Müller and Jacob 2003; Tarnowski et al. 2005; Needham et al. 2006; Jeon 2008; Rowe 2005; Rowe and Rimal 2008a, 2008b; Rowe et al. 2008, 2009, 2010b; Rimal and Rowe 2009) and is generally considered to consist of three stages (Figure 7.1): (1) Stage A – depletion of antioxidants; (2) Stage B – induction time to onset of polymer degradation; and (3) Stage C – polymer degradation and decrease in key physical properties (Hsuan and Koerner 1998).

During Stage A, antioxidants present in the geomembrane are progressively volatized, diffused, and/or oxidized (Koerner 1998). The duration of Stage A is important because the active antioxidants protect the geomembrane polymer from degradation. During Stage B, polymer degradation commences but there is no measurable change in geomembrane engineering properties even though the antioxidants have been significantly reduced or removed (Koerner 1998). Induction of polymer degradation continues in Stage B until the effects of the oxidation-induced scission of polyethylene chains becomes measurable (Koerner 1998). During Stage C, measurable changes in the engineering properties of the geomembrane occur (Koerner 1998) until the service

life of the geomembrane is reached. The duration of each of the three stages is referred to as depletion time (Stage A), induction time (Stage B), and degradation time (Stage C), respectively. The service life of a geomembrane is the sum of the duration of these three stages. Table 7.1 provides the service life of HDPE geomembranes subject to temperatures of 20ºC to 60ºC in a laboratory simulated landfill liner system (Rowe 2005) using 50% reduction in the tensile strength at break as the end of service life.

Figure 7.2 shows the decrease in service life with increasing temperature. Only the results for Stage A, or antioxidant depletion, are based on laboratory testing that simulates landfill disposal conditions. Stage B and C degradation are based on polyethylene pipe test results presented by Viebke et al. (1994). Although the estimated service life values assume a constant temperature, even a short duration of elevated temperature can significantly reduce HDPE geomembrane service life to several decades (see Figure 7.2) and, by extrapolation, to as little as a few years at higher temperatures (Rowe and Islam 2009).

7.3 Elevated Temperature Case History

The effects of elevated temperatures on a Subtitle D compliant composite liner system are illustrated using a case history and some of the liner system issues that can develop when a facility experiences elevated temperatures. This case is described in detail by Stark et al. (2011) so only a brief review is provided herein. The facility accepted approximately 540,000 metric tons (600,000 tons) of aluminum production waste (mostly black dross or salt cake) from 1991 through 2004. According to the March 2007 Findings and Orders issued by the Ohio EPA, from 1993 to 2006 the facility placed the aluminum production wastes (mostly black dross or salt cake) in Cells 1, 3, 4, and 6A (see Figure 7.3). Around 2005, it became obvious that the facility was experiencing an abnormal reaction because of the extremely bad odors, elevated temperatures, increased gas and liquid pressures, and rapid settlement of the waste. Based on observations and gas and leachate compositions, it was concluded that an exothermic aluminum reaction was occurring and generating considerable heat. Figure 7.4 illustrates increasing gas wellhead temperatures from April 2006 to December 2007. It is evident that between April 2006 and December 2006, temperatures increased to approximately 100°C in Cells 3, 4, and 6A. However, Cells 1 and 2 did not exhibit elevated temperatures above 55°C because the haul road (see Figure 7.4 black line)

used by disposal trucks to reach the working face of the landfill acted as a thermal barrier and prevented heat from spreading to Cells 1 and 2.

At this site, the engineered barrier system consists of a single composite liner with the following components in Cells 1 through 4 (Figure 7.5):

- 0.3 m (1 ft) leachate collection system (LCS) washed sand (Cell 1) or pea gravel (Cells 2, 3, and 4),
- 400 g/m^2 (12 oz/yd^2) to 540 g/m^2 (16 oz/yd^2) protective nonwoven (NW) geotextile,
- 1.5 mm (60-mil) HDPE geomembrane,
- 1.5 m (5 ft) low hydraulic conductivity soil liner (LHCSL).

In Cells 5A through 5D and Cell 6, the composite liner system consists of the following components (Figure 7.5):

- 0.3 m (1 ft) leachate collection system pea gravel (Cells 5D and 6) or 0.45 m (1.5 ft) shredded tires (Cells 5A, 5B, and 5C) ,
- 270 g/m^2 (12 oz/yd^2) to 540 g/m^2 (16 oz/yd^2) protective nonwoven geotextile,
- 1.5 mm (60-mil) HDPE geomembrane,
- Needle-punched reinforced geosynthetic clay liner (GCL), and
- 0.9 m (3 ft) low hydraulic conductivity soil liner (LHCSL).

In May 2007, the facility installed thermocouples in the leachate collection pipes (LCP, see Figure 7.3 for locations of thermocouples) to monitor temperature conditions at the geomembrane in the single composite liner system. The measured temperatures shown in Figure 7.6 exceed 70°C (176°F) at LCP 3B, 3C, and 4E and are sustained for the entire monitoring period. Temperatures between 38°C to 44°C were measured at LCP 1C and 2C. Temperatures at LCP 5A/B and 4C started at 40°C but increased during the monitoring period to 60°C, a result of the APW reaction expanding to the west. Given the sustained elevated temperatures, the integrity of the HDPE geomembrane was investigated.

7.3.1 Idealized Temperature Variation in a Landfill

To predict service life of an HDPE geomembrane, it is necessary to assume an idealized temperature variation with time (Figure 7.7). The temperature at the base of the landfill is assumed to start at T_o (typical ground temperature in the absence of landfilling) and remains constant until a time t_1. The temperature then increases linearly to an intermediate value of T_i (due to waste decomposition) at time t_2 and remains constant until a time t_3. The temperature increases again linearly to a peak value of T_p (due to exothermic reaction, smoldering combustion, etc.) at time t_4 and remains constant until a time t_5. After time t_5, the temperature decreases linearly and reaches the initial ground temperature T_o at time t_6 and remains constant thereafter.

Table 7.2 summarizes six idealized landfill liner time-temperature histories based on data from Figure 7.6. Cases 1 and 2 simulate LCP 1C and 2C (located in Cells 1 and 2 away from the APW reaction). They represent geomembrane service life for normal MSW landfills. Cases 3-6 evaluate the effect of peak temperatures on the geomembrane service life. As an example, Figure 7.7 illustrates the liner time-temperature history for Case 6 in context to the timeline of landfill operations. Permitted in 1991, the facility operated as a dry cell (no leachate recirculation) for the first 5 years. In April 1996, leachate recirculation began and continued until 2006, when the ongoing exothermic reaction between APW and recirculated leachate became obvious in Cells 3, 4, and 6A. As a result, the initial temperature T_o is assumed to start at 20°C and remains constant for 5 years (until 1996). After leachate recirculation commences, accelerated waste biodegradation causes temperatures to reach T_i (35°C to 45°C in Figure 7.6). Koerner et al. (2008) monitored the temperatures on the primary geomembrane at two landfill cells designated as “dry” and “wet.” Because the temperatures of the wet cell increased rapidly from 20°C to 50°C after 5.7 years of landfilling, the time t_2 corresponds to 5 years after time t_1. Gas wellhead temperatures shown in Figure 7.4 indicate that elevated temperatures escalate from 65°C (149°F) to 90°C (194°F) in April and December of 2006, respectively. Thus, the intermediate temperature T_i remains constant from 2001 to April 2006 (~4.5 years) and the time t_4 to reach T_p is about 6 months (October 2006). After December 2006, the temperatures follow the measured temperatures in Figure 7.6. Because data reflecting long-term temperatures on landfill liners during an elevated temperature scenario is not available, the idealized temperature is assumed to remain at peak temperature T_p for 5 years (end of present data in Figure 7.6). After time t_5, the temperature decreases linearly and reaches the initial temperature T_o at time t_6 and remained constant thereafter.

7.3.2 Prediction of Geomembrane Service Life

The service life of HDPE geomembranes is normally evaluated using a three-stage degradation model, i.e., Stages A, B, and C. The boundaries between Stages A, B, and C are not, in practice, as distinct and the end of Stages B and C may vary depending on the parameters being considered, e.g., tensile break strength, tensile break strain, and stress crack resistance. Because stress cracking is the mode of final failure, the authors consider this to be the most appropriate determinant of end-of-life when the data is available.

The equations used in predicting the duration of each stage of geomembrane service life considering the idealized liner temperature history are presented herein. A detailed description of these equations is beyond the scope of this chapter and can be found in Rowe and Islam (2009). The depletion of antioxidants (Stage A) is evaluated using the following equation (Hsuan and Koerner 1998):

$$\mathrm{OIT}_t = \mathrm{OIT}_o \exp\left(-\mathrm{st}\right) \tag{7.1}$$

where OIT_t = OIT remaining at any time t (min), OIT_o = initial OIT (min), s = antioxidant depletion rate (month^{-1}), t = time (month). The antioxidant depletion rate at a temperature of interest is evaluated using the Arrhenius equation (Hsuan and Koerner 1998):

$$\mathrm{s} = \mathrm{A}\exp\left(\frac{-\mathrm{E}_a}{\mathrm{RT}}\right) \tag{7.2}$$

where E_a = activation energy (J/mol), R = universal gas constant (8.314 J/mol·K), T = absolute temperature (K), and A = a constant called the collision factor. Equation 7.2 can be used directly to predict the antioxidant depletion rate at a constant temperature.

To accurately establish Stage B for a given geomembrane and exposure condition, it is necessary to first deplete the antioxidants and determine the initiation of a change in the physical properties of the geomembrane. The Arrhenius parameters for the geomembranes during Stage B are not available because laboratory experiments have not been published at more than one elevated temperature (85°C). As a result, the duration of Stage B was calculated using laboratory

data at 85°C and activation energy of 75 kJ/mol as reported by Viebke et al. (1994) for air-water exposed polyethylene pipe together with the following equations:

$$\frac{s_{85}}{s_T} = \exp\left(\frac{-E_a}{R}\left(\frac{1}{T_{85}} - \frac{1}{T}\right)\right) \tag{7.3}$$

$$\xi = \frac{s_{85}}{s_T} \times \xi_{85} \tag{7.4}$$

where T = temperature of interest (K), T_{85} = 85°C = 358 K, S_T and S_{85} are the reaction rates of Stage B at temperatures T and T_{85}, respectively, ξ = Stage B time (years) at temperature T, and ξ_{85} = Stage B (years) at 85°C. Equation 7.3 and Equation 7.4 are applicable for predicting Stage B at a constant temperature.

The calculation procedure for prediction of Stage C time is the same as that of the Stage B time described previously. Because Stage C Arrhenius parameters are not yet available, the duration of Stage C was calculated using the laboratory data at 85°C and the activation energy of 80 kJ/mol used by Viebke et al. (1994) for air-water exposed polyethylene pipe together with Equation 7.3:

$$\lambda = \frac{s_{85}}{s_T} \times \lambda_{85} \tag{7.5}$$

Antioxidant depletion times were not performed for the geomembrane installed at the case history facility, so consideration is given to three different 1.5 mm thick (60 mil) geomembranes (see Table 7.3) for which data is available with respect to Stage A, B, and C of the service life. The data from the aging tests cited in Table 7.3 are used to make the predictions. Geomembrane GM1a, GM1b, and GM2 were manufactured by GSE Lining Inc., Texas, USA and geomembrane GM3a GM3b are manufactured by Solmax International, Quebec, Canada.

For aging method “A”, the geomembrane was immersed in simulated MSW leachate (no applied stress). This is the most common aging test reported in the literature (Hsuan and Koerner 1998; Sangam and Rowe 2002; Gulec et al. 2004; Rowe 2005; Rowe et al. 2008, 2009) but is likely

to be over conservative because it implies the geomembrane is exposed to leachate on both sides. If the geomembrane is located away from holes in a composite landfill liner, the top may be exposed to leachate but the bottom is usually in contact with a LHCSL and not leachate (Rowe 2005). Aging method "B" (Rowe and Rimal 2008a) simulated a composite liner with the top face of the geomembrane exposed to leachate and the bottom face exposed to a hydrated GCL. In this method, there was no applied stress. Aging method "C" (Rowe et al. 2010b) is the most realistic and involves a full simulated composite liner (from bottom up: a sand foundation layer, geosynthetic clay liner (GCL), geomembrane, geotextile protection layer, and gravel drainage layer with circulating simulated MSW leachate) subject to a 250 kPa stress applied to the gravel leachate collection layer. Table 7.4 summarizes the time to complete Stage A, for six idealized cases.

In cases where the geomembrane was aged by immersion in leachate (GM1a, GM2, and GM3a), the time to antioxidant depletion is relatively small (12-20 years depending on the case). The higher end of the range (20 years, Case 1) corresponds to an idealized dry cell, i.e., no leachate recirculation, and 14 years (Case 2) for a wet cell (leachate recirculation). The lower end of the range is 12 to 14 years (Cases 5 and 6) for peak temperatures ranging from 70°C to 80°C. Comparing GM1a, GM2, and GM3a, initial OIT and the synthetic leachate do not significantly affect the time to deplete antioxidants for the idealized time-temperature history. As illustrated by Cases 3 and 4, the effect of intermediate temperature T_i was shown not to be a critical variable for this case study because the time-temperature history and peak temperatures controlled antioxidant depletion. For the geomembranes aged in simulated composite liner systems, e.g., GM3b, Stage A varied from 16 to 87 years for the six idealized cases.

The predictions based on leachate immersions are conservative for the geomembrane that is intact and leachate is only in contact with the upper portion of the geomembrane. In June 2006, the south slope near the juncture of Cells 5A and 6A failed due to elevated gas pressures, leachate outbreaks, and thermally degraded MSW. In March 2011, while the facility was excavating waste and installing a toe drain, an irregular fold, approximately 1.5 m to 1.8 m in length, of geomembrane was discovered near the junction of Cells 5A and 6A. Additional excavation showed that the irregular fold was a series of smaller folds and a tear of approximately 5 cm in width in the geomembrane. The tear resulted in leachate coming in contact with both sides of the geomembrane (simulating an immersion test) so antioxidant depletion time is expected to be less

than predicted from simulated landfill liner experiments (GM3b and GM1b). Because Stage A for geomembranes located at the facility is quite short, there is a need to examine the other stages of the service life to assess whether the geomembrane service life is adequate.

The estimated time to complete Stages B and C and evaluate the integrity of the geomembrane are summarized in Table 7.5 and Table 7.6, respectively, for GM3a and GM3b. For Cases 1 and 2, the geomembrane service life is likely adequate because Stage A was completed after temperatures returned to the original ground temperature. For Cases 3 and 4, by the end of Stage A there was only a very limited time remaining at the peak temperature (e.g., 1 year for Case 3 and GM3b), thus the predicted time in Stage C is long. Cases 5 and 6 illustrate that peak temperatures of 70°C and 80°C, respectively, cause substantially shorter geomembrane service life and the integrity of the geomembrane may be compromised. The service life of HDPE geomembranes (Table 7.7) is calculated by adding the durations of Stages A through C presented in Table 7.4 through Table 7.6. The service life varied from 20 to 960 years. For situations like Case 6, the service life of the geomembrane could well be reached within the contaminating lifespan. The substantial difference in predicted time is significant and highlights the need to consider the possible effects of elevated temperatures and landfill time-temperature history when designing landfills.

The predictions of Stages B and C are based on available data for stress crack resistance (GM3a). Although there was no data for GM3b in a simulated liner, available data from immersion of GM3a in leachate was used for predicting Stage B times for GM3b. Stage C has not been completed at any elevated temperature. The reported values are based on the time in Stage C at 85°C in the laboratory immersion experiments together with the E_a= 80 kJ/mol used by Viebke et al. (1994) for air-water exposed polyethylene pipe. As a result, the data used to predict Stages B and C are presented in Table 7.5 and Table 7.6 only to illustrate the impact of elevated temperatures on geomembrane service life. For example, the geomembrane service life of GM3b for Case 6 is approximately 20 years for the geomembrane aged with leachate present on only one side. However, the slope failure in 2006 caused the liner to tear and allowed leachate to contact both sides of the geomembrane and hence the service life could be shorter than 20 years. Given the sustained elevated temperatures and exposure conditions, the next sections investigate possible indicators of the integrity of the composite liner system.

7.3.3 Integrity of Geomembrane Liner

Waste containment system performance data, e.g., groundwater monitoring wells, are used to assess the integrity of the composite liner system. Because the composite liner system for the case history is located below the groundwater surface, one possible indication of the loss of integrity of the composite liner system is reflected in the increased leachate volume (groundwater inflow due to an inward gradient) pumped from Cells 1-6. From 1999 until 2005, most of the leachate generated (103 million liters) was recirculated so the volume of leachate transported off-site during this period was minimal. In 2004, the transported leachate volume was 12 million liters (3.1 million gallons) and continued to increase in subsequent years with 109 million liters (29 million gallons) in 2006 and 127 million liters (33.6 million gallons) in 2008. The amount of leachate generated by the effects of the reaction and subsequent combustion significantly exceeds the total amount of leachate recirculated, which may be evidence that the composite liner system is compromised. However, other potential sources of the excess leachate are: (1) water generated by the heating and/or combustion of organic wastes (i.e., initial waste moisture content); (2) possible groundwater inflow due to an inward gradient through the slope movement damaged liner system; and (3) rainfall infiltration.

Thermal dehydration of the MSW drives moisture from the waste and the resulting liquid is removed via the leachate collection system or gas extraction system. The initial moisture content of the MSW was estimated to be about 20% because of the leachate recirculation prior to the reaction. Cells 1-6 contain an estimated 10.9 million m^3 (14.3 million yd^3) of airspace. Assuming both complete thermal dehydration of MSW and half of the moisture is removed by the gas extraction system, a total increase in leachate of 605.7 million liters (160 million gallons) may be generated from the waste. The leachate volume was estimated using a reaction area of about 16 hectares (~45% airspace) multiplying it by 20% and a MSW unit weight of 12 kN/m^3. From 2006 to 2011, approximately 654.2 million liters (~172.8 million gallons) of leachate was transported offsite.

The sidewall liner on the south side of the landfill in the vicinity of Cell 6 was damaged due to gas pressures, leachate chemical composition, and the 2006 slope failure. Because the liner system was compromised, groundwater from the confining mine spoil and underlying shale and siltstone bedrock could have migrated into the waste mass and contributed to the excessive leachate volume because the liner system is below the zone of saturation in the mine spoil. Based

on the earlier discussion, a sustained temperature of 80°C for four years (and even less at higher temperature) may have been sufficient to cause failure of the geomembrane. Thus, some of the excess leachate could be the result of water ingress through the liner system if the geomembrane failed.

Infiltration of precipitation is not thought to have contributed significantly to the increased leachate volume because a significant portion of the 35.7 hectares (Cells 1 through 6 in Figure 7.3) was covered with a 2.0 mm (80 mil) thick HDPE geomembrane to control odors after 2006. However, prior to placement of this cover geomembrane, surface water ponding occurred within a large bowl-shaped area at the top of the landfill created by rapid settlement of the underlying waste, which may have contributed some moisture to the leachate quantity.

7.4 Evaluation of HDPE Geomembrane Service Life

The presence of elevated temperatures at or near a liner system in the case history described above, as well as others, raises the question of how should service life of the liner system and in particular the geomembrane be assessed. This question is usually raised after elevated temperatures have been detected and leads to many questions, such as, what criteria should be used to assess service life, how should the criteria be investigated, and what remedial measures should be implemented for the liner system.

7.4.1 Examples of Possible Service Life Criteria

This issue is complicated in the United States because there is no regulation on the required service life of a HDPE geomembrane. In contrast, Ontario (Canada) Regulation 232/98 requires a service of 150 years for the primary liner system and 350 years for the secondary liner system in the double composite liner system required for a Subtitle D compliant landfill (OMoE 1998). Based on the data presented in Table 7.7, the geomembranes described in the elevated temperature case history above would not meet Ontario Regulation 232/98 because the time-temperature history service life analyses of the 1.5 mm thick HDPE geomembrane is significantly less than 150 years. Because the Subtitle D in the United States does not specify a service life as Ontario Regulation 232/98 does, some possible service life durations are listed below:

- 150 years as required by Ontario Regulation 232/98;

- Long term performance based on monitoring criteria;
- Service life of HDPE geomembrane (Stages A, B, and C) using time-temperature history.

The Ontario Regulation 232/98 is clear about the required service life, and suggests that this might be achieved for a geomembrane used in a normal MSW landfill where liner temperatures are 30-40ºC (it was not written for bioreactor landfills and did not envisage co-disposal with aluminum production waste) provided the following requirements are met:

- The initial oxidation induction time of the geomembrane exceeds 100 minutes as determined by ASTM D3895 or 250 minutes as determined by ASTM D5885;
- The oxidation induction time of the geomembrane after oven aging at 85°C for 90 days as described in ASTM D5721 must exceed (a) 80% of the value for the original geomembrane as determined by ASTM D3895 or (b) 80% of the value for the original geomembrane as determined by ASTM D5885.

Of course, a sample of the impacted geomembrane must be obtained from the facility to assess the oxidation induction time, which may be difficult because of the presence of waste and elevated temperatures.

Long-term performance of a containment barrier system, i.e., integrity of the liner system and the components over time, can be evaluated using direct and indirect monitoring methods. The primary liner in a double-liner system is perhaps the only type of engineered barrier system in which post construction integrity is routinely monitored directly. Liquids collected in the leak detection layer between the primary and secondary liners provide a direct assessment of the performance of the primary liner system. For example, a double composite liner system consisting of (from top to bottom) GMB, GCL, GDC, and GMB can be an effective barrier system and provide direct performance of the primary liner. Although leak detection layers are advantageous for monitoring large areas of barriers, the data can be difficult to distinguish the effects of LHCSL consolidation from induced flow in systems (Bonaparte et al. 2002). Indirect monitoring of engineered barrier performance by monitoring for contaminant migration downstream of the waste containment system is mandated by regulations. However, there will be a time lag between the loss of the hydraulic effectiveness of the geomembrane and contaminants being detected. The length of this time lag will depend on site hydrogeology and the type and location of the

groundwater monitoring wells being used to detect the leakage. The time lags may cause a change in economic viability of the facility before leakage is detected resulting in insufficient funds being available for an expensive cleanup.

Hsuan and Koerner (1995) selected the criterion for geomembrane service life as when a specific design property has been reduced by 50% of its initial value. This is referred to as the half-life of the geomembrane. Although the design property, e.g., tensile strength or strain at break, may be reduced by 50% and the geomembrane becomes brittle, the geomembrane may still function as a hydraulic barrier. Thus, this half-life concept may not be appropriate for estimating the service life of a geomembrane for containment purposes (Rowe 2012).

Using geosynthetic landfill liner simulators (GLLS), Rowe (2012) reports that when geomembranes reach the end of their service life they experience extensive stress cracking and the number of holes goes from a few holes/ha to 30 to 100 holes/m^2. The geomembrane can no longer be considered functional so leakage will be controlled by the LHCSL and/or GCL underlying the geomembrane. It seems appropriate then to define the service life of HDPE geomembranes as the time from installation to onset of stress cracking, i.e., total time to complete Stages A, B, and C where Stage C is completed when leakage begins. Although the time to complete Stage A is well-established in laboratory experiments, to accurately establish Stage B for a given geomembrane and exposure condition it is necessary to complete Stage A (depletion of antioxidants), observe the initiation of a change in the physical properties (end of Stage B), and perform the experiment at least three temperatures (Rowe and Islam 2009). Given the quality of geomembranes, this takes a long time at all but the highest temperature examined, so limited experimental data is available to calculate Stages B and C (Rowe and Islam 2009). As geomembrane aging experiments continue to mature, it is anticipated that better estimates of Stage B and C durations will become available. In addition, not all HDPE geomembranes exhibit the same durations, e.g., antioxidant packages differ between manufacturers so the duration of Stage A will vary. There is a large uncertainty associated with evaluating the service life using Stage B through C degradation model from laboratory experiments.

The activation energies used for Stages B and C were also obtained for pipes and not geomembranes so service life predictions may change when data becomes available. Because of geomembrane variations, it is recommended that service life criteria for HDPE geomembranes consider Stages A, B, and C where failure is defined as leakage due to stress cracking. The

duration of Stage A is calculated using the time-temperature history of the site and Arrhenius parameters determined from laboratory experiments. The analyses presented in the section above titled: “Elevated Temperature Case History” highlight the importance of the time-temperature history and exposure conditions in evaluating the service life of a geomembrane. For example, Cases 1 and 2 for GM3b have long Stage A completion times and hence a service life can be expected while the geomembrane is still in Stage A. Cases 3 and 4 show antioxidants are depleted near the end of the peak temperatures. For Cases 5 and 6, the antioxidants deplete at the beginning of the peak temperature and so the service life of the geomembrane and remedial actions may require careful examination.

7.4.2 Location of Service Life Assessment

It is implicit in Ontario Regulation 232/98 (although not clearly stated) that the location where geomembrane service life should be assessed is the most critical location (i.e. that which would allow an escape of contaminant to the environment that might exceed the maximum allowable concentrations as defined in §10 of OMoE 1998). One such critical location is the sump where sustained liquid and gas pressures may be present that could facilitate advective and diffusive flow. Of course, this assumes there is no clogging of the leachate collection system that could result in sustained liquid and gas pressures accumulating at other places above the liner system besides the sump. For example, most geomembranes are placed with some wrinkles (Chappel et al. 2012; Rowe 2012). These wrinkles can result in local ponding of leachate, especially on a relatively flat landfill base, until the leachate level is high enough to flow over the wrinkle.

Another area where service life could be evaluated is landfill side slopes because the liner system, in particular the geosynthetics and the LHCSL, are subjected to tensile stress imposed by the waste especially if it is settling due to overburden stresses, waste degradation, or waste reaction or combustion. Thus, it seems the service life would need to be met everywhere.

7.5 Possible Remedial Measures

Some of the possible remedial measures that could be implemented after sustained elevated temperatures are measured on or near the liner system include:

- Excavate the waste so the liner system can be repaired as was done for a hazardous waste landfill containing industrial waste sludges and other chemical manufacturing by-products that experienced temperatures near the liner system of about 800ºC (Adams et al. 1997). Adams et al. (1997) describe the damage to the geosynthetic components of the liner system in the immediate vicinity of the combustion as complete disintegration, melting, and/or fusing of the various components together near the center of the heated area. Rippling and stretching of the materials along the perimeter of the visibly damaged area also occurred. In several areas, melted geosynthetic materials were observed in desiccation cracks in the secondary LHCSL (Adams et al. 1997).
- Install additional ground water monitoring wells down gradient of the area subjected to elevated temperature to facilitate detection of leakage. If leakage is detected, the closer spaced monitoring wells should trigger a quicker remedial action. One of the drawbacks of this approach is that if leakage is detected, the contaminants, i.e., leachate and gas, have already entered the subsurface which can substantially increase remediation costs.
- Stop active filling in the portion of the landfill experiencing elevated temperatures and apply a suitable low hydraulic conductivity cover to prevent infiltration.
- In addition to installing additional ground water monitoring wells down gradient of the elevated temperature area, increase the required post-closure bonding to compensate for possibly higher remediation costs.
- The facility can perform aggressive leachate removal to minimize leachate head on the composite liner system. However, this may introduce other challenges, e.g., the case study described above yielded leachate quality that could not be treated locally and had to be shipped about 400 km for treatment at considerable cost.

7.6 Summary and Conclusions

This chapter highlights some of the questions that can arise when assessing the integrity of a composite liner system in the presence of sustained elevated temperatures. Based on experiences with landfills with elevated temperatures, the following conclusions and recommendations are presented based on data and the case history presented:

1. The presented case history shows temperatures at a MSW facility increased from normal operating conditions (35°C to 45°C) to elevated temperatures (70°C to 85°C) due to APW

reactions and smoldering combustion of MSW. Thermocouples installed in leachate collection pipes were used to develop a time-temperature history plot to assess the service life of the geomembrane. For GM3b, Cases 1 and 2 temperatures are in the range of normal MSW landfills; the geomembrane is expected to have a service life of several centuries. When peak temperatures reach 60°C to 80°C, the geomembrane service life can be reduced to decades for the conditions examined and thus raises concerns regarding the integrity of the geomembrane at high temperatures.

2. Although laboratory experiments evaluating the geomembrane activation energies used for Stages B and C have not been completed, the recommended criterion to estimate the service life of a geomembrane is the sum of time to complete antioxidant depletion (Stage A), Stage B, and time to stress cracking of HDPE geomembrane (Stage C). Using Arrhenius parameters for geomembranes determined via laboratory experiments and a time-temperature history plot, Stage A duration can be evaluated from Equation 7.1 and Equation 7.2. An approximation of Stage B and C can computed using Equation 7.3 through Equation 7.5.
3. Assuming proper construction and operations, the service life of a geomembrane liner used in a Subtitle D landfill will depend on temperature and time-temperature history, the chemical composition of the leachate, and the geomembrane properties. With respect to wide range of HDPE geomembranes, the resin and antioxidant package used may have a significant impact on the geomembrane's long-term performance in landfill applications. Therefore, the selection of an appropriate geomembrane is critical to the system's long term performance. The standard specification (GRI-GM13 1997) represents a basic starting point. While the minimum requirements may be sufficient for some applications, the specification GRI-GM13 may not be adequate for other applications such as elevated temperatures. Prior to geomembrane installation in landfills, laboratory experiments simulating higher temperatures and exposure conditions by the manufacturer or the designer are recommended to ensure adequate performance of the antioxidant package and resin to elevated temperatures.
4. Assessing the integrity of a composite liner and geomembrane is difficult and dependent on site geology and location of ground monitoring wells. For the design of new landfill cells, the barrier system should reflect the type of waste, e.g., MSW, APW, incinerator ash,

etc., and mode of operation (dry cell, leachate recirculation, bioreactor). Installing a leak detection layer below the primary liner and thermocouples to monitor the temperature provides direct monitoring of the liner performance. In addition, various strategies can be adopted to control the liner temperature (Hoor and Rowe 2012) and maintain an adequate geomembrane service life.

7.7 Tables and Figures

Table 7.1 Estimated HDPE geomembrane service life based on 50% reduction in tensile strength at break for different temperatures (based on Rowe 2005)

Temperature (ºC)	Service Life (years)
20	565-900
30	205-315
35	130-190
40	80-120
50	35-50
60	15-20

Table 7.2 Summary of liner temperature histories examined

	Time (years)						Temperature (°C)		
Case	t_1	t_2	t_3	t_4	t_5	t_6	T_o	T_i	T_p
1	5	10	---	---	20	35	20	35	---
2	5	10	---	---	20	35	20	45	---
3	5	10	14.5	15	20	35	20	35	60
4	5	10	14.5	15	20	35	20	45	60
5	5	10	14.5	15	20	35	20	45	70
6	5	10	14.5	15	20	35	20	45	80

Table 7.3 Initial properties and aging conditions of 1.5 mm thick geomembranes

GMB	Aging Condition	Leachate	Std-OIT (min) [ASTM D3895]	Arrhenius equation	Ea (kJ/mol)
GM1a	A	X	135	$\ln(s) = 19.85 - \frac{7084}{T}$	58.9
GM1b	B	X	135	$\ln(s) = 20.06 - \frac{7540}{T}$	62.7
GM2	A	Y	174	$\ln(s) = 20.32 - \frac{7315}{T}$	60.8
GM3a	A	Y	135	$\ln(s) = 20.37 - \frac{7304}{T}$	60.7
GM3b	C	Y	135	$\ln(s) = 20.63 - \frac{7703}{T}$	64

A: geomembrane immersed in simulated MSW leachate
B: simulated composite liner system with MSW leachate on one side
C: simulated composite liner system with MSW leachate on one side with 250 kPa overburden
X: synthetic leachate consisted of inorganic nutrients, volatile fatty acids, surfactant, trace metals, and reducing agent;
Y: synthetic leachate consisted of surfactant, trace metals, and reducing agent

Table 7.4 Time to complete Stage A

	Antioxidant Depletion (years)				
Case	GM1a	GM1b	GM2	GM3a	GM3b
1	15	90	20	19	87
2	12	28	14	13	26
3	15	19	16	16	19
4	12	18	14	13	17
5	12	17	14	13	16
6	12	15	14	13	16

Table 7.5 Estimated time to complete Stage B

	Time to complete Stage B (years)					
GMB	Case 1	Case 2	Case 3	Case 4	Case 5	Case 6
GM3a	110	19	4	5	3	2
GM3b	140	120	5	4	2	1

Table 7.6 Estimated time to complete Stage C

	Time to complete Stage C (years)					
GMB	Case 1	Case 2	Case 3	Case 4	Case 5	Case 6
GM3a	690	690	450	390	6	3
GM3b	690	690	620	560	49	3

Table 7.7 Summary of geomembrane service life

	Service Life (years)					
GMB	Case 1	Case 2	Case 3	Case 4	Case 5	Case 6
GM3a	820	720	470	410	22	18
GM3b	920	850	650	590	68	20

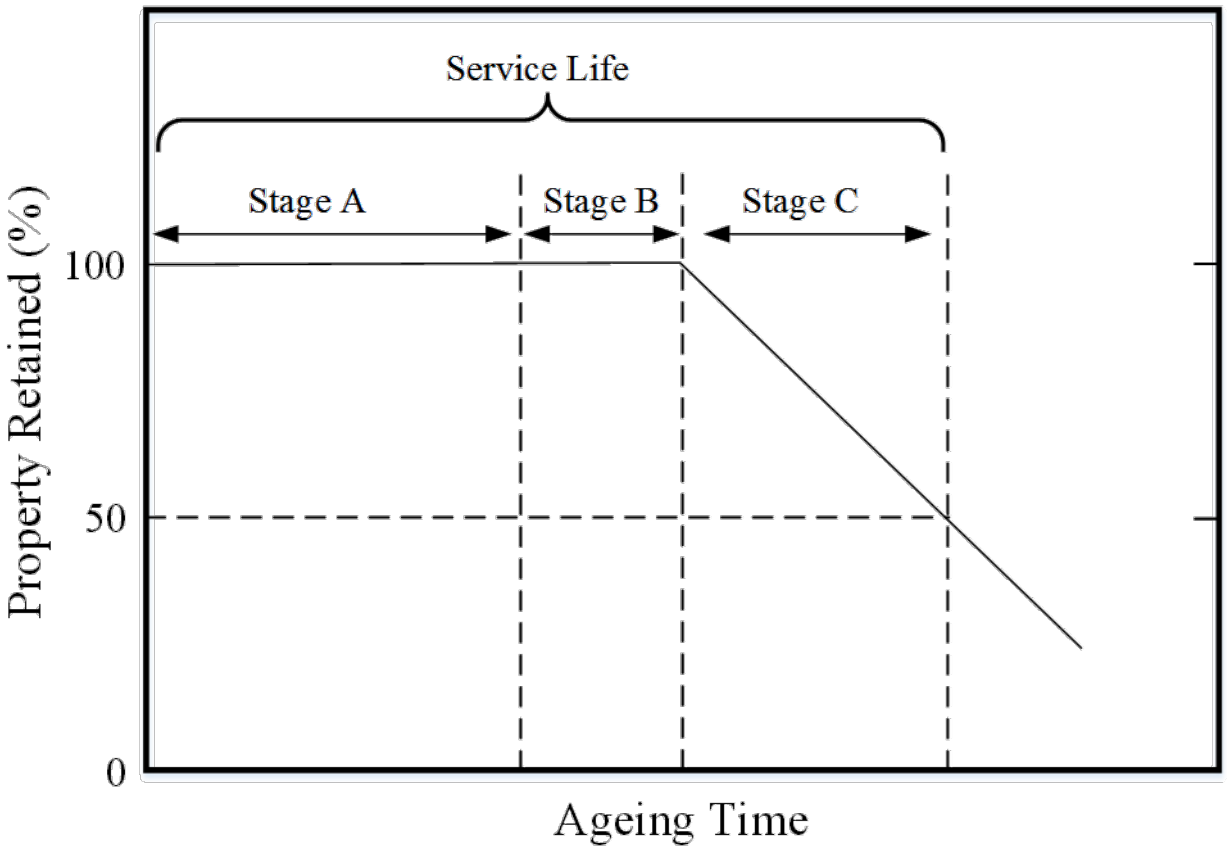

Figure 7.1 Three conceptual stages in chemical ageing of HDPE geomembranes

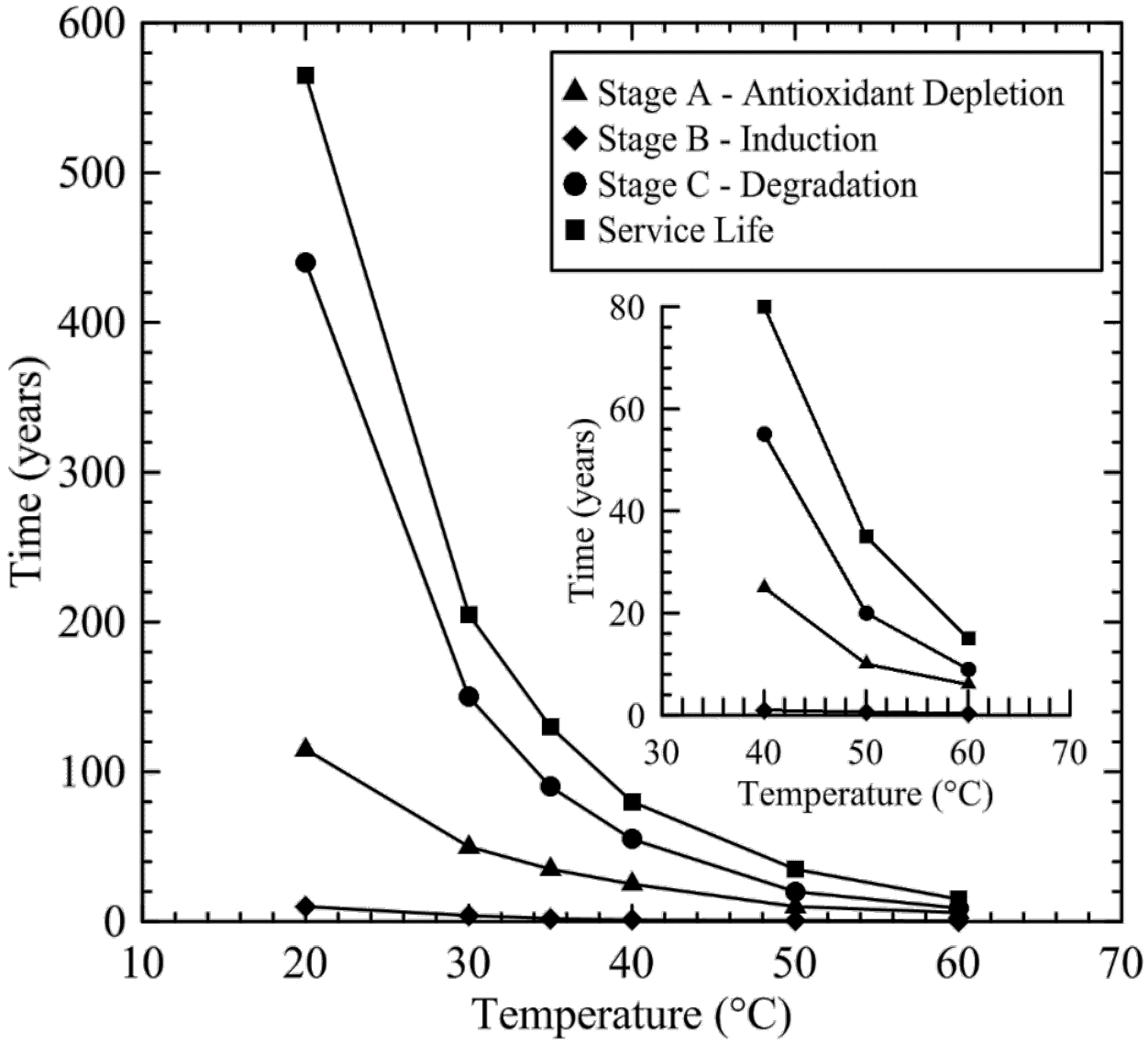

Figure 7.2 Duration of degradation stages A, B, and C and total service life based on 50% reduction in tensile strength at break (data from Rowe 2005)

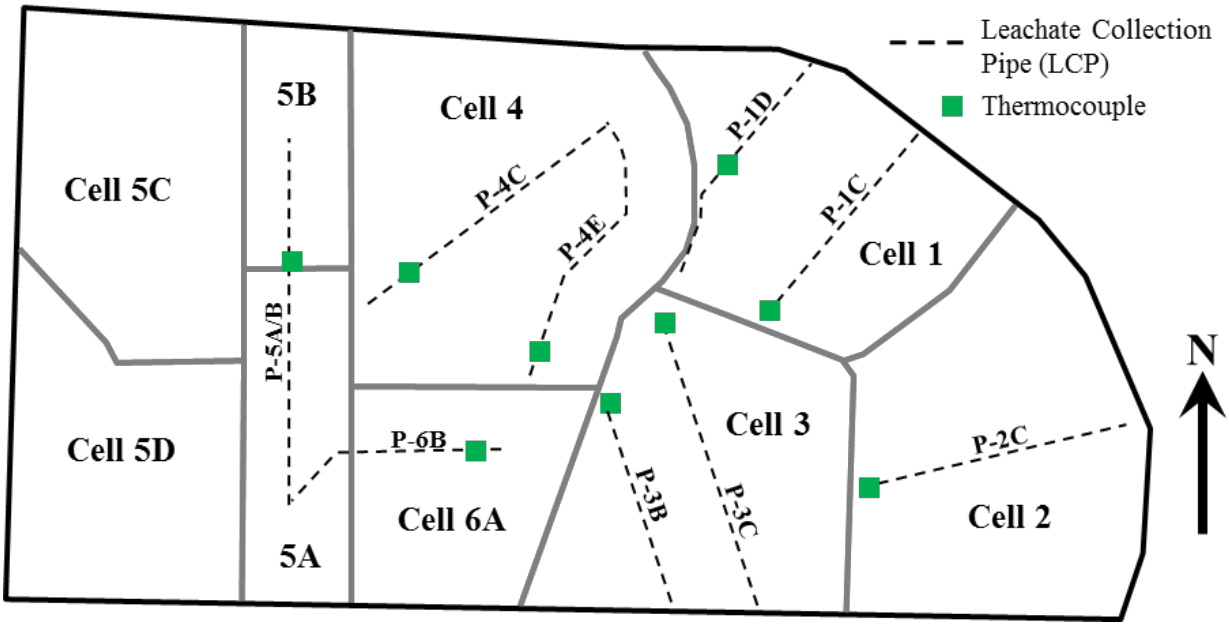

Figure 7.3 Sketch of Cells 1-6 and thermocouple locations

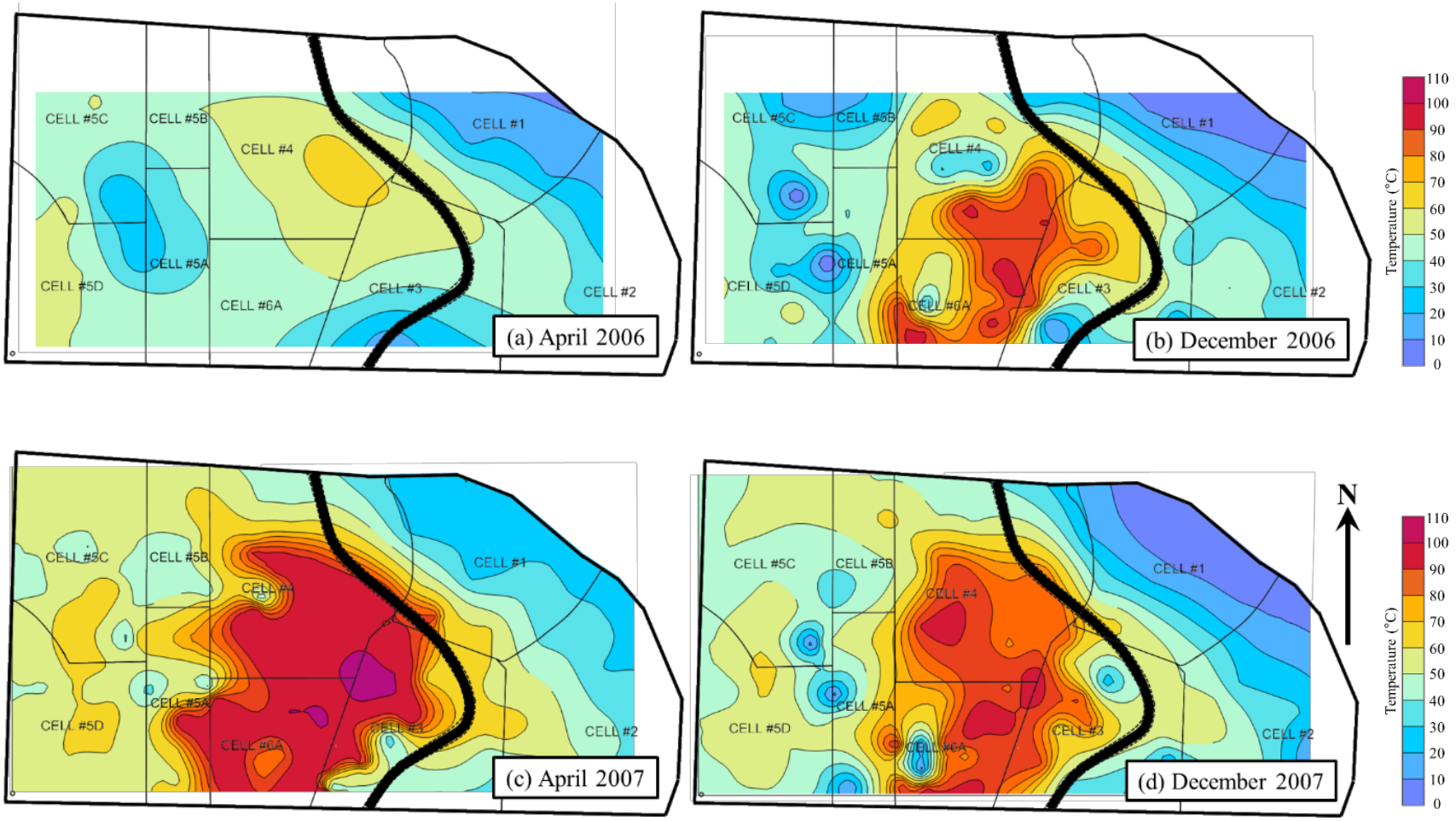

Figure 7.4 Spatial expansion of elevated gas wellhead temperatures at MSW landfill (Jafari et al. 2014)

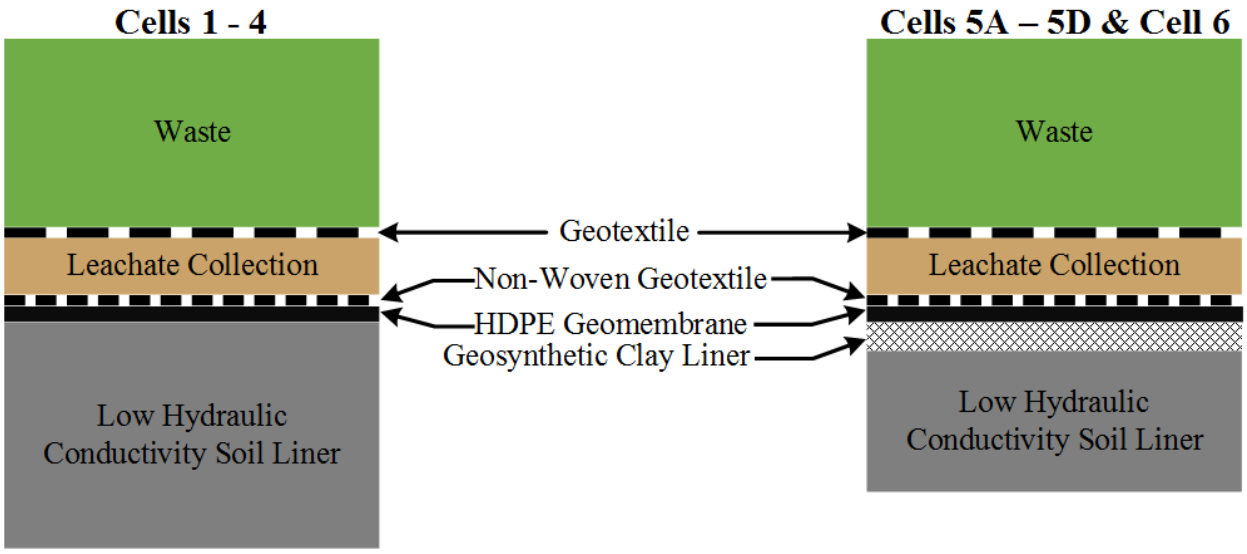

Figure 7.5 Schematic of composite liner systems for Cells 1-4, Cells 5A – 5D, and Cell 6

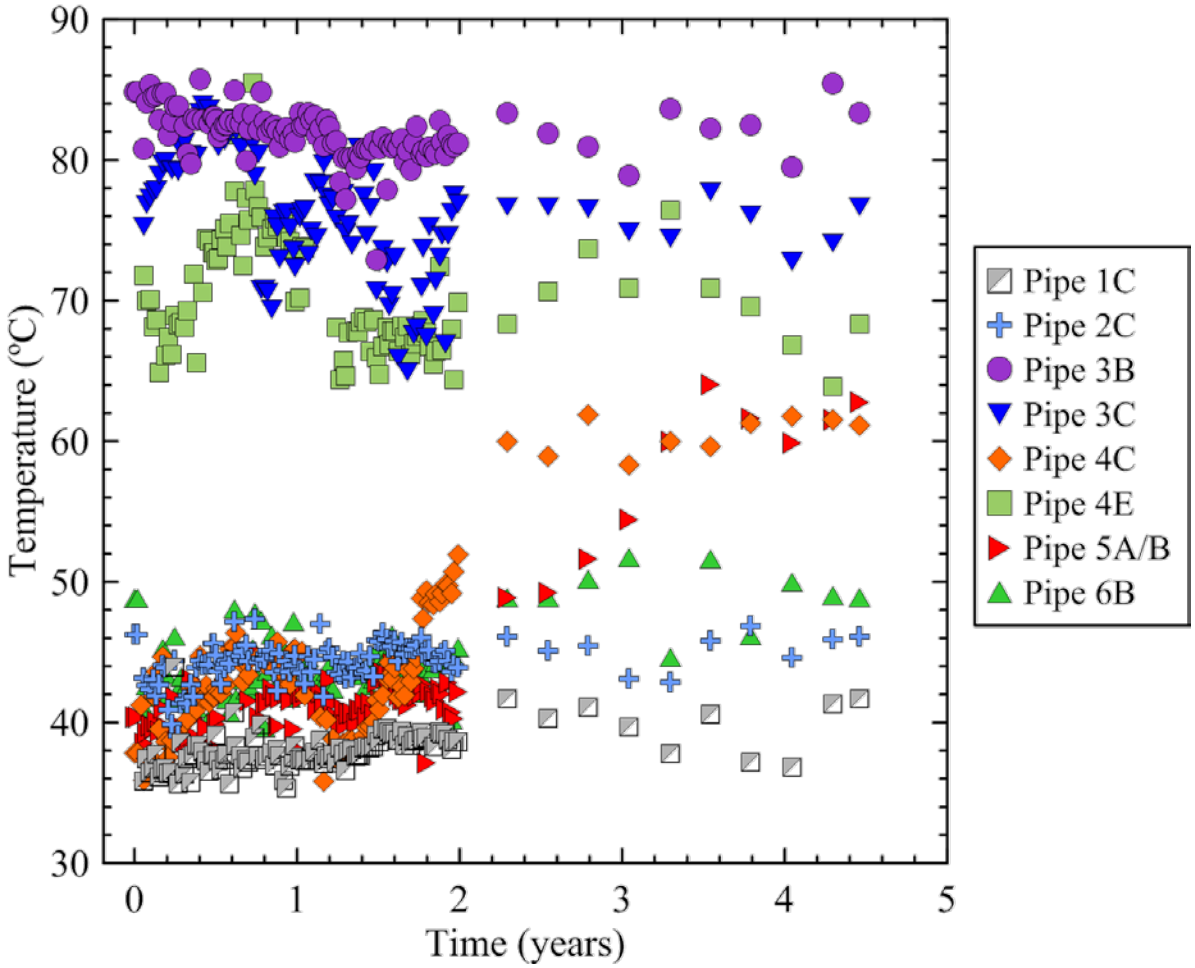

Figure 7.6 Leachate collection system temperatures as a function of time

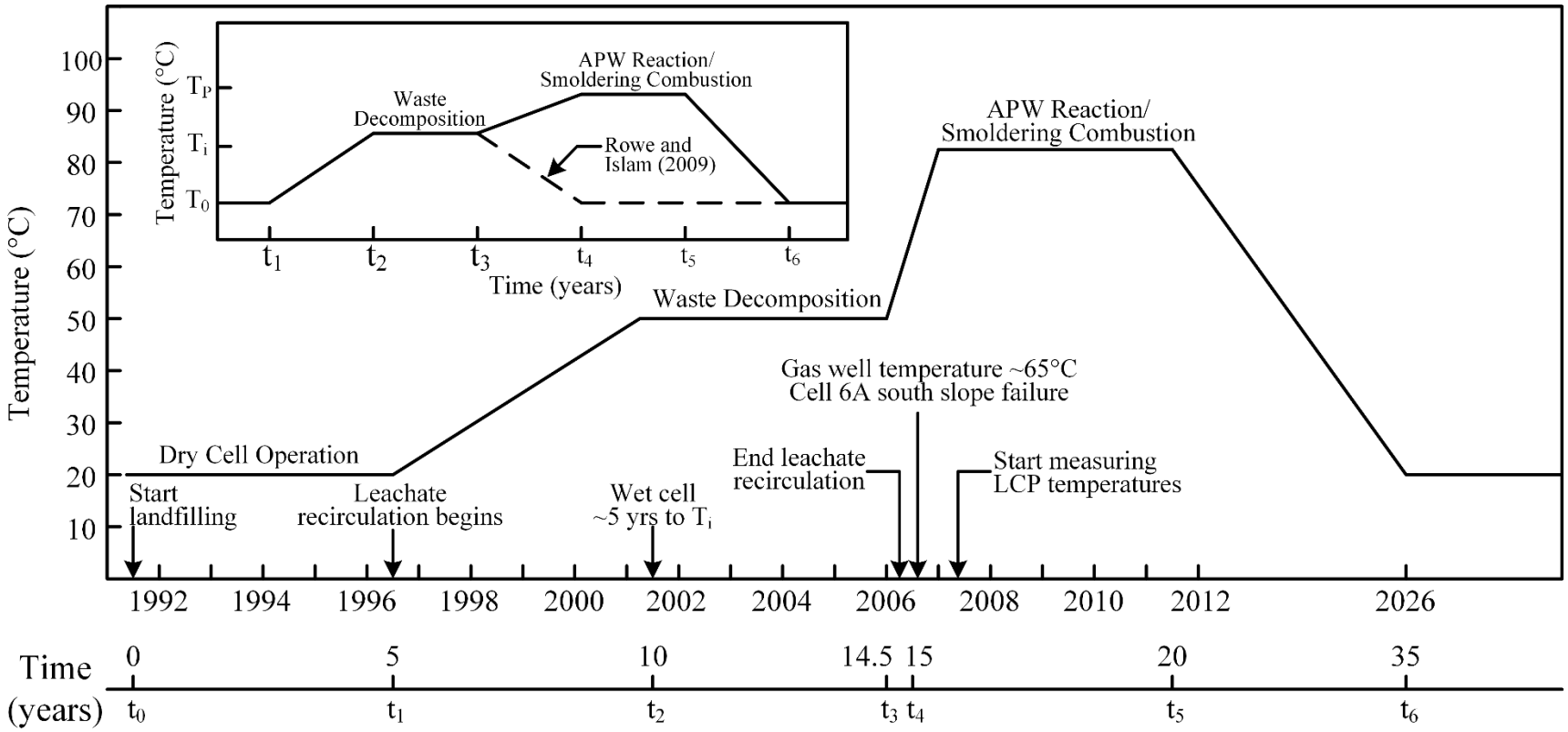

Figure 7.7 Idealized temperature variation with time in a landfill under elevated temperatures

CHAPTER 8

SUMMARY AND CONCLUSIONS

8.1 Summary

The presence of elevated temperatures in waste containment landfills can impact the integrity of the cover and liner systems, leachate quality, gas composition, slope stability and differential settlement, odor mitigation, and abatement operations. In addition, they present a significant threat to the environment by emitting to the atmosphere incomplete combustion byproducts, reduced sulfur compounds, and particulate matter.

A review of case histories found that elevated temperatures occur throughout the world. FEMA (2002) estimates that ~8,400 landfill fires occur every year in the U.S.A. Ettala et al. (1996) states that ~60% of operational landfills in Finland reported fires annually, and 200 to 250 fires were reported in 400 Swedish landfills (Ruokojarvi 1995; Naturvardverket 1994). In the United Kingdom, 57 incidents were reported to the environmental agency over a 10 month period in 2002 (Environmental Agency 2007). Poorly managed sanitary landfills and dumps in the Philippines and Indonesia resulted in waste slides and hundreds of deaths.

Several factors can lead to elevated landfill temperatures, including aerobic decomposition, self-heating, partially extinguished surface fires, exothermic chemical reactions, and spontaneous combustion. The leading mechanism of landfill fires is air ingress and subsequent spontaneous combustion. Recently, landfills are experiencing elevated temperatures due to exothermic reactions from reactive wastes. In particular, the disposal of aluminum production waste in landfills is causing environmental pollution through its high reactivity with leachate, precipitation, or even humidity in air, leading to the heat generation and formation of toxic, explosive, and odorous gases. A review of two case studies found that aluminum production waste does not meet hazardous waste classification criteria so it is disposed in MSW landfills. As a result, this thesis focused on developing a calorimeter test procedure to simulate reactivity, or heat generation potential, under landfill conditions. APW is used as an example of industrial waste to show the efficacy of the reactivity test to evaluate heat generation potential and prevent reactive waste for being landfilled. In addition, this study developed an experimental setup to measure gas production

and ammonia concentrations. Gas generation rates for several APW samples are presented and corroborated with x-ray diffraction results.

Aluminum wastes, air ingress, or other mechanisms can lead to elevated temperatures in a localized area, but over time they can expand and consume entire landfill facilities. Thus, the present thesis used a case study to develop a progression of landfill indicators to show these events follow a systematic spatial and temporal sequence. The progression of indicators allows landfill operators and first responders to detect and identify the location of elevated temperatures. Expanding on the progression of indicators, the current study used two case histories to investigate the spatial and temporal changes in landfill indicators. The first case study illustrates spatial movements with gas extraction wells and settlement points. The second case study demonstrates subsurface temperature migration. This case study also provides a comparison of waste temperatures to gas wellhead gas composition and temperatures. These two case studies along with the progression of indicators were used to classify MSW landfills into five zones.

Furthermore, elevated temperatures can negatively impact engineered components in composite bottom liners, cover systems, leachate collection, and gas extraction and recovery systems. A case study is used to investigate the effect of elevated temperatures on HDPE geomembrane service life. Geomembrane service life criteria and possible remedial measures are also proposed.

8.2 Conclusions

Based on this study, the following conclusions are drawn concerning reactivity of aluminum production waste:

- Aluminum production wastes are reactive but not necessarily hazardous under 40 CFR Sec. 261, Subpart C. Calorimeter experiments at varying NaOH strengths show temperatures rise to 100°C. The optimal concentration of NaOH was determined to be 1M to 2M NaOH, which provides sufficient alkalinity to react the metallic Al and fulfill the objectives of a rapid procedure to evaluate APW reactivity per hazardous waste classification. XRD analyses or hydrogen gas production can complement the reactivity tests by corroborating the amount of Al present and similar temperature increase and reaction rates. The maximum recommended temperature for the calorimeter test is 65°C (~150°F) to permit waste decomposition in MSW

landfills and prevent elevated temperatures from impacting engineered components (composite liner system, gas vents, and leachate collection system).

- Preliminary laboratory gas experiments show cumulative gas volumes increase with increasing NaOH strength, where 5M NaOH was determined to provide sufficient alkalinity to maximize gas production. Ammonia concentrations range from 2,600 to 6,200 ppmv and methane concentrations were <2% v/v. In addition, hydrogen was the dominant gas generated from the APW reaction because of the correlation to total gas generated.

Based on this study, the following conclusions are drawn concerning the progression of indicators, spatial movement, and classification of MSW landfills during elevated temperatures:

- Landfill temperatures can be measured: (1) at the gas wellhead, (2) from samples recovered during drilling, and (3) with thermocouple arrays installed at various depths in gas extraction well pipes, in boreholes, and in leachate collection pipes. For one-time sampling events, such as the thermal infrared camera, temperatures are less accurate because heat gain or loss may occur during drilling operations or during removal of samples from landfills. Gas wellhead temperatures can be about 20°C lower than downhole temperatures because wellhead temperatures are influenced by mixing with surrounding gases in the wellhead and convective heat loss from waste to the ground surface. In addition, a gas wellhead represents a composite temperature over finite waste thickness.
- The case study in Chapter 5 shows that the initiation and expansion of elevated temperatures results in a sequence of indicators that delineates the location, boundary, and movement. These indicators follow the systematic progression: (1) changes in landfill gas composition; (2) elevated waste and gas temperatures; (3) increased leachate volume and migration; (4) elevated gas and leachate pressures; (5) slope movement; and (6) excessive and rapid settlement.
- Evidence of carbon monoxide suggests that smoldering combustion is occurring and generating heat for pyrolysis to occur. Pyrolysis can produce hydrogen when temperatures exceed 600°C or at lower temperatures through the water-gas shift reaction. It is also possible that before the elevated temperatures advance to areas where methanogenesis prevails, waste is heated to the thermophilic range and acetogenesis produces hydrogen gas. However,

temperatures in the settlement bowl should be 240 to 380°C to degrade the cellulosic fraction of MSW, while temperatures ranging from 410 and 500°C degrade the plastic components.

- Based on the vertical strain rate behavior of Site 1 in Chapter 6, strain rates below 2%/yr indicate normal biodegradation settlement while vertical strain rates greater than 3%/yr indicate elevated temperatures.
- Contour plots of the ratio of CH_4 and CO_2 and vertical strain rate can capture the spatial migration of elevated temperature events. The ratio of CH_4 to CO_2 of 1.0 to 0.6 is used to depict the transition from anaerobic biodegradation to elevated temperatures. The strain rate contour plots provide a useful method to characterize the location where thermal degradation is the dominant process. When combining ratio of CH_4 to CO_2 and vertical strain rate contour plots, gas ratio contours are in front of accelerated strain rates because heat is transferred by conduction and time is required to thermally degrade the waste.
- The installation of DTAs provides four important pieces of information to evaluate internal landfill processes: (1) validate the wellhead gas composition and determine if methanogenesis is the dominant landfill process; (2) allow comparison between subsurface and gas wellhead temperatures; (3) provide the elevated temperature thickness and depth, which is important for determining whether or not waste excavation is a possible containment technique and the condition of the liner system components; (4) allow evaluation of progression of subsurface temperatures, which can be used to estimate rate of movement.
- A landfill zone framework is proposed to account for the spatial and subsurface movement with time. The five zones are: (1) anaerobic biodegradation, (2) gas front, (3) heating front, (4) smoldering front, and (5) combustion/pyrolysis. Anaerobic biodegradation is represented by temperatures below 60°C and typical ratio of CH_4 to CO_2 greater than unity. The gas and heating front are located between anaerobic biodegradation and the smoldering front. The smoldering front follows the heating front and is the driving force of elevated temperatures. The heat generated from the smoldering front permits pyrolysis of MSW, which yields increased gas flow and water vapor, emits toxic and odorous gases, and causes excessive settlement.
- The heating front is the zone adjacent to the heat source and is defined by increasing wellhead temperatures and decreasing ratio of CH_4 to CO_2. The gas front projects outward to areas

unaffected by the hot spot to a greater extent than the heating front. This region is characterized by decreasing ratio of CH_4 to CO_2 and mesophilic landfill temperatures.

- The smoldering front can be defined by elevated carbon monoxide concentrations and subsurface temperatures, e.g., a carbon monoxide concentration of 1,500 ppmv and subsurface temperatures ranging from 80 to 100°C.
- The case history in Chapter 7 shows temperatures at a MSW facility increased from normal operating conditions (35°C to 45°C) to elevated temperatures (70°C to 85°C) due to APW reactions and smoldering combustion of MSW. Thermocouples installed in leachate collection pipes were used to develop a time-temperature history plot to assess the service life of the geomembrane. For GM3b, Cases 1 and 2 temperatures are in the range of normal MSW landfills; the geomembrane is expected to have a service life of several centuries. When peak temperatures reach 60°C to 80°C, the geomembrane service life can be reduced to decades for the conditions examined and thus raises concerns regarding the integrity of the geomembrane at high temperatures.
- Assessing the integrity of a composite liner and geomembrane is difficult and dependent on site geology and location of ground monitoring wells. For the design of new landfill cells, the barrier system should reflect the type of waste, e.g., MSW, APW, incinerator ash, etc., and mode of operation (dry cell, leachate recirculation, bioreactor). Installing a leak detection layer below the primary liner and thermistors to monitor the temperature provides direct monitoring of the liner performance. In addition, various strategies can be adopted to control the liner temperature (Hoor and Rowe 2012) and maintain an adequate geomembrane service life.

8.3 Recommendations for Future Research

The present study makes the following recommendations for future research:

- Test additional secondary aluminum production wastes using the calorimeter and laboratory gas generation experiments.
- Develop a pretreatment process that APW reduces potential for ammonia emissions and heat generating reactions while also using heat and hydrogen gas as an energy resource.
- Analyze additional case histories for progression of indicators and landfill classification.

- Develop numerical models to account for landfill heat, gas, leachate, and settlement.
- Develop numerical model for combustion of MSW in landfills.
- Evaluate the efficacy of vertical ground heat exchangers to contain and isolate elevated temperature areas.
- Investigate effect of elevated temperatures on geosynthetic clay liner desiccation.
- Investigate combustion emissions from landfills and impact to the environment.

REFERENCES

Adams, F.T., Overmann, L.K., and Cotton, R.L. (1997). "Evaluation and remediation of a fire damaged geosynthetic liner system." *Proc. of Geosynthetics '97*, IFAI, CA, 379-392.

Aderemi, A., Otitoloju, A. (2012). "An Assessment of Landfill Fires and their potential health effects- A Case study of a Municipal solid waste landfill in Lagos, Nigeria." *International Journal of Environmental Protection*.

Agency for Toxic Substances and Disease Registry (ATSDR). (2001). "Chapter 2: Landfill gas basics." Landfill gas primer—An overview for environmental health professionals, Atlanta, 3–14.

Ahring, B.K. (1995). "Methanogensis in thermophilic biogas reactors." *Antonie Leeuwenhoek*, 67, 91-102.

AIHA. (1971). "Anhydrous ammonia." *Hygienic guide series*. Am Ind Hyg Assoc, 32,139-142

Alawi, M.A, Wichmann H., Lorenz, W., and Bahadir, M. (1996). "Dioxins and Furans in the Jordanian environment. Part 1: Preliminary study on a municipal landfill site with open combustion nearby AMMAN-Jordan." *Chemosphere*, 32(5).

Alberta Environment (2012). "Air quality monitoring in response to a fire at the Tsuu T'ina First Nation Landfill."

Amer, A. M. (2002). "Extracting aluminum from dross tailings." *J. Mater*., 54(11), 72–75.

Antal, M.J., Friedman, H.L., and Rogers, F.E. (1980). "Kinetics of cellulose pyrolysis in nitrogen and steam." *Comb. Sci. Tech*., 21, 141-152.

Anthony, E.J., Jia, L., Caris, M., Preto, F., and Burwell, S. (1999). "An examination of the exothermic nature of fluidized bed combustion (FBC) residues." *Waste Manag.*, 19(4), 293-305.

ASTM. (2006). "Standard test method for oxidative induction time of polyolefins geosynthetics by high-pressure differential scanning calorimetry." *D5885*, West Conshohocken, Pa.

ASTM. (2007). "Standard test method for oxidative-induction time of polyolefins by differential scanning calorimetry." *D3895*, West Conshohocken, Pa.

ASTM. (2008). "Standard practice for air-oven aging of polyolefin geomembranes." *D5721*, West Conshohocken, Pa.

ASTM. (2011). "Standard test method for hydrogen gas generation of aluminum emulsified asphalt used as a protective coating for roofing." *D6356-11*, West Conshohocken, Pa.

Azad, F., Rowe, R.K., El-Zein, A., and Airey, D. (2011). “Laboratory investigation of thermally induced desiccation of gcls in double composite liner systems.” *Geotext. Geomembr.,* 29 (6) 534-543.

Azad, F., El-Zein, A., Rowe, R.K., and Airey, D. (2012). “Modelling of thermally induced desiccation of geosynthetic clay liners in double composite liner systems”, *Geotextiles and Geomembranes*, 34: 28-28.

Babrauskas, V., (2003). *Ignition Handbook: Principles and Applications to Fire Safety Engineering, Fire Investigation, Risk Management and Forensic Science*. Fire Science Publishers, Issaquah WA and Society of Fire Protection Engineers, ISBN: 0-9728111-3-3, Chapter 2, 13-23.

Baggio, P., Baratieri, M., Gasparella, A., and Longo, G. (2008). “Energy and environmental analysis of an innovative system based on municipal solid waste (MSW) pyrolysis and combined cycle.” *Applied Thermal Engineering*, 28, 136-144.

Bahr, A., Kues, J. (1978). “Processing of salt slags from aluminum remelting plants.” *M.J Jones (Ed.),* Complex Metallurgy’78, The Institution of Mining and Metallurgy, London, 134-143.

Bates, M. (2004). “Managing Landfill Site Fires in Northamptonshire: A research study by the University College Northampton for the Environment and Transport Scrutiny Committee.” Northamptonshire County Council. Sustainable Wastes Management Centre (SITA), University College Northampton, Boughton Green Road, Northampton, Northamptonshire, NN2, 7AL.

Barlaz, M.A., Staley, B.F., and de los Reyes, F.L. (2010). “Anaerobic Biodegradation of Solid Waste.” *Environmental Microbiology*, Wiley, Ralph Mitchell, ed., Chapter 12.

Barlaz, M.A., Bareither, C.A., Hossain, A., Saquing, J., Mezzari, I., Benson, C.H., Tolaymat, T.M., and Yazdani, R. (2010). "Performance of North American Bioreactor Landfills. II: Chemical and Biological Characteristics." J. Environ. Engrg., 136(8), 839-853.

Beckman, M., 1991. “Salt slag reclamation in the state of Nordheim– Westfalen. Aluminium-67.” *Jahrgang*, 1981, 6, 589–593.

Belitskus, D. (1971). “Reaction of aluminum with sodium hydroxide solution as a source of hydrogen.” *J. Electrochem. Soc. Electrochemical Technology*, 117(8), 1097-1099.

Benson, C.H., Barlaz, M.A., Lane, D.T., and Rawe, J.M. (2007). “Practice review of five bioreactor/recirculation landfills.” *Waste Manage*. 27, 13–29.

Bergstrom, J. & Bjorner, B. (1992). “Dioxins and fires in waste storage.” *Report no. 68.* REFORSK Foundation.

Blight, G. (2008). “Slope failures in municipal solid waste dumps and landfills: a review.” *Waste Manag Res.*, 26, 448-463.

Bodnar, R.J., Hryn, J.N., Mavrogenes, J., and Vityk, M.O. (1997). “Phase equilibrium in the system H_20-NaCl-KCl-$MgCl_2$ relevant to salt cake processing.” *Light Metals: Proceedings of sessions*, TMS Annual Meeting, Orland, USA, 1195-1207.

Bogner, J., Rose, C., Vogt, M., and Gartman, D. (1988). “Understanding landfill gas generation and migration.” *Proceedings of the 11th annual international landfill gas symposium*, Houston, Texas, GRCDA, Silver Spring, MD, USA, 225-242.

Bonaparte, R., Daniel, D.E., and Boutwell, G.P. (2002). “Assessment and recommendations for improving the performance of waste containment systems.” *EPA Report EPA/600/R-02/099*, U.S. Environmental Protection Agenc, Washington, D.C.

Bothman, P. (1994). “Experience with landfill fires and fire protection measure in baden-wurttemberg.” *Brandschutz und Brandbekampfung bei Deponien und Zwischenlagern auf Deponien*: 26th Seminar of UTECH Berlin, Berlin.

Bott, M., Thauer, R. K. (1987). “Proton-motive-force-driven formation of CO from CO2, and H2 in methanogenic bacteria.” *Eur. J. Biochem*., 168, 407-412.

Brownring, J., Crone, H. (1950). “Rate of Combustion of Carbon.” *In Colloques Internationaux du Centre National de la Recherché Scientifique XX,* Service des Publications du Centre National de la Recherché Scientifique, 85-88.

Bruckard, W.J., Woodcock, J.T. (2007). “Characterization and treatment of Australian salt aqueous leaching.” *Minerals Engineering*.

Brune, M., Ramke, H. G., Collins, H., and Hanert, H. H. (1991). “Incrustation process in drainage systems of sanitary landfills.” *Proc., 3rd Int. Landfill Symp.*, CISA, Cagliari, Italy, 999–1035.

Buah, W.K., Cuncliffe, A.M., and Williams, P.T. (2007). “Characterization of products from the pyrolysis of municipal solid waste.” *Process Safety and Environmental Protection*, 85(5), 450-457.

Buggeln, R., Rynk R. (2002). “Self-Heating in Yard Trimmings: Conditions Leading to Spontaneous Combustion.” *Compost science and utilization,* 10(2), 162-182.

Buivid, M. G., Wise, D. L., Blanchet, M. J., Remedios, E. C., Jenkins, B. M., Boyd, W. F. and Pacey, J**.** G. (1981). “Fuel gas enhancement by controlled landfilling of municipal solid waste.” *Resources Conserv.*, 6,3-20.

Calder, G.V., Stark, T.D. (2010). “Aluminum reactions and problems in municipal solid waste landfills." *Journal of Hazardous, Toxic, and Radioactive Waste Management*, 15(1), 1-8.

Cecchi, F., Pavan, P., Musacco, A., Mata-Alvarez, J., and Vallini, G. (1993). “Digesting the organic fraction of municipal solid waste: Moving from mesophilic (37°C) to thermophilic (55°C) conditions.” *Waste Manage. Res*., 11, 403–414.

Chang, R. (2005). *Chemistry*, 7th Ed., McGraw Hill, Burr Ridge, IL.

Chappel, M.J., Brachman, R.W.I., Take, W.A., and Rowe, R.K. (2012). “Large-scale quantification of wrinkles in a smooth, black, HDPE geomembrane.” *J. Geotech. and Geoenviron. Engrg.* 138(6), 671-679.

Chatterjee, B, and Thomas, R.W. (1976). “The chemical etching of aluminum in caustic soda solutions.” *Trans. Inst. Metal Finish.*, 54(1), 17-24.

Chen, W. Y. (1955). “Aluminum-water hazards.” *Ind. Eng. Chem. Letters*, 47(7), 32A–34A.

Chiblow, S. (2004). “Final report on survey of garbage disposal/burning in first nation communities in Ontario.” Chiefs of Ontario and Environment Canada-Ontario Region.

Christensen, T.H., Kjeldsen, P., Albrechtsen, H.J., Heron, G., Nielsen, P.H., Bjerg, P.L., and Holm, P.E. (1994). “Attenuation of landfill leachate pollutants in aquifers.” *Crit. Rev. Environ. Sci. Technol.*, 24(119).

Christensen, T.H., Cossu, R., Stegmann, R. (1996). *Landfilling of Waste: Biogas*. E & Spoon, Bury St. Edmunds, Suffolk, Great Britain.

Christensen, T.H., Manfredi, S. (2011). “Landfilling: Reactor Landfills.” *Solid Waste Technology & Management*. Blackwell Publishing.

Chrysikou, L., Gemenetzia, P., Kouras, A., Manoli, E., Terzi, E., Constantini, S. (2008). “Distribution of persistent organic pollutants, polycyclic aromatic hydrocarbons and trace elements in soil and vegetation following a large scale landfill fire in northern Greece.” *Environment International*, 34(2).

Crutcher, A.J., Rovers, F.A., and McBean, E.A. (1982). “Temperature as an indicator of landfill behavior.” *Water, Air, and Soil Pollution*, 17, 213-223.

David, E., and Kopac, J. (2012). “Hydrolysis of aluminum dross material to achieve zero hazardous waste.” *J. Hazard. Mater.*, 209-210, 501-509.

Dash, B., Bhattacharya, S.C., Das, B.R., Das, S.C., Tripathy, B.C. (2008). “Acid dissolution of alumina from waste aluminum dross.” *Hydrometallurgy*, 92, 45-53.

DeHann, J.D. (2007). *Kirk’s fire investigation*, 6th Ed., Pearson Prentice Hal, Upper Saddle River, NJ.

Demirel, E., Azan, N. (2012). “Thermodynamic modeling of water-gas shift reaction in supercritical water.” *Proceedings of the World Congress on Engineering and Computer Science*, October 24-26, San Francisco, USA, 1-4.

Diekert, G., Hansch, M., and Conrad, R. (1984). “Acetate synthesis from 2 CO_2 in acetogenic bacteria: is carbon monoxide an intermediate?” *Arch. Microbial.* 138(3), 224-228.

Doutre, D.A. (2010). “Hazards associated with the use of bone ash in contact with molten aluminum.” *Light Metals 2010*.

Drysdale, D. (1999). *An Introduction to Fire Dynamics*, 2nd Edition. Wiley. New York.

Ehrig, H.-J. (1983). "Quality and quantity of sanitary landfill leachate." *Waste Mgmt. Res.*, 1(1), 53-68.

El-Fadel, M., Findikakis, A., and Leckie, J. (1977). “Environmental impacts of solid waste landfilling.” *J. Environ Manag.*, 50, 1-25.

EMCON Associates. (1981). “State-of-the-Art of Methane Gas Enhancement in Landfills,” *Report ANL/CNSV-23*. Argonne National Laboratory, Argonne, IL.

Environment Hawaii. (1998). “Ma’aleae landfill fire sparks state effort to develop guidelines.” Environment Hawaii, Inc., 9(4), < http://www.environment-hawaii.org/?p=3426>.

Ettala, M., Rahkonen, P., Rossi, E., Mangs, J., and Keski-Rahkonen, O. (1996). “Landfill fires in Finland.” *Waste Management & Research*, 14, 377-384.

Fair, K.J., Toguri, J.M., Smith, H.W. (1987). “Upgrading of aluminum dross by selective comminution and sizing.” *CIM Bulletin*, 80, 73-78.

Farquhar, G. J., Rovers, F. A. (1973). “Gas production during refuse decomposition.” *Water, Air, Soil Pollut.*, 2(4), 483–495.

Federal Emergency Management Agency (FEMA). (2002). "Landfill Fires – Their Magnitude, Characteristics, and Mitigation." *FA-225*. TriData Corporation, 1000 Wilson Boulevard, Arlington, Virginia for FEMA United States Fire Administration, National Fire Data Center.

Fire, F.L. (1996). "Chapter 6: Fire and Pyrolysis. The common sense approach to hazardous materials." *Fire Engineering Books and Videos*, 2nd Edition, PennWell, Tulsa, Oklahoma, 105-123.

Frid, V., Doudkinski, D., Liskevich, G., Shafran, E., Averbakh, A., Korostishevsky, N., and Prihodko, L. (2009). "Geophysical-geochemical investigation of fire-prone landfills." *Environ Earth Sci*., 60(4), 787-798.

Fukumoto, S., Ho'okabe, T., and Tsubakino, H. (2001). "Leaching reactions of aluminum dross in various aqueous solutions." *J. Japan Inst. Light Metals*, 51(1), 34–39.

Gale, C. (2007). "Landfill fire case study: Identifying the ambient air source if half the battle." *SWANA*.

Geosyntec consultants. (2008). "Effect of landfill operating temperatures on liner containment capability. Waimanalo Gulch Sanitary Landfill Ewa Beach, Oahu, Hawaii." *Waste Management of Hawaii*. Kapolei, Hawaii.

Geosynthetic Institute. (1997). Test methods, test properties, testing frequency for high density polyethylene (HDPE) smooth and textured geomembranes, GRI-GM13, Folsom, PA.

Gil, A. (2003). "Management of the salt cake from secondary aluminum fusion processes." *Ind. ENG. Chem. Res.*, 44, 8852-8857.

Golden Software, (2014). Surfer® 12. http://www.goldensoftware.com/products/surfer

Graczyk, D.G., Essling, A.M., Huff, E.A., Smith, F.P., and Snyder, C.T. (1997). "Analyticalchemistry of aluminum salt cake." *Light Metals: Proceedings of Sessions*, TMS Annual Meeting, Warrendale, PA, 1997, 1135-1140.

Griffiths, J. F., Barnard, J. A. (1995). *Flame and combustion*, 3rd Ed., Blackie Academic and Professional, Bishopbriggs, Glasgow, Scotland.

Gulec, S.B., Edil, T.B., Benson, C.H. (2004). "Effect if acidic mine drainage on the polymer properties of an HDPE geomembrane." *Geosynthetics International*, 2(11), 60-72.

Hall, D., Drury, D., Keeble, R., Morgans, A., and Wyles, R. (2007). "Review and investigation of deep-seated fires within landfill sites". *UK Environment Agency Science Report:*

SC010066. Environment Agency, Bristol, Rio House, Waterside Drive, Aztec West, Almondsbury, Bristol, BS32 4UD.

Hamilton County Public Health. (2014). "Rumpke Sanitary Landfill Odor Complaint Hotline Summary/Analysis 2014." *Hamilton County Public Health Department of Environmental Health Services*. Cincinnati, Ohio.

Hanson, J. L., Yesiller, N., and Kendall, L. A. (2005). "Integrated temperature and gas analysis at a municipal solid waste landfill." *Proc., 16th Int. Conf. on Soil Mech. and Geotech. Engrg., Geotechnology in Harmony with the Global Environment*, Millpress Science, Rotterdam, The Netherlands, 4, 2265–2268.

Hanson, J. L., Liu, W.-L., and Yesiller, N. (2008). "Analytical and numerical methodology for modeling temperatures in landfills." *Geotechnics of waste management and remediation, ASCE GSP No. 177*, M. V. Khire, A. N. Alshawabkeh, and K. R. Reddy, eds., ASCE, Va., 24–31.

Hanson, J.L., Yesiller, N., and Oettle, N. (2010). "Spatial and temporal temperature distributions in municipal solid waste landfills." *J. Environ. Eng.*, 136 (8), 804–814.

Hartz, K.E., Klink, R.E., and Ham, R.K. (1982). "Temperature effects: methane generation from landfill samples." *J. Environ. Eng.*, 108 (EE4), 629–638.

Haug, R.T. (1997). "Feedstocks, condition, and fire prevention." *Biocycle.*, 38(4), 68-70.

Hendron, D.M., Fernandez G., Prommer P.J., Giroud J.P., and Orozco L.F. (1999). "Investigation of the cause of the 27 September 1997 slope failure at the Doña Juana landfill." *Proc. Sardinia'99—7th Int. waste management and landfill symposium*, Cagliari, Italy.

Hogland, W., Marques, M. (2003). "Physical, biological, and chemical processes during storage and spontaneous combustion of waste fuel." *Resource conservation and recycling*, 40, 53-69.

Hollingworth, E.H., and Hunsicker, H.Y. (1990). Corrosion of aluminum and aluminum alloys. Metal Handbook AM Vol. 2, p 608.

Hoor, A., and Rowe, R.K. (2012). "Application of tire chips to reduce the temperature of secondary geomembranes in municipal solid waste landfills." *Waste Management*, 32, 901-911.

Houi, D., Paul, E., and Couturier, C. (1997). “Heat and mass transfer in landfills and biogas recovery.” *Proc., 6th Int. Waste Management and Landfill Symp.*, T. H. Christensen et al., eds., Vol. I, CISA, Italy, 101–108.

Hsuan, Y.G., Koerner, R.M. (1995). “The single point-notched constant tensile load test: A quality control test for assessing stress crack resistance.” *Geosynthet. Int.*, 2 (5), 831-843.

Hsuan, Y. G., and Koerner, R. M. (1998). “Antioxidant depletion lifetime in high density polyethylene geomembranes.” *J. Geotech.and Geoenviron. Engrg.*, 124(6), 532–541.

Huang, X., Tolaymat, T., Ford, R., and Barlaz, M. (2014). “Characterization of Secondary Aluminum Processing Waste.” *Report US EPA Contract EP-C-11-006*, U.S. EPA, Cincinnati, OH.

Hudgins, M., Harper, S. (1999). “Operational characteristics of two aerobic landfill systems.” *Proc. 7th International Waste Management and Landfill Symposium*, Sardinia, 1-9.

Huggett, C. (1980). “Estimation of rate of heat release by means of oxygen consumption measurements.” *Fire and Materials*, 4(2), 61-65.

Hwang, J.Y., Huang, X., and Xu, Z. (2006). “Recovery of metals from aluminum dross and salt cake.” *J. Min. Mat. Charact. Eng.*, 5(1), 47-62.

Illinois Environmental Protection Agency (EPA). (2012). “Monthly Progress Report Congress Landfill.” *No. 06 CH 1438*. Environmental Information Logistics, Wheaton, Il.

Institute of Materials Processing (IMP). (2002). “Recycling and reuse of aluminum wastes.” DE-FC07-98ID13663, Michigan Technological University.

Ishigaki, T., Yamada, M., Nagamori, M., Ono, Y., and Inoue, Y. (2005). “Estimation of Methane Emission from Whole Waste Landfill Site Using Correlation Between Flux and Ground Temperature.” *Environmental Geology*, 48(7), 845-853.

Jafari, N.H., Stark, T.D., and Merry, S.M. (2013). “The 10 July 2000 Payatas landfill slope failure.” *International Journal of Geoengineering Case Histories*, 2(3), 208-228.

Jafari, N.H., and Stark, T.D. (2014). “Calorimeter test for assessment of aluminum production waste reactivity.” ASCE GeoCongress 2014 Geo-Characterization and Modeling for Sustainability, in press.

Jafari, N.H., Stark, T.D., and Rowe, K. (2014a). “Service life of HDPE geomembranes subjected to elevated temperatures.” *Journal of Hazardous, Toxic, and Radioactive Waste*, 18(1), 16-26.

Jafari, N.H., Stark, T.D., and Roper, R. (2014b). “Classification and reactivity of aluminum production waste.” *ASCE Journal of Hazardous, Toxic, and Radioactive Waste*, 18, 1-11.

Jeon, H.-Y., Bouazza, A., and Lee, K.-Y. (2008). “Depletion of antioxidants from an HDPE geomembrane upon exposure to acidic and alkaline solutions.” *Polymer Testing*, 27, 434-440.

Kadioglu, Y., Varamaz, M. (2003). “The Effect of Moisture Content and Air-Drying on Spontaneous Combustion Characteristics of Two Turkish Lignites.” *Fuel*, 82, 1685-1693.

Karvelas, D., Daniels, E., Jody, B., and Bonsignore, P. (1991). “An economic and technical assessment of black dross and salt cake recycling systems for application in the secondary aluminum industry.” *ANL/ESD-11.* Argonne National Laboratory, Argonne, IL.

Kasali, G. B., Senior, E. (1989). “Effect of temperature and moisture on the anaerobic digestion of refuse.” *J. Chern. Tech. Biotechnol.*, 44, 31-41.

Kerfoot, H.B. (1993). “Landfill gas effect on groundwater samples at a municipal solid waste facility.” *Proceedings Sardinia 93, Fourth International Landfill Symposium*, Cagliari, Italy, 1141-1154.

Kjeldsen, P., Fischer, E. (1995). “Landfill gas migration – field investigations at Skellingsted Landfill, Denmark.” *Waste Management & Research*, 13, 467-484.

Kjeldsen, P., Barlaz, M. A., Rooker, A. P., Baun, A., Ledin, A., and Christensen, T. H. (2002). “Present and long term composition of MSW landfill leachate—A review.” *Crit. Rev. Environ. Sci. Technol.*, 32(4), 297–336.

Klein, R., Baumann, T., Kahapka, E., and Niessner, R. (2001). “Temperature development in a modern municipal solid waste incineration (MSWI) bottom ash landfill with regard to sustainable waste management.” J. Hazard. Mater., 83(3), 265–280.

Klein, R., Nestle, N., Niessner, R., and Baumann, T. (2003). “Numerical modelling of the generation and transport of heat in a bottom ash monofill.” *J. Hazardous Materials*. B100, 147-162.

Koelsch, F., Fricke, K., Mahler, C., and Damanhuri, E. (2005). “Stability of landfills – the Bandung dumpsite disaster.” *Sardinia 2005, 10th Int. Waste Manag. Landfill Sympm.*, Cagliari, Italy.

Koerner, G. R., and Koerner, R. M. (2006). “Long-term temperature monitoring of geomembranes at dry and wet landfills.” *Geotext. Geomembr.*, 24(1), 72–77.

Koerner, R. M., Koerner, G. R., Eith, A. W., and Ballod, C. P. (2008). "Geomembrane temperature monitoring at dry and wet landfills." *Proc. of the 1st Global Waste Management Symp.*, NSWMA, Copper Mountain, CO (CD-ROM).

Koerner, R.M. (1998). *Designing with geosynthetics*, 4th Ed. Prentice-Hall, New Jersey.

Kotze, J. P., Thiel, P. G., and Hattingh, W. H. J. (1969). "Characterization and control of anaerobic digestion." Water Research, 7(3), 459-494.

Kubler, H. (1982). "Heat Release in Thermally Disintegrating Wood." *Wood and Fiber*, 14(3), 166-177.

Kubler, H. (1987). "Heat Generation Processes as Cause of Spontaneous Ignition in Forest Products." *Forest Products Abstracts*, 10(11).

Kucuk, A., Kadioglu, Y., and Gulaboglu, M. (2003). "A Study of Spontaneous Combustion Characteristics of Turkish Lignite: Particle Size, Moisture of Coal, Humidity of Air." *Combustion and Flame*, 133, 255-261.

Kulik, G.J, and Daley, J.C. (1990). "Aluminum dross processing in the 90's." *Proc., 2nd Int. Symp. Recycl. Met. Eng. Mater*, TMS-AIME, Warrendale, PA, 427.

Kumar, A. (2007). "Temperature inside the Landfill: Effects of Liquid Injection and ambient Temperature." M.S. Thesis, University of Central Florida., Orlando, FL, USA.

Kuo, K. (1986). *Principles of Combustion.* John Wiley & Sons, Inc, New York, USA.

LandTec. (2010). "GEM™ 2000 gas analyzer and extraction monitors." *Instruments Operation Manual*, 64.

Lee, M.Y., Cheon, J.H., Hidaka, T., and Tsuno, H. (2008). "The performance and microbial diversity of temperature phased hyperthermophilic and thermophilic anaerobic digestion system fed with organic waste." *Water Science & Technology*, 57(2), 283-289.

Lefebvre, X., Lanini, S., and Houi, D. (2000). "The role of aerobic activity on refuse temperature rise, I. Landfill experimental study." *Waste Manage. Res.*, 18, 444–452.

Lewicki, R. (1999). "Early Detection and Prevention of Landfill Fires." *Proceedings Sardinia 99, Seventh International Waste Management and Landfill Symposium*, CISA, Environmental Sanitary Engineering Centre, Cagliari, Italy.

Lin, K.S., Wang, H.P., Liu, S.H., Chang, N.B., Huang, Y.J. and Wang, H.C. (1999). "Pyrolysis kinetics of refuse-derived fuel." *Fuel Processing Technology*, 60(2), 103–110.

Liu, N., Chou, M. (2013). “Degree of hazardous reduction of secondary aluminum dross using ferrous chloride.” *ASCE*.

Lönnermark, A., Blomquist, P., and Marklund, S. (2008) “Emission from simulated deep-seated fires in domestic waste.” *Chemosphere*, 70, 626-639.

Lorber, K.E., Antrekowitsch, H. (2009). “Treatment and disposal of residues from aluminum dross recovery.” Institute for Sustainable Waste Management and Technology (IAE), Montan University Leobeben, Leoben, Austria.

Lucheva, B., Tsonev, T.S., and Petkov, R. (2005). “Non-waste aluminum dross recycling.” *J. Univ. Chem. Technol. Metall.*, 40(4), 335–338.

Manfredi, O., Wuth, W., and Bohlinger, I. (1997). “Characterizing the physical and chemical properties of aluminum dross.” *J. Mater.*, November Issue, 48–51.

Martin, J.W., Stark, T.D., Thalhamer, T., and Gerbasi, G.T. (2012). “Detection of aluminum waste reactions and associated waste fires.” *ACCEPTED to J. of Hazardous, Toxic, and Radioactive Waste*, ASCE, June, 2011.

Martin, J.W., Stark, T.D., Thalhamer, T., Gerbasi-Graf, G.T., and Gortner, R.E. (2013). “Detection of aluminum waste reactions and associated waste fires.” *J. of Haz., Toxic, and Rad. Waste*, 17(3), 164-174.

Mata-Alvarez, J., Martinez-Viturtia, A. (1986). “Laboratory simulation of municipal solid waste fermentation with leachate recycle.” *J. Chem. Tech. Biotechnol.*, 36, 547-556.

McBean, E.A., Rovers, F.A., and Farquhar, G.J. (1995). *Solid Waste Landfill Engineering and Design*, Prentice Hall PTR, Englewood Cliffs, NJ.

Meima, J.A., Mora-Naranjo, N., and Haarstrick, A. (2008). “Sensitivity analysis and literature review of parameters controlling local biodegradation processes in municipal solid waste landfills.” *Waste Management*, 28, 904-918.

Meraz, L., Dominguez, A. (1998). “A Calorimetric Description of the Digestion of Organic Matter in Landfills.” *The Chemical Educator*, 3(6).

Merry, S.M., Fritz, W.U., Budhu, M., and Jesionek, K. (2005). “Effect of gas on pore pressures in wet landfills.” *J. Geotech. and Geoenvir. Engrg.*, 132(5), 553-561.

Merz, R.C. (1969). “Special studies of a sanitary landfill.” Final report Bureau of Solid Waste Management, Grant No. UI00518-08, Univ. of Southern California.

Merz, R.C., Stone, R. (1966). “Sanitary Landfill Behavior in an Aerobic Environment,” *Public Works*, 97(1), 67-70.

Miller, J.B. (2007). “Elevated temperature investigation of landfill gas wells.” *SWANA Landfill Gas Symposium*, 1-9.

Miškufová, A., Štifner, T., Havlik, T., and Jančok, J. (2006). “Recovery of valuable substances from aluminum dross.” *Acta Metall. Slovaca*, 12, 303–312.

Missouri DNR. (2014). “Bridgeton Landfill, LLC Monthly Data Submittals Required by section 52.E of Agreed Order, Case No. 13SL-CC01088 Effective May, 13, 2013”. *Bridgeton LLC.*

Moqbel, S.Y. (2010). “Characterizing spontaneous fires in landfills.” Ph.D. dissertation, University of Central Florida, Orlando, Florida.

Mora-Naranjo, N., Meima, J.A., Haarstrick, A., and Hempel, D.C., (2004). “Modelling and experimental investigation of environmental influences on the acetate and methane formation in solid waste.” *Waste Management*, 24, 763-773.

Mulder, J.S., Van der Zahm, H.O. (1967). “Fatal case of ammonium poisoning.” *TydschriftVoor Sociale Geneeskunde*, Amsterdam, 45,458-46.

Müller, W., and Jacob, I. (2003). “Oxidative resistance of high density polyethylene geomembranes.” *Polym. Degrad. Stab.*, 79(1), 161–172.

Nammari, D., Hogland, W., Marques, M., Nimmermark, S., and Moutavtchi, V. (2004). “Emission from uncontrolled fire in municipal solid waste bales.” *Waste Management*, 24, 9-18.

Narayanan, R., Sahai, Y. (1997). “Chemical Interactions of dross with water and water vapor in aluminum scrap remelting.” *Mater. Trans.*, 38(1), 85–88.

Nastev, M., Therrien, R., Lefebvre, R., and Gelinas, P. (2001). “Gas Production and migration in landfills and geological materials.” *Journal of Contaminant Hydrology*, 52, 187-211.

Naturvardsverket. (1994). “Fires at landfill sites.” *Naturvardsverket*. Rapport 4320.

Needham, A.D., Smith, J.W.N., Gallagher, E.M.G. (2006). “The service life of polyethylene geomembrane barriers.” *Eng. Geol.*, 85 (1-2), 82–90.

Neves, D., Thunman, H., Matos, A., Tarelho, L., and G´omez Barea, A. (2011). “Characterization and prediction of biomass pyrolysis products.” *Prog. Energy Combust. Sci*., 37(5), 611–630.

Nikolaou, K. (2008). “Environmental management and landfill fire accidents.” *J. Environ Protection Ecology*. 9(4), 830-834.

New Zeland Ministry of Environment (NZ MOE). (1997). "Landfill guidelines: Hazards of burning at landfills." Pollution and Waste Group, Ministry for the Environment.

Ohio EPA. (2011). "Subsurface heating events at solid waste and construction and demolition debris landfills: Best management practices." *Guidance document #1009*, p. 12.

Ohlemiller, T.J. (1995). "Smoldering Combustion." *SFPE Handbook of Fire Protection Engineering*, 2nd. Ed., Bethesda, MD., 2-11, 2-171 – 2-179.

Ontario Ministry of the Environment. (OMOE). (1998). *Landfill standards: a guideline on the regulatory and approval requirements for the new or expanding landfilling sites*, Ontario Ministry of the Environment, Ontario Regulation 232/98. Queen's Printer for Ontario, Toronto.

Øygard, J. K., Måge, A., Gjengedal, E., and Svane, T. (2005). "Effect of an uncontrolled fire and the subsequent fire fight on the chemical composition of landfill leachate." *Waste Management*, 25, 712-718.

Parker, R. J., Thornton, P. N. and Leonard, C. (2001). "Remediation of a landfill that contained an underground fire." *International waste management and landfill symposium*; Sardinia 2001, Cagliari, Italy, CISA, 623-632.

Peterson, R.D., and Newton, L. (2002). "Review of aluminum dross processing." *Light Metals: Proc. of Sessions*, TMS Annual Meeting, Warrendale, PA, 1029-1037.

Pfeffer, J. T. (1974). "Temperature effects on anaerobic fermentation of domestic refuse." *Biotechnol. Bioeng.*, 16(6), 771–787.

Pitts, W. M. (2007). "Ignition of cellulosic fuels by heated and radioactive surfaces." *National Institute of Standards and Technology Technical Note 1482*, NIST, Gaithersburg, MD, 3–4.

Pitts, W.M., Johnsson, E.L., and Bryner, N.O. (1994). "Carbon monoxide formation in fires by high-temperature anaerobic wood pyrolysis." *25th Symposium on Combustion, the Combustion Institute*, 1455-1462.

Poffet, M., Kaeser, K., and Jenni, T.A. (2008). "Thermal runaway of dried sewage sludge granules in storage tanks." *Chimica*, 62, 29–34.

Powell, J., Jain, P., Kim, H., Townsend, T., and Reinhart, D. (2006). "Changes in landfill gas quality as a result of controlled air injection." *Environmental Science and Technology*, 40, 1029-1034.

Quintiere, J.G., Birky, M., Macdonald, F., and Smith, G. (1982). “An analysis of smoldering fires in closed compartments and their hazard due to carbon monoxide.” *Fire and Materials*, 6(3 & 4), 99-110.

Rampling, T.W., Hickey, T.J. (1988). “The laboratory characterization of refuse derived fuel.”, *Report No LR643*, Department of Trade and Industry, HM Government, HMSO, London, UK.

Read, A, Hudgins, M., Harper, S., Philips, P., and Morris, J. (2001a). “The Successful Demonstration of aerobic landfilling- The Potential for a More Sustainable Solid Waste Management Approach.” *Resources, Conservation and Recycling*, 32(2), 115.

Read, A, Hudgins, M., and Philips, P. (2001b). “Perpetual Landfilling Through Aeration of The Waste Mass; Lessons from Test Cells in Georgia USA.” *Waste Management*, 21(7), 617-629.

Rees, J.F. (1980). “Optimization of Methane Production and Refuse Decomposition in Landfills by Temperature Control.” *Journal of Chemical Technology and Biotechnology*, 30, 458-465.

Reinhart, D, McCreanor, P., Townsend, T. (2002). “The Bioreactor Landfill; Its Status and Future.” *Waste Management Research*, 4(2), 172-186.

Rettenberger, G., Stegmann, R. (1996). *Landfill gas components*. 58-81.

Richardson Smith Gardner & Associates (RGSA). (2010). “Aluminum Processing Waste Gas Study.” *House Engineering*, Nashville, TN.

Rimal, S., and Rowe, R. K. (2009). “Diffusion modelling of OIT depletion from HDPE geomembrane in landfill applications.” *Geosynthet. Int.*,16(3), 183–196.

Rim-Rukeh, A. (2014). “An assessment of the contribution of municipal solid waste dump site fires to atmospheric pollution.” *Open Journal of Air Pollution*, 3, 53-60.

Riquier, L., Guerbois, M., Budka, A., Hebe I., and Riviere, S. (2003). “Underground fires characterization in landfills: Investigation methods.” *Proc. Sardinia 2003, Ninth International Waste Management and Landfill Symposium*, Cagliari, Italy, CISA, Italy.

Riviere, S., Goumand, J.C., Guerbois, M., and Hebe, I. (2003). “Characterization of underground fires in landfills using geophysical methods: a case study.” *Proceedings Sardinia 2003, Ninth International Waste Management and Landfill Symposium*, Cagliari, Italy, CISA, Italy.

RMT, Inc. (2007). “Response to request for additional information: Permit renewal Wabash Alloys.” Indiana Dept. of Environmental Management, Indianapolis, IN.

Rowe, R. K. (2005). “Long-term performance of contaminant barrier systems: 45th Rankine lecture.” *Geotechnique*, 55(9), 631–678.

Rowe, R. K. (2012). “Short- and long-term leakage through composite liners. The 7th Arthur Casagrande Lecture.” *Can. Geotech. J.*, 49(12) 141-169.

Rowe, R.K., and Islam, M.Z. (2009). “Impact on landfill liner time-temperature history on the service-life of HDPE geomembranes.” *Waste Management*, **29**(10) 2689-2699.

Rowe, R. K., and Rimal, S. (2008a). “Aging of HDPE geomembrane in three composite liner configurations.” *J. Geotech. Geoenviron. Eng.*, 134(7), 906–916.

Rowe, R. K., and Rimal, S. (2008b). “Ageing and long-term performance of geomembrane liners.” *GeoAmericas 2008*, Industrial Fabrics Association International, Cancun, Mexico, 425–434.

Rowe, R.K., Hoor, A., and Pollard, A. (2010). Examination of a method for reducing the temperature of MSW landfill liners, *J. of Environ. Engrg.*, 136(8) 794-803.

Rowe, R. K., Islam, M. Z., and Hsuan, Y. G. (2008). “Leachate chemical composition effects on OIT depletion in HDPE geomembranes.” *Geosynthet. Int.*,15(2), 136–151.

Rowe, R. K., Quigley, R. M., Brachman, R. W. I., and Booker, J. R. (2004). *Barrier systems for waste disposal facilities*, Taylor and Francis, London.

Rowe, R. K., Rimal, S., and Sangam, H. P. (2009). “Ageing of HDPE geomembrane exposed to air, water and leachate at different temperatures.” *Geotext. Geomembr.*, 27(2), 137–151.

Rowe, R. K., and Hoor, A. (2009). “Predicted temperatures and service lives of secondary geomembrane landfill liners.” *Geosynthet. Int.*, 16(2), 71–82.

Rowe, R.K., Islam, M.Z., Brachman, R.W.I., Arnepalli , D.N. and Ewais, A. (2010). “Antioxidant depletion from an HDPE geomembrane under simulated landfill conditions.” *J. of Geotech and Geoenvir. Engrg.*, 136(7), 930-939.

Ruokojarvi, P., Ruuskanen, J., Ettala, M., Rahkonen P., and Tarhanen, J. (1995b). “Formation of Polyaromatic Hydrocarbons and Polychlorinated Organic Compounds in Municipal Waste Landfill Fires.” *Chemosphere*, 31(8), 3899-3908.

Sangam, H. P., and Rowe, R. K. (2002). “Effects of exposure conditions on the depletion of antioxidants from high-density polyethylene HDPE geomembranes.” *Can. Geotech. J.*, 39(6), 1221–1230.

Skoch, J.T., Collins, R.L. (1995). “Reduction of salt cake waste by removing low value oxide fines.” *Third International Symposium on Recycling of Metals and Engineered Materials, Light Metals: Proceedings of sessions*, TMS Annual Meeting, Warrendale, PA, 937-946.

Sreenivasarao, K., Patsiogiannis, F., Hryn, J.N., and Daniels, E.J. (1997). “Concentration and precipitation of NaCl and KCl from salt cake leach solutions by electrodialysis.” *Light Metals, Proc. of TMS*, Orlando, FL, 1153–1158.

Schaefer. (2008). *Global Waste Conference*, Colorado.

Shafizadeh, F. (1982). “Chemistry of pyrolysis and combustion of wood.” *Pro-gress in Biomass Conversion*, 3, Academic Press, London, UK.

Shafizadeh, F., Bradbury, G. (1979). “Thermal Degradation of Cellulose in Air and Nitrogen at Low Temperatures.” *Journal of Applied Polymer Science*, 23, 1431-1442.

Shea, F., Jr., Hsu, H. (1971). “Self-Heating of Carbonaceous Materials.” *Industrial and Engineering chemistry, products research and development*, 11(2), 184-187.

Shinzato, M. C., Hypolito, R. (2005). “Solid waste from aluminum recycling process: Characterization and reuse of its economically valuable constituents.” *Waste Manage. J.*, 25(1), 37–46.

Smyth, H.F. (1956). “Improved communication: hygienic standards for daily inhalation.” *Am Ind Hyg Assoc Q*, 17(2), 129-185.

SØrum, L., Gronli, M.G., and Hustan, J.E. (2001). “Pyrolysis characteristics and kinetics of municipal solid wastes.” *Fuel*, 80(9), 1217-1227.

Southen, J. M., and Rowe, R. K. (2004). “Investigation of the behavior of geosynthetic clay liners subjected to thermal gradients in basal liner applications.” *J. ASTM Int.*,1(2), JAI11470.

Southen, J. M., and Rowe, R. K. (2005a). “Laboratory investigation of geosynthetic clay liner desiccation in a composite liner subjected to thermal gradients.” *J. Geotech. and Geoenviron. Engrg.*, 131(7), 925–935.

Southen, J. M., and Rowe, R. K. (2005b). “Modelling of thermally induced desiccation of geosynthetic clay liners.” *Geotext. Geomembr.*, 23(5), 425–442.

Southen, J.M., and Rowe, R.K. (2011). “Numerical modelling of thermally induced desiccation of geosynthetic clay liners observed in laboratory experiments”, *Geosynthet. Int.*, 18(5) (In press: Accepted 8/7/11; GI-512).

Sperling, T., Henderson, J.P. (2001). “Understanding and controlling landfill fires.” *SWANA landfill symposium*, San Diego, California.

Springer, E., Hajny, G., and Fiest, W. (1971). “Spontaneous Heating in Piled Wood Chips: II. Effect of Temperature.” *Tappi*, 5(4), 589-591.

Stanforth, R.R. (1991). “Method for reduction of heavy metal leaching from hazardous waste under acidic and nonacidic conditions.” US Patent 5,037,479.

Stark, T.D., Huvaj-Sarihan, N., and Li, G. (2009). Shear strength of municipal solid waste for stability analyses. Envir. Geology, 57(8), 1911-1923.

Stark, T.D., Akhtar, K., and Hussain, M. (2010). “Stability analyses for landfills experiencing elevated temperatures.” *Proceedings of Specialty Conference GeoFlorida 2010: Advances in Analysis, Modeling and Design*, ASCE, Orlando, FL, March, 2010, 1-8.

Stark, T.D., Martin, J.W. Gerbasi, G.T., and Thalhamer, T. (2012). “Aluminum waste reaction indicators in an MSW landfill.” *J. of Geotech. Geoenvir. Engrg.*, 138(3), 252-261.

Stearns, R.P., Petoyan, G.S. (1984). “Identifying and controlling landfill sites.” *Waste Manag Res*., 2, 303-309.

Stessel, R., Murphy, R. (1992). A Lysimeter Study of the Aerobic Landfill Concept. *Waste Management Research*, 6(6), 485-503.

Swackhamer, R. D. (2006). “Interim remedial action plan RAMCO aluminum waste disposal site, Port of Klickitat Industrial Park.” Report Washington State Dept. of Ecology Toxics Cleanup Program, Dallesport, WA.

Szczygielski, T. (2008). “Fire in the Hole: Aluminum Dross in Landfills.” *Journal of Natural Resources and Environmental Law*, 22(2), 159-174.

Tarnowski, C., Baldauf, S., and Sost, E. (2005). “Assessment of the durability of HDPE-geomembranes in landfills: Practical approach under consideration of material examination performed during service life.” *Proc., 10th Int. Waste Management and Landfull Symp.*, Caligari, Italy, (CD-ROM).

Thauer, R.K. (1998). “Biochemistry of methanogenesis: a tribute to Marjory Stephenson.” *Microbiology*, 144, 2377-2406.

Totten, G. E., and MacKenzie, D. S. (2003). “Handbook of aluminum: Alloy production and materials manufacturing.” Vol. 2, Marcel Dekker, Inc, New York.

Ueno, Y., Fukui, H., and Goto, M. (2007). “Operation of a two-stage fermentation process producing hydrogen and methane from organic waste.” *Environmental Science & Technology*, 41(4), 1413-1419.

Unger, T.W., and Beckmann, M. (1992). "Salt slag processing for recycling." *Light Metals: Proceedings of Sessions*, TMS Annual Meeting, San Diego, CA, 1159–1162.

U.S. Army Corps of Engineers (USACE). (2008). “Landfill off-gas collection and treatment systems.” EM 1110-1-4016, Washington D.C..

U.S. Environmental Protection Agency (EPA). (1994). “Brantley landfill site Island, Kentucky.” EPA/ROD/-95/201, Atlanta, GA.

U.S. EPA. (1999). “Summary of the requirements for the New Source Performance Standards and Emission Guidelines for municipal solid waste landfills.” EPA-453R/96-004, Research Triangle Park, NC.

Vargel, C. (2004). *Corrosion of aluminum*, 1st Ed, Elsevier New York, 626.

Viebke, J., Elble, E., Ifwarson, M., and Gedde, U. W. (1994). “Degradation of unstabilized medium-density polyethylene pipes in hot-water applications.” *Polym. Eng. Sci.*, 34(17), 1354–1361.

Wappett, H.L., Zornberg, J.G. (2006). “Full scale monitoring for assessment of exothermal reactions in waste tires.” *Final Report Recycled Materials Resource Center Project No. 27*, 312.

Warnatz, J., Maas, U., and Dibble, R.W. (1996). *Combustion*, Springer-Verlag Berlin, Heidelberg.

Williams, G.M., Aitkenhead, N. (1991). “Lessons from Loscoe: the uncontrolled migration of landfill gas.” *Quarterly Journal of Engineering Geology*, 24, 191-207.

Williams, P.T., Besler, S. (1993). “The pyrolysis of rice husks in a thermogravimetric analyzer and static bed reactor.” *Fuel*, 72, 151.

Williams, P.T., Besler, S. (1996). “Thermogravimetric analysis of the components of biomass.” *Renewable Energy*, 7(3): 233-250.

Wittmann, S.G. (1985). “Landfill gas migration: Early warning signs, monitoring techniques and migration control systems.” *Proceedings 23rd Annual International Seminar, Equipment, Services, and Systems Show*, Denver, CO, USA, 317-328.

Xiao, Y., Reuter, M.A., and Boin, U. (2005). “Aluminum recycling and environmental issues of salt slag treatment.” *J. Environ. Sci. Heal. A*, 40, 1861-1875.

Yesiller, N., Hanson, J., and Liu, W. (2005). “Heat generation in municipal solid waste landfills.” *J. Geotech. Geoenviron. Eng.*, ASCE 131(11), 1330–1344.

Yazdani, R., Kieffer, J., Sananikone, K., and Augenstein, D. 2006. “Full scale bioreactor landfill for carbon sequestration and greenhouse emission control.” *Final Technical Progress Rep., DOE Award # DEFC26-01NT41152*.

Yoshida, H., and Rowe, R. K. (2003). “Consideration of landfill liner temperature.” *Proc., 9th Int. Waste Management and Landfull Symp.*, Caligari, Italy, (CD-ROM).

Young, A. (1992). “Application of computer modelling to landfill processes.” *DoE Rep. No. CWM 039A/92*, Dept. of Environment, London.

Zerlottin, M., Refisci, D., Della Zassa, M., Biasin, A., and Canu, P. (2013). “Self-heating of dried wastewater sludge.” *Waste Manag.* 33, 12-137.

Zinder, S. H. (1993). “Physiological ecology of methanogenesis.” *Ferry, J. G. (ed.), Methanogenesis: Ecology, Physiology, Biochemistry and Genetics*. Chapman & Hall, New York, 128–206.

Zinder, S.H., Anguish, T., and Cardwell, S.C. (1984). “Effects of temperature on methanogenesis in a thermophilic (58C) anaerobic digester.” *Applied and Environ. Microbiol.*, 47, 808-813.